MULTISCALE MODELING OF THE DOSIMETRIC AND RELATIVE BIOLOGICAL EFFECTIVENESS OF DIAGNOSTIC X-RAYS AND HIGH LINEAR ENERGY TRANSFER PARTICLES

by

Seth William Streitmatter

A dissertation submitted to the faculty of
The University of Utah
in partial fulfillment of the requirements for the degree of

Doctor of Philosophy

in

Nuclear Engineering

Department of Civil and Environmental Engineering

The University of Utah

December 2017

The University of Utah Graduate School

STATEMENT OF DISSERTATION APPROVAL

The dissertation of **Seth William Streitmatter**

has been approved by the following supervisory committee members:

Tatjana Jevremovic	, Chair	**8/9/17** Date Approved
Terry Arthur Ring	, Member	**7/26/17** Date Approved
Jules John Magda	, Member	**7/26/17** Date Approved
Premavathy Rassiah	, Member	**7/26/17** Date Approved
Robert Stewart	, Member	**7/26/17**
Peter Jenkins	, Member	**8/3/17** Date Approved

and by **Michael Ernest Barber** , Chair/Dean of

the Department/College/School of **Civil and Environmental Engineering**

and by David B. Kieda, Dean of The Graduate School.

ABSTRACT

The concept of relative biological effectiveness (RBE) in radiation therapy and diagnostic imaging for a particular radiation type is defined by the ratio of absorbed dose of a reference radiation, typically a low linear energy transfer (LET) radiation to the absorbed dose of a test radiation of typically higher LET that achieves the same biological effect. It is used to quantify and compare expected outcomes (therapy) and deterministic and stochastic risk (imaging, radiation protection) from different types of ionizing radiation. Numerical modeling of RBE and other metrics related to the biological response to ionizing radiation in radiation therapy, diagnostic X-ray imaging, and other related fields is becoming increasingly important as hadron therapy becomes more prevalent and as the concerns associated with diagnostic X-ray dose increase. This dissertation develops and tests a multiscale biophysical model to aid in both estimating clinically relevant biological metrics and to further understand the underlying mechanisms in the special cases examined. The investigation of these special, asymptotic cases in clinical applications of ionizing radiation are used to further refine and improve the multiscale model.

On the therapy side, the high-LET binary radiation therapy of boron neutron capture therapy (BNCT) is used to test the multiscale model. In this therapy modality, there is both dependence on the primary neutron source and biodistribution of the boron with respect to the targeted cells. The radiobiology of these densely ionizing, short range

particles are much different than that of sparsely ionizing photons. On the diagnostic imaging side, the RBE and dosimetric characteristics of computed tomography (CT) are examined with the multiscale model, looking specifically at effects of iodine enhancement. Recent experimental data showing that kV X-rays and electrons have an RBE greater than unity are in line with predictions from the multiscale model. Furthermore, the reported studies also provide strong support for the hypothesis that the RBE for DSB induction is within a few percent of the RBE for cell survival over a wide range of photon and electron energies. The final part of this research focuses on the further integration and expansion of the multiscale model.

I would like to dedicate this work to my wife and family for all their support, patience, and sacrifice throughout this endeavor. I am forever grateful for their help and understanding.

TABLE OF CONTENTS

LIST OF TABLES

Tables

LIST OF FIGURES

Figures

ACKNOWLEDGEMENTS

I would like to thank all the family, friends, colleagues, and mentors who have made this work possible. Special thanks and appreciation to my wife, Marni, for being so supportive and patient, and my friends and family that have always been there to provide encouragement and support along the way. Special thanks to Dr. Robert Stewart for his mentorship, advice, and knowledge all these years, from when I was first interested in the field of medical physics and nuclear engineering, and his instrumental guidance and assistance throughout my graduate work. I thank Dr. Peter Jenkins, for both his career and research mentorship, Dr. Francine Mahak for her invaluable help with my writing. Also, appreciation to Dr. Terry Ring, Dr. Jules Magda, and Dr. Prema Rassiah-Szegedi for serving on my supervisory committee. Finally, I would like to thank my advisor, Dr. Tatjana Jevremovic, for all of her inspiration, advice and motivation over the course of my PhD work. This work would not have been possible without her.

CHAPTER 1

INTRODUCTION

1.1 Contributions

This dissertation develops a novel multiscale model to estimate pertinent biological effects in the clinical applications of ionizing radiation. The special cases examined were chosen to 1) represent the effects of adding compounds that enhance absorbed dose, relative biological effectiveness (RBE), or both 2) highlight the different mechanism at work for high linear energy transfer (LET), high-dose versus those at low-LET and low-dose over a wide range of radiation qualities, 3) determine any weaknesses the system of models that needed to be improved and 4) examine the sensitivity of the model to selected biophysical parameters with an eye towards minimizing the number of adjustable parameters. The multiscale model is tested against measured data from *in vitro* and *in vivo* experiments for the endpoints of double-strand break (DSB) induction and cell survival.

1.2 Motivation

The optimization of proton and heavy ion beam therapy relies on modeling to simulate the transport of the primary particles and secondary ions into patients, and, to predict the relative effectiveness of high-LET ions relative to the MV X-rays more

widely used in radiation oncology. Considering the complexity of biological systems, multiscale approaches are necessary for relating the primary physical and chemical events induced by the radiation field to the clinical outcomes for patients both in healthy tissues and tumors. Compared to conventional photon-based therapies, proton and heavy ion beam therapy typically have a RBE greater than unity, which is known to vary as a function of dose, depth in tissue and the molecular, cellular, or clinical endpoint of interest. Assuming a constant RBE for proton and heavy ion treatment misses an opportunity to fully exploit the potential of hadron therapy in cancer treatments and may, in some instances, cause harmful treatment side effects. In the context of therapeutic applications of radiation, the most relevant endpoint of interest is considered cell survival (or, conversely, cell killing) as it is directly related to the tumor control probability (TCP). Therefore, accurate *a priori* estimates of tumor cell survival are desirable from a therapeutic radiation treatment planning perspective.

In diagnostic X-ray imaging, the primary goal is to optimize the balance of image quality, diagnostic precision and radiation dose. As the prevalence of diagnostic X-ray imaging and X-ray imaging guided procedures and therapies increases, the importance of modeling the impacts of lower energy X-rays, secondary electrons, dose, dose rate, and contrast agents' effects is an increasingly important consideration. In the context of diagnostic X-ray imaging, the biological endpoint of interest is the increased stochastic risk of cancer. Although this is difficult to model and quantify, initial DSB induction, as well as other types of DNA damage formed by ionizing radiation, contribute to radiation mutagenesis and, ultimately, carcinogenesis. The multiscale model developed and tested in this work provide potentially useful information to help quantify the cancer risks

associated with CT scans.

To illustrate the utility and efficiency of a coupled, multiscale model that estimates macroscale dosimetry, particle energy distribution and subsequent biological impact for the endpoints of initial DSB and cell survival, two "extreme" cases are examined. First, the model is applied to the binary treatment of boron neutron capture therapy (BNCT), a high-dose, high RBE treatment. The efficacy of this treatment relies on the localization of ^{10}B in the malignant cells and the capture reaction, $n(^{10}B, \alpha)^{7}Li$, releases two densely ionizing, high linear-energy-transfer (LET), high relative biological effectiveness (RBE) particles that deposit their energy within 10 μm. The compound biological effectiveness (CBE) is heavily influenced by the proximity and spatial distribution of ^{10}B with respect to target cells. The heterogeneous nature of boron distribution *in vivo* for the currently used boron carriers is examined. Second, the model is used to assess the impact of X-ray contrast agents on absorbed dose and RBE in diagnostic CT. Like BNCT, increases in absorbed dose and RBE due to added contrast agents are correlated with the compound's proximity to the cell. Here, the secondary particles are electrons, with short range but lower LET than the alpha particles produced in BNCT. Beyond the special cases examined in this work, the multiscale dosimetric and RBE model can be applied to a myriad of other cases, for example, space and cosmic ray radiation RBE, radiation protection, etc.

The foundation of the multiscale model presented here is based on a few key pieces of research.[1-6] While other multiscale or coupled solutions for RBE modeling have been proposed, one of the goals of this work is to show that the model proposed here has several advantages over the other approaches, which are addressed throughout Chapters

2-4. Figure 1.1 illustrates the system of models used in this work, which aspects they address and how they relate to each other. MCNP (Monte Carlo N-Particle) is a general purpose three-dimensional simulation tool that transports 37 different particle types and has been used for many applications, including nuclear criticality, radiation shielding, dosimetry, and detector response. In this work, version 6.1.1b[7,8] is primarily used, but MCNPX[9], its predecessor, was also used in some early stages of the project. The MCDS[4,5] (Monte Carlo Damage Simulation) Version 3.10A is software that generates nucleotide-level maps of DNA damage for electrons and ions with atomic numbers up to Z = 26 with kinetic energies a few GeV down to kinetic energies corresponding to a continuous slowing down approximation (CSDA) range on the order of a few nanometers.

Estimates of DSB, single strand break (SSB) and base damage (BD) are integrated into MCNP by modifying standard dosimetric tallies by an ion-specific dose-response (i.e., RBE) function. Finally, the RMF (Repair-Misrepair-Fixation) model[3,4,6] is used to relate initial DSB induction to reproductive cell death. The system of models (MCNP, MCDS and RMF model) effectively constitutes a biophysical framework that key events and biological effects on a spatial scale that ranges from the macroscopic (> 1 mm) down to the subcellular (~ 5 to 10 μm) and molecular (tens of nanometers) scales.

1.3 References

1. Stewart, R. D.; Streitmatter, S. W.; Argento, D. C.; Kirkby, C.; Goorley, J. T.; Moffitt, G.; Jevremovic, T.; Sandison, G. A. Rapid MCNP Simulation of DNA Double Strand Break (DSB) Relative Biological Effectiveness (RBE) for Photons, Neutrons, and Light Ions. *Phys. Med. Biol.* **2015**, *60* (21), 8249–8274 DOI: 10.1088/0031-9155/60/21/8249.

2. Frese M. C.; Yu V. K.; Stewart R. D.; and Carlson D. J. A Mechanism-Based Approach to Predict the Relative Biological Effectiveness of Protons and Carbon Ions in Radiation Therapy. *Radiat. Oncol. Biol.* **2012**, *83* (1), 442–450 DOI: 10.1016/j.ijrobp.2011.06.1983.

3. Carlson, D. J.; Stewart, R. D.; Semenenko, V.; Sandison, G. A. Combined Use of Monte Carlo DNA damage Simulations and Deterministic Repair Models to Examine Putative Mechanisms of Cell Killing. *Radiat. Res.* **2008**, *169* (4), 447–459.

4. Semenenko, V.; Stewart, R. D. Fast Monte Carlo Simulation of DNA Damage Formed by Electrons and Light Ions. *Phys. Med. Biol.* **2006**, *51*, 1693.

5. Stewart, R. D.; Yu, V. K.; Georgakilas, A. G.; Koumenis, C.; Park, J. H.; Carlson, D. J. Effects of Radiation Quality and Oxygen on Clustered DNA Lesions and Cell Death. *Radiat. Res.* **2011**, *176* (5), 587–602 DOI: 10.1667/RR2663.1.

6. Carlson, D. J. Mechanisms of Intrinsic Radiation Sensitivity: The Effects of DNA Damage Repair, Oxygen, and Radiation Quality. Ph.D. Dissertation, Purdue University, West Lafayette, IN, 2006.

7. Goorley, T.; James, M.; Booth, T.; Brown, F.; Bull, J.; Cox, L. J.; Durkee, J.; Elson, J.; Fensin, M.; Forster, R. A.; *et al.* Initial Mcnp6 Release Overview. *Nucl. Technol.* **2012**, *180* (3), 298–315.

8. Mckinney, G. W.; Brown, F. B.; Hughes, H. G. I.; James, M. R.; Martz, R. L.; McMath, G. E.; Wilcox, T. MCNP 6.1.1 - New Features Demonstrated. *LA-UR-14-28473. Los Alamos, NM: Los Alamos National Laboratory (LANL).* **2014**.

9. Pelowitz, B D (ed), MCNPX User's Manual, v2.7.0 LA-CP-11-00438. *Los Alamos, NM: Los Alamos National Laboratory (LANL).* **2011**

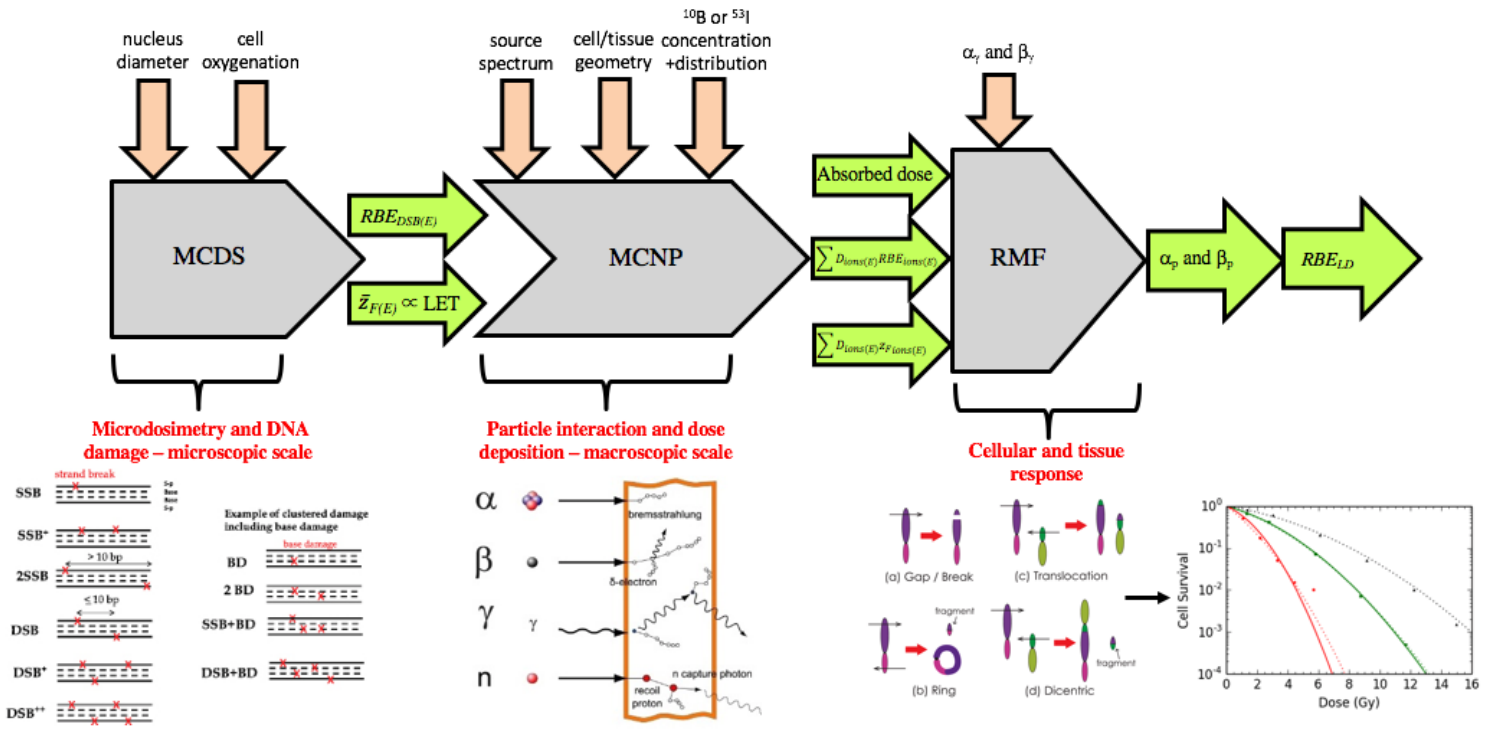

Figure 1.1. Flowchart of a multiscale system of models to assess the dosimetry, microdosimetry, and particle RBE *in vitro* or *in vivo*. Models (grey), input parameters (orange) and output (green). Here, $\bar{z}_F$ is the mean-frequency specific energy, α_γ and β_γ are the linear quadratic (LQ) model parameters for the reference radiation (e.g., ^{60}Co γ-rays) and α_p and β_p are the linear quadratic variables for the test radiation (e.g., BNCT). The main output summations from system of models is the dose-averaged RBE_{DSB}, $\bar{z}_F$ and estimates of α_p and β_p weighted by dose and averaged over all particle types and kinetic energies. The RBE for cell survival in the asymptotic limit of absorbed dose D that is small compared to $(\alpha/\beta)_\gamma$ is $RBE_{LD} \equiv \alpha_p/\alpha_\gamma$

CHAPTER 2

MECHANISTIC MODELING OF THE RELATIVE BIOLOGICAL EFFECTIVENESS (RBE) OF BORON NEUTRON CAPTURE THERAPY[1]

2.1 Introduction

A published coupled (multiscale) framework for estimating the initial DNA damage arising from interactions with photons, neutrons, and light ions (Stewart *et al.* 2015) is applied to the complex, mixed radiation field encountered in boron neutron capture therapy (BNCT). Further, the mechanistic repair-misrepair-fixation (RMF) model (Carlson *et al.* 2008, Frese *et al.* 2012) is used to explicitly link α and β parameters in the linear quadratic (LQ) cell survival model to the initial numbers and spatial distribution of DSB obtained from the multiscale simulations. A MCNP model (Moffitt *et al.* 2016) of the University of Washington Clinical Neutron Therapy System (UW CNTS) and a few other neutron source models are used in combination with the system of biophysical models to validate it with existing experimental data based on the use of BPA (boronophenylalanine) as well as examine the potential efficacy of BNCT using other boron carriers in development. The impact of the microdistribution of ^{10}B

[1] This chapter is adapted from an article in preparation for submission to *Physics in Medicine and Biology*.

within and near representative cells on the relative biological effectiveness (RBE), compound sources. The results of these studies suggest that BNCT with fast, conformal neutron therapy beams may provide superior local tumor control compared to three-dimensional conformal neutron therapy alone or BNCT with nonconformal neutron sources.

BNCT has been investigated as a potential treatment for glioblastoma multiforme (GBM), head and neck cancers, melanoma, and tumor sites for many decades. Although efforts to develop neutron sources and new boron delivery agents for BNCT are ongoing (Barth 2009), BPA and BSH (sodium borocaptate) are currently the only boron compounds approved for use in clinical trials (Hopewell *et al. 2*012). Although doses of BPA are non-toxic for doses as high as 250 mg BPA/kg of body weight and tumor to blood ratios up to 3.5:1 (Coderre *et al.* 1997), the use of non-conformal thermal and epithermal neutron beams are limited by normal brain tolerances and some clinical trials have confirmed radiation necrosis in non-tumor brain tissue (Laramore *et al.* 1996). Additionally, BSH is much more toxic than BPA and doesn't possess the specificity of BPA and is thus characterized as a global (nonspecific) boron delivery agent (Hawthorne *et al. 2*003). For GBM, BSH was first used with thermal neutron beams in clinical trials started in Japan during the mid-1960s and then in the United States. Clinical trials of BNCT for the treatment of GBM ended in the United States in the early 1990's (Coderre *et al.*1999), although in other countries clinical trials of BNCT continued. Early studies of BNCT with nonconformal neutron beams ultimately concluded that BNCT using BSH is not superior to 3D conformal photon therapy in terms of patient survival (Laramore *et al.* 1996). Although BNCT with nonconformal neutron beams for the treatment of GBM

has not proven advantageous when compared to current photon therapy, it has shown promise for the treatment of superficial melanoma lesions (Laramore 1996a, Menéndez *et al. 2*009). The potential efficacy of BNCT using well-collimated, higher energy neutron beams (Nigg *et al. 2*000, Laramore *et al. 2*001) is at an early stage of development, in part because very few facilities have the ability to deliver neutron beams shaped to the beams-eye view of an irregularly shaped tumor target. The University of Washington (UW) Clinical Neutron Therapy System (CNTS) is the only remaining operational facility in the U.S. with the ability to deliver 3D conformal fast neutron beams for the treatment of cancer (Kalet *et al.* 1997, 2013, Moffitt *et al.* 2016).

The production and modeling of optimal neutron spectrum that maximize the dose from boron capture reactions has been extensively studied (Riley *et al. 2*003, 2004). However, additional research on ^{10}B pharmaceutical development is needed to further advance the overall use of BNCT for the treatment of cancer. Advances in tumor-specific boron delivery agents have the potential to greatly improve BNCT using nonconformal and conformal neutron beams. Some mAbs (monoclonal antibodies) are especially promising due to their high tumor selectivity. For example, Trastuzumab, an anti-HER2 mAb, may prove to be an especially useful delivery agent for some cancers with over-expression of HER2, specifically breast cancer (Mundy *et al. 2*006, Sztejnberg Gonçalves-Carralves and Jevremovic 2007). This over-expression is present in 20 - 30% of breast cancer cases (Mitri *et al. 2*012). Current PET (Positron Emission Tomography) imaging studies show very good specificity of Trastuzumab, up to 18:1 tumor to healthy tissue ratio (Dijkers *et al. 2*010). Although, due to the size of mAbs diffusion is slow and optimal uptake of Trastuzumab, for example, occurs 3-5 days after injection (Dijkers *et*

al. 2010). In addition to having a highly specific neutron capture therapy (NCT) targeting compound, the use of highly conformal neutron beams, such as the UW CNTS may overcome limits of early studies of BNCT with nonconformal neutron beams. Exploiting the benefits of a fractionated regime may also show promise.

2.2 Methods

2.2.1 Conceptual aspects of a multiscale radiobiological model

Consider a small region of tissue or culture medium that receives a uniform absorbed dose *D* of ionizing radiation, as conceptually illustrated in Figure 2.1b. In ICRU Report 36 on *Microdosimetry* (1983), the absorbed dose in a region of interest (ROI) is the product of the average event frequency ν times the frequency-mean specific energy, i.e., $D \equiv \nu \bar{z}_F \cong (\Phi A)\bar{z}_F$. Here, Φ is the particle fluence and *A* denotes the cross-sectional area of a subcellular, cellular or multicellular target of interest within the ROI. By definition, the absorbed dose distribution in a ROI may be considered *uniform* when, for any target within the ROI, the product $\nu \bar{z}_F$ or $(\Phi A)\bar{z}_F$ is the same at all locations within the ROI. However, because of the stochastic nature of particle interactions within cellular and subcellular targets, the specific energy (stochastic analog to absorbed dose) imparted to different targets within a uniformly irradiated ROI may be quite different. That is, the absorbed dose in the ROI is the average (*expected value*) of the specific energy distribution of the cellular or subcellular targets within the ROI.

As a first approximation, the mean specific energy for a spherical target of diameter *d* irradiated by a charged particle of defined linear energy transfer (LET) randomly passing through a spherical target with mass density ρ is $\bar{z}_F \cong LET / \rho d^2$

(ICRU 1983). When a ROI is irradiated by a low LET radiation, such as the energetic electrons arising from the interactions of ^{60}Co γ-rays or MV X-rays, the mean specific energy per event is small (~ 1.6 mGy for a 0.2 keV/μm electron passing through a 5 μm in diameter target) and the number of events per unit absorbed dose is two or three orders of magnitude larger (ν ~ 600 for a 5 μm target and 0.2 keV/μm electrons). For higher LET radiations, such as the particles produced in BNCT (n,α) reactions, the mean specific energy increases in approximately linear fashion with particle LET, and the number of events per unit absorbed dose therefore decreases in linear fashion with increasing particle LET. Numerous published studies provide compelling evidence that, for the same absorbed dose, the severity and frequency of biological damage (e.g., initial DNA damage to cell killing) is larger for a small number of large energy deposition events (high-LET, large $\overline{z}_F$) than for a large number of small energy deposition events (low LET, small $\overline{z}_F$). The effects of low and high-LET radiations arising from stochastic differences in dose on the small scale even when the average absorbed dose on the larger (multicellular, macroscopic) scale is uniform motivates the definition of a radiation's relative biological effectiveness (RBE). For two different types of radiations that result in the same biological effect *E*, the RBE of a radiation relative to another is defined as the absorbed dose of the (usually low LET) reference radiation D_γ to the absorbed *D* of the other (usually higher LET) radiation, i.e., $RBE \equiv D_\gamma/D$.

Although often used in the literature to define the characteristics of one type of radiation relative to another, the RBE concept is easily generalized to the irradiation of a ROI by a mixture of particles of varying type, energy and charge. From the definition RBE, one can also define the RBE weighted dose (RWD) as the product of ($RBE \times D$).

Conceptually, the RWD is the dose of the (usually higher LET) test radiation that produces the same biological effect as the reference radiation. For a ROI that receives a uniform absorbed dose of radiation, the overall RWD is the sum of ($RBE_i \times D_i$) integrated over all *i* particle types (charge and mass) and kinetic energies, i.e.,

$$RWD = \sum_i \int_0^\infty dED_i(E)RBE_i(E) \tag{2.1}$$

The corresponding RBE, averaged over all particle types and energies is

$$RBE = \frac{1}{D}\sum_i \int_0^\infty dED_i(E)RBE_i(E),\ where\ D \equiv \int_0^\infty dED_i(E) \tag{2.2}$$

Eq. (2.1) and (2.2) provide a rigorous quantitative and conceptual framework to define a relevant RBE and RWD for one or more cells in a (*macroscopic*) ROI receiving a uniform absorbed dose of radiation. Conceptually, $RBE_i(E)$ is a biological dose-response function that primarily corrects for the small-scale, cellular, and multicellular ionization density (track structure) of the *i*th type of particle with kinetic energy *E*. On a larger multicellular level, there is good evidence in the literature that cell-to-cell signaling (e.g., bystander effects) and the interactions of cells with their environment (e.g., *in vitro* vs. *in vivo* environment) has a substantial impact on the dose-response characteristics of biological endpoints ranging from initial DNA damage to neoplastic transformation and cell death. On an even larger scale, at the tissue and organ level, immune response and inflammation can also influence the effects of radiation (Georakilas 2015 and references therein), but mechanistic models have not yet been proposed for these complex pathways and reactions to ionizing radiation.

For a nonuniform dose distribution, subdivide the ROI into a series of *j* smaller ROI that receive a uniform absorbed dose. Then, compute the overall dose-averaged RBE by summing the RWD over all *j* ROI and then dividing by the sum of the doses to

all *j* regions, i.e.,

$$RBE = \frac{1}{D}\sum_j RWD_j,\ where\ D \equiv \sum_j D_j \quad (2.3)$$

Experimental determinations of a radiation's RBE are attributed to the small-scale (cellular and subcellular) ionization density (track structure) of one type of radiation relative to another. However, almost all experimental determinations of RBE quantify the molecular and cellular damage arising from a macroscopic absorbed dose of one type of radiation to a collection of cells (*in vitro* or *in vivo*) relative to a macroscopic absorbed dose of another type of radiation to a collection of cells (*in vitro* or *in vivo*), regardless of the underlying mechanisms of action. For the same conceptual reasons, mathematical models that accurately reproduce the results of *in vitro* or *in vivo* experiments implicitly or explicitly include all mechanisms of action for the experimental conditions in which the RBE models fit the measured data.

In experimental determinations of radiation RBE, uncertainties in the dosimetry (e.g., nonuniform dose across a collection of cells *in vitro* or *in vivo*) as well as uncertainties in the measurement of a biological endpoint using a specific assay (e.g., γ-H2AX foci or PFGE for the measurement of DSB induction) contribute to uncertainties in RBE estimates. It is not uncommon to have experimental uncertainty of 10% or greater. Uncertainties arise from random or systematic errors in the biological assay as well as random and systematic errors in the dosimetry. The dosimetry of low energy, very short range (high-LET and RBE) particles is especially challenging.

2.2.2 MCDS+MCNP model for a mixed radiation field

The MCDS algorithm has been extensively tested and benchmarked against track structure simulations (Nikjoo *et al.* 1997, 1999, 2001, Friedland *et al.* 2003, Campa *et al.* 2009, Alloni *et al.* 2010) and experimental data in previous work (Hsiao and Stewart 2008, Stewart *et al.* 2011). Details of the computationally efficient method used to integrate information from the MCDS into larger-scale MCNP simulations are described in Stewart *et al.* 2015. To apply the MCDS+MCNP system of models to a mixed radiation field, consisting of ions of varying charge, mass and kinetic energy, a standard MCNP F6 heating tally is modified by an ion-specific RBE_{DSB} dose–response function (DE DF card in MCNP). The modified F6 heating tally records the RWD averaged over a target region of interest. The dose-averaged value of the RBE_{DSB} is then computed by summing $(\text{RBE} \times \text{dose})_i$ over all i ions and dividing by the total absorbed dose, as described in Eq. 2.2. The dose-averaged values of $\bar{z}_F$ is obtained in the same manner for subsequent use in the model of cell survival.

2.2.3 RMF model for a mixed radiation field

Within the RMF model (Carlson *et al.* 2008, Frese *et al.* 2012), the effects of particle type and kinetic energy (and hence LET) on α and β in the linear quadratic (LQ) cell survival model are explicitly linked to the initial numbers and spatial distribution of DSB. In the RMF model, the biological processing of initial DSB into lethal chromosome aberrations or point mutations is modeled by a coupled system of nonlinear differential equations. From combined MCDS+MCNP simulations, dose-weighted RBE_{DSB} and $\bar{z}_F$ are computed for each ion contribution and within the RMF, low and

high-dose RBE (asymptotic limits) for the endpoint of reproductive cell death are computed (Streitmatter *et al.* 2017) as

$$RBE_{LD} = \frac{a_p}{\alpha_\gamma} = RBE_{DSB}\left(1 + \frac{2\bar{z}_F RBE_{DSB}}{(\alpha/\beta)_\gamma}\right), RBE_{HD} = \sqrt{\frac{\beta_p}{\beta_\gamma}} = RBE_{DSB} \quad (2.4)$$

These formulas are derived under the assumption that intra-track binary misrepair is negligible (≤ 1%) for the low-LET reference radiation, e.g., the cell-specific adjustable biological parameter $\kappa = 2\beta_\gamma/\Sigma_\gamma$ and $\theta = \alpha_\gamma/\Sigma_\gamma$ within the RMF (Figure 3A in Carlson *et al.* 2008). Here, Σ_γ is the DSB Gy^{-1} Gbp^{-1} for the reference radiation and Σ_p is the DSB Gy^{-1} Gbp^{-1} for the test radiation, and hence, the ratio $\Sigma_p/\Sigma_\gamma = RBE_{DSB}$.

$$RBE_{LD} = \frac{\alpha_p}{\alpha_\gamma} = \frac{\theta\Sigma_p + \kappa\Sigma_p^2\bar{z}_F}{\alpha_\gamma} = \frac{\frac{\alpha_\gamma}{\Sigma_\gamma}\Sigma_p + \frac{2\beta_\gamma}{\Sigma_\gamma^2}\Sigma_p^2\bar{z}_F}{\alpha_\gamma} = RBE_{DSB}\left(1 + \frac{2\bar{z}_F RBE_{DSB}}{(\alpha/\beta)_\gamma}\right)$$

$$RBE_{HD} = \sqrt{\frac{\beta_p}{\beta_\gamma}} = \sqrt{\frac{\frac{\kappa}{2}\Sigma_p^2}{\beta_\gamma}} = \sqrt{\frac{\frac{2\beta_\gamma}{2\Sigma_\gamma^2}\Sigma_p^2}{\beta_\gamma}} = RBE_{DSB}$$

For direct comparison to experimental cell survival, the two terms in Eq. 2.4 are simply solved for the linear (α_p) and quadratic (β_p) variable of the test radiation. Here α_γ and β_γ are the LQ parameters for the low-LET radiation (e.g. - ^{60}Co γ-rays, 200-250 kVp X-rays, etc.) and α_p and β_p are the LQ parameters for the test radiation, in this case, the dose-

weighted LQ parameters are for the combined ion contributions of the neutron or BNCT field. Because biophysically meaningful values of the RBE_{DSB} as well as $\overline{z}_F$ and $(\alpha/\beta)_\gamma$ must be nonnegative, Eq. (2.4) implies that the RBE for reproductive cell death must fall within the range of values defined by RBE_{DSB} (minimum RBE) and RBE_{LD} (maximum RBE) for a given cell line or tissue. For a single large absorbed dose of radiation, as is typical with conventional BNCT [$D > (\alpha/\beta)_\gamma$], RBE_{DSB} is the more relevant metric, while a fractionated regime of smaller absorbed doses, as is seen in fast neutron therapy [$D < (\alpha/\beta)_\gamma$], RBE_{LD}, is the more relevant metric. The RMF formulas in combination with first principle estimates of RBE_{DSB} have been shown to reproduce trends in cell survival for electrons, protons and other charged particles with an LET up to at least 100 to 200 keV/μm. This framework has been used to predict cell survival for the mixed radiation field encountered in helium ion therapy (Mairani *et al.* 2016) and heavy ion therapy (Kamp *et al.* 2015), proton and carbon ion therapy (Frese *et al.* 2012) and for X-rays (Streitmatter *et al.* 2017), monoenergetic deuterons and alpha particles (Carlson *et al.* 2008).

For the lithium recoil ions encountered in BNCT, with LET ~370-390 keV/μm and ranges ~4-5 μm, which is comparable to the size of the nucleus (see Table 2.1), the RMF may overestimate the level of cell killing compared to experimental data for particles with LET > ~100 keV/μm (Figure 4 in Carlson *et al.* 2008, Figure 1 in Frese *et al.* 2012). Currently within the RMF, all DSBs have equal chances of contributing to cell killing, regardless of their proximity to one another and cell killing is predicted continue to increase past ~100-200 keV/ μm. The MCDS corrects for CSDA range and changes in stopping power as particles pass through a cell nucleus 5 μm (default) in diameter for

estimates of $\bar{z}_F$, where the equation $\bar{z}_F \cong LET/\rho\, d^2$ will overestimate $\bar{z}_F$ in this special case. Here, LET is the LET in water (keV/μm), ρ is the density of the nucleus (1.0 g/cm^2) and d is the diameter of the nucleus (~ 5 μm). Figure 2.2 shows the trends in relative DSBs per track and μm per DSB vs. $(z_{eff}/\beta)^2$ for alpha particles and ^{7}Li ions; $\bar{z}_F$ values used are calculated via MCDS. As $(z_{eff}/\beta)^2$ increases each particle reaches a specific peak in DSB per track and minimum DSB spacing. For the alpha particles, this corresponds to a $(z_{eff}/\beta)^2$ ~ 4,500, with a corresponding LET ~ 200 keV/μm, which is comparable to what has been seen in experimental studies of RBE vs. LET. This may play an important role in the RBE predictions for the high-LET capture products in BNCT and is discussed further in Section 2.4.3. The range of alpha particle energies seen in BNCT, as denoted in Figure 2.2, precede the particle-specific peak, while the lithium ion energies occur at the peak and a bit past, where the effectiveness starts to decline. However, this peak occurs at higher LET then seen in experimental data, suggesting that the minimum DSB spacing is smaller than the threshold the cell "sees" for processing. The increase in spacing after the minimum in Figure 2.2 is an artifact of using the mean chord length in the calculation, rather than the CSDA range.

2.2.4 Simulation of the secondary charged-particle spectrum

Neutrons undergo a number of interactions in soft tissue important to radiobiology. The dominant interaction for fast neutrons is (n, p) with hydrogen, while slow and thermal neutrons have a high probability of being captured via ^{1}H(n, γ)^{2}H and ^{14}N(n, p)^{14}C reactions. These are nonspecific dose components that affect all irradiated tissue. In addition, there is the localized dose arising from ^{10}B capture reactions that

create short-range, high-LET alphas, and recoil ^{7}Li nuclei. MCNPX was used to track all the secondary ions within the water/tissue phantom and cellular model, including ^{1}H, ^{2}H, ^{3}H, ^{3}He, ^{4}He^{2+}, ^{7}Li^{3+}, and ions with Z > 2. To separate the ^{7}Li^{3+} contribution from the rest of the heavy ions such as ^{14}C, the special tally treatment card FT RES 3007 in MCNP6 was used.

The neutron capture ion algorithm (NCIA) model was enabled by setting the 7th entry on the PHYS:N card to 4 in MCNPX; this allowed for the production of ions from the n(^{10}B, α)^{7}Li reaction as well as enabling light ion recoil physics. This setting accounts for the ionization potential and uses the proper two-body kinematics to bank recoil particles with the proper energy and angle. Simulations were performed with a proton, alpha and heavy ion cutoff energy of 1 keV (lowest allowed by the code) and the Vavilov energy straggling model with the finest-allowed energy resolution in stopping power (efac=0.99). CEM03 and LAQGSM models were selected over the default physics in the LCA card, as recommended in the User's Manual (Pelowitz 2011) and the neutron cross-section data used are primarily from ENDF/B-VII.0. Absorbed dose tallies (F6) were setup for all charged particles of interest (all possible secondary ions from neutrons and photons) to determine the physical and biological dose. Additionally, modified F6 tallies were setup with dose response functions that relate particle energy to DNA and cellular damage, as discussed in Sections 2.3.1 and 2.3.2.

2.2.5 Model for cellular dosimetry

In order to assess microdosimetry of BNCT treatment and the impact of subcellular ^{10}B distributions, a simple cell model was developed and parameters were

evaluated using MCNPX. The cell model is shown in Figure 2.2 and consists of concentric spheres representing the cell cytoplasm and nucleus, which is a common approach in microdosimetry studies. Others (Elbast *et al. 2*012) have shown that Monte Carlo simulation is a suitable method to assess the stochastic and heterogeneous nature of alpha particle and other heavy ion energy depositions. They show that MCNPX simulations of specific energy *(z)* deposited in the cell nucleus, the single-hit density of specific energy $f_1(z)$ and the mean-specific energy $\langle z_1 \rangle$ were in good agreement when compared with the literature using simple geometry as small as 1 μm.

Uniform ^{10}B distributions, as well as heterogeneous distributions, which more realistically mimics clinically used BNCT pharmaceuticals, are assessed. Using data collected from experimental studies related to subcellular localization of BPA (Nguyen *et al.* 1993), ^{10}B was incorporated into the representative cell compartments. Brain tissue composition (ICRU 1992) was selected as representative of the composition of 9L rat gliosarcoma surrounding the cells *in vivo*. The extracellular matrix was modeled as a cube of tissue, with the cell model embedded in the center of the cube at a depth of 2 mm. The 2-mm size of the cube was selected to be larger than the continuous slowing-down approximation (CSDA) of the charged particles of interest (Table 2.1) but small compared to the range of the incident neutron mean free path. The neutron source was modeled as a uniform, monodirectional disk source. For the sake of computational efficiency, Monte Carlo simulations were performed in two steps. First, neutrons from a disk source incident on a tissue phantom are scored along the central axis of the beam (Figure 2.1a). The tally of neutron energy-dependent fluence at the depth of interest (1.5-1.7 cm) was used as the source in a second, microdosimetric simulation mimicking an *in*

vitro experiment (as shown in Figure 2.2b). The secondary charged particle energy distribution and the DNA damage are based on tallies within the cell nucleus as the critical (sensitive) volume. The MCDS contains a subcellular dosimetry model for charged particles passing through water (Stewart *et al.* 2011), while MCNP handles larger scale dosimetry and accounts for any charged particle equilibrium (CPE) effects. Notice the divergence of the MCDS and analytic ICRU formula for $\bar{z}_F$ when the CSDA range approaches 5 μm or less as shown in Table 2.1.

2.2.6 Neutron source models for BNCT

To assess normal tissue RBEs and overall cell survival, the four neutron sources we considered are:

(a) Massachusetts Institute of Technology Fission Convertor Beam (MIT-FCB) (Riley *et al. 2*004). The MIT-FCB is a commonly used source for analyzing BNCT because of the purity and intensity of epithermal neutrons (Riley *et al. 2*003). It has a very similar neutron spectrum and microdosimetric properties to the Brookhaven Medical Research Reactor (BMRR) (Burmeister *et al.* 2003, Binns *et al.* 2005).

(b) A compact neutron source or "neutron multiplier" source (NM source). This source uses a D-T reaction to generate neutrons (Rasouli and Masoudi 2012). All of the reported results are for this source are based on a published MCNPX model (Pelowitz 2011)

(c) A new CN source derived from the NM by removing the uranium sphere from the NM source.

(d) The UW CNTS (Bichsel *et al.*1974, Stelzer *et al.*1994, Kalet *et al.* 1997, Douglas *et al. 2*003, Kalet *et al.* 2013 and Moffitt *et al. 2*016), which uses 50.5 MeV protons incident on a Be target to produce a fast neutron energy spectrum.

The neutron fluence in the MIT-FCB source corresponds to a reactor power at 5 MW, which produces ~3×10^9 n cm^{-2} s^{-1} epithermal (0.5 eV – 10 keV) fluence (Riley *et al. 2*003). Spectral data for this fission source were acquired from literature (Auterinen *et al. 2*004) without the need for additional modeling of the MIT-FCB beam. D-T sources were a major focus of interest due to their compactness, lower cost, and greater feasibility in a hospital setting than a reactor-based neutron source. Rasouli and Masoudi (2012) proposed using a fissionable material as a neutron multiplier, effectively increasing the number of neutrons emitted from the D-T neutron generation. Their work built on the initial work of Verbeke *et al.* (2000) on D-T and D-D neutron sources. The proposed beam shaping assembly (BSA) uses a combination of TiF_3, Al_2O_3 as moderators, Pb as a reflector, Ni as a shield and Li-Poly (Lithiated Polyethylene) as collimation. This BSA combination was reproduced in MCNPX with two tally planes past the aperture to record the neutron spectrum and flux, as seen in Figure 2.3. Neutrons produced by D-T reaction of this source vary around 14.1 MeV by only ±7% (Rasouli and Masoudi 2012), thus, it is assumed that neutrons are emitted isotropically and monoenergetically from the target in this model.

2.2.6.1 MCNP6 model of the Clinical Neutron Therapy System (CNTS)

While not a traditional neutron source for BNCT, the UW CNTS is the only remaining fast neutron therapy facility in clinical operational within the U.S. Currently,

the CNTS is mainly used for palliative treatments of tumors refractory to photons and for selected head and neck cancers, including salivary gland tumors (Stelzer *et al.* 1994, Douglas *et al. 2*003). However, it may be feasible to further enhance the usefulness of fast neutron therapy by combining 3D conformal neutron therapy with BNCT (Maughan *et al.*1993, Laramore *et al.*1994, Buchholz *et al.*1997, Nigg *et al.* 2000) or by using fast, conformal BNCT in combination with 3D conformal and intensity modulated photon or proton therapy.

In the UW CNTS, fast neutrons are produced by 50.5 MeV protons incident on a 10.5 mm thick beryllium target, primarily through (p, n) and (p, $n + p$) reaction, but a small portion are created through (p, $2n$), (p, $3n$), and (p, $n + \alpha$) reactions (Moffitt *et al. 2*016). The incident proton beam was modeled in MCNP6 as a monoenergetic, monodirectional disk source of 0.5 cm radius, uniformly sampled. The beam originates in the vacuum above the beryllium target. Neutrons and photons are transported through the geometry as illustrated in Figure 2.4 and tallied in a volume of air below the target housing. The neutron spectrum and fluence at this point is recorded in a phase space file, using a SSW card in MCNP6, and then transported as a secondary source through the multileaf collimator (MLC) (Figure 2.4b) and then into a water or tissue phantom. All of the simulations reported in this work are for an open 10.4×10.3 cm^2 field at a depth of 1.7 cm in water, no wedge, small flattening filter, 148.5 cm source to surface distance or SSD.

2.3 Results

2.3.1 Energy fluence of the MIT-FCB, NM, CN and UW CNTS neutron sources

Figure 2.5 shows a comparison of the neutron energy fluence for the MIT-FCB, NM, CN and UW CNTS sources. The NM source (configuration d with a Ni shield and Li-Poly collimator) can produce fluence as high as 5×10^{12} n/s at the target, with a resulting epithermal fluence rate of ~ 4×10^{8} n cm^{-2} s^{-1} at the beam port (tally planes). This configuration was chosen due to its maximum epithermal flux compared to other material combinations (Rasouli and Masoudi 2012). With the removal of the uranium sphere (i.e., CN source), the neutron fluence rate decreases to ~ 2×10^{8} n cm^{-2} s^{-1}. In the UW CNTS, an open 10.4×10.3 cm^2 field (small filter, 148.5 cm SSD) produces a neutron fluence rate along the central axis of the beam at a depth of 1.5 cm in water of 1.91×10^{8} n cm^{-2} s^{-1}, which corresponds to an absorbed dose rate in water of 60 cGy min^{-1} at the depth of maximum dose (1.7 cm). The fluence-averaged neutron energy for the MIT-FCB, NM, CN and UW CNTS sources are 11.0 keV, 0.46 MeV, 0.36 MeV, and 21.0 MeV, respectively. The average energy of the CNTS neutron energy spectrum varies with depth and lateral position within the field because of beam hardening as well as in-field and out-of-field nuclear interactions. As illustrated in Figure 2.5, all of the sources produce large numbers of thermal and epithermal neutrons. The NM and CM sources produce nearly identical neutron energy spectra over the entire energy range. Below about 20-30 keV, the MIT-FCB source also produces a neutron energy spectrum very similar to the NM and CN sources; however, the MIT-FCB source has been optimized to reduce the number of higher-energy neutrons. Unlike the MIT-FCB, NM, and CN sources, the UW CNTS beam also produces substantial numbers of very energetic

neutrons (> 10 MeV), which is advantageous for the delivery of a conformal neutron dose to tumor targets (i.e., MLC are used to shape the field to the beam's eye tumor contour) but does little to enhance $^{10}B(n,\alpha)^{7}Li$ reactions.

2.3.2 Proton and alpha particle cell survival benchmarks

To test the accuracy of the proposed system of models, it is applied to experimental cell survival data for monoenergetic protons and alpha particles. The work of Goodhead *et al.* (1992) compared cell survival of alpha particles and protons of equal LET, finding that protons had a statistically significant increase in biological effectiveness in the V79 cell line. They concluded that this must be due to differences in track structure. Table 2.2 shows the experimental results against model estimates, confirming that the track structure level effects are reflected in our system of models and not based on LET alone. At 1.4 MeV, the experimentally-derived value of α is larger than expected compared to the other experimental data and MCDS+RMF estimates. At 0.42 Gy^{-1}, it is significantly larger than the α estimate for a 1.2 MeV alpha particle. This is likely due to the experimentally uncertainty inherent in the dosimetry and cell counting statistical variations for these short-range, high-LET particles. It is expected that the α values for the 1.2 and 1.4 MeV alpha particle will only differ by a small amount since their $(z_{eff}/\beta)^2$ values are similar.

Additional tests of the model were performed for a range of alpha particle kinetic energies. In the work of Tracy *et al.* (2015) cell survival in the V79 cell line was assessed for alpha energies from 1.1 to 4 MeV, which covers the energy range seen in ^{10}B capture reactions. Figure 2.6 shows the comparison of experimental cell survival results and model estimates for the alpha particle energies examined and Table 2.3 shows

comparisons of variables derived from the work their work and our system of models' estimates. For high-LET particles, such as alpha particles in this range, note that MCDS+MCNP estimates of LET are very good for higher energy, longer range but start to diverge a bit for the lower energies, where path length straggling and LET variations in the ion track come into play. In experimental irradiation conditions, truly monoenergetic beams are rarely achieved; there is at least some spread in the particle energy. Monoenergetic simulations were compared to simulations of the reported energy distributions, finding that the impact on RBE_{DSB} was > 0.5%, while the impact on $\bar{z}_F$ was relatively large (4 – 14%) for the 1.1 – 1.8 MeV alpha particles, but < 2% for the 2.4 – 4 MeV alpha particle energy distributions. Since Tracy *et al.* reports a distribution of cell sizes in their cell survival experiments, nucleus diameters of 3-6 μm were assessed in MCDS+MCNP simulation. This variable (ndia) has a quite large impact on estimates of $\bar{z}_F$, but a small impact on RBE_{DSB} within the current version of MCDS. Table 2.3 shows that there is good agreement between MCDS+MCNP estimates of $\bar{z}_F$ and the computed values $\bar{z}_F$ from RMF-fits to the experimental data (using Eq. 2.4, RBE_{LD}) for 1.1 and 1.5 MeV alpha particles, but exhibiting opposite trends at higher energy, opposite of the LET comparisons. This finding indicates that the accuracy of the RBE_{DSB} estimates or some other aspect of the RMF model may need to be refined in order to improve the accuracy of the model for very low energy (short-range, high-LET) alpha particles. Other work (Mairani *et al.* 2016) supports the hypothesis that the RBE for cell survival of alpha particles can be reliably estimated within the RMF for clinically relevant scenarios in helium ion radiotherapy, although they were looking at much higher kinetic energies.

2.3.3 RBE of selected ions produced in BNCT reactions

Table 2.4 lists estimates of the dose-averaged RBE_{DSB} and RBE_{LD} for selected ions in BNCT reactions. All of the results in this table are based on a representative ^{10}B subcellular distribution of 40 μg/g in the cell cytoplasm. It can be seen that the recoil protons from ^{14}N capture and the fast recoil protons from hydrogen elastic interactions with fast neutrons are lumped together in the single RBE value, but weighted appropriately by absorbed dose. The ^{14}N content of the tissue can have a significant effect on the dose-weighted proton RBE because the capture reactions release higher RBE protons than the protons from hydrogen scattering. One of the more striking aspects of the results shown in Table 2.4 is that the proton low dose RBE with α/β = 3 Gy is not much higher than $RBE_{HD} \cong RBE_{DSB}$ whereas RBE_{LD} is much larger than RBE_{HD} for particles with $Z > 2$. These effects arise in the RMF model because intra-track DSB interactions (also referred to as "proximity effects" in the literature) are much more significant for ions with $Z > 2$ than for protons. In terms of equation (2.4), the product of $2\,\overline{z}_F RBE_{DSB} / (\alpha/\beta)_\gamma$ is ≤ 1 for protons (with kinetic energies above 1 keV) and large (compared to unity) for heavier ions for α/β = 3. The results from Table 2.4 also suggest that the effects of α/β on the overall RBE_{LD} arise in the RMF model from intra-track (proximity) effects associated with heavier ions from BNCT reactions rather than protons.

2.3.4 *In vitro* and *in vivo* testing of the dosimetry and CBE Models

To calibrate the RMF model for BNCT, we first obtained the LQ parameters α_γ and β_γ for the 9L rat gliosarcoma cell line irradiated by 200-250 kVp X-rays, which was published in Coderre *et al.* (1993). It follows from Eq. 2.4 that the only further

parameters needed to estimate α_p and β_p for the BNCT experiment are $\bar{z}_F$ and RBE_{DSB}, which are calculated with the MCDS and integrated into MCNP to produce dose-averaged values. The ^{10}B concentrations of 40 μg/g and 27 μg/g for *in vivo/in vitro* and *in vitro* experiments, respectively, were modeled according to the Coderre *et al.* data (1993). For the *in vivo/in vitro* experiments, ^{10}B was distributed outside the nucleus and for the *in vitro* experiment, it was homogenously distributed, according to the findings of Nguyen *et al.* (1993) and Bennett *et al.* (1994). As illustrated in Figure 2.7, estimates of the surviving fraction for the BNCT experiments of Coderre (1993) with BPA *in vivo/in vitro* agree within 5% (solid red line) and neutron-only cell survival estimates for both the *in vivo/in vitro,* as well as *in vitro* experiments (solid blue lines) are also in good agreement. This provides some measure of confidence that the model may also be useful for predicting the photon isoeffective doses for other neutron sources and known boron distrubutions. For comparison to the neutron source used by Coderre, estimates of cell survival for the CN, NM and CNTS sources with the same concentration of ^{10}B are also shown in Figure 2.7. Estimates of cell survival are slightly higher for the CN, NM, and CNTS sources than for the source used by Coderre *et al* (1993).

For simplicity and uniformity, the dose-weighted RBE values in Table 2.5 use the RBE_{LD} formulation (Eq. 2.4) with ^{60}Co as the reference radiation. However, if a different low-LET reference radiation is desired, a correction factor can be applied (e.g., 1.1 for 250 kVp X-rays, 1.3 mm Cu filtration) (Stewart *et al.* 2015). For fraction sizes that are small compared to α/β, which encompasses the most clinically relevant range of doses used in fast neutron therapy (~ 1 Gy per day to a total as high as 16 or 18 Gy), RBE_{LD} is the relevant metric and is always ≥ RBE_{HD} (RBE_{DSB}). In past clinical trials of BNCT

treatment, a photon-equivalent dose of about 50 Gy is typically delivered in a single fraction (Coderre *et al.*1997). Estimates of the photon-isoeffective dose based on the RBE_{LD} are a more relevant metric of the potential effectiveness of a fractionated BNCT treatment with fast neutrons. For a single acute dose or hypofractionated BNCT, estimates of the photon isoeffective dose based on $RBE_{HD} \cong RBE_{DSB}$ is the more relevant metric of potential treatment effectiveness.

The cumulative RBE estimates are based on a cytoplasmic ^{10}B concentration of 40 μg/g for BPA and 100 μg/g for mAb. The $(\alpha/\beta)_\gamma$ values of 87 Gy, 3 Gy, and 10 Gy are for the 9L rat gliosarcoma cell line (*in vivo/in vitro*), mammary carcinoma and a typical early responding tissue or tumor, respectively. The high-dose RBE (RBE_{DSB}) is effectively the same for the NM, CN, and UW CNTS neutrons and slightly larger for the MIT-FCB neutrons, which supports the idea that the MIT-FCB source produces a secondary charged particle energy distribution with a closer to optimal LET distribution. The same general trends hold for the reproductive cell death in the limit when the dose per fraction is small compared to β/α (RBE_{LD}). However, the models predict that the low-dose RBE will always be greater than or equal to the high-dose RBE. Also, the RBE_{LD} is predicted to increase with decreasing β/α. For the lower energy, MIT-FCB, NM, and CN neutron sources, RBE_{LD} is predicted to be the same as RBE_{HD} (~ 3) for all tumor or tissue types with β/α above 10 Gy; RBE_{LD} is also approximately equal to 3 for the UW CNTS with β/α = 87 Gy. For tumors or tissue with β/α = 3 Gy, RBE_{LD} may be as large as 4.3 for the NM beam or 7.4 for the UW CNTS beam. These observations suggest that BNCT may be most effective for the treatment of tumors with a low β/α ratio, such as tumors of the breast and prostate. However, with the UW CNTS beam,

RBE_{LD} is ~ 4 even when α/β = 10 Gy. Fractionated BNCT treatments using the UW CNTS may be a very effective treatment even for tumors with larger α/β, especially since beams can be directed towards the patient and tumor targets from any direction (i.e., any couch position and gantry angles) and shaped to the beams eye view of the tumor using 40 individually movable leaves. The CNTS offers a degree of dose conformity not possible with thermal and epithermal neutron sources traditionally used for BNCT and the combination of dose escalation and conformity should prove advantageous. Figures 2.8 – 2.11 illustrate the potential advantage the CNTS has for deep seated tumors, using fractionation (RBE_{LD}) over epithermal beams. The use of a mAb as the boron carrier instead of BPA could also offer some modest increases in the potential effectiveness of BNCT (Mundy *et al.* 2006, Sztejnberg Goncalves-Carralves and Jevremovic 2007) and better quantification of uptake, and hence, tumor to healthy tissue ratios using immuno-PET (van Dongen *et al.* 2007). However, additional experimental work is still needed to confirm that mAbs can be an effective and targeted boron carrier.

Currently, RBE and CBE weighting factors and isoeffective dose calculations derived from cell survival experiments have been universally applied to calculate biologically equivalent dose for BNCT clinical trials and treatment on human subjects. This involves many assumptions that have mainly been derived from nonhuman experiments (Jung *et al. 2*009 and references therein). Although we assume boron concentration and biodistribution based on experimental data, the method put forth here offers a mechanistic prediction of biological weighting factors, LQ parameters and hence, isoeffective doses, based on the specific tissue and endpoint of interest.

2.4 Discussion and Conclusions

A system of dosimetry and radiobiological models is presented to predict RBE, CBE, and other important biological metrics for selected neutron sources, tissue types, and boron distributions. With only the $(\alpha/\beta)_\gamma$ from the reference radiation, RBE_{DSB} and $\bar{z}_F$ (which are estimation from first principles), as *ad hoc* biological (input) parameters, the presented BNCT model accurately predicts the cell survival for *in vitro* and *in vivo/in vitro* experiments with the neutron beam alone and with BPA to within a few percent (Figure 2.7). Applying the model to a hypothetical mAb boron carrier that targets HER2+ cells, even conservatively assuming no localization in the cell nucleus, shows a significant increase in CBE. Compounded with the macroscopic advantage of having a higher tumor to healthy tissue ratio of ^{10}B, this methodology shows promising applications for other, theoretical, or in development, boron carrier pharmaceuticals. However, the strength of the estimates from the system of models is ultimately limited by the accuracy of the experimental determination of the ^{10}B subcellular distribution and α_γ and β_γ. Although the predicted cumulative RBE values for the compact, D-T produced neutron sources and the fast neutron source are less than that for the MIT-FCB neutron source, evidence shows the high tumor uptake and high tumor to healthy tissue ratios achievable with the proposed pharmaceutical (Dijkers *et al.* 2010), which has the potential to overcome the fluence and CBE restraints seen with compact neutron sources. The results suggest that BNCT with fast, conformal neutron therapy beams should provide superior local tumor control compared to 3D conformal neutron therapy alone or BNCT with nonconformal neutron sources. In addition to the increased dose conformity and uniformity the CNTS can achieve, the differences in RBE_{LD} and RBE_{HD} can be

exploited to increase the therapeutic ratio of BNCT treatments. The primary limitation is patient tolerance to repeated administration of BPA or another pharmaceutical.

The most compelling argument for applying our system of models to BNCT is the ease of implementation and the minimal number of adjustable parameters. In the RMF model, the cell, tumor and tissue-specific kinetics and fidelity of DSB repair are contained solely in α_γ and β_γ, the low-LET experimentally-derived LQ parameters, and dose-weighted values of RBE_{DSB} and $\bar{z}_F$, which are obtained from the MCDS+MCNP simulations, are needed to estimate the α_p and β_p of all the ion components in the mixed field and the subsequent values of RBE_{LD} and RBE_{HD}. As described above, this approach has been successfully applied for other mixed fields of light and heavy ions. Mairina *et al.* (2016) concluded that the RMF framework was a good candidate for predicting cell survival with He ion beams, especially considering that its implementation only required $\alpha_\gamma/\beta_\gamma$ as input, without requiring tuning and adjustment with other light ion cell survival data (Mairina *et al.* 2013, 2016). However, from our investigation of the low-energy, high-LET alpha particles and previous work (Carlson *et al.* 2008, Frese *et al.* 2012), there is evidence that refinements are needed for this subset of particles. Proximity effects, discussed earlier, which aren't explicitly considered in the RMF, likely have an increasing importance as charged particles reach very high-LET. In the case of fast neutron therapy or boron neutron capture enhanced fast neutron therapy, this overestimation will likely not have a significant impact on RBE estimates, considering the other uncertainties in biological parameters.

Horiguchi *et al.* (2014) used the particle transport simulation code (PHITS) coupled with the microdosimetric kinetic model (MKM) to estimate the relative

biological effectiveness factors for BNCT. Within the MKM, cell survival is estimated from the probability densities of specific energies in a subcellular structure contained in the cell nucleus (domain). This adds at least one additional adjustable parameter as compared to the RMF, where the entire nucleus is considered. Additionally, as compared to our method, the PHITS+MKM model simulated the four BNCT dose components separately, where we obtained the biophysical variables for all components in one simulation. Subsequent fitting and optimization was also needed to update the domain radius. This framework has also been used to estimate biological dose and cell survival fraction in charged particle therapy (Sato *et al.* 2009, 2012).

Gonzalez and Santa Cruz (2012) proposed a method to calculate the photon-isoeffective dose in BNCT to replace the old paradigm of using "RBE-weighted" doses for calculating the photon-equivalent dose. They show that using the fixed-RBE approach is not suitable to understand the observed clinical results in terms of the photon radiotherapy data and always predicted much higher equivalent doses that the isoeffective approach. They use a modified linear quadratic (MLQ) model to account for synergistic effects between low and high-LET components (i.e. – sublesions produced by one radiation can combine with the sublesions produced by any other radiation to form lethal lesions). While not explicitly shown in the RMF equations, synergistic (inter-track and intra-track) DSB interactions are embedded in the RBE_{DSB} and $RBE_{DSB} \times \bar{z}_F$ terms, with the RBE_{DSB} (relative DSB Gy^{-1} Gbp^{-1}) and $RBE_{DSB} \times \bar{z}_F$ (relative DSB $track^{-1}$ Gbp^{-1}) representing the intra-track and inter-track (proximity) effects, respectively. Within the RMF, the RBE_{HD} is only dependent on the dose-averaged RBE_{DSB}, making it straightforward to implement as compared to Eq. (15) in Gonzalez and Santa Cruz (2012).

Also note that the LQ parameters in MLQ were obtained from fitting of experimental data, requiring at least four variables. The range of survival fractions, S(D), and isoeffective doses, DR(D), can be obtained with some simple rearrangement of the RMF formulas.

Additionally, optimized target (Nigg *et al. 2*000) and filtration of the UW CNTS and the advantage of the more conformal neutron beam have not been taken into consideration here, but may very well show promise for BNCT applications. Current applications using BPA for tumor treatments other than GBM (e.g., melanoma) may also benefit from more accurate RBE models.

2.5 References

Alloni D, Campa A, Belli M, Esposito G, Facoetti A, Friedland W, Liotta M, Mariotti L, Paretzke H G and Ottolenghi A 2010 A Monte Carlo study of the radiation quality dependence of DNA fragmentation spectra *Radiat. Res.* **173** 263–71

Auterinen I, Serén T, Anttila K, Kosunen A and Savolainen S 2004 Measurement of free beam neutron spectra at eight BNCT facilities worldwide *Appl. Radiat. Isot.* **61** 1021–6

Ballarini F, Bakeine J, Bortolussi S, Bruschi P, Cansolino L, Clerici A M, Ferrari C, Protti N, Stella S, Zonta A, Zonta C and Altieri S 2011 Cell death following BNCT: A theoretical approach based on Monte Carlo simulations *Appl. Radiat. Isot.* **69** 1745–7

Barth R F 2009 Boron neutron capture therapy at the crossroads: Challenges and opportunities *Appl. Radiat. Isot.* **67** S3–S6

Bennett B D, Mumford-Zisk J, Coderre J A and Morrison G H 1994 Subcellular localization of p-boronophenylalanine-delivered boron-10 in the rat 9L gliosarcoma: cryogenic preparation *in vitro* and *in vivo*. *Radiat. Res.* **140** 72–8

Burmeister J, Riley K, Coderre J A, Harling O K, Ma R, Wielopolski L, Kota C and Maughan R L 2003 Microdosimetric intercomparison of BNCT beams at BNL and MIT. *Med. Phys.* **30(8)** 2131-39

Bichsel H, Eenmaa J, Weaver K, Williams D L, Wootton P and Wyckoff W G 1974 A physics cyclotron adapted for fast neutron beam therapy *Phys. Med. Biol.* **19** 236

Binns P J, Riley K J and Harling O K 2005 Epithermal neutron beams for clinical studies of boron neutron capture therapy: a dosimetric comparison of seven beams. *Radiat. Res.* **164** 212–20

Blaumann H R, González S J, Longhino J, Santa Cruz G A, Calzetta Larrieu O A, Bonomi M R and Roth B M C 2004 Boron neutron capture therapy of skin melanomas at the RA-6 reactor: a procedural approach to beam set up and performance evaluation for upcoming clinical trials. *Med. Phys.* **31** 70–80

Buchholz T A, Laramore G E, Stelzer K J, Risler R, Wootton P and Griffin T W 1997 Boron neutron capture enhanced fast neutron radiotherapy for malignant gliomas and other tumors. *J. Neurooncol.* **33** 171–8

Carabe-Fernandez A, Dale R G, Hopewell J W, Jones B and Paganetti H 2010 Fractionation effects in particle radiotherapy: implications for hypo-fractionation regimes *Phys. Med. Biol.* **55** 5685–700

Campa A *et al* 2009 DNA fragmentation induced in human broblasts by ^{56}Fe ions: experimental data and Monte Carlo simulations *Radiat. Res.* **171** 438–45

Carlson D, Stewart R, Semenenko V and Sandison G 2008 Combined use of Monte Carlo DNA damage Simulations and deterministic repair models to examine putative mechanisms of cell killing *Radiat. Res.* **169** 447–59

Coderre J A and Morris G M 1999 The radiation biology of boron neutron capture therapy. *Radiat. Res.* **151** 1–18

Coderre J A, Elowitz E H, Chadha M, Bergland R, Capala J, Joel D D, Liu H B, Slatkin D N and Chanana A D 1997 Boron neutron capture therapy for glioblastoma multiforme using p-boronophenylalanine and epithermal neutrons: trial design and early clinical results. *J. Neurooncol.* **33** 141–52

Coderre J A, Makar M S, Micca P L and Nawrocky M M 1994 Major compound-dependent variations of ^{10}B(n, α)^{7}Li RBE for the 9L rat gliosarcoma *in vitro* and *in vivo* In Topics in Dosimetry and Treatment Planning for Boron Neutron Capture Therapy (R. G. Zamenhof, G. Solares and O. Harling, Eds.), pp. 37-47. Advanced Medical Publishing, Madison, WI

Coderre JA, Makar MS, Micca PL, Nawrocky MM, Liu HB, Joel DD, *et al.*1993 Derivations of relative biological effectiveness for the high-let radiations produced during boron neutron capture irradiations of the 9L rat gliosarcoma *in vitro* and *in vivo Int. J. Radiat. Oncol. Biol. Phys.* **127(5)** 1121–9

Costantini D L, Chan C, Cai Z, Vallis K A and Reilly R M 2007 ^{111}In-labeled trastuzumab (Herceptin) modified with nuclear localization sequences (NLS): an Auger electron-emitting radiotherapeutic agent for HER2/neu-amplified breast cancer. *J. Nucl. Med.* **48** 1357–68

Dijkers E C, Oude Munnink T H, Kosterink J G, Brouwers A H, Jager P L, de Jong J R, van Dongen G A, Schröder C P, Lub-de Hooge M N and de Vries E G 2010 Biodistribution of ^{89}Zr-trastuzumab and PET imaging of HER2-positive lesions in patients with metastatic breast cancer. *Clin. Pharmacol. Ther.* **87** 586–92

Douglas J G, Koh W-J, Austin-Seymour M and Laramore G E 2003 Treatment of salivary gland neoplasms with fast neutron radiotherapy. *Arch. Otolaryngol. Head Neck Surg.* **129** 944–8

Elbast M, Saudo A, Franck D, Petitot F and Desbree A 2012 Microdosimetry of alpha particles for simple and 3D voxelised geometries using MCNPX and Geant4 Monte Carlo codes *Rad. Prot. Dosim.***150** 342–9

Frese M, Yu V, Stewart R, and Carlson D 2012 A Mechanism-Based Approach to Predict the Relative Biological Effectiveness of Protons and Carbon Ions in Radiation Therapy *Radiat. Oncol. Biol.* **83** 442–50

Friedland W, Jacob P, Bernhardt P, Paretzke H G and Dingfelder M 2003 Simulation of DNA damage after proton irradiation *Radiat. Res.* **159** 401–10

Fukuda H, Hiratsuka J, Honda C, Kobayashi T, Yoshino K, Karashima H, Takahashi J, Abe Y, Kanda K and Ichihashi M 1994 Boron neutron capture therapy of malignant melanoma using 10B-paraboronophenylalanine with special reference to evaluation of radiation dose and damage to the normal skin. *Radiat. Res.* **138** 435–42

Furusawa Y, Fukutsu K, Aoki M, Itsukaichi H, Eguchi-Kasai K, Ohara H, Yatagai F, Kanai T and Ando K 2000 Inactivation of aerobic and hypoxic cells from three different cell lines by accelerated 3He-, 12C- and 20Ne-ion beams. *Radiat. Res.* **154** 485–96

Georgakilas A G 2015 Role of the immune system and inflammation in ionizing radiation effects. Cancer Lett. **368** 154–5

González S J and Cruz G A S 2012 The Photon-Isoeffective Dose in Boron Neutron Capture Therapy *Radiat. Res.* **178** 609–21

Goorley J T *et al. 2*013 Initial MCNP6 Release Overview *Nucl. Technol.* **180** 298-315

Hall E J and Giaccia A J 2006 *Radiobiology for the Radiologist 6th ed* (Philadelphia,

PA: Lippincott Williams & Wilkins)

Hawthorne M F and Lee M W 2003 A critical assessment of boron target compounds for boron neutron capture therapy. *J. of Neuro Oncology.* **62** 33–45

Hirayama R, Uzawa A, Obara M, Takase N, Koda K, Ozaki M, Noguchi M, Matsumoto Y, Li H, Yamashita K, Koike S, Ando K, Shirai T, Matsufuji N and Furusawa Y 2015 Determination of the relative biological effectiveness and oxygen enhancement ratio for micronuclei formation using high-LET radiation in solid tumor cells: An *in vitro* and *in vivo* study. *Mutat. Res. Genet. Toxicol. Environ. Mutagen* **793** 41–7

Hopewell J W, Morris G M, Schwint A, Coderre J A, Sauerwein W, Wittig A, Moss R L and Nakagawa Y 2012 Boron neutron capture therapy: Application of radiobiological principles *Textbook of neutron capture therapy*

Hopewell J.W. *et al.*, 2010. Boron neutron capture therapy: application of radiobiological principles. In: Texbook of Neutron Capture Therapy, eds Sauerwein, W *et al.*, Springer.

Horiguchi H, Sato T, Kumada H, Yamamoto T and Sakae T 2014 Estimation of relative biological effectiveness for boron neutron capture therapy using the PHITS code coupled with a microdosimetric kinetic model. *J. Radiat. Res.* **56** 382–90

ICRU 1992 *Photon, Electron, Proton and Neutron Interaction Data for Body Tissues* (*ICRU Report No. 46)* (Bethesda, MD: International Commission on Radiation Units and Measurements)

ICRU 1983 *Microdosimetry* (*ICRU Report No. 35)* (Bethesda, MD: International Commission on Radiation Units and Measurements)

ICRU 1970 *Linear Energy Transfer* (*ICRU Report No. 16)* (Bethesda, MD: International Commission on Radiation Units and Measurements)

Jung S H, Yoon S M, Park S H, Choi I S, Kim J K, Choi E K, Ahn S D, Lee S-W, Song S Y and Kim J H 2009 A treatment planning study on glioblastoma with different techniques using boron neutron capture therapy, 3-dimensional conformal radiotherapy, and intensity modulated radiotherapy. *Appl. Radiat. Isot.* **67** 1180–4

Kalet I J, Jacky J P, Risler R, Rohlin S, Wootton P. Integration of radiotherapy planning systems and radiotherapy treatment equipment: 11 years experience 1997 *Int. J. Radiat. Oncol. Biol. Phys.* **38(1)** 213-21

Kalet A M, Sandison G A, Phillips M H, Parvathaneni U 2013 Validation of the Pinnacle™ photon convolution-superposition algorithm applied to fast neutron

beams. *J. Appl. Clin. Med. Phys.* **14(6)** 133-54

Kamp F, Cabal G, Mairani A, Parodi K, Wilkens J J and Carlson D J 2015 Fast biological modeling for voxel-based heavy ion treatment planning using the mechanistic repair-misrepair-fixation model and nuclear fragment spectra *Int. J. Radiat. Oncol. Biol. Phys.* **93** 557–68

Kirkby C, Ghasroddashti E, Poirier Y, Tambasco M and Stewart R D 2013 RBE of kV CBCT radiation determined by Monte Carlo DNA damage simulations *Phys. Med. Biol.* **58** 5693–704

Laramore G E, Risler R, Griffin T W, Wootton P, Wilbur D S 1996 Fast neutron radiotherapy and boron neutron capture therapy: application to a human melanoma test system *Bull. Cancer Radiother.* **83** 191s-7s

Laramore G E and Spence A M 1996 Boron neutron capture therapy (BNCT) for high-grade gliomas of the brain: a cautionary note *Radiat. Oncol. Biol.* **36** 241–6

Laramore G E, Wootton P, Livesey J C, Wilbur D S, Risler R, Phillips M, Jacky J, Buchholz T A, Griffin T W and Brossard S 1994 Boron neutron capture therapy: a mechanism for achieving a concomitant tumor boost in fast neutron radiotherapy *Radiat. Oncol. Biol.* **28** 1135–42

Mairani A, Dokic I, Magro G, Tessonnier T, Kamp F, Carlson D J, Ciocca M, Cerutti F, Sala P R, Ferrari A, Böhlen T T, Jäkel O, Parodi K, Debus J, Abdollahi A and Haberer T 2016 Biologically optimized helium ion plans: calculation approach and its *in vitro* validation *Phys. Med. Biol.* **61** 4283–99

Maughan R L, Chuba P J, Porter A T, Ben-Josef E and Lucas D R 1997 The elemental composition of tumors: kerma data for neutrons. *Med. Phys.* **24** 1241–4

Maughan R L, Kota C and Yudelev M 1993 A microdosimetric study of the dose enhancement in a fast neutron beam due to boron neutron capture *Phys. Med. Biol.* **38** 1957–61

Menéndez P R, Roth B M C, Pereira M D, Casal M R, González S J, Feld D B, Santa Cruz G A, Kessler J, Longhino J, Blaumann H, Jiménez Rebagliati R, Calzetta Larrieu O A, Fernández C, Nievas S I and Liberman S J 2009 BNCT for skin melanoma in extremities: updated Argentine clinical results *Appl. Radiat. Isot.* **67** S50–3

Mitri Z, Constantine T and O' Regan R 2012 The HER2 receptor in breast cancer: pathophysiology, clinical use, and new advances in therapy *Chemother. Res. Pract.* **2012** 743193

Moffitt G B, Stewart R D, Sandison G A, Goorley J T, Argento D C and Jevremovic T 2016 MCNP6 model of the University of Washington clinical neutron therapy system (CNTS). *Phys. Med. Biol.* **61** 937–57

Mundy D W, Harb W and Jevremovic T 2006 Radiation binary targeted therapy for HER-2 positive breast cancers: assumptions, theoretical assessment and future directions *Phys. Med. Biol.* **51** 1377–91

Nguyen T, Brownell G L, Holden S A, Kahl S, Miura M and Teicher B A 1993 Subcellular distribution of various boron compounds and implications for their efficacy in boron neutron capture therapy by Monte Carlo simulations *Radiat. Res.* **133** 33–40

Nigg D W, Wemple C A, Risler R, Hartwell J K, Harker Y D and Laramore G E 2000 Modification of the University of Washington Neutron Radiotherapy Facility for optimization of neutron capture enhanced fast-neutron therapy. *Med. Phys.* **27** 359–67

Nikjoo H, Bolton C E, Watanabe R, Terrissol M, O'Neill P and Goodhead D T 2002 Modelling of DNA damage induced by energetic electrons (100 eV to 100 keV) *Radiat. Prot. Dosim.* **99** 77–80

Nikjoo H, O'Neill P, Terrissol M and Goodhead D T 1999 Quantitative modelling of DNA damage using Monte Carlo track structure method *Radiat. Environ. Biophys.* **38** 31–8

Nikjoo H, O'Neill P, Goodhead D T and Terrissol M 1997 Computational modelling of low-energy electron-induced DNA damage by early physical and chemical events *Int. J. Radiat. Biol.* **71** 467–83

Pelowitz B D (ed) 2011 *MCNPX User's Manual, v2.7.0 LA-CP-11-00438* (Los Alamos, NM: Los Alamos National Laboratory)

Polster L, Schuemann J, Rinaldi I, Burigo L, McNamara A L, Stewart R D, Attili A, Carlson D J, Sato T, Faddegon B, Perl J, and Paganetti H 2014 Extension of TOPAS for the simulation of proton radiation effects considering molecular and cellular endpoints. *Phys. Med. Biol.*

Qi X S, White J and Li X A 2011 Is α/β for breast cancer really low? *Radiother. Oncol.* **100** 282–8

Rasouli F S and Masoudi S F 2012 Design and optimization of a beam shaping assembly for BNCT based on D–T neutron generator and dose evaluation using a simulated head phantom *Appl. Radiat. Isot.* **70** 2755–62

Rassow J, Sauerwein W, Wittig A, Bourhis-Martin E, Hideghéty K and Moss R 2004

Advantage and limitations of weighting factors and weighted dose quantities and their units in boron neutron capture therapy *Med. Phys.* **31** 1128–34

Riley K J, Binns P J and Harling O K 2004 A state-of-the-art epithermal neutron irradiation facility for neutron capture therapy *Phys. Med. Biol.* **49** 3725–35

Riley K J, Binns P J and Harling O K 2003 Performance characteristics of the MIT fission converter based epithermal neutron beam *Phys. Med. Biol.* **48** 943–58

Rossi H H and Zaider M 1992 Compound dual radiation action. I. General aspects *Radiat. Res.* **132** 178–83

Santa Cruz G A S 2016 Microdosimetry: principles and applications *Rep. Pract. Oncol. Radiother.* **21** 135–9

Sato T and Furusawa Y 2012 Cell survival fraction estimation based on the probability densities of domain and cell nucleus specific energies using improved microdosimetric kinetic models *Radiat. Res.* **178** 341–56

Sato T, Kase Y, Watanabe R, Niita K and Sihver L 2009 Biological dose estimation for charged-particle therapy using an improved PHITS code coupled with a microdosimetric kinetic model *Radiat. Res.* **171** 107–17

Semenenko V A and Stewart R D 2004 A fast Monte Carlo algorithm to simulate the spectrum of DNA damages formed by ionizing radiation *Radiat. Res.* **161(4)**, 451-457

Semenenko V A and Stewart R D 2006 Fast Monte Carlo simulation of DNA damage formed by electrons and light ions *Phys. Med. Biol.* **51(7)** 1693-1706

Smith D R, Chandra S, Barth R F, Yang W, Joel D D and Coderre J A 2001 Quantitative imaging and microlocalization of boron-10 in brain tumors and infiltrating tumor cells by sims ion microscopy relevance to neutron capture therapy *Cancer Res.* **61** 8179–87

Solares G R and Zamenhof R G 1995 A novel approach to the microdosimetry of neutron capture therapy. Part I. High-resolution quantitative autoradiography applied to microdosimetry in neutron capture therapy *Radiat. Res.* **144** 50–8

Specht H M, Neff T, Reuschel W, Wagner F M, Kampfer S, Wilkens J J, Petry W and Combs S E 2015 Paving the road for modern particle therapy - what can we learn from the experience gained with fast neutron therapy in Munich? *Front. Oncol.* **5** 262

Stelzer K J, Laramore G E, Griffin T W, Koh W J, Austin-Seymour M, Russell K J and Buchholz T A 1994 Fast neutron radiotherapy. The University of Washington

experience. *Acta. Oncol.* **33** 275–80

Stewart R D, Streitmatter S W, Argento D C, Kirkby C, Goorley J T, and Moffitt G 2015 Rapid MCNP simulation of the dna double strand break (dsb) relative biological effectiveness (RBE) of photons, neutrons, electrons, and light ions *Phys. Med. Biol.* **60** 8249-74

Stewart R D, Yu V K, Georgakilas A G, Koumenis C, Park J H and Carlson D J 2011 Effects of radiation quality and oxygen on clustered DNA lesions and cell death *Radiat. Res.* **176** 587–60

Stewart R D and Li X A 2007 BGRT: Biologically Guided Radiation Therapy – the future is fast approaching! *Med. Phys.* **34** 3739-3751

Streitmatter S W, Stewart R D, Jenkins P A and Jevremovic T 2017 DNA double strand break (DSB) induction and cell survival in iodine-enhanced computed tomography (CT) *Phys. Med. Biol.* **62** 6164–84

Sztejnberg Gonçalves-Carralves M L and Jevremovic T 2007 Numerical assessment of radiation binary targeted therapy for HER-2 positive breast cancers: advanced calculations and radiation dosimetry *Phys. Med. Biol.* **52** 4245–64

van Dongen G A M S, Visser G W M, Lub-de Hooge M N, de Vries E G and Perk L R 2007 Immuno-PET: a navigator in monoclonal antibody development and applications *Oncologist* **12** 1379–89

Verbeke J M, Vujic J L and Leung K N 2000 Neutron beam optimization for boron neutron capture therapy using the DD and DT high-energy neutron sources *Nucl. Technol.* **129** 257–78

Whelan T J, Kim D-H and Sussman J 2008 Clinical experience using hypofractionated radiation schedules in breast cancer *Semin. Radiat. Oncol.* **18** 257–6

Zamenhof R G 1997 Microdosimetry for boron neutron capture therapy: a review *J. Neurooncol.* **33** 81–92

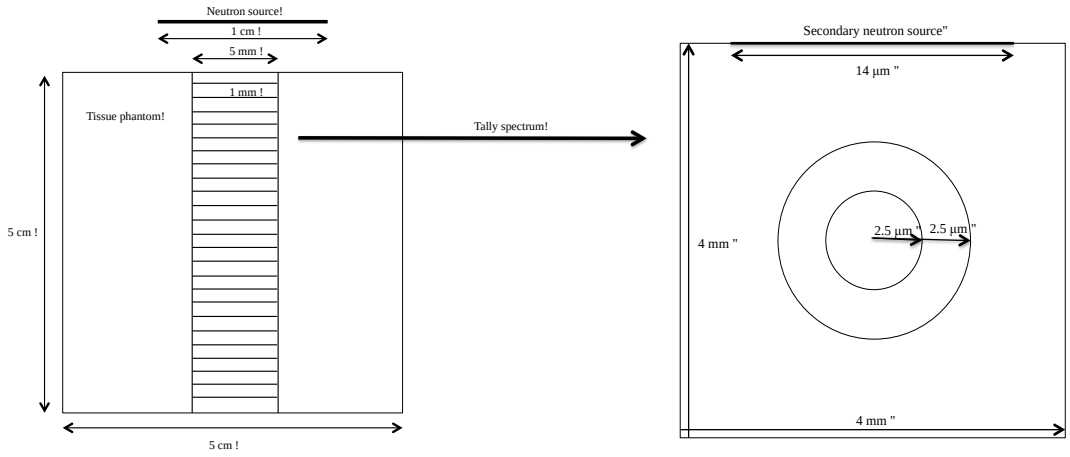

Figure 2.1. MCNPX models for: (left) water and tissue phantom, and (right) cellular microdosimetry.

Table 2.1. LET, CSDA ranges and $\bar{z}_F$ calculations for selected ions computed using Monte Carlo Damage Simulation (Stewart *et al.* 2011)

particle	E (MeV)	LET (keV/µm)	CSDA range (µm)	$\bar{z}_F$ (Gy)[a]	$\bar{z}_F$ (Gy)[a] (ICRU def.)[b]
$^{1}H^{1+}$	0.59	38.03	11.09	0.34	0.31
$^{4}He^{2+}$	1.47	186.5	8.28	1.69	1.52
$^{4}He^{2+}$	1.78	170.4	10.02	1.54	1.39
$^{7}Li^{3+}$	0.84	369.1	4.18	1.79	3.01
$^{7}Li^{3+}$	1.01	386.1	4.63	2.07	3.15

[a] d_{target} = 5 µm
[b] $\bar{z}_F = 0.204\text{LET}/\rho d^2$, ρ = 1 g/cc, $d = d_{nucleus}$

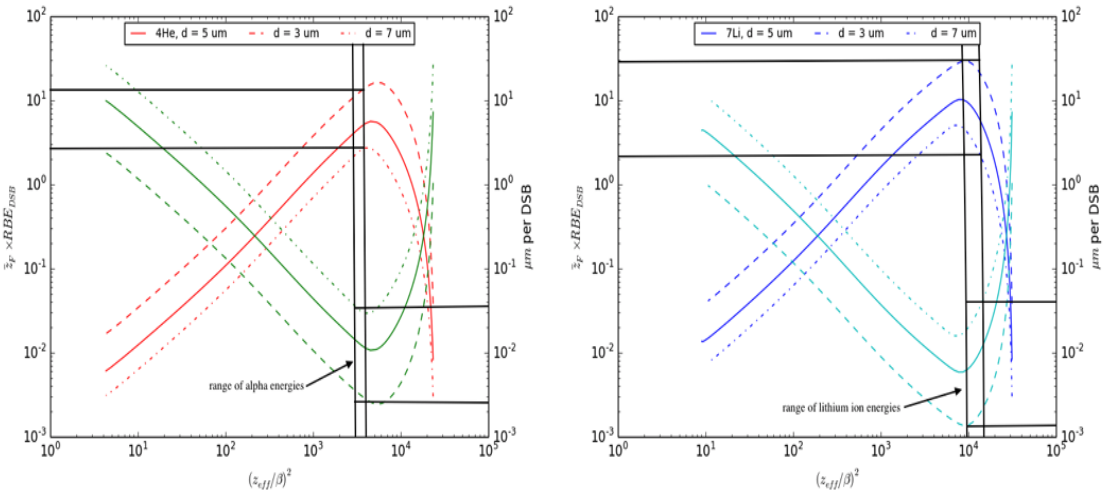

Figure 2.2. Plot of $\bar{z}_F\ RBE_{DSB}$ (relative DSBs per track), solid lines, and μm per DSB, dashed lines, vs. $(z_{eff}/\beta)^2$ for alpha particles and ^{7}Li ions, illustrating the particle-specific maximum DSB per track and minimum distance between DSBs, formulas used are described in Stewart *et al.* (2015).

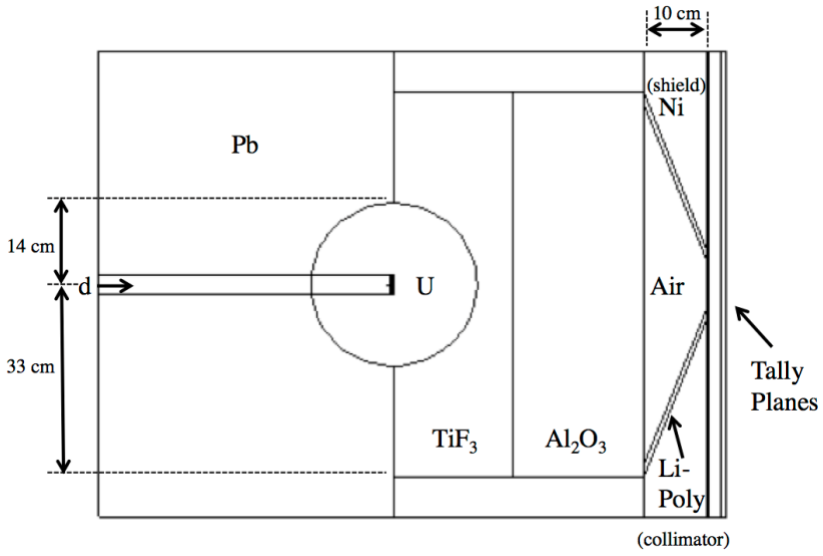

Figure 2.3. MCNPX model of the neutron multiplier and beam shaping assembly as proposed by Rasouli and Masoudi (2012).

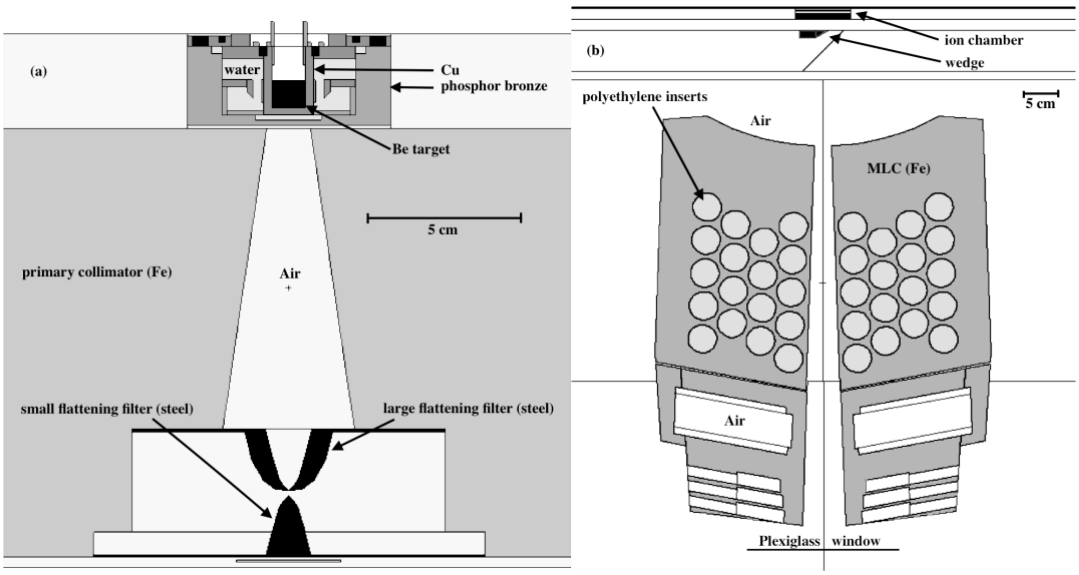

Figure 2.4. UW CNTS treatment head, (a) primary neutron production and collimation, and (b) the MLC downstream from (a). Additional details and benchmarks of the MCNP6 model of the CNTS are described in Moffitt *et al.* (2016) .

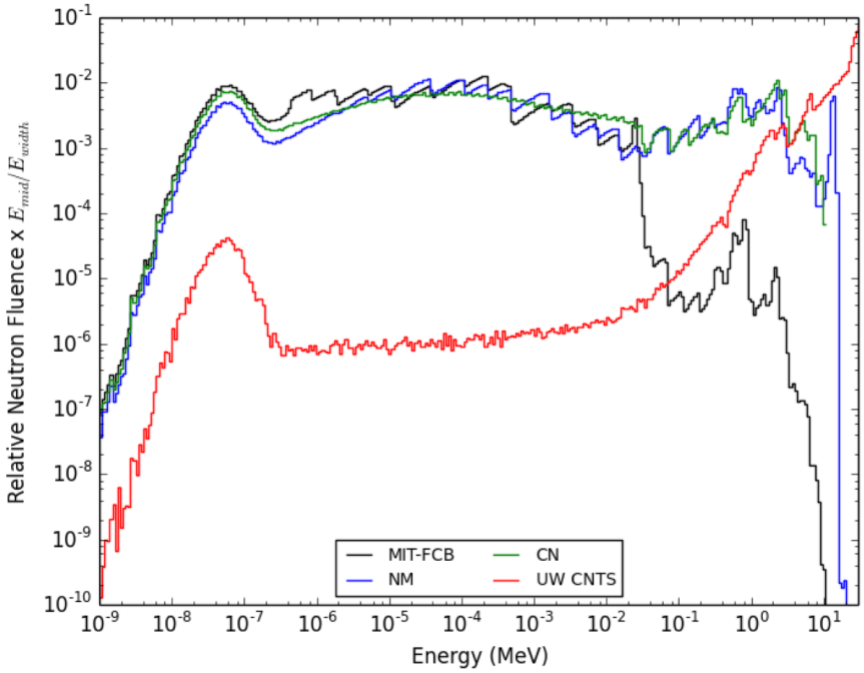

Figure 2.5. Comparison of the MIT-FCB, NM, CN and UW CNTS relative neutron fluence at a depth of 1.5 cm in a water phantom (geometry in Figure 2.1) obtained using MCNPX.

Table 2.2. Comparison of experimental results and model estimates for alpha particles and protons with approximately the same LET

particle	LET (keV/μm)		α (Gy^{-1})		RBE_{DSB}
	Goodhead *et al.*	MCDS	Goodhead *et al.*	MCDS+RMF	MCDS
1.2 MeV ^{+}H	22.02	23.65	0.30	0.29	1.80
1.4 MeV ^{+}H	19.67	21.13	0.42	0.27	1.71
30 MeV α	23.00	22.72	0.21	0.25	1.56
35 MeV α	20.45	20.07	0.25	0.23	1.50

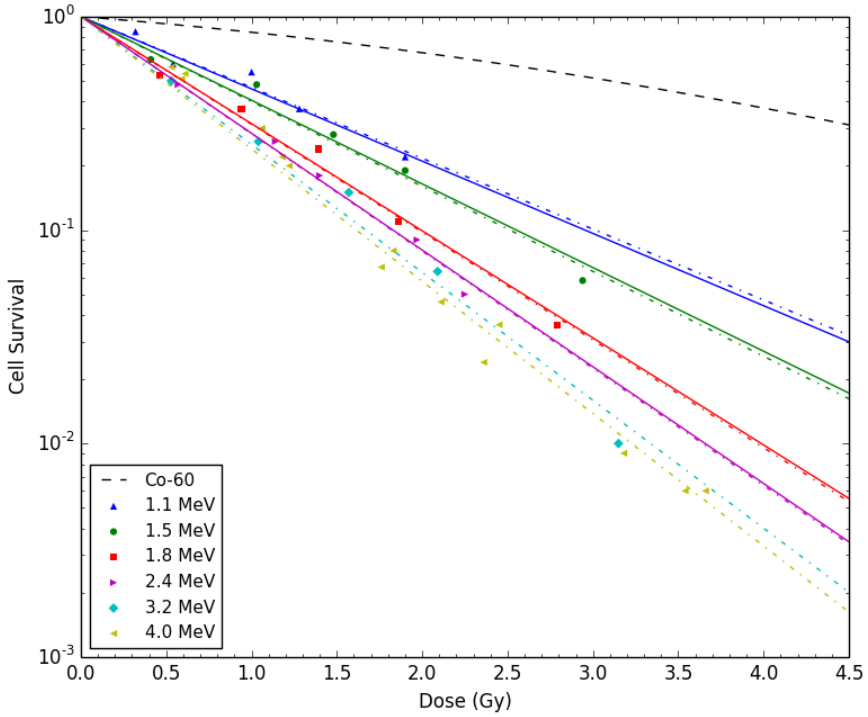

Figure 2.6. Comparison of cell survival in V79 cells irradiated by low-energy alpha particles (Tracy *et al.* 2015). Dashed lines are LQ fits to the experimental data and solid lines are RMF estimates. For 1.1 and 1.5 MeV (blue and red lines), $\bar{z}_F$ is obtained from MCDS+MCNP simulations, for 1.8 and 2.4 MeV (red and magenta lines), $\bar{z}_F$ is obtained from an RMF-fit.

Table 2.3. Comparison of experimentally-derived parameters, MCDS+MCNP estimates and RMF fits

α energy (MeV)	Dose-weighted LET (keV/μm)		$\bar{z}_F$ (Gy)			RBE_{DSB}
	Tracy *et al.*	MCDS+MCNP	MCDS+MCNP		RMF-fit	MCDS+ MCNP
			5 μm	3-6 μm		
1.1	181	203	1.09	3.76-0.67	1.03	3.30
1.5	201	213	1.60	5.33-1.16	1.66	3.24
1.8	190	195	1.69	4.67-1.16	2.68	3.19
2.4	161	161	1.44	3.84-1.02	3.32	3.09
3.2	131	130	1.13	3.06-0.79	4.21	2.96
4.0	112	110	0.94	2.56-0.66	4.90	2.84

Table 2.4. Predicted RBE values for BNCT secondary charged particles (using Eq. 2.4)

neutron source	protons		alphas		lithium		heavy ions	
	$RBE_{HD} = RBE_{DSB}$	RBE_{LD} (α/β = 3)	$RBE_{HD} = RBE_{DSB}$	RBE_{LD} (α/β = 3)	$RBE_{HD} = RBE_{DSB}$	RBE_{LD} (α/β = 3)	$RBE_{HD} = RBE_{DSB}$	RBE_{LD} = (α/β = 3)
MIT-FCB	2.85	3.42	3.06	8.79	3.39	7.05	3.15	6.39
NM	2.57	3.47	3.02	8.74	3.39	7.08	3.15	6.55
CN	2.54	3.38	3.04	9.06	3.39	6.82	3.15	5.59
UW CNTS	2.22	3.01	2.79	7.86	3.39	7.05	3.15	11.2

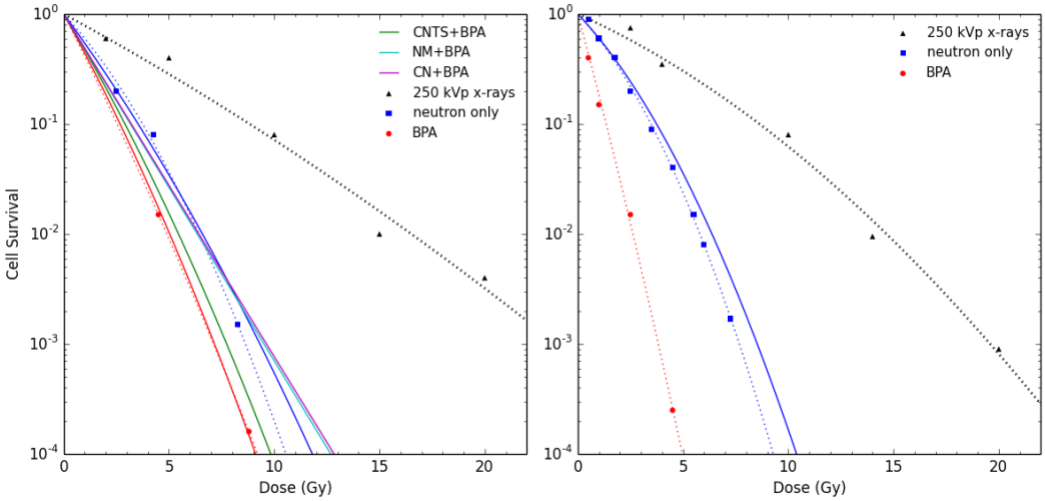

Figure 2.7. Cell survival predictions for the 9L rat gliosarcoma cell line with BPA and varying neutron source (parameter details in Section 2.3.2), *in vivo*/*in vitro* (left) and *in vitro* (right). Dotted lines are LQ-fits, solid lines are RMF predictions.

Table 2.5. Dose-weighted RBE estimates for selected neutron sources and ^{10}B carriers. Estimates are reported using asymptotic low and high-dose RBE models

	$RBE_{HD} = RBE_{DSB}$			RBE_{LD} (α/β = 87)			RBE_{LD} (α/β = 3)			RBE_{LD} (α/β = 10)
Neutron source	no ^{10}B	BPA	mAb	no ^{10}B[a]	BPA	mAb	no ^{10}B[a]	BPA	mAb	no ^{10}B
MIT-FCB	2.87	2.97	3.04	2.89	3.06	3.17	3.46	5.78	6.99	3.09
NM	2.63	2.66	2.69	2.68	2.71	2.75	3.99	4.08	4.34	3.02
CN	2.62	2.63	2.69	2.66	2.68	2.75	3.71	3.94	4.47	2.94
UW CNTS	2.66	2.66	2.72	2.80	2.81	2.88	6.86	6.88	7.40	4.03

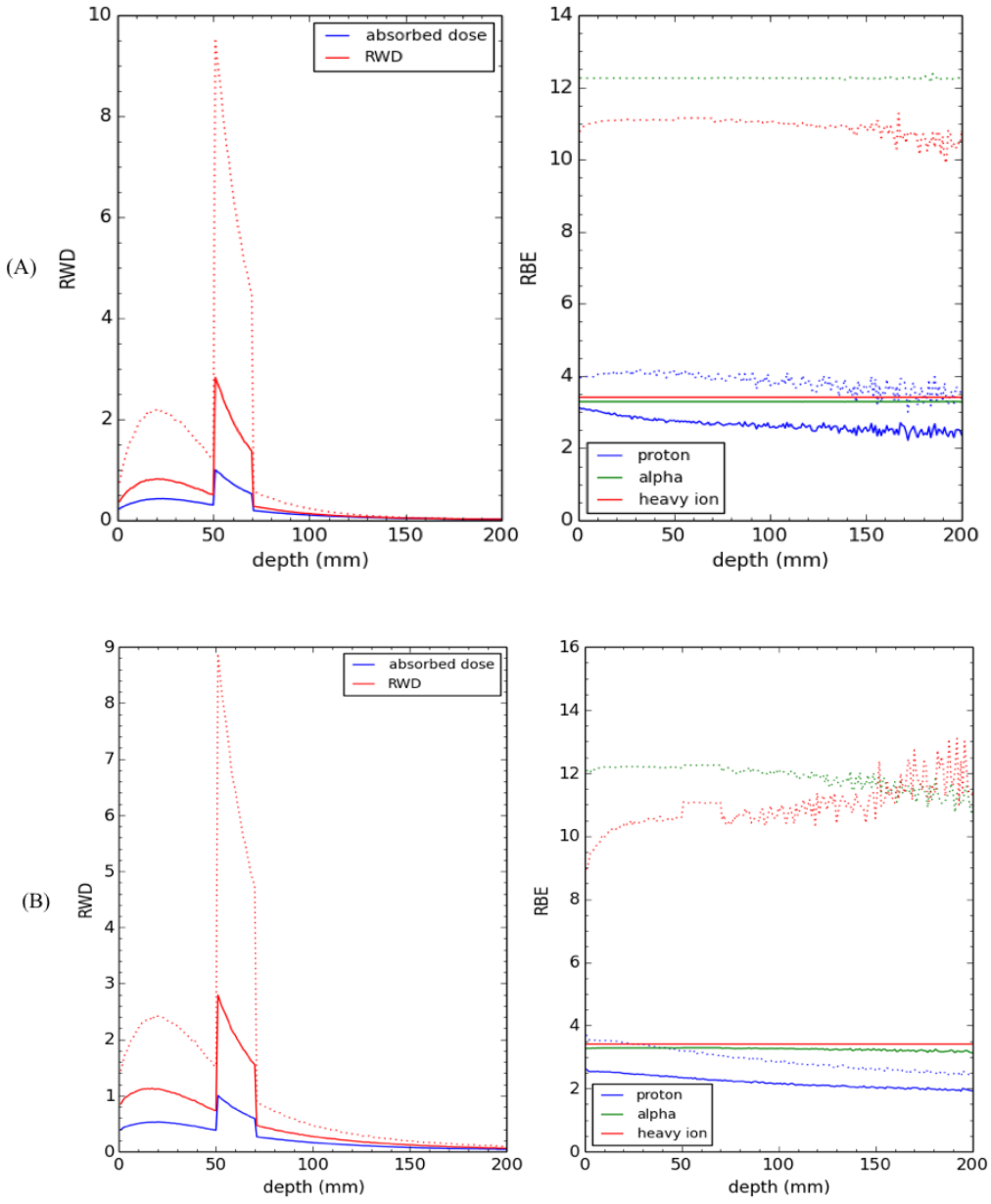

Figure 2.8. Soft tissue phantom, mass at 5 cm depth, 2 cm wide, 10:1 tumor to tissue ratio, 100 μg/g ^{10}B in tumor, solid lines RBE_{DSB}, dotted lines RBE_{LD} (β/α=3). PDD, RWD, and RBE for the MIT-FCB neutron source (A, left and right panel, respectively) NM neutron source (B, left and right panel, respectively).

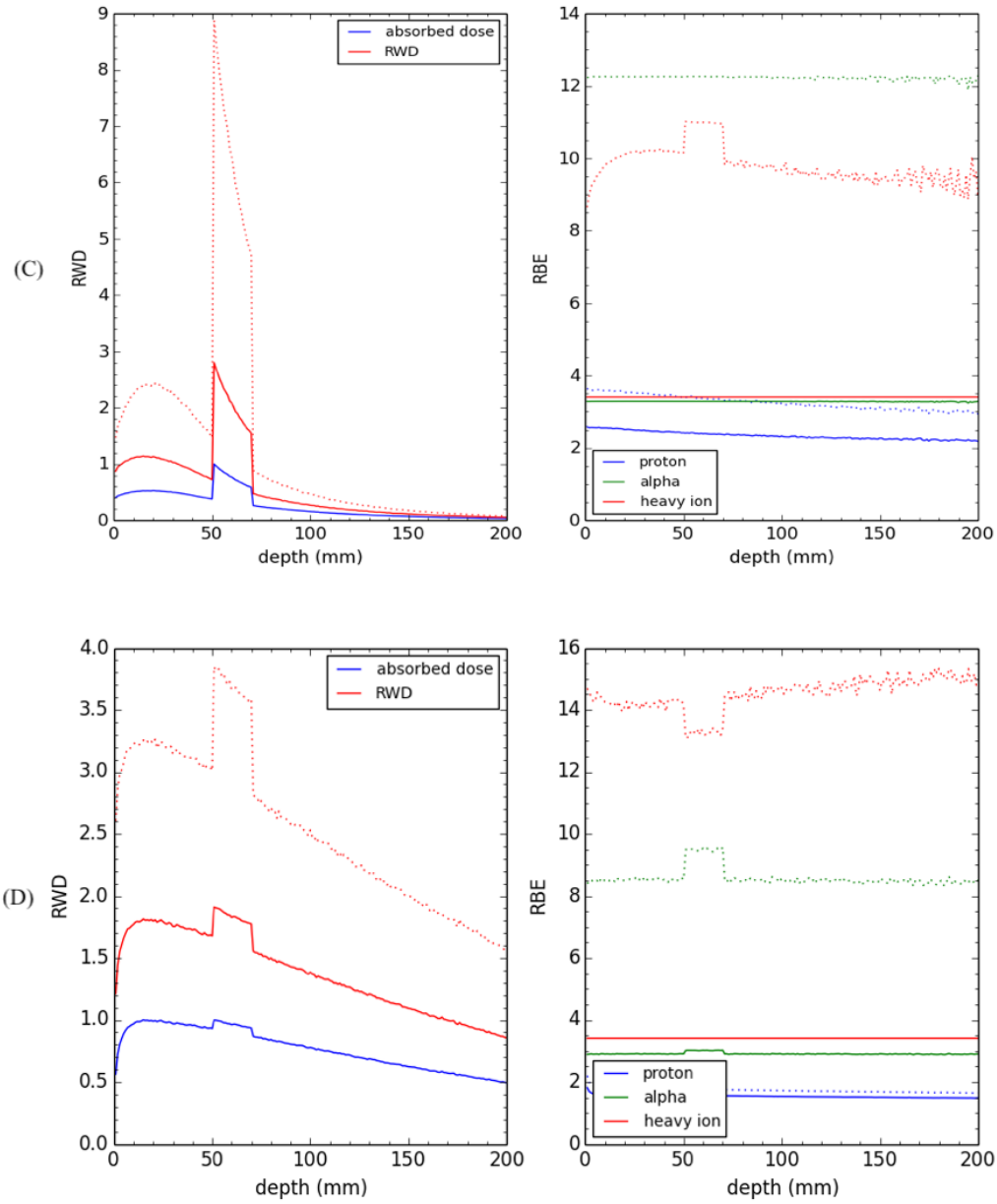

Figure 2.9. Soft tissue phantom, mass at 5 cm depth, 2 cm wide, 10:1 tumor to tissue ratio, 100 μg/g ^{10}B in tumor, solid lines RBE_{DSB} dotted lines RBE_{LD} (β/α=3). PDD, RWD, and RBE for the CN neutron source (C, left and right panel, respectively) and CNTS neutron source (D, left and right panel, respectively).

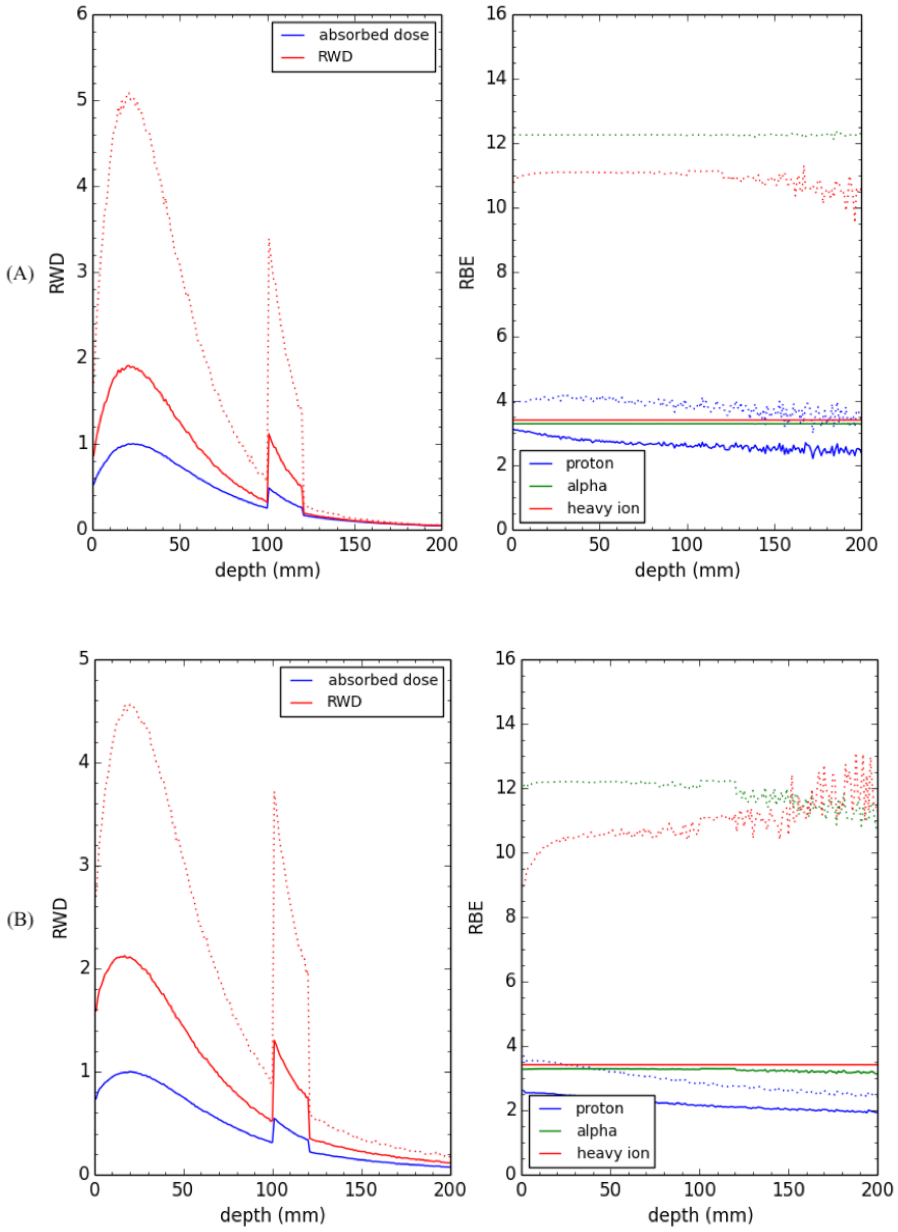

Figure 2.10. Soft tissue phantom, mass at 10 cm depth, 2 cm wide, 10:1 tumor to tissue ratio, 100 μg/g ^{10}B in tumor, solid lines RBE_{DSB}, dotted lines RBE_{LD} (β/α=3). PDD, RWD, and RBE for the MIT-FCB neutron source (A, left and right panel, respectively) NM neutron source (B, left and right panel, respectively).

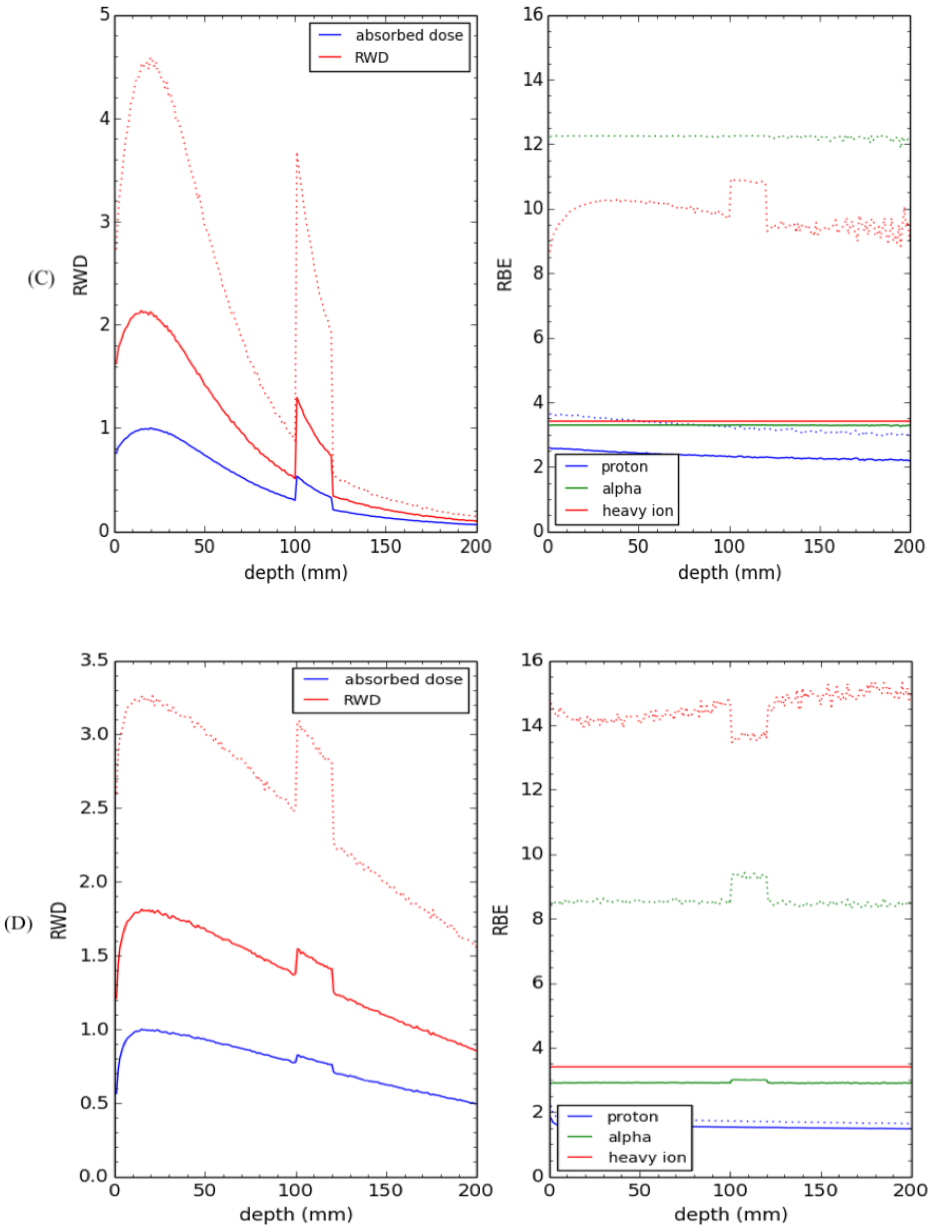

Figure 2.11. Soft tissue phantom, mass at 10 cm depth, 2 cm wide, 10:1 tumor to tissue ratio, 100 μg/g ^{10}B in tumor, solid lines RBE_{DSB} dotted lines RBE_{LD} (β/α=3). PDD, RWD, and RBE for the CN neutron source (C, left and right panel, respectively) and CNTS neutron source (D, left and right panel, respectively).

CHAPTER 3

DNA DOUBLE STRAND BREAK (DSB) INDUCTION AND CELL SURVIVAL IN IODINE-ENHANCED COMPUTED TOMOGRAPHY (CT)[2]

3.1 Abstract

A multiscale Monte Carlo model is proposed to assess the dosimetric and biological impact of iodine-based contrast agents commonly used in computed tomography (CT). As presented, the model integrates the general purpose MCNP6 code system for larger-scale radiation transport and dose assessment with the Monte Carlo Damage Simulation (MCDS) to determine the subcellular characteristics and spatial distribution of initial DNA damage. The repair-misrepair-fixation model is then used to relate DNA double strand break (DSB) induction to reproductive cell death. Comparisons of measured and modeled changes in reproductive cell survival for ultrasoft characteristic k-shell X-rays (0.25 – 4.55 keV) up to orthovoltage (200 – 500 kVp) X-rays indicate that the relative biological effectiveness (RBE) for DSB induction is within a few percent of the RBE for cell survival. Because of the very short range of secondary

[2] Streitmatter SW, Stewart R D, Jenkins PA, Jevremovic T, DNA Double Strand Break (DSB) Induction and Cell Survival in Iodine-Enhanced Computed Tomography (CT). Submitted to *Physics in Medicine and Biology* December 19, 2016 (PMB-105153), formally accepted June 5, 2017 (PMB-105153.R1).

electrons produced by low energy X-ray interactions with contrast agents, the concentration and subcellular distribution of iodine within and near cellular targets have a significant impact on the estimated absorbed dose and number of DSB produced in the cell nucleus. For some plausible models of the cell-level distribution of contrast agent, the model predicts an increase in RBE-weighted dose (RWD) for the endpoint of DSB induction of 1.22 – 1.40 for a 5 - 10 mg/mL iodine concentration in blood compared to an RWD increase of 1.07 ± 0.19 from a recent clinical trial. The modeled RWD of 2.58 is also in good agreement with the measured RWD of 2.3 ± 0.5 for an iodine concentration of 50 mg/mL relative to no iodine. The good agreement between modeled and measured DSB and cell survival estimates provides some confidence that the presented model can be used to accurately assess biological dose for other concentrations of the same or different contrast agents.

3.2 Introduction

At present, the effects of image contrast media on the absorbed dose and RBE are not considered in clinically reported estimates of patient absorbed or effective dose in computed tomography (CT) (ICRU 2012), although there is likely some impact on the absorbed dose and DNA damage a patient receives, at least to the blood (Amato *et al.* 2010, Pathe *et al.* 2011 and references therein). We will demonstrate a useful multiscale system of models for the assessment of the absorbed dose enhancement and relative biological effectiveness for double strand break induction (RBE_{DSB}) arising from the use of an iodine-based contrast agent commonly used in CT scans. We will also provide further insight into the mechanisms at work for different biological endpoints for photons

and electrons. Because the biological processing of DSBs into chromosome aberrations is widely considered an important mechanism underlying both cell reproductive death (Cornforth and Bedford 1987, Bedford 1991, Hlatky *et al* 2002, Carlson *et al* 2008, Stewart *et al* 2011), mutagenesis (Frankenberg 1994), genome instability (Jeggo and Löbrich 2015, Terasawae *et al.* 2014), oncogenic transformation (Byrne *et al.* 2014), and radiation carcinogenesis (Byrne *et al.* 2014, Rothkamm and Löbrich 2002), RBE_{DSB} may be useful as a reasonable surrogate for the radiation weighting factors recommended in the ICRP 92 report (ICRP 2003) for diagnostic X-rays. The approach proposed could potentially improve the accuracy of patient-specific absorbed dose arising from CT scans, specifically contrast-enhanced CT scans.

The average linear energy transfer (LET) of secondary electrons produced from photon interactions tends to increase as the energy of the primary photons decreases, with a resultant increase in the RBE of at least 10-20% (Nikjoo *et al.* 2010). *In vitro* and *in vivo* experiments support the hypothesis that lower energy X-rays and secondary electrons have higher a RBE when compared to ^{60}Co or ^{137}Cs (Prise *et al.* 1989, Cornforth *et al.* 1989, Spadinger and Palcic 1992, Botchway *et al.* 1997, Fayard *et al.* 2002, Nikjoo *et al.* 2010, Kirkby *et al.* 2013, Hsaio and Stewart 2008). Monte Carlo simulations of DNA DSB induction indicate that X-ray voltage (> 20 keV) and anode composition have a small impact, whereas the type and thickness of filtration have a significant impact on RBE_{DSB} (Stewart *et al.* 2015). The former has a small impact because higher-energy (> 30-50 keV) photo- and Compton electrons have an RBE close to unity, and filtration substantially reduces the number of low-energy (high-RBE) electrons. The intra- and extracellular media in which the X-rays interact are also a very important consideration

due to the strong dependence of the photoelectric effect on atomic number.

Contrast agents designed to maximize photoelectric absorption, such as the k-edge of iodine-based (Z=53) agents, are widely used in CT and angiography to improve image quality, contrast and diagnostic precision. Theoretical and experimental evidence suggests that the presence of iodine will locally enhance absorbed dose due to its large absorption coefficient for kilovoltage photons compared to the low-*Z* components of soft tissue (e.g. – C, H, O and N) (Callisen *et al.* 1979). Figure 3.1 illustrates the magnitude of differences between the total and individual photon cross sections for water and iodine using the latest low energy electron-photon-relaxation data available in MCNP6 (Hughes 2013).

Recent studies have examined the impact of contrast agents on absorbed dose (Amato *et al.* 2010, 2013, Jost *et al.* 2009) and DNA damage/repair and chromosomal aberrations (Grudzenski *et al.* 2009, Jost *et al.* 2009, Pathe *et al.* 2011, Piechowiak *et al.* 2015, Matsubara *et al.* 1997), with most of them confirming that there are indeed statistically significant increases in *γ-H2AX* foci and chromosomal abberations, and its impact should not be overlooked. However, Jost *et al.* (2009) concluded that, at the level of absorbed dose typically encountered in diagnostic CT, no significant differences in the yields of dicentrics and *γ-H2AX* foci were observed in the absence or presence of 5 mg/mL iodine in blood, an outlier among all the other studies. Although it is likely that higher iodine concentrations are present for clinical administration. For diagnostic X-ray imaging, the benefit of medical diagnosis and treatment is weighed against the stochastic risks of patient harm. For CT exams that utilize image contrast media, there are further local dose enhancements and radiobiological effects that are of potential concern, but are

not yet considered. A phosphorylated form of H2AX histone variant (i.e., *γ–H2AX* foci) has been used to retrospectively estimate radiation dose in patients who received CT exams by analyzing the foci produced in blood lymphocytes (Golfier *et al.* 2009, Rothkamm *et al.* 2007). The numbers of *γ–H2AX* foci produced by ionizing radiation are approximately equal to the number of DNA DSBs (Rothkamm *et al.* 2003) because phosphorylation of H2AX is one of the earliest steps in the cellular response to DSB induction. DSBs are any cluster of two or more individual DNA lesions (strand breaks, abasic sites, base damage) containing (at least) a pair of opposed strand breaks within ~10 base pairs (bp) of each other. Although *γ–H2AX* foci can tend to underestimate DSBs for high-LET radiation when several foci are counted as one (e.g., several DSB occur in such close proximity that they are counted as a single foci), the effect for low-LET photons and electrons are negligible (Antonelli *et al.* 2015).

For diagnostic X-ray imaging, the benefit of medical diagnosis and treatment is weighed against the stochastic risks of patient harm. For CT exams that utilize image contrast media, there are further local dose enhancements and RBE effects that are of potential concern (Amato *et al.* 2010, 2013, Grudzenski *et al.* 2009, Piechowiak *et al.* 2015). One experimental metric currently used is termed the dose enhancement factor (DEF)[†]. While the DEF-based method is analytic and easy to implement, it assumes a homogenous distribution of iodine within critical cellular targets. The DEF method also neglects the RBE of the secondary electrons produced by the interactions of low energy

---

[†] $DEF \equiv \int_{E=0\ keV}^{\infty} \left(\frac{f\left(\frac{\mu_{en}}{\rho}\right)_E^{iodine} + (1-f)\left(\frac{\mu_{en}}{\rho}\right)_E^{blood}}{\left(\frac{\mu_{en}}{\rho}\right)_E^{blood}} \cdot N(E) \right) dE$, where: (μ_{en}/ρ) - mass energy absorption coefficient (cm^2/g) for iodine or blood at a given energy E, obtained from the NIST reference database (http://www.nist.gov/pml/data/xraycoef/), f - mass fraction of iodine in blood and $N(E)$ - relative quantity of photons at each energy E for a given X-ray source spectrum.

X-rays with the contrast agent, hence the need for a better metric to assess the biological dose for relevant clinical endpoints, such as *γ–H2AX* foci formation.

As illustrated in Figure 3.2, we have developed a system of models to better assess the absorbed dose and biological effects of iodine-enhanced CT. Our system of models uses MCNP6.1.1b (Goorley *et al.* 2013, 2014), a general-purpose Monte Carlo radiation transport code with the ability to simulate the interactions of photons and electrons with energies as low as 1 eV and 10 eV, respectively, to model the larger scale (> 1 mm) interactions of photons in laboratory experiments and diagnostic scans. Larger scale MCNP simulations of electron and photon transport are needed to more accurately account for charged particle disequilibrium and related effects that arise from the macro-scale cellular and *in vivo* distribution of an iodine within the irradiated blood and tissue during a CT scan. The MCDS (Monte Carlo Damage Simulation) is a cell-level model for the induction of clusters of DNA lesions, including DSB, by electrons, protons and other charged particles ($Z \leq 26$) with kinetic energies up to a few GeV (Semenenko and Stewart 2004, 2006 and Stewart *et al.* 2011). Finally, the repair-misrepair-fixation (RMF) model (Carlson *et al.* 2008) is utilized to relate the biological processing of initial DSB into lethal damage that impacts on reproductive cell survival.

Here, we report for the first time some additional low-energy X-ray benchmarks of the MCDS+RMF system of models for the endpoint of *in vitro* cell survival. Additional benchmarks of the MCDS+MCNP system of models for DSB induction by ultrasoft X-rays are also reported. The model benchmarks, as well as theoretical considerations arising from the RMF model, collectively indicate that, for ionizing electrons and photons with kinetic energies up to at least a few hundred keV, RBE_{DSB} is an effective surrogate

endpoint for the RBE for cell survival. The reported comparisons of measurements and results from the multiscale system of models reported here provide new information and insights into fundamental molecular mechanisms underlying particle RBE, as well as absorbed dose and radiobiological effects of iodine-enhanced CT scans in particular. These findings have the potential to aid in more precise clinical estimates and reporting of the increased absorbed dose to patients for such exams.

3.3 Methods

3.3.1 General framework of the system of models

We used the MCDS to generate lookup tables (dose-response functions) for the induction of DSB by monoenergetic electrons with kinetic energies from 10 eV to 1 GeV. As described in detail elsewhere (Stewart *et al.* 2015), a standard MCNP6 dose (F6:e tally) modified by the dose-response function for DSB induction was used to compute the dose, (dose × RBE_{DSB}) and RBE_{DSB} in the nucleus of a human cell (d = 5 μm). After simulating the initial numbers and spatial distribution of DSB through a combined MCDS+MCNP simulation, analytic formulas arising from the RMF model (Carlson *et al.* 2008) are used to determine how linear-quadratic (LQ) cell survival model parameters vary with electron kinetic energy and linear energy transfer (LET). The RMF model was developed to better link DSB induction to cell survival through an intra- and inter-track binary misrepair process. The RMF formulas in combination with first principle estimates of RBE_{DSB} have been shown to reproduce trends in cell survival for electrons, protons and other charged particles with an LET up to at least 100 to 200 keV/μm (Carlson *et al.* 2008, Frese *et al.* 2012, Mairani *et al.* 2016). Figure 3.2 illustrates the

components of the system of models and the respective input and ouput parameters.

3.3.2 MCDS+MCNP model for DSB induction by ultrasoft X-rays and ^{60}Co γ-rays

Figure 3.3 shows an idealized schematic of the MCDS+MCNP model developed to simulate DNA damage induction in a monolayer cell culture irradiated by ultrasoft characteristic X-rays. Similar Monte Carlo models have been used by others (Hsaio and Stewart 2008, Kirkby *et al.* 2013, Stewart *et al.* 2015) to simulate the induction of DNA damage by X-rays, γ-rays, neutrons and many other types of charged particles. In the MCNP simulations, the cutoff energies for photon and electrons transport are set to 1 eV and 15 eV, respectively. Tabulations of electron stopping power in MCNP are on the finest allowed energy grid (EFAC = 0.99). At electron energies < 1 keV, MCNP switches from a condensed-history transport method to single-event transport. This is due to the failure of condensed-history electron transport physics in MCNP associated with limitations in the data and semi-analytic methods used in the transport of higher energy electrons. The single-event method provides a successful and potentially much more accurate approach to low-energy electron transport and dosimetry (Hughes 2014). Fluence, absorbed dose, RBE_{DSB}, LET and related dose-response functions (e.g., mean-frequency specific energy) are recorded in the sensitive volumes shown in Figure 3.3.

The results of the MCDS+MCNP model for DSB induction are compared to measurements (de Lara *et al.* 2001) of the numbers of DSB Gy^{-1} Gbp^{-1} produced in V79-4 cells irradiated by ^{60}Co γ-rays, 0.28 keV (carbon K-shell), 0.96 keV (copper L-shell), 1.49 keV (aluminum K-shell) and 4.55 keV (titanium K-shell) X-rays. In the de Lara

experiments, the medium between the photon source and cell monolayer is adjusted based on the X-ray energy to minimize beam attenuation, using helium or hydrogen instead of air, which is also reflected in our MCNP model of the cell culture model (Figure 3.3).

3.3.3 MCDS+MCNP model to evaluate DSB induction in lymphocytes irradiated by 120 kVp X-rays with and without contrast

As an idealized *in vivo* model for lymphocyte irradiation, we developed a two-stage Monte Carlo modeling approach to determine the dosimetric and RBE characteristics of a 120 kVp X-rays with varying amounts of contrast media. Figure 3.4 (stage 1 of the model) shows an idealized MCNP model of a CT tube with a lead collimator and aluminum filtration to approximate the X-ray energy spectrum produced by a general CT tube with a 7° anode angle. In a second Monte Carlo simulation, X-rays from the stage 1 (CT scanner) model are transported through the idealized model of lymphocytes surrounded by a thin layer of medium with or without contrast, as illustrated in Figure 3.5. In the model for blood lymphocytes, the sensitive cell volume is surrounded by blood (ICRU 1992) or by a mixture of blood and the iodine contrast agent Ultravist® (Iompromide, $C_{18}H_{24}I_3N_3O_8$).

To efficiently model bremsstrahlung photon production in the tungsten anode of the CT tube, a variance reduction technique called the bremsstrahlung biasing is applied (Ay *et al.* 2004, Zoubair *et al.* 2013), which increases the number of photon tracks per electron, but reduces the particle weight in a way that to preserves the correct average number of tracks per electron. A "surface-source-write" file is recorded at 10 cm

downstream from the focal spot, capturing the energies and vectors of the photons produced. The second stage simulation, downstream of the phase space plane, is used to insert varying types and thicknesses of filtration without re-running the bremsstrahlung production, which is computationally expensive. Filtration is experimentally measured on a CT scanner using the Radcal™AGMS-DM+ solid-state multisensor at the isocenter, which is capable of determining half value layer (HVL) and filtration in a single measurement. The resulting filtered photon energy spectrum is scored with an energy fluence tally (F4) at 75 cm from the focal spot, with an energy bin width of 0.5 keV.

Most modern nonionic iodine compounds used as intravenous contrast are described as highly hydrophilic, biologically inert, extracellular and renally excreted; their pharmacokinetics in normal subjects conform to an open two-compartment model with first order elimination (Lusic *et al.* 2013, Ultravist® 2015, Isovue® 2012). While there is a statistically significant increase in *γ-H2AX foci*, and hence DSBs, in the presence of iodine contrast agents post irradiation, it is independent of the contrast agent used and the increase is solely attributed to the amount of iodine applied (Deinzer *et al.* 2012). Pharmokinetic studies also show that negligible amounts of iodine will cross into the cellular compartments of blood lymphocytes (Bourin *et al.* 1997), hence iodine is excluded from the representative nucleus and cytoplasm (sensitive volumes) in our lymphocyte model (Figure 3.5).

3.3.4 Relationship between the RBE for DSB induction and the RBE for cell survival – the repair-misrepair-fixation (RMF) model

In the RMF model (Carlson *et al.* 2008), the effects of particle type and kinetic energy (and hence LET) on α and β in the linear quadratic (LQ) cell survival model are explicitly linked to the initial numbers and spatial distribution of DSBs. In the RMF model, the biological processing of initial DSB into lethal chromosome aberrations or point mutations is model by a coupled system of nonlinear differential equations. In the work of Carlson *et al.* (2008), they were unable to find any category of complex DSB that was intrinsically less capable of initiating reproductive cell death than any other category of DSB. They concluded that the numbers of DSB per cell is the most significant determinant of cell killing efficiency. The number of DSB per electron (or other particle) track plays a significant role in determining particle RBE. There is compelling evidence in the literature that the number of DSB/Gy/Gbp of DNA tends to increase in a monotonic fashion with increasing particle LET up to an ion-specific peak before beginning to plateau or (possibly) decrease (Stewart *et al.* 2011 and references therein, Campa *et al.* 2005, Stenerlow *et al.* 2002). Some earlier studies seemed to suggest that the number of RBE for DSB induction was a weak or independent function of the radiation quality (e.g., Prise *et al.* 1998). However, there are known artifacts in the use of neutral filter elution for the measurement of DSB induction (Prise *et al.* 1998), and the measurement of DSB with pulsed-field gel electrophoresis (PFGE) can also be challenging because of issues related to cell lysis at elevated temperatures and the use of data analysis methods that convert fragment size distributions into estimates of the number of DSB (Alloni *et al.* 2013, Cedervall *et al.* 1995, Cedervall *et al.* 2002,

Ratnayake *et al.* 2005 and references therein), especially at low absorbed doses. As a first approximation, the RMF system of differential equations predicts that RBE_{DSB} is related to the RBE for cell survival for doses that are small compared to α/β (low-dose RBE or RBE_{LD}) by

$$RBE_{LD} = \frac{\alpha}{\alpha_\gamma} = RBE_{DSB}\left(1 + \frac{2\bar{z}_F RBE_{DSB}}{(\alpha/\beta)_\gamma}\right) \tag{3.1}$$

where $\bar{z}_F \cong LET/\rho d^2$ (ICRU Report 36, 1983); d is the diameter of the cell nucleus (~ 4-6 μm). The subscript γ denotes a parameter for the reference radiation (e.g., γ-rays from ^{60}Co). In the alternate limit of doses that are very large compared to α/β (high-dose RBE or RBE_{HD}), the RMF model predicts that

$$RBE_{HD} = \sqrt{\frac{\beta}{\beta_\gamma}} = RBE_{DSB} \tag{3.2}$$

For high and low energy electrons, the product of $2\bar{z}_F RBE_{DSB}/(\alpha/\beta)_\gamma$ in Eq. (1) is small or negligible (~0.01 or less) for most mammalian cells because (1) $\bar{z}_F$ is on the order of a mGy or less, (2) electron $RBE_{DSB} \geq 1$ regardless of kinetic energy, and (3) $(\alpha/\beta)_\gamma$ is often greater than 1 Gy for most mammalian cells. Therefore, Eqs. (1) and (2) indicate that, for electrons, $RBE_{LD} \cong RBE_{HD} = RBE_{DSB}$. If this approximation is sufficiently accurate, then the radiosensitivity parameters for ultrasoft and orthovoltage X-rays are related to the radiosensitivity parameters for ^{60}Co γ-rays by

$$\alpha = \alpha_\gamma \cdot RBE_{DSB}\,, \quad \beta = \beta_\gamma \cdot RBE_{DSB}{}^2 \tag{3.3}$$

3.4 Results

3.4.1 Comparison of measured and MCDS+MCNP estimates of DSB induction by ultrasoft X-rays, orthovoltage X-rays and ^{60}Co γ-rays

Table 3.1 shows the comparison of RBE predictions using the MCDS+MCNP model and de Lara's (2001) experimental results. The MCDS+MCNP model estimates are 10-20% larger than the measured numbers of DSB Gy^{-1} Gbp^{-1} whereas the RBE_{DSB} is ≤ 10%. The simulated absolute DSB yields may be larger than the measured ones because of limitations and uncertainties of the experimental assays (Löbrich *et al.* 1996, Pinto *et al.* 2002, Stenerlöw *et al.* 2003, Ratnayake *et al.* 2006 and references therein) and because some second-order effects are neglected in the MCDS+MCNP simulations, such as chromatin structure effects (Ljungman 1991, Oleinick *et al.* 1994, Venkatesh *et al.* 2016). Regardless, as indicated by Eqs. (3.1), (3.2) and (3.3), it is the relative numbers of DSB that are important in the cell survival model rather than the absolute numbers of DSB Gy^{-1} Gbp^{-1}, and the observed differences in RBE_{DSB} estimates of 10% or less are well within the uncertainties in the measured data. Prior to the release of MCNP6, which extends photon and electron transport down to 1 eV and 10 eV from 1 keV, respectively (Hughes 2014), it was not possible to explicitly model DNA damage from lower energy photons and electrons, such as the 0.28 keV (carbon K-shell X-rays) and 0.96 keV (copper L-shell X-rays) used by the De Lara study, within the framework of a combined MCDS+MCNP simulation. However, earlier studies (Hsaio and Stewart 2008, Stewart *et al.* 2011, Kirkby *et al.* 2013) comparing MCDS estimates of the absolute or relative numbers of DSB to measurements are also in reasonable agreement for low and higher energy photons and electrons.

3.4.2 Tests of the RMF model prediction that $RBE_{LD} = RBE_{HD} = RBE_{DSB}$ for electrons and photons

Figure 3.6 compares estimates of the cell surviving fraction computed using the RMF model formula (i.e., Eq. 3.3) to relate α and β for the reference radiation to the α and β for lower-energy kilovoltage, orthovoltage and ultrasoft X-rays. Experimental data is analyzed using a nonlinear regression analysis of the measured data for each type of radiation (Figure 3.6 dashed and dotted lines). For comparison, the measured data were also analyzed using the RMF-motivated analysis [i.e., Eq. (3.3)] in which α and β for the reference radiation (^{60}Co γ-rays) and the RBE_{DSB} for each type of radiation is treated as an adjustable parameter (Figure 3.6 solid lines). The key advantage of the RMF-motivated analysis of the cell survival data is that the number of adjustable parameters is reduced from 40 parameters (2 parameters for each type of radiation) to 26 parameters (2 parameters for the reference radiation plus 1 additional RBE_{DSB} parameter for each additional type of radiation) with only a small impact on the quality of the fits (compare dotted/dashed lines to solid lines in Figure 3.6). As an additional test of the multiscale system of models, we then compared the estimates of the RBE_{DSB} from the analysis of the cell survival data to a first principle MCDS+MCNP simulation of DSB induction as a way to independently examine the relationship between RBE_{DSB} and the RBE for cell survival.

Table 3.2 compares the RBE_{DSB} values computed from RMF-fits of the cell survival data in Figure 3.6 and MCDS+MCNP simulations. For the Spadinger and Palcic (1992) dataset, the first-principle Monte Carlo simulations of RBE_{DSB} are within 3% of the values derived from the nonlinear regression analysis of the measured cell survival

data. For the de Lara *et al.* (2002) dataset, where both DSBs and cell survival were investigated, measured and calculated RBE_{DSB} are in excellent (~ 5%) agreement. Comparison of the Frankenberg *et al.* (2002) data shows excellent agreement for 29 kVp, mammography quality X-rays as well as 200 kVp X-rays. For the lowest photon energies examined here, from the work of Fayard *et al.* (2002), there is excellent agreement at 340 eV. However, there is a puzzlingly large difference in the RBE estimates for the very low energy (250 eV) photons derived from the Fayard *et al.* dataset, especially in view of the observation that the RBE estimates derived from the de Lara *et al.* dataset are in excellent agree for 280 eV photons. The differences in the fitted and model-predicted estimates for the 250 eV photons in the Fayard *et al.* may relate to uncertainties in the dosimetry, particularly in the mean Mylar window thickness and mass absorption coefficients used. With the exception of the Hoshi *et al.* (1988) study, the estimates of RBE_{DSB} from the first principle Monte Carlo simulations are in excellent (~5-10% or less) agreement with the estimates derived from the nonlinear regression analysis of the cell survival data. The systematically low predictions of RBE_{DSB} for the Hoshi *et al.* data may be due to a systematic bias in the dosimetry associated with the absolute calibration of the X-ray source and/or to uncertainties in the MCNP modeling of the filtration and other components of the X-ray source. Collectively, the analysis of the cell survival data and first principle Monte Carlo simulations of RBE_{DSB} provide strong evidence supporting the RMF-motivated hypothesis that $RBE_{LD} = RBE_{HD} = RBE_{DSB}$ for photons and electrons across a wide range of energies.

3.4.3 Iodine effects on the spectra and interactions of secondary electrons

Table 3.3 shows the photon/electron interactions dependence on iodine concentration and distributions based on the MCNP6 model. The generation of Auger electrons is linearly dependent on the quantity of photons absorbed, and thus directly proportional to the increase in iodine concentration. Due to the very low energies (~20-500 eV) and short ranges (~1-10 nm) of Auger electrons (Howell 2009), for iodine contrast outside of the cell, a trivial amount of dose will be deposited in the cell by these high-LET electrons (Regulla *et al.* 2002) and that is also shown in the data in Table 3.3. The photoelectrons around the k-edge of iodine are also short range (~20 μm) (Callisen *et al.* 1979).

Figure 3.7 illustrates the difference in energy spectrum in the sensitive 5 μm layer with the modeled iodine concentration (refer to Figure 3.5). From Figure 3.7, a clear dose enhancement as the iodine concentration increases is observed, but it is much more pronounced for a homogenous distribution compared to an extracellular distribution. For instance, to achieve the same dose increase for a homogenous distribution of 0.48% iodine by weight, an extracellular concentration of 2.48% is required. Differences in RWD are even more pronounced: an extracellular iodine concentration of 4.81% is needed to equal the same RWD as 0.48% of homogenously distributed. Using the DEF doesn't take into account the finer details of the subcellular iodine distribution and range of the secondary electrons that are considered in MCDS+MCNP system of models. In the work of Jost *et al.* (2009), the calculated DEF exceeded the relative increase in *γ–H2AX* foci nearly 3-fold.

3.4.4 Comparison of measured and Monte Carlo simulated estimates of absorbed dose and RBE_{DSB} for the *in vivo* irradiation of lymphocytes by 120 kVp X-rays

Simulations of RWD in a 5 μm sensitive volume exposed to 120 kVp X-rays with an extracellular iodine/blood concentration of 5 mg/mL (0.48% iodine by weight) results in 122% increase in the number of DSBs from a combination of absorbed dose and RBE changes compared to blood without iodine. For 50 mg/mL (4.81% iodine by weight), the Monte Carlo model predicts an increase of 258%. Experimental values of *γ–H2AX foci* induction in Jost *et al.* (2009) are used for comparison. For 0.48% and 4.81% iodine concentrations, an enhancement factor of 1.35 ± 0.08 and 2.3 ± 0.5 is observed, respectively. These values are much lower than expected from the analytical estimates of physical dose enhancement of 1.56 and 6.3, but are within 10% of the Monte Carlo predictions. Additionally, Pathe *et al.* (2011) found that the number of γ–*H2AX foci* increased by a factor of 1.58 *in vivo* for 120 kVp CT scans with Ultravist administered compared to unenhanced scans, consistent with our findings of 1.22 – 1.94 that bracket the likely clinical concentration (Table 3.4). The work of Piechowiak *et al.* (2015) concluded that iodine-enhanced CT scans increases the number of γ–*H2AX foci* by 107 ± 19% compared to unenhanced studies. This is also consistent with our predicted factor of 1.22 – 1.40. The large standard deviation of his study is likely due to uncertainties of iodine concentration in blood at the time of scan among the patients. Therefore, we examined a range of possible iodine concentrations: ~5-25 mg/mL (0.48 - 2.41% by weight) iodine in blood signifying the clinical range for diagnostic imaging applications. Table 3.4 shows the MCDS+MCNP estimated RWD and related quantities for varying concentrations of iodine in blood for 120 kVp X-rays, 10.5 mm Al filtration in a 5 μm

layer of medium (refer to Figure 3.3). Assuming a homogenous distribution of iodine results in much higher estimates of the absorbed dose, especially for the low-energy region. When modeling the more realistic scenario of extracellular iodine, estimates of RWD are in good agreement with the *in vitro* and *in vivo* experiments reporting a ~20-30% increase in RWD determined by *γ-H2AX foci* measurements (Grudzenski *et al.* 2009, Piechowiak *et al.* 2015). For extracellular iodine, the RBE remains essentially constant regardless of the iodine concentrations, while homogenous iodine concentrations show a substantial increase of 45% in RBE as the iodine concentration by weight increases from 0.48 to 4.81%. The same trends are seen for dose-averaged LET.

3.5 Discussion

Enumerating *γ-H2AX* foci formation in blood lymphocytes is a sensitive method for quantifying absorbed dose due to CT scan with or without iodine contrast present and is a good measure of initial DSB formation. As noted in Golfier *et al.* (2009), both assays of scoring *γ-H2AX* foci and chromosomal aberrations are appropriate methods for assessing impact of dose-modifying effects such as in the use of iodine-based contrast. Of the two, chromosome aberrations are the more clinically relevant endpoint because they represent the persistence of a biologically significant form of unrepaired or misrepaired DNA damage whereas the vast majority of the *γ-H2AX* foci, a marker for initial DSB induction, are ultimately repaired and are much less biologically significant. However, *γ-H2AX* foci assay can detect DSB after lower doses of ionizing radiation (~ 1-6 mGy) than the assays used for the measurement of chromosome aberrations (Rothkamm *et al.* 2007, Rothkamm and Löbrich 2003). Comparatively, the low-dose detectability limit of chromosomal

aberration analysis is about 50-100 mGy (IAEA 1986). For this reason, *γ–H2AX* foci are particularly well suited for biological dosimetry in CT and other diagnostic X-ray scans. *In vitro* and *in vivo* studies of *γ-H2AX* foci formation in blood lymphocytes were compared and benchmarked against results from a multiscale (MCDS+MCNP) model simulations of relative increases in DSBs using a more realistic distribution of iodine around the cells. Good agreement was found for both the *in vitro* and *in vivo* experiments, which provides evidence to support the use of this system of models as a predictive tool to explore and help quantify the effects of iodine contrast agenda in diagnostic X-ray scans. Others (Joubert *et al* 2005) have shown that repair of DSB can be inhibited from the radiolysis products of iodine compounds, and this may be a factor to consider when applying the RMF model to account for the repair and misrepair of initial DSB. The significance of any iodine-related decreased DSB repair in the context of low doses of diagnostic X-rays is an open question in need of additional study.

In the RMF model for the conversion of initial DSB into lethal forms of damage, RBE effects primarily arise from (*1*) the tendency for DSB induction to increase with increasing LET up to a particle-specific peak before reaching a plateau or beginning to decrease (Stewart *et al* 2011, Stewart *et al* 2015) and (*2*) the numbers of DSB per electron (or other particle) track tends to increase with increasing LET. The former effect determines the rate of *inter-track* DSB interactions (pairs of DSB formed by different electrons interact to form lethal damage) whereas the latter mechanism of action determines the rate of *intra-track* DSB interactions (pairs of DSB formed by a single electron interact to form lethal damage). Because electrons are very unlikely to create, on average, more than one DSB per track per cell (right panel of Figure 2 in Stewart *et al*

2015), the RMF model predicts that the RBE for cell survival should be approximately equal to the RBE for DSB induction (i.e., RBE_{DSB}). The results reported in Table 3.2 provide strong support for the RMF-motivated hypothesis that the RBE for cell survival and DSB induction are about the same for electrons (all kinetic energies) as well as diagnostic and MV X-rays. A practical consequence of this observation is that exploratory modeling as well as patient-specific determinations of RWD for contrast-enhanced diagnostic scans can potentially be determined from first principle Monte Carlo simulations with (effectively) no *ad hoc* adjustable biological parameters. That is, estimates of RBE_{DSB} can be determined through combined MCDS+MCNP simulations without the need to define any additional cell-or tissue specific parameters. The extensively benchmarked MCDS handles the cellular and subcellular physiochemical interaction that create DSB, and MCNP simulations handle the larger-scale (> cellular) interactions of photons and secondary particles. In contrast to our approach, other RBE models, such as the local-effect-model (LEM) (Friedrich *et al.* 2012, Tommasino *et al.* 2013, 2015) and the microdosimetric kinetic (MK) model (Hawkins 1998, 2003, 2009) require the specification of two or more cell- or tissue specific parameters and rely on extensive databases of cell biophysical parameters that may or may not be fully representative of cell, tissue and patient specific biology.

For patient-specific dosimetry, one of the largest sources of uncertainty in the RWD estimates is likely to be the iodine concentration in blood at the time of scan. As seen in Table 3.4, small variations in the estimated iodine content in blood can have a significant impact on estimates of absorbed dose, RBE_{DSB} and hence RWD. Since the induction of *γ-H2AX* foci, and hence DSB, are dependent on both the absorbed dose and

RBE effects, uncertainty in the absorbed dose between the pre-contrast and post-contrast scan will impact the calculated excess RWD due to the iodine. Although not investigated here, beam hardening and attenuation in a patient will likely have some minor effect on effective RBE. In the context of the models, the MCNP input parameters, which include the X-ray spectra, cell/tissue geometry and iodine concentration and distribution (Figure 3.2), are critical for determinations of RWD. Better characterization of these three parameters in a clinical CT scan is important for the most accurate estimates of RWD. The MCDS parameters are fixed (independent or weak function of cell and tissue type) and since the mean-frequency specific energy term in Eq. 3.1 was found to be negligible for the investigated scenarios, the nucleus diameter parameter doesn't effect MCDS+MCNP estimates.

Since the absorbed dose and RBE enhancement arising from the interactions of kilovoltage photons with iodine contrast is confined to the blood in circulation, there is still a question as to whether this translates into increased stochastic risk, at least to the extent it is currently calculated using the ICRP's methodology (ICRP 2007). The endothelial cells of the vessels containing iodine-based contrast at the time of scan likely receive additional dose (Joubert *et al.* 2005). Organs which are perfused by contrast laden blood may receive additional dose in the immediate proximity to the vessels, but more animal-based studies need to be performed to more accurately assess if organs receive any appreciable absorbed dose and RBE enhancements due to iodine-enhanced CT. Regardless, optimization of contrast-enhanced CT protocols is desirable, since there is a measurable enhancement in RWD in blood for CT scans that utilize iodine contrasts. Application of our system of models could aid in determining the best balance between

kVp, iodine concentration and RWD. However, since the desired image enhancement is directly related to the iodine concentration, and thus resulting RWD at the time of scan, much is dependent on the interpreting physician and the threshold for acceptable image-contrast enhancement needed for diagnosis or intervention.

To better quantify patient-specific risks from contrast-enhanced CT, we envision using our model to calculate the excess RWD from CT scans with inputs of only the change in HU from noncontrast to contrast scan, the Bremsstrahlung spectrum and operating kVp for the specific CT machine. Since many CT clinical protocols employ multiple scans at different circulatory phases after administration of contrast, a method that correlates change in HU to *in vivo* concentrations of iodine (Chandarana *et al.* 2011, Amato *et al.* 2010) and ultimately determination of RWD, could improve estimates of whole body absorbed dose and also aid in potential protocol optimizations. Further development of the proposed system of models is in progress to address patient CT datasets in conjunction with a helical CT source.

3.6 Summary and Conclusions

This paper describes a useful multiscale system of models for the assessment of changes in absorbed dose and the RBE for DSB induction and cell survival arising from the use of iodine-based contrast agent commonly used in CT scans. Model estimates of the absorbed dose and radiobiological enhancements of DSB induction from iodine contrast agents are in good agreement with experimental observations *in vitro* and *in vivo* (Grudzenski *et al.* 2009, Jost *et al.* 2009, Piechowiak *et al.* 2015) indicating an RWD ~20-60% for the iodine concentrations seen clinically in contrast-enhanced CT. The

RBE_{DSB} estimate of about 1.2 is insensitive to the extracellular concentration of contrast agent whereas the absorbed dose increases in linear fashion with the extracellular concentration of contrast. It is concluded that iodine-enhanced CT scans can increase the RWD to the blood by at least 20% compared to unenhanced scans.

In addition to quantifying the increased biological dose in iodine-enhanced CT, the reported studies provide compelling new evidence for the RMF-model hypothesis that, for photons and electrons with energies up to at least a few hundred keV, RBE_{DSB} is an effective surrogate endpoint for the RBE for cell survival, i.e., $RBE_{DSB} = RBE_{LD} = RBE_{HD}$. This finding, in addition to the reported comparisons of measurements and results from the multiscale system of models reported here, provides new information and insights into fundamental molecular mechanisms underlying particle RBE.

In the future, the Amato *et al* (2010) method to quantify the *in vivo* iodine concentration at the time of CT scan could be used in combination with the presented multiscale Monte Carlo model to determine patient-specific biological dose estimates because in reality, iodine concentrations *in vivo* will vary with scan parameters, injection timing and variations in patient physiology and habitus (Bae 2010 and references therein). While we have compared our system of models with the few *in vivo* real-time fluorescence imaging of γ-*H2AX* foci studies of iodine-enhanced CT scans, there still is a need for larger cohort studies with various types of CT angiography exams and correlation of HU to iodine concentration to test the usefulness of the model for patient-specific quantification of biological dose. A validated approach for accurate patient-specific RWD estimates would allow for better assessments of the risks and benefits of contrast-enhanced CT scans. The same approach is also extensible to interventional

radiology cases which utilize iodine contrast, although further modeling of the beam quality would be needed.

3.7 Acknowledgements

The authors would like to thank the University of Utah Department of Radiology and Imaging Sciences for their assistance with testing CT beam filtration and the on-site engineers for providing information on X-ray tube schematics and specifications.

3.8 References

Alloni D, Campa A, Friedland W, Mariotti L and Ottolenghi A 2013 Integration of Monte Carlo simulations with PFGE experimental data yields constant RBE of 2.3 for DNA double-strand break induction by nitrogen ions between 125 and 225 kev/μm let *Radiat. Res.* **179** 690–7

Amato E, Salamone I, Naso S, Bottari A, Gaeta M and Blandino A 2013 Can contrast media increase organ doses in CT examinations? A Clinical Study *Am. J. Roentgenol.* **200** 1288–93

Amato E, Lizio D, Settineri N, Di Pasquale A, Salamone I and Pandolfo I 2010 A method to evaluate the dose increase in CT with iodinated contrast medium *Med. Phys.* **37** 4249–8

Antonelli F, Campa A, Esposito G, Giardullo P, Belli M, Dini V, Meschini S, Simone G, Sorrentino E, Gerardi S, Cirrone G A P and Tabocchini M A 2015 Induction and repair of DNA DSB as revealed by H2AX phosphorylation foci in human fibroblasts exposed to low- and high-LET radiation: relationship with early and delayed reproductive cell death *Radiat. Res.* **183** 417–31

Ay M R, Shahriari M, Sarkar S, Adib M and Zaidi H 2004 Monte Carlo simulation of x-ray spectra in diagnostic radiology and mammography using MCNP4C *Phys. Med. Biol.* **49** 4897–917

Bae K T 2010 Intravenous contrast medium administration and scan timing at CT: considerations and approaches *Radiology* **256** 32–61

Bedford J S 1991 Sublethal damage, potentially lethal damage, and chromosomal

aberrations in mammalian cells exposed to ionizing radiations *Int. J. Radiat. Oncol. Biol. Phys.* **21** 1457–69

Botchway S W, Stevens D L, Hill M A, Jenner T J and O'Neill P 1997 Induction and rejoining of DNA double-strand breaks in Chinese hamster V79-4 cells irradiated with characteristic aluminum K and copper L ultrasoft X rays. *Radiat. Res.* **148** 317–24

Bourin M, Jolliet P and Ballereau F 1997 An overview of the clinical pharmacokinetics of X-ray contrast media *Clin. Pharmacokinet.* **32** 180–93

Byrne M, Wray J, Reinert B, Wu Y, Nickoloff J, Lee S H, Hromas R and Williamson E 2014 Mechanisms of oncogenic chromosomal translocations *Ann. New York Acad. Sci.* **1310** 89–97

Callisen H H, Norman A and Adams F H 1979 Absorbed dose in the presence of contrast agents during pediatric cardiac catheterization *Med. Phys.* **6** 504–9

Campa A, Ballarini F, Belli M, Cherubini R, Dini V, Esposito G, Friedland W, Gerardi S, Molinelli S, Ottolenghi A, Paretzke H, Simone G and Tabocchini M A 2005 DNA DSB induced in human cells by charged particles and gamma rays: experimental results and theoretical approaches. *Int. J. Radiat. Biol.* **81** 841–54

Carlson D, Stewart R, Semenenko V and Sandison G 2008 Combined use of Monte Carlo DNA damage Simulations and deterministic repair models to examine putative mechanisms of cell killing *Radiat. Res.* **169** 447–59

Cedervall B E and McMillan T J 2002 The fraction of DNA released on pulsed field gel electrophoresis gels may differ significantly at low levels of double-strand breaks *Radiat. Res.* **158(2)** 247-9

Cedervall, B., Wong, R., Albright, N., Dynlacht, J., Lambin, P. and Dewey, W.C. 1995 Methods for the quantification of DNA double-strand breaks determined from the distribution of DNA fragment sizes measured by pulsed-field gel electrophoresis. *Radiat. Res.* **143(1)** 8-16

Chandarana H, Megibow A J, Cohen B A, Srinivasan R, Kim D, Leidecker C and Macari M 2011 Iodine quantification with dual-energy ct: phantom study and preliminary experience with renal masses *Am. J. Roentgenol.* **196** W693–W700

Cornforth M N, Schillaci M E, Goodhead D T, Carpenter S G, Wilder M E, Sebring R J and Raju M R 1989 Radiobiology of ultrasoft X-rays. III. Normal human fibroblasts and the significance of terminal track structure in cell inactivation *Radiat. Res.* **119** 511–22

Cornforth M N and Bedford J S 1987 A quantitative comparison of potentially lethal

damage repair and the rejoining of interphase chromosome breaks in low passage normal human fibroblasts *Radiat. Res.* **111** 385–405

Deinzer C K W, Danova D, Kleb B, Klose K J and Heverhagen J T 2013 Influence of different iodinated contrast media on the induction of DNA double-strand breaks after *in vitro* X-ray irradiation *Contrast Media Mol. Imaging* **9** 259–67

De Lara C M, Hill M A, Jenner T J and Papworth D 2001 Dependence of the yield of DNA double-strand breaks in Chinese hamster V79-4 cells on the photon energy of ultrasoft X-rays *Radiat. Res.* **155** 440–8

Fayard B, Touati A, Abel F, Herve du Penhoat M A, Despiney-Bailly I, Gobert F, Ricoul M, L'Hoir A, Politis M F, Hill M A, Stevens D L, Sabatier L, Sage E, Goodhead D T and Chetioui A 2002 Cell inactivation and double-strand breaks: the role of core ionizations, as probed by ultrasoft X rays. *Radiat. Res.* **157** 128–40

Frankenberg D, Kelnhofer K, Bär K and Frankenberg-Schwager M 2002 Enhanced neoplastic transformation by mammography X-rays relative to 200 kVp X rays: indication for a strong dependence on photon energy of the RBE(M) for various end points *Radiat. Res.* **157** 99–105

Frankenberg D 1994 Repair of DNA double-strand breaks and its effect on RBE *Adv. Space Res.* **14(10)** 235-48

Friedrich T, Durante M and Scholz M 2012 Modeling cell survival after photon irradiation based on double-strand break clustering in megabase pair chromatin loops *Radiat. Res.* **178** 385–94

Frese M, Yu V, Stewart R, and Carlson D 2012 A mechanism-based approach to predict the relative biological effectiveness of protons and carbon ions in radiation therapy *Radiat. Oncol. Biol.* **83** 442–50

Golfier S, Jost G, Pietsch H, Lengsfeld P, Eckardt-Schupp F, Schmid E and Voth M 2009 Dicentric chromosomes and γ-H2AX foci formation in lymphocytes of human blood samples exposed to a CT scanner: a direct comparison of dose response relationships *Rad. Prot. Dosim.* **134** 55–61

Goorley J T *et al* 2013 Initial MCNP6 Release Overview *Nucl. Technol.* **180** 298-315

Goorley J T 2014 MCNP6.1.1-Beta Release Notes LA-UR-14-24680

Grudzenski S, Kuefner M A, Heckmann M B and Uder M 2009 Contrast medium–enhanced radiation damage caused by ct examinations *Radiology* **253(3)** 706-714

Hawkins R B 1998 A microdosimetric-kinetic theory of the dependence of the RBE for cell death on LET *Med. Phys.* **25** 1157–70

Hawkins R B 2003 A microdosimetric-kinetic model for the effect of nonPoisson distribution of lethal lesions on the variation of RBE with LET *Radiat. Res.* **160** 61–9

Hawkins R B 2009 The relationship between the sensitivity of cells to high-energy photons and the RBE of particle radiation used in radiotherapy *Radiat. Res.* **172** 761–76

Hlatky L, Sachs R K, Vazquez M and Cornforth M N 2002 Radiation-induced chromosome aberrations: insights gained from biophysical modeling *Bioessays* **24** 714–23

Hoshi M, Antoku S, Nakamura N, Russell W J, Miller R C, Sawada S, Mizuno M and Nishio S 1988 Soft X-ray dosimetry and RBE for survival of Chinese hamster V79 cells *Int. J. Radiat. Biol.* **54** 577–91

Howell R W 2009 Auger processes in the 21st century *Int J Radiat Biol* **84** 959–75

Hsiao Y-Y, Hung T-H, Tu S-J and Tung C-J 2014 Fast Monte Carlo simulation of DNA damage induction by Auger-electron emission *Int. J. Radiat. Biol.* **90** 392–400

Hsiao Y and Stewart R 2008 Monte Carlo simulation of DNA damage induction by x-rays and selected radioisotopes *Phys. Med. Biol.* **53** 233

Hughes H G 2014 Recent developments in low-energy electron/photon transport for MCNP6 *Prog. Nucl. Science and Technology* **4** 454-58

Hughes H G 2013 An electron/photon/relaxation data library for MCNP6 *Los Alamos National Laboratory Report* LA-UR-13-27377

IAEA 1986 Biological dosimetry: chromosomal aberration analysis for dose assessment *IAEA Reports Series No. 260* (Vienna, Austria: International Atomic Energy Agency)

ICRP 2003 Relative Biological Effectiveness (RBE), Quality Factor (*Q*), and Radiation Weighting Factor (w_R) *ICRP Publication 92 (Ann. ICRP* **33** 4*)*
ICRU 1983 Microdosimetry *ICRU Report No. 36* (Bethesda, MD: International Commission on Radiation Units and Measurements)

ICRU 1989 *Tissue Substitutes in Radiation Dosimetry and Measurement (ICRU Report No. 44)* (Bethesda, MD: International Commission on Radiation Units and

Measurements)

ICRU 1992 *Photon, Electron, Proton and Neutron Interaction Data for Body Tissues (ICRU Report No. 46)* (Bethesda, MD: International Commission on Radiation Units and Measurements)

ICRU 2012 *Radiation Dose and Image-Quality Assessment in Computed Tomography (ICRU Report No.87)* (Bethesda, MD: International Commission on Radiation Units and Measurements)

Isovue® Injection [package insert]. Princeton, New Jersey, USA: Bracco Diagnostics; 2012

Jeggo P A and Lobrich M 2015 How cancer cells hijack DNA double-strand break repair pathways to gain genomic instability *Biochem. J.* **471** 1–11

Jost G, Golfier S, Pietsch H, Lengsfeld P, Voth M, Schmid T E, Eckardt-Schupp F and Schmid E 2009 The influence of X-ray contrast agents in computed tomography on the induction of dicentrics and γ-H2AX foci in lymphocytes of human blood samples *Phys. Med. Biol.* **54** 6029–39

Joubert A, Biston M-C, Boudou C, Ravanat J-L, Brochard T, Charvet A-M, Estève F, Balosso J and Foray N 2005 Irradiation in presence of iodinated contrast agent results in radiosensitization of endothelial cells: Consequences for computed tomography therapy *Int. J. Radiat. Oncol. Biol. Phys.* **62** 1486–96

Kirkby C, Ghasroddashti E, Poirier Y, Tambasco M and Stewart R D 2013 RBE of kV CBCT radiation determined by Monte Carlo DNA damage simulations *Phys. Med. Biol.* **58** 5693–704

Kuo L J and Yang L-X 2008 γ-H2AX - a novel biomarker for DNA double-strand breaks *In vivo* **22** 305–9

Ljungman M 1991 The influence of chromatin structure on the frequency of radiation-induced DNA strand breaks: a study using nuclear and nucleoid monolayers *Radiat. Res.* **126(1)** 58-64

Löbrich M, Cooper PK, Rydberg B 1996 Non-random distribution of DNA double-strand breaks induced by particle irradiation *Int. J. Radiat. Biol.* **70(5)** 493-503

Lusic H and Grinstaff M W 2013 X-ray computed tomography contrast agents *Chem. Rev.* **113** 1641–66

Mairani A, Dokic I, Magro G, Tessonnier T, Kamp F, Carlson D J, Ciocca M, Cerutti F,

Sala P R, Ferrari A, Böhlen T T, Jäkel O, Parodi K, Debus J, Abdollahi A and Haberer T 2016 Biologically optimized helium ion plans: calculation approach and its *in vitro* validation *Phys. Med. Biol.* 4283–99

Matsubara S, Kong Z S, Omura M, Kurihara H, Torigoe S, Iwasawa T, Yoshida T and Kubota N 1997 The effect of iodine-based contrast agents on the levels of radiation-induced chromosomal aberrations *Radiat. Res.* **147** 263–8

Nikjoo H and Lindborg L 2010 RBE of low energy electrons and photons *Phys. Med. Biol.* **55** R65–109

Obe G, Pfeiffer P, Savage J R, Johannes C, Goedecke W, Jeppesen P, Natarajan A T, Martinez-Lopez W, Folle G A and Drets M E 2002 Chromosomal aberrations: formation, identification and distribution *Mutat. Res.* **504** 17–36

Oleinick NL1, Balasubramaniam U, Xue L, Chiu S 1994 Nuclear structure and the microdistribution of radiation damage in DNA *Int. J. Radiat. Biol.* **66(5)** 523-9

Pathe C, Eble K, Schmitz-Beuting D, Keil B, Kaestner B, Voelker M, Kleb B, Klose K J and Heverhagen J T 2011 The presence of iodinated contrast agents amplifies DNA radiation damage in computed tomography *Contrast Media Mol. Imaging* **6** 507–13

Pinto M, Prise K M and Michael B D 2002 Quantification of radiation induced DNA double-strand breaks in human fibroblasts by PFGE: testing the applicability of random breakage models *Int. J. Radiat. Biol.* **78(5)** 375-88

Prise K M, Ahnström G, Belli M, Carlsson J, Frankenberg D, Kiefer J, Lobrich M, Michael B D, Nygren J, Simone G and Stenerlöw B 1998 A review of DSB induction data for varying quality radiations *Int. J. Radiat. Biol.* **74** 173–84

Piechowiak E I, Peter J-F W, Kleb B, Klose K J and Heverhagen J T 2015 Intravenous iodinated contrast agents amplify DNA radiation damage at CT *Radiology* **275** 692–7

Ratnayake R K, Semenenko V A, Stewart R D 2006 Retrospective analysis of double-strand break rejoining data collected using warm-lysis PFGE protocols *Int. J. Radiat. Biol.* **82(2)** 139

Regulla D, Schmid E, Friedland W, Panzer W, Heinzmann U and Harder D 2002 Enhanced values of the RBE and h ratio for cytogenetic effects induced by secondary electrons from an X-irradiated gold surface *Radiat. Res.* **158** 505–15

Rothkamm K, Balroop S, Shekhdar J, Fernie P and Goh V 2007 Leukocyte DNA

damage after multi-detector row CT: a quantitative biomarker of low-level radiation exposure. *Radiology* **242** 244–51

Rothkamm K and Löbrich M 2003 Evidence for a lack of DNA double-strand break repair in human cells exposed to very low X-ray doses *Proc. Natl. Acad. Sci. U.S.A.* **100** 5057–62

Rothkamm K and Löbrich M 2002 Misrepair of radiation-induced DNA double-strand breaks and its relevance for tumorigenesis and cancer treatment (review). *Int. J. Oncol.* **21** 433–40

Semenenko V and Stewart R 2004 A fast Monte Carlo algorithm to simulate the spectrum of DNA damages formed by ionizing radiation *Radiat. Res.* **161** 451–7

Semenenko V and Stewart R 2006 Fast Monte Carlo simulation of DNA damage formed by electrons and light ions *Phys. Med. Biol.* **51** 1693
Spadinger I and Palcic B 1992 The relative biological effectiveness of ^{60}Co gamma-rays, 55 kVp X-rays, 250 kVp X-rays, and 11 MeV electrons at low doses. *Int. J. Radiat. Biol.* **61** 345–53

Stenerlöw B, Karlsson KH, Cooper B, Rydberg B 2003 Measurement of prompt DNA double-strand breaks in mammalian cells without including heat-labile sites: results for cells deficient in nonhomologous end joining *Radiat. Res.* **159(4)** 502.10.

Stenerlöw B, Hoglund E and Carlsson J 2002 DNA fragmentation by charged particle tracks *Adv. Space Res.* **30** 859–63

Stewart R D, Streitmatter S W, Argento D C, Kirkby C, Goorley J T, and Moffitt G 2015 Rapid MCNP simulation of the DNA double-strand break (dsb) relative biological effectiveness (RBE) of photons, neutrons, electrons, and light ions *Phys. Med. Biol.* **60** 8249-74

Stewart R D, Yu V K, Georgakilas A G, Koumenis C, Park J H and Carlson D J 2011 Effects of radiation quality and oxygen on clustered dna lesions and cell death *Radiat. Res.* **176** 587–60

Terasawa M, Shinohara A and Shinohara M 2014 Double-strand break repair-adox: Restoration of suppressed double-strand break repair during mitosis induces genomic instability *Cancer Sci.* **105** 1519–25

Tommasino F, Friedrich T, Scholz U, Taucher-Scholz G, Durante M and Scholz M 2013 A DNA double-strand break kinetic rejoining model based on the local effect model *Radiat. Res.* **180** 524–38

Tommasino F, Friedrich T, Scholz U, Taucher-Scholz G, Durante M and Scholz M 2015 Application of the local effect model to predict DNA double-strand break rejoining after photon and high-let irradiation *Radiat. Prot. Dosim.* **166** 66–70

Ultravist® Injection [package insert]. Berlin, Germany: Bayer HealthCare Pharmaceuticals; 2015

Venkatesh P, Panyutin I, Remeeva E, Neumann R and Panyutin I 2016 Effect of Chromatin Structure on the Extent and Distribution of DNA Double Strand Breaks Produced by Ionizing Radiation; Comparative study of hESC and differentiated cell lines *Int. J. Mol. Sci.* **17** 58–15

Worku M, Fersht N, Martindale C, Funes J M and Short S C 2013 Sequential transformation of mesenchymal stem cells is associated with increased radiosensitivity and reduced DNA repair capacity *Radiat. Res.* **179** 698–706

Zoubair M, Bardouni El T, Allaoui O and Boulaich Y 2013 Computing efficiency improvement in monte carlo simulation of a 12 mv photon beam medical LINAC *World J. Nucl. Sci. Technol.* **3** 14-21

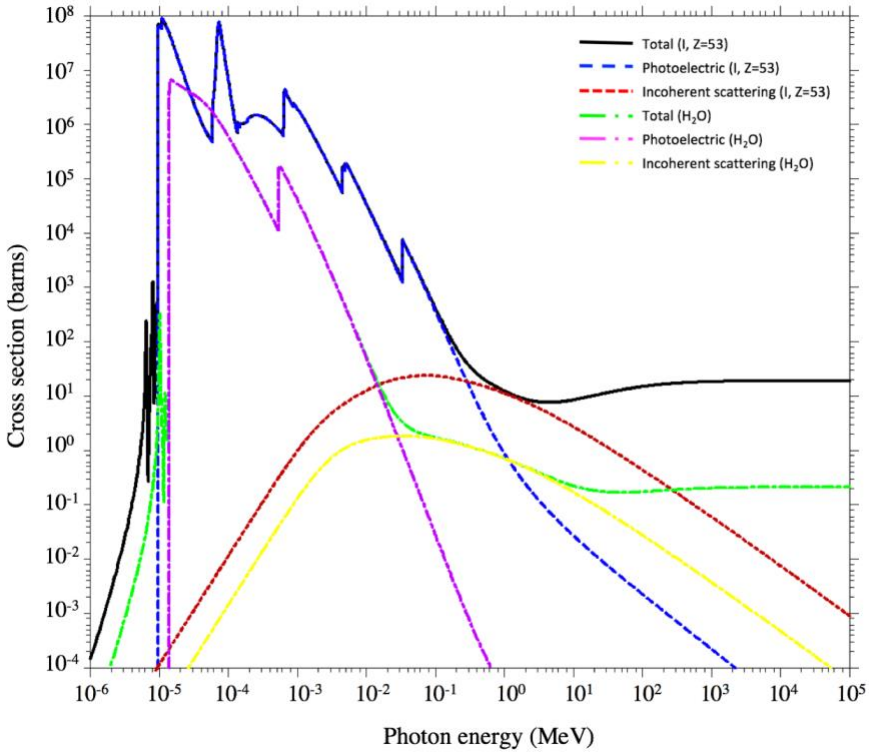

Figure 3.1. Independent photon cross sections for water and iodine, plotted with MCPLOT in MCNP6.1.1b, data from ENDF/B VI, version 8, eprdata (electron-photon-relaxation data) 12 (Hughes 2013).

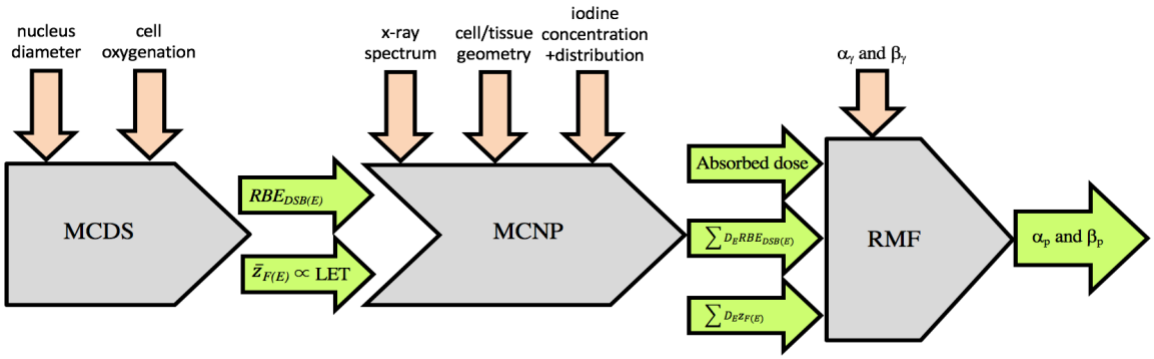

Figure 3.2. Flowchart of system of models. Models (grey), input parameters (orange) and output (green). Here, $\bar{z}_F$ is the mean-frequency specific energy, α_γ and β_γ are the linear and quadratic cell survival model parameters for the reference radiation (e.g., ^{60}Co γ-rays), respectively, and α_P and β_P are the predicted cell survival parameters for the test radiation (e.g., CT beam spectrum, CT beam spectrum + iodine contrast). The output summations from MCDS+MCNP are dose-averaged RBE_{DSB} and $\bar{z}_F$ from the spectrum of electrons with kinetic energy E.

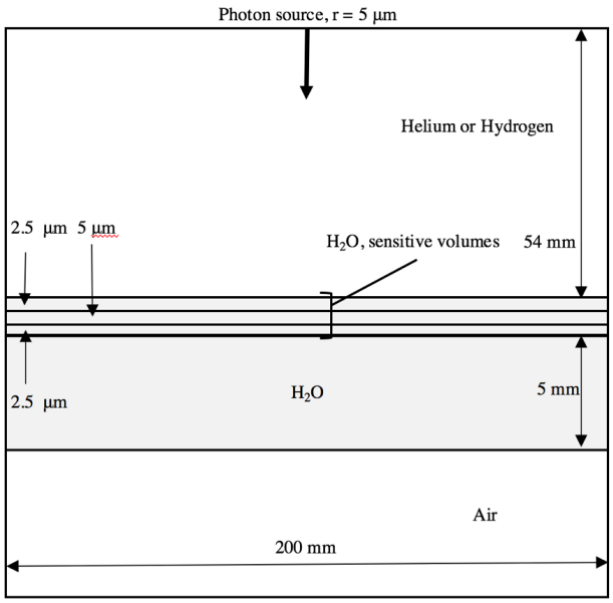

Figure 3.3. Idealized MCDS+MCNP model of a cell culture monolayer (not to scale).

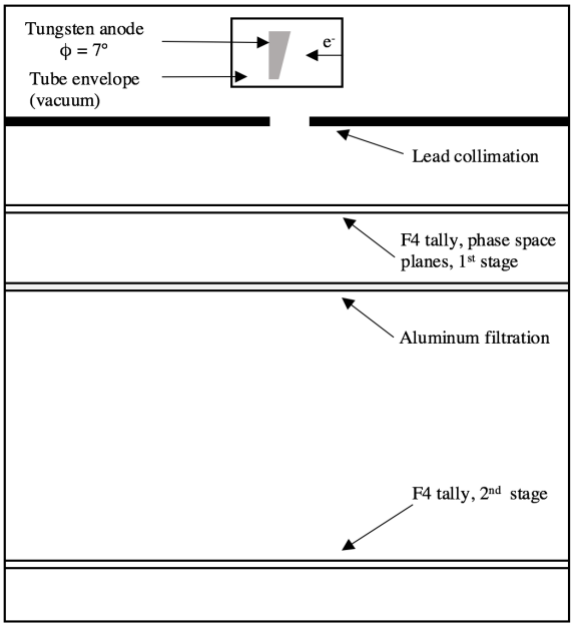

Figure 3.4. MCNP6 model bremsstrahlung model of photon production and filtration: Top to bottom, X-ray tube containing a tungsten wedge with an anode angle of 7° within a vacuum envelope, a 0.8 x 0.9 cm monodirectional, monoenergetic beam of electrons is incident the tungsten wedge, lead collimation, F4 tally to record photon energies and directions, aluminum or other filtration, and the last F4 tally, which records the final diagnostic photon spectra.

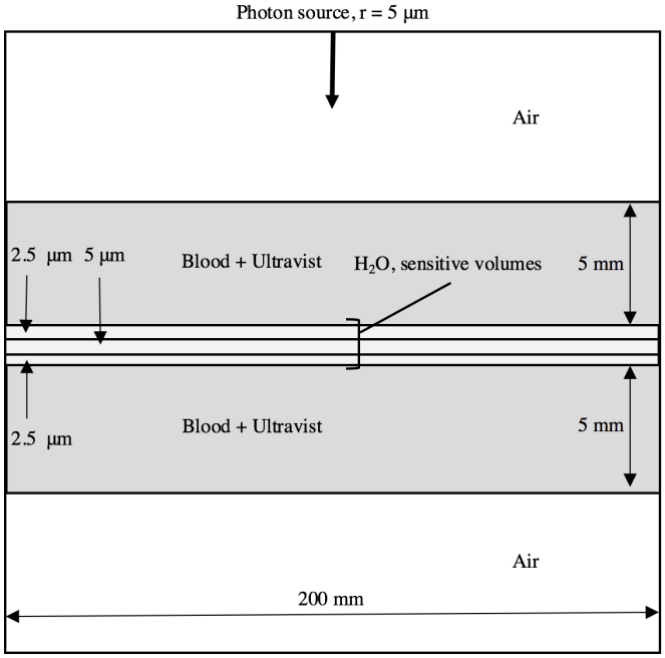

Figure 3.5. Idealized MCDS+MCNP model of lymphocytes in blood (not to scale).

Table 3.1. Comparison of measured and simulated estimates of the absolute and relative numbers of DSB created by ultrasoft X-rays in Chinese hamster V79-4 cells

Photon energy (keV)	DSB/Gy/Gbp (de Lara *et al.*)	DSB/Gy/Gbp (MCDS+MCNP)	RBE_{DSB} (de Lara *et al.*)	RBE_{DSB} (MCDS+MCNP)
0.28	20.7	23.2	2.7	2.7
0.96	17.4	20.8	2.3	2.4
1.49	14.3	18.3	1.9	2.1
4.55	10.4	13.3	1.4	1.5
^{60}Co γ-rays	7.6	8.6	1.0	1.0

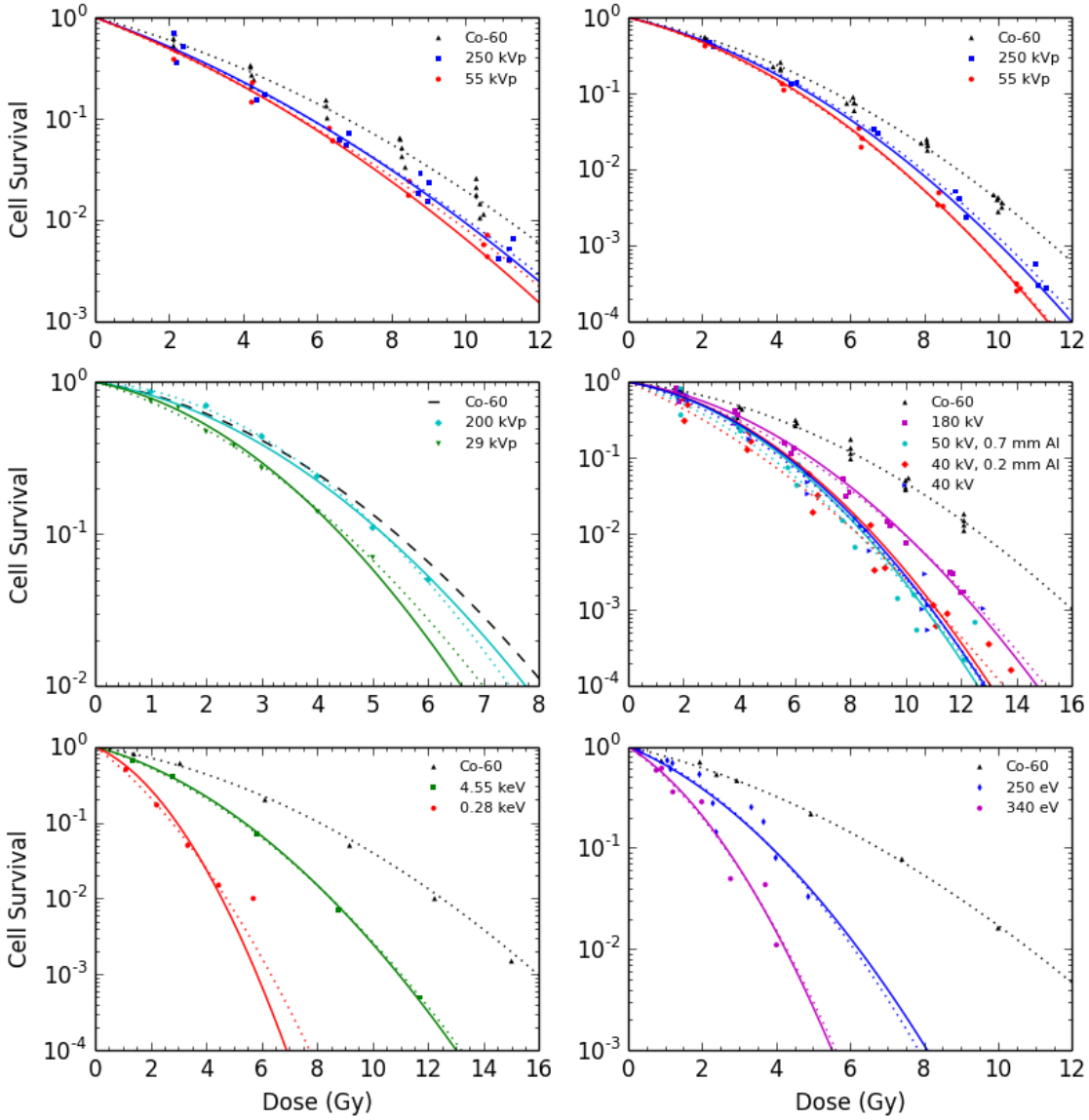

Figure 3.6. Cell survival as a function of dose due to exposure to low-energy X-rays. Spadinger and Palcic (1992) cell survival data for V79 and CHO cell lines (upper left and right graphs, respectively), Frankenberg *et al.* (2002) cell survival data for CGL1 cells (middle left graph), Hoshi *et al.* (1988) cell survival data for V79 cells (middle right graph), de Lara *et al.* (2002) cell survival data for V79 cells (lower left graph), and Fayard *et al.* 2002 data for V79 cells (lower right graph). Dotted lines represent linear quadratic fits; solid lines represent an RMF-fit (Eq. 3.3).

Table 3.2. Comparison of RBE_{DSB} estimates using an RMF-fit (Eq. 3.3) and MCDS+MCNP simulations

Reference	Cell line	Photon energy (keV)	RBE_{DSB} (RMF-fit)	RBE_{DSB} (MCDS+MCNP)	% diff, rel. to RMF-fit
Spadinger and Palcic	V79	250	1.13	1.14	0.88
	CHO	250	1.12	1.14	1.75
	V79	55	1.17	1.21	3.41
	CHO	55	1.21	1.21	0.00
Frankenberg *et al.*	CGL1	200	1.13	1.10	-2.65
	CGL1	29	1.17	1.18	0.85
Hoshi *et al.*	V79	180[a]	1.28	1.14	-11.0
	V79	50[b]	1.49	1.17	-21.5
	V79	40[c]	1.44	1.23	-14.6
	V79	40	1.47	1.32	-10.2
De Lara *et al.*	V79	4.55	1.42	1.50	5.63
	V79	0.28	2.67	2.70	1.12
Fayard *et al.*	V79	0.25	1.74	2.85	63.8
	V79	0.34	2.55	2.57	0.78

[a]0.5 mm Al + 1mm Cu
[b]0.7 mm Al
[c]0.2 mm Al

Table 3.3. Photon/electron interaction dependence on iodine concentration and distribution from MCNP6 Table 130

Iodine distribution	% iodine by weight	Compton recoil	Photo-electric	Auger
Homogenous	0.00	53.6%	8.5%	37.9%
	0.48	17.7%	8.5%	73.8%
	4.81	2.8%	7.9%	89.3%
Extracellular	0.48	49.4%	10.2%	40.5%
	4.81	33.6%	14.9%	51.6%

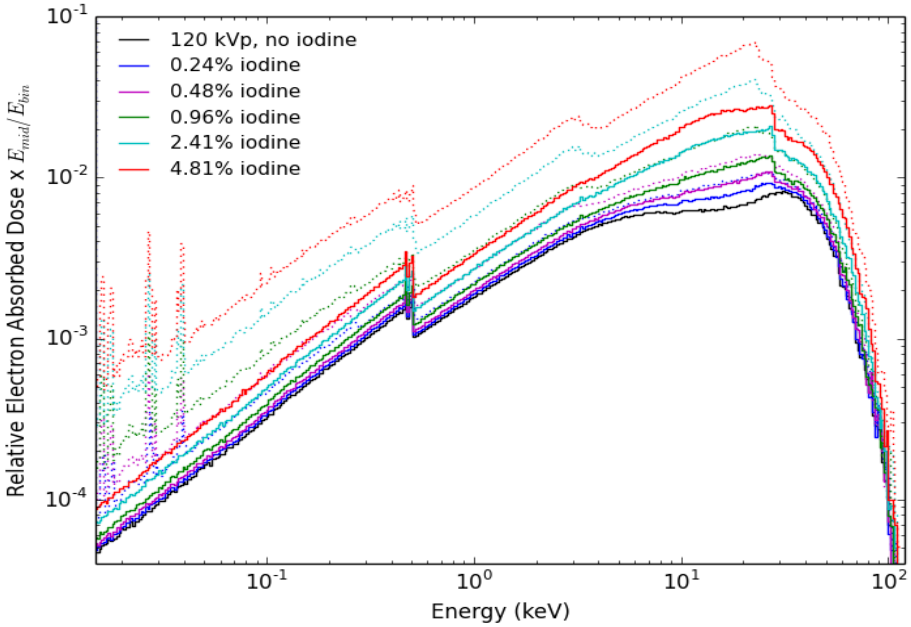

Figure 3.7. Dependence of the relative electron absorbed dose in a 5 μm layer on iodine concentration in blood (by weight) surrounding the center sensitive volume, normalized to blood without contrast. Solid lines indicate the absorbed dose for an extracellular iodine distribution in the microdosimetry phantom shown in Figure 3.5 (outside sensitive volumes), while dotted lines indicate a homogenous iodine distribution (throughout the phantom and sensitive volumes).

Table 3.4. Absorbed dose, RBE_{DSB} and RWD prediction for varying concentrations of iodine in blood for 120 kVp X-rays, 10.5 mm Al filtration in a 5 μm layer (Figure 3.5).

Distribution	% iodine by weight	E_{MEAN}[1] (keV)	$D/D_{I=0}$ (DEF)	LET[1] (keV/μm)	RBE_{DSB}[1,2]	RWD/ ΔD	RWD/ $RWD_{I=0}$	Exp. comparison *in vitro*	Exp. comparison *in vivo*
Homogenous	0.00	15.83	1.00	4.17	1.22	—	1.00		
	0.24	13.31	1.51	6.19	1.52	1.25	1.88		
	0.48	12.36	2.01	7.72	1.59	1.29	2.60		
	0.96	11.35	2.92	8.71	1.69	1.38	4.04		
	2.41	10.57	5.36	9.45	1.77	1.45	7.75		
	4.81	10.53	8.45	9.51	1.77	1.45	12.28		
Extracellular	0.24	15.86	1.11	4.07	1.21	1.00	1.11		
	0.48	16.01	1.22	3.97	1.21	1.00	1.22		
	0.96	16.11	1.43	3.85	1.20	0.98	1.40		1.07±0.19[3], 1.58[5], 1.30[6]
	2.41	16.47	2.00	3.63	1.18	0.97	1.94	2.35±0.59[5]	
	4.81	16.83	2.70	3.45	1.17	0.96	2.58	2.3±0.5[4]	

[1]Reflects dose-weighted averages
[2]Reference low-LET radiation of ^{60}Co γ-rays
[3]Piechowiak *et al.* 2015
[4]Jost *et al.* 2009
[5]Pathe *et al.* 2011
[6]Gruzenski *et al.* 2009

CHAPTER 4

MCNP6 TALLYX IMPLEMENTATION FOR EFFICIENT MULTISCALE RELATIVE BIOLOGICAL EFFECTIVENESS (RBE) MODELING[3]

4.1 Introduction

This work proposes a more efficient and unified way to integrate information from the cell-level DNA damage software, the Monte Carlo Damage Simulation (MCDS)[1-3], with the general-purpose Monte Carlo code, Monte Carlo N-Particle (MCNP6)[4]. With the advancement of proton and heavy ion therapy, accurate relative biological effectiveness (RBE) modeling is key to the optimization and success of such treatments. It is desirable to have a computationally efficient and integrated solution that requires a minimal number of adjustable parameters and reliance on experimental data. While most radiobiological studies have focused on DSB-induction as the primary initiating event for other effects such as chromosomal aberrations and cell death, SSB and BD have received far less attention. A DSB, defined as at least two strand breaks on opposite side of the DNA strand within 10 base-pairs (bp) of each other, are the most difficult to repair. Within the DSB classification there are subsets of varying complexity, where DSBs

[3] This chapter is adapted from an article in preparation for submission to *Medical Physics*

include other strand breaks and base damages. However, the quantity of single-strand break (SSB) and base damage (BD) induction is much larger when compared to DSB, for example, for low-LET radiation, ~1,000 SSBs and up to 25,000 BDs per Gy per cell are induced, compared to only about 40 DSBs.[1] DSBs and clustered lesions (consisting of >2 SSB, abasic (AP) sites, oxidized purine or pyrimidine bases, or double strand breaks (DSB), formed within one or two helix turns), also termed local multiply damaged sites (LMDS)[5-7], are likely the initiating events in biological effects like reproductive cell death. Others have proposed that further investigation is warranted to determine the degree which clusters of non-DSB lesions attribute to finding some situations in which DSBs alone cannot describe biological effects, such as loss of plasmid DNA functionality[6]. Therefore, part of this work focuses on also integrating functions of SSB and BD induction functions into the MCNP6 source code.

Utilizing the MCNP6 tallyx subroutine to integrate biophysical models into general purpose Monte Carlo codes is beneficial for efficient multiscale RBE modeling, especially for mixed fields of radiation. It provides an easy way to generate dose-averaged biological metrics within a single function, without the need for a custom lookup table for every particle type. It is also easier to modify the function if necessary for high-LET corrections, as compared to generating new tables of data, making it easier for the end-user and future applications.

4.2 Methods

4.2.1 MCDS functions of RBE_{DSB}, RBE_{SSB} and RBE_{BD}

As presented in Stewart *et al.*,[8] the MCDS estimates of DSB induction produced in both aerobic and anoxic cells with respect to the particle's $(z_{eff}/\beta)^2$ have been fit to empirical formulas across a wide range of particle types and energies – electrons up to ^{56}Fe ions, with $2 \leq (z_{eff}/\beta)^2 \leq 10^5$. Here, z_{eff} is the effective charge of the ion, which accounts for screening due to atomic electrons, and β is the velocity of the ion with respect to the speed of light. Empirical formulas already derived (Eq. 4.1, 4.4), as well as newly fitted functions for SSB and BD induction (Eq. 4.2, 4.3, 4.5, 4.6) were used. The TableCurve 2D Version 5.01.01 (SYSTAT Software Inc. 2002) software was used to perform an automated regression analysis of the MCDS estimates; utilizing the formula with the best r^2. Parameters used in Eq. 4.1 to 4.6 are contained in Table 4.1.

Reference low-LET values to convert the number of cluster types per Gy per Gbp to respective RBE were obtained by modeling a ^{60}Co source on a monolayer of cells and computing the dose-averaged RBE values in MCNP6. For aerobic conditions the resultant values are 8.32 DSB, 188.63 SSB and 425.26 BD $Gy^{-1}Gbp^{-1}$. Under anoxic conditions the values are 2.86 DSB, 115.53 SSB and 293.98 BD $Gy^{-1}Gbp^{-1}$. Figure 4.1 reflects the RBE using these reference values, from electrons up to ^{56}Fe. Here $x=(z_{eff}/\beta)^2$

Aerobic Cells (100% pO_2)

$$RBE_{DSB} = a + b - \left\{b^{(1-d)} + cx(d-1)\right\}^{\frac{1}{1-d}} \quad (4.1)$$

$$RBE_{SSB} = \frac{a+c\sqrt{x}+ex}{1+b\sqrt{x}+dx+fx^{1.5}} \tag{4.2}$$

$$RBE_{BD} = \frac{a+c\sqrt{x}+ex}{1+b\sqrt{x}+dx+fx^{1.5}} \tag{4.3}$$

Anoxic Cells (0% pO_2)

$$RBE_{DSB} = \frac{a+\sqrt{x}\{c+\sqrt{x}[e+\sqrt{x}(g+i\sqrt{x})]\}}{1+\sqrt{x}\{b+\sqrt{x}[d+\sqrt{x}(f+h\sqrt{x})]\}} \tag{4.4}$$

$$RBE_{SSB} = \frac{a+cln(x)+eln(x)^2+gln(x)^3+iln(x)^4}{1+bln(x)+dln(x)^2+fln(x)^3+hln(x)^4+jln(x)^5} \tag{4.5}$$

$$RBE_{BD} = \frac{a+cln(x)+eln(x)^2+gln(x)^3+iln(x)^4}{1+bln(x)+dln(x)^2+fln(x)^3+hln(x)^4+jln(x)^5} \tag{4.6}$$

4.2.2 Microdosimetric functions

Past the absolute and relative yields of different DNA damage, it is advantageous to be able to estimate important microdosimetric quantities in a larger-scale general purpose Monte Carlo code. For instance, to compute the average DSBs, SSBs or BDs per particle track, an important factor in the repair-misrepair-fixation (RMF) model of cell survival[8,9] (and other RBE models), the mean-frequency specific energy must be known. The RMF has been applied to helium ion therapy[10] and heavy ion therapy[11] using a different combination of codes. In the ICRU report 36[12], the mean-frequency specific energy is defined as $\bar{z}_F = 0.204\text{LET}/\rho d^2$, where ρ is the density of water (1 g/cc) and d is the diameter of the nucleus (5 μm). For particles with CSDA ranges > mean chord length

through the nucleus ($2d/3$), this is a good approximation and can be easily integrated into MCNP using its computed stopping power values. For CSDA ranges ≤ the mean chord length $\bar{z}_F$ will be overestimated under the ICRU definition, while the MCDS computes $\bar{z}_F$ to account for these "stoppers." The ICRU definition was integrated into the tallyx.F90 subroutine for these cases, the variables for ρ and d could then be user-defined in the MCNP6 input file if desired. Furthermore, by introducing the formulation of $\bar{z}_F$ directly into MCNP6, the impact of the chemical compositions of the nucleus of $\bar{z}_F$ can be assessed, as others have shown there can be significant differences in the number of ionization events using realistic molecular compositions and densities of cellular components when compared to a simple water medium,[12] which MCDS and most other microdosimetry codes use.

4.2.3 MCNP integration using the tallyx.f90 subroutine

One current solution for computing dose-averaged values of RBE_{DSB}, RBE_{SSB}, RBE_{BD} and other relevant physical and radiobiological metrics as applied to MCNP6 is the use of dose response (DE/DF) functions. The dose response functions modify a standard F6 heating tally with a lookup table that contains particle energy (DE) and corresponding RBE_{DSB}, RBE_{SSB}, RBE_{BD} values (DF) obtained from MCDS simulations. When assessing a mixed field of radiation, a DE/DF table is required for each particle type being tracked. This approach has been used to test a variety of experimental and clinical scenarios, looking at electrons, light ions and neutron fields.[6] Since this and past work has shown that all the DNA cluster types analyzed here follow the same trends with respect to $(z_{eff}/\beta)^2$, it follows that a function describing these trends could serve as a

generalized equation embedded in MCNP6 that could be called for any simulation, regardless of mode or particle(s) type. For accurate RBE calculations, all possible secondary particles must be tracked, as they mediate the absorbed dose and RBE effects. Using dose response functions, 2*n* tallies are required, where *n* is the number of particle types tracked. Using tallyx, only 2 tallies are required regardless of the quantity of particle types tracked; one tally for total absorbed dose and one tally for the total RBE-weighted dose (RWD).

The tallyx.f90 subroutine is part of the MCNP6 source code that allows the user to modify and customize the standard tallies. The tallyx implementation described here integrates Eq.1-6 derived above to modify any standard MCNP6 tally, including lattice tallies. The tallyx subroutine, as used here, pulls data for the rest mass, kinetic energy and charge of the particle(s) from other subroutines to calculate $(z_{eff}/\beta)^2$. Using the card *FUn* in the MCNP6 input file calls the tallyx subroutine to modify the tally, where *n* is the tally number. The resultant output is a dose-weighted or dose-weighted RBE. Using F6:# (all heavy ions, Z > 2) or +F6 (all charged particles), the output is defined as:

$$RWD_i = \sum_j \int_0^\infty D_j\,(E) RBE_{i,j}(E) \tag{4.7}$$

Here, the product $D_j(\mathrm{E})\cdot RBE_{i,j}(\mathrm{E})$ is integrated over all particle types *j* and kinetic energies *E* for the desired endpoints *i* (e.g., DSB, SSB, BD). As it relates to the dose response table option, each modified tally only contributes to the output of a one specific particle *j* and must be weighted and summed with any other transported particles dose response output.

In the same manner, LET and $\bar{z}_F$ are dose-weighted, but using the built-in physics models of MCNP, rather than lookup tables. Since the MCNP-computed stopping powers are easy to access in the source code, it is called to compute LET as well as $\bar{z}_F$ for CSDA ranges >> mean chord length through the nucleus using the ICRU formula in Section 4.3.2. At ranges approaching the nucleus diameter, it will integrate the LET over the path length to estimate $\bar{z}_F$. For particle ranges < mean chord length, it is assumed that all the energy of the particle is deposited within the target (cell nucleus) and hence, logic is built into the tallyx.F90 subroutine to switch over to the formulation of $\bar{z}_F$ = KE (kinetic energy of incident particle)/ mass of nucleus. This inclusion allows for all necessary radiobiological variables to be obtained/computed within MCNP without external libraries or lookup tables from MCDS.

4.3 Results

4.3.1 Comparisons of DE/DF with TALLYX Results

As an initial test, a monoenergtic and polyenergetic selection of protons, alpha particles and carbon ions were simulated on a cell monolayer in aerobic and anoxic conditions (utilizing Eq. 1 and Eq. 4, respectively) and dose and dose × RBE_{DSB} are tallied using both the tallyx approach and dose response approach. Table 4.2 shows the results of the RBE_{DSB} using the different approaches, with differences < 0.5%.

Further simulations were performed for a mixed particle field. Table 4.3 shows some result for some simple mixed fields. The examples use a mix of alpha particles, carbon ions and protons. For the DE/DF implementation, two custom dose response tables are needed and the dose-averaging of the RBE is computed manually from four

separate tally results (DE/DF output + absorbed dose output). For the tallyx implementation only the +F6 tally is needed and all particle dose and RBE contributions and weighting is computed in one tally. Functions of RBE_{SSB} and RBE_{BD} were also tested for monoenergetic and mixed fields, results are tabulated in Tables 4.4 and 4.5. With the exception of some of the carbon ion simulations, which are still less than ~3% different, the two approaches agree within 0.5%. This may be due to the differences in $(z_{eff}/\beta)^2$ calculations between MCDS and MCNP, but it is still a minor discrepancy.

4.4 Discussion and Conclusions

A new approach to integrating RBE models into MCNP6 is proposed and benchmarked with an existing solution. While the tallyx approach has not been found to speed up computational time to any significant degree compared to dose response functions in the cases tested here, its utility is apparent, from a simplification and efficiency standpoint, during simulations involving mixed radiation fields (using either the F6:# (heavy ion heating tally) or +F6 (total heating tally) in a mixed-field simulation). To properly assess the RBE in a mixed field of radiation, all possible secondary charged particles are tracked and weighted. Using tallyx, all ion RBE parameters are computed with a single function and multiple lookup tables are unnecessary. The microdosimetric functions of LET and $\bar{z}_F$ are also integrated, but utilizing MCNP's built-in physics models. Additionally, new empirical formulas for the endpoints of SSB and BD induction have been derived across a large range of particle types and charges that they can be implemented within the tallyx.f90 subroutine in the same manner as the RBE_{DSB} formulas were. This provides further means to investigate these lesser studied lesions in

the context of a multiscale model.

The tallyx implementation discussed in this paper is still at an early stage of development and needs some work to further refine the user interface and variable selection in the MCNP source code to make it more accessible to all users who may wish to implement the source code modification. However, initial results are encouraging and as treatment planning optimization shifts from physical constraints (e.g., dose-volume) to biological response models[15], this implementation should prove a useful tool in this ongoing emphasis. Described here, equations 1-6 can also be utilized in other general-purpose Monte Carlo codes or treatment planning systems (TPS) that have the ability to modify the tally or scoring function as a function of $(z_{eff}/\beta)^2$.

4.5 References

1. Semenenko V, Stewart R. A fast Monte Carlo algorithm to simulate the spectrum of DNA damages formed by ionizing radiation. *Radiat Res.* 2004;161(4):451-457.

2. Semenenko V, Stewart R. Fast Monte Carlo simulation of DNA damage formed by electrons and light ions. *Phys Med Biol.* 2006;51:1693-1706.

3. Stewart RD, Yu VK, Georgakilas AG, Koumenis C, Park JH, Carlson DJ. Effects of radiation quality and oxygen on clustered DNA lesions and cell death. *Radiat Res.* 2011;176(5):587-602. doi:10.1667/RR2663.1.

4. Goorley T, James M, Booth T, *et al.* Initial Mcnp6 release overview. *Nucl Technol.* 2012;180(3):298-315.

5. Ward J. DNA damage produced by ionizing radiation in mammalian cells: identities, mechanisms of formation, and reparability. *Prog Nucleic Acid Res Mol Biol.* 1988;35(1):95-125.

6. Saloua KS, Sonia G, Pierre C, Léon S, Darel HJ. The relative contributions of DNA strand breaks, base damage and clustered lesions to the loss of DNA functionality induced by ionizing radiation. *Radiat Res.* 2014;181(1):99-110.

7. Sage E, Shikazono N. Radiation-induced clustered DNA lesions: Repair and mutagenesis. *Free Radic Biol Med*. 2016;107(2017):125-135

8. Stewart RD, Streitmatter SW, Argento DC, Kirkby C, Goorley JT, Moffitt G, Jevremovic T and Sandison GA. Rapid MCNP simulation of DNA double strand break (DSB) relative biological effectiveness (RBE) for photons, neutrons, and light ions. *Phys Med Biol*. 2015;60(21):8249-8274. doi:10.1088/0031-9155/60/21/8249.

9. Carlson D, Stewart R, Semenenko V, Sandison G. Combined use of Monte Carlo DNA damage Simulations and deterministic repair models to examine putative mechanisms of cell killing. *Radiat Res*. 2008;169(4):447-459.

10. Frese M, Yu V, Stewart R, and Carlson D. A mechanism-based approach to predict the relative biological effectiveness of protons and carbon ions in radiation therapy. *Radiat Oncol Biol*. 2012;83(1):442-450. doi:10.1016/j.ijrobp.2011.06.1983.

11. Mairani A, Dokic I, Magro G, *et al.* Biologically optimized helium ion plans: calculation approach and its *in vitro* validation. *Phys Med Biol*. 2016;61:4283-4299. doi:10.1088/0031-9155/61/11/4283.

12. Kamp F, Cabal G, Mairani A, Parodi K, Wilkens JJ, Carlson DJ. Fast biological modeling for voxel-based heavy ion treatment planning using the mechanistic repair-misrepair-fixation model and nuclear fragment spectra. *Int J Radiat Oncol Biol Phys*. 2015;93(3):557-568. doi:10.1016/j.ijrobp.2015.07.2264.

13. ICRU. Microdosimetry. Report No. 36. *International Commission on Radiation Units and Measurements*. 1983.

14. Douglass M, Bezak E, Penfold S. Development of a randomized 3D cell model for Monte Carlo microdosimetry simulations. *Am Assoc Phys Med.* 2012;39(6):3509-3519. doi:10.1118/1.4719963.

15. Allen Li X, Alber M, Deasy JO, *et al.* The use and QA of biologically related models for treatment planning: short report of the TG-166 of the therapy physics committee of the AAPM. *Am Assoc Phys Med.* 2012;39(3):1386-1409. doi:10.1118/1.3685447.

Table 4.1. Parameter values for empirical formulas (Eq. 4.1-4.6) to estimate RBE_{DSB}, RBE_{SSB} and RBE_{BD} for aerobic and anoxic cells as a function of $(z_{eff}/\beta)^2$

parameter	Aerobic (100% pO_2)			Anoxic (0% pO_2)		
	RBE_{DSB} (4.1)	RBE_{SSB} (4.2)	RBE_{BD} (4.3)	RBE_{DSB} (4.4)	RBE_{SSB} (4.5)	RBE_{BD} (4.6)
a	9.902×10^{-1}	1.001	9.932×10^{-1}	1.502	9.995×10^{-1}	1.000
b	2.411	-3.754×10^{-3}	5.621×10^{-1}	1.611	-4.457×10^{-1}	-4.074×10^{-1}
c	7.32×10^{-4}	-3.468×10^{-3}	5.693×10^{-1}	1.037	-4.439×10^{-1}	-4.109×10^{-1}
d	1.539	6.658×10^{-4}	1.375×10^{-1}	-1.15×10^{-2}	7.667×10^{-2}	6.145×10^{-2}
e	—	2.142×10^{-4}	1.384×10^{-1}	1.35×10^{-1}	7.574×10^{-2}	6.544×10^{-2}
f	—	1.028×10^{-7}	2.724×10^{-3}	-6.096×10^{-4}	-5.974×10^{-3}	-3.025×10^{-3}
g	—	—	—	-8.230×10^{-3}	-5.922×10^{-3}	-4.821×10^{-3}
h	—	—	—	3.047×10^{-5}	1.601×10^{-4}	-1.619×10^{-4}
i	—	—	—	3.077×10^{-4}	1.818×10^{-4}	1.410×10^{-4}
j	—	—	—	—	2.176×10^{-6}	1.740×10^{-5}

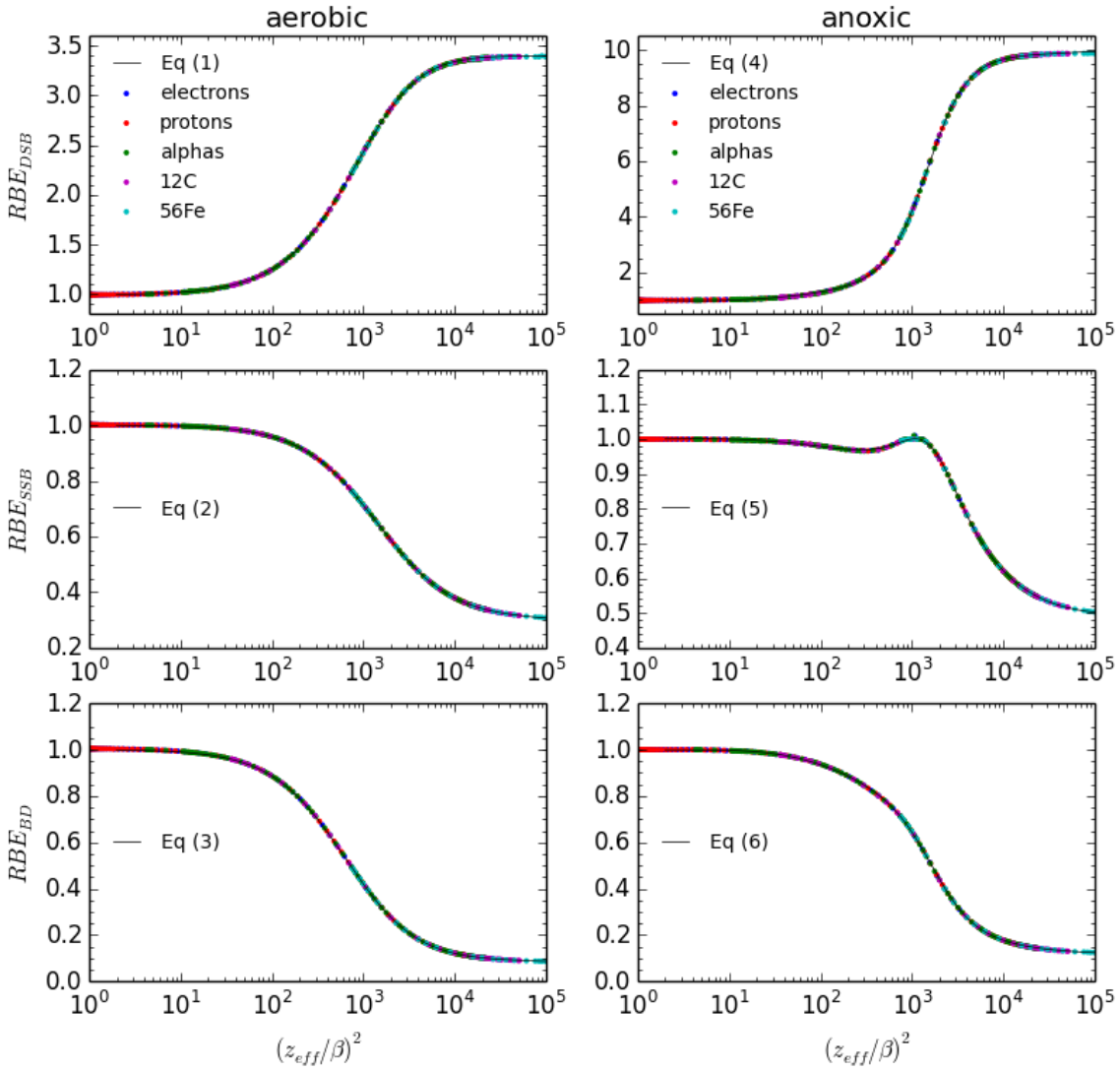

Figure 4.1. Plots of RBE_{DSB}, RBE_{SSB} and RBE_{BD} vs. $(z_{eff}/\beta)^2$ for mammalian cells ($d_{nucleus}$ = 5 μm) in aerobic (100% pO_2) and anoxic (0% pO_2) environments with respect to ^{60}Co γ-rays. Data from MCDS version 3.10A simulations.

Table 4.2. Comparison between DE/DF and TALLYX dose-averaged *RBE$_{DSB}$* results, single ion tallies for mono and polyenergetic sources

			RBE_{DSB}		
particle	% O_2	E (MeV)	DE/DF	TALLYX	Diff (%)*
$^{1}H^{+}$	100	20	1.0644	1.0638	-0.048
$^{1}H^{+}$	0	20	1.0675	1.0662	-0.118
$^{1}H^{+}$	100	0.5-16	1.5085	1.5073	-0.076
$^{1}H^{+}$	0	0.5-16	1.9254	1.9282	0.141
$^{4}He^{2+}$	100	5	2.7287	2.7298	0.039
$^{4}He^{2+}$	0	5	5.9464	5.9533	0.115
$^{4}He^{2+}$	100	0.5-3	3.2243	3.2268	0.077
$^{4}He^{2+}$	0	0.5-3	9.0719	9.0949	0.254
$^{12}C^{6+}$	100	20	3.3228	3.3333	0.313
$^{21}C^{6+}$	0	20	9.5893	9.6262	0.385

*difference in tallyx with respect to de/df result

Table 4.3. Comparison between DE/DF (F6:# + F6:A) and TALLYX (+F6) dose-averaged *RBE$_{DSD}$* results, mixed ion tallies for polyenergetic sources

				RBE_{DSB}		
particles	% O_2	E (MeV)	weight	DE/DF	TALLYX	Diff (%)*
$^{4}He^{2+}$	100	5	0.75	3.1437	3.1441	0.011
$^{12}C^{6+}$		20	0.25			
$^{4}He^{2+}$	0	5	0.75	8.4818	8.4724	-0.111
$^{12}C^{6+}$		20	0.25			
$^{1}H^{+}$	100	10	0.5	2.5190	2.5194	0.016
$^{4}He^{2+}$		3	0.5			
$^{1}H^{+}$	0	10	0.5	5.2533	5.2693	0.304
$^{4}He^{2+}$		3	0.5			

*difference in tallyx with respect to de/df results

Table 4.4. Comparison between DE/DF and TALLYX dose-averaged RBE_{SSB} and RBE_{BD} results, single ion tallies for mono and polyenergetic sources

			RBE_{SSB}			RBE_{BD}		
particles	% O_2	E (MeV)	DE/DF	TALLYX	Diff (%)*	DE/DF	TALLYX	Diff (%)*
$^{1}H^{+}$	100	20	0.9899	0.9904	0.047	0.9710	0.9698	-0.132
$^{1}H^{+}$	0	20	0.9945	0.9950	0.057	0.9842	0.9857	0.148
$^{1}H^{+}$	100	0.5-16	0.9046	0.9032	0.156	0.7835	0.7840	0.067
$^{1}H^{+}$	0	0.5-16	0.9751	0.9747	-0.034	0.8688	0.8694	0.070
$^{4}He^{2+}$	100	5	0.6309	0.6312	0.047	0.3211	0.3218	0.215
$^{4}He^{2+}$	0	5	0.9823	0.9822	-0.011	0.5139	0.5156	0.330
$^{4}He^{2+}$	100	0.5-3	0.4408	0.4410	0.053	0.1616	0.1613	-0.155
$^{4}He^{2+}$	0	0.5-3	0.7246	0.7242	-0.061	0.2427	0.2423	-0.179

*difference in tallyx with respect to de/df results

Table 4.5. Comparison between DE/DF (F6:# + F6:A,H) and TALLYX (+F6) dose-averaged RBE_{SSB} and RBE_{BD} results, mixed ion tallies for polyenergetic sources

				RBE_{SSB}			RBE_{BD}		
particles	% O_2	E (MeV)	wgt.	DE/DF	TALLYX	Diff (%)*	DE/DF	TALLYX	Diff (%)*
$^{4}He^{2+}$	100	5	0.75	0.6160	0.6300	2.272	0.1361	0.1398	0.272
$^{12}C^{6+}$		20	0.25						
$^{4}He^{2+}$	0	5	0.75	0.3835	0.3917	2.145	0.2015	0.2081	3.27
$^{12}C^{6+}$		20	0.25						
$^{1}H^{+}$	100	10	0.5	0.6715	0.6720	0.076	0.4005	0.4004	-0.250
$^{4}He^{2+}$		3	0.5						
$^{1}H^{+}$	0	10	0.5	0.9350	0.9343	-0.080	0.5652	0.5653	0.018
$^{4}He^{2+}$		3	0.5						

*difference in tallyx with respect to de/df results

CHAPTER 5

CONCLUSIONS AND FUTURE WORK

5.1 Contributions

In this work, the accuracy of a useful multiscale RBE model has been tested against *in vitro* and *in vivo* laboratory experiments and then applied to a range of clinical issues arising radiology (diagnostic X-ray imaging) and in radiation oncology. The special cases examined found 1) the RBE for high-LET, short-range particles can be modeled in the multiscale framework, but some correction may be needed to improve the accuracy of the model may be needed 2) for low-LET particles, specifically the range of secondary electrons encountered in diagnostic X-ray imaging, the RBE_{DSB} alone can be used to accurately predict (within a few percent) other photon and electron cell survival with the α and β parameters for a reference radiation and essentially no *ad hoc* variables (e.g., the low-dose term in the RMF model is negligible) and 3) beyond DSB, empirical formulas can be fitted to SSB and BD induction, as they follow the same trends across a wide range of particle types and energies. These empirical formulas have been integrated in MCNP as generalized formulas for generating a wide-variety of biological metrics from macroscopic simulations of radiation transport. This can greatly simplify and streamline the multiscale implementation for a variety of different, complex radiation fields.

5.1.1 RBE for high-LET particles and effects of boron distribution

In the case of BNCT, past *in vitro/in vivo* were benchmarked with the multiscale model with good agreement. Several neutron sources, including one used for fast neutron therapy (UW CNTS) were examined for their impact on dose and RBE as well as to assess hypothetical boron distributions. The high-LET ^{7}Li particles and alpha particles tested the limits of the multiscale model, LET > 200 keV/μm and CSDA ranges ≤ 5 μm, but it was shown that even these scenarios can be assessed with the model with some modifications. This will aid the efforts in advancing RBE modeling in heavy ion therapy modalities, as these special cases are encountered near the end of the particle's track (Bragg peak), where there is a buildup of high-energy nuclear fragments. As heavier ions (Z > 2) are of interest for radiotherapy, the need for accurate RBE modeling becomes increasingly important.

5.1.2 RBE for low-LET particles and effects of X-ray contrast

The most important finding from examining the RBE of diagnostic CT X-rays (with or without contrast) within the repair-misrepair-fixation (RMF) model was a further simplification of the framework to quantify cell survival. As discussed in Chapter 3, it was determined that for the range of secondary electron energies encountered in diagnostic X-ray exams, and further, really the entire range of electron energies applied to mammalian cells, that $RBE_{LD} = RBE_{HD} = RBE_{DSB}$. This provides support that, regardless of the secondary electron energy spectra, estimates of RBE_{DSB} alone can be used to accurately predict other photon and electron cell survival curves with no other knowledge than the survival curve for a reference radiation (e.g., ^{60}Co or ^{137}Cs γ-rays).

Benchmarking the model-predicted estimates DSB induction against results from *in vitro* and *in vivo* experiments in blood lymphocytes showed good agreement for high and low concentrations of contrast. The findings also showed that the more plausible case in iodine-enhanced CT, that the iodine was extracellular with respect to the blood lymphocytes, yielded model-predicted results in-line with experimental data, where homogeneous distribution would overestimate dose and RBE effects. There still remains the question of whether the impact of these enhancements to the blood will translate into increased long-term cancer risk in patients undergoing these exams, but the tools laid out here can aid in further studies.

5.1.3 Refinements, additions, and simplification of the model

The last part of this work develops a method to further integrate and streamline the computational implementation of the model in MCNP. It also expands the scope of the model to encompass categories of DNA damage other than the DSB (SSB and base damage). The majority of the reported studies (Chapter 2-3) used dose response functions, or essentially look up tables in MCNP6 to compute the RBE values, requiring a unique table generated from MCDS output per particles type. With the work contained in Chapter 4, general, empirical formulas are integrated into the source code of MCNP6 which can be called for any particle(s) for dose-averaged output of RBE_{DSB}, $RBE_{SSB,}$ and $RBE_{BD.}$ Additional microdosimetric parameters are also integrated, which are needed for integration of the RMF model and other applications. As mentioned in the chapter, it is still at an early stage of development and there is much potential for expansion.

5.2 Future Work

There are several aspects of this work that can be investigated further and validated with experimental data:

- Further examination of the so called "overkill" phenomenon that occurs with high-LET particles, such as the $^{7}Li^{3+}$ ions in BNCT and fragmentation ions from heavy ion therapy. That is, the decrease in RBE or cell killing per unit dose past a certain "peak" LET (usually ~100-250 keV/μm). Most common approaches use a saturation or correction factor to account for RBE decreases at high-LET, but the mechanism of this phenomenon is still not fully understood and a mechanistic model of this would be very beneficial. This is briefly discussed in Chapter 2, specifically the description of Figure 2.1, and, as mentioned in Chapter 4, some theorize that changes in yields of other simpler forms of DNA damage have effects on higher-order biological effects.
- Regarding contrast-enhanced CT, it is clear that there is a dose-enhancing effect when using X-ray contrasts that is not yet considered in patient dose estimates. Establishing a method to calculate the excess dose a patient received from injected contrast using a combination of the CT data (increase in HU) and the multiscale model would be a beneficial tool that could be developed. Further studies are needed to assess long-term effects.
- Additionally, investigation into the dose and RBE effects for interventional radiology and cardiology procedures that utilize contrast is worthwhile, since it is expected that the effect is even greater due to the lower kVp and

filtration used in fluoroscopy and angiography.

- Even though the multiscale model captures all the major trends in RBE, other effects that aren't explicitly considered with the presented model, such as bystander effects and immune response warrant further review.
- As experimental detection methods and studies of SSB and BD induction improve, the proposed multiscale model can be further benchmarked
- Beyond the special case scenarios examined in this work, this multiscale model can be applied to a myriad of other cases, for example, space and cosmic ray radiation RBE, radiation protection, etc. A new feature in MCNP6.1.1b is the addition of the cosmic-source heavy ion upgrade, which includes ^{14}N, ^{28}Si and ^{56}Fe, which represents a range of actual cosmic-ray heavy ions. This improvement generally increases the production of secondary particles within the earth's atmosphere and the data is location dependent. The multiscale model used throughout this work could be used to assess both alphas, protons and the new heavy ion data of cosmic rays and provide guidance for radiation protection.

5.3 Other Related Publications and Abstracts

Stewart, R. D.; Streitmatter, S. W.; Argento, D. C.; Kirkby, C.; Goorley, J. T.; Moffitt, G.; Jevremovic, T.; Sandison, G. A. Rapid MCNP Simulation of DNA Double Strand Break (DSB) Relative Biological Effectiveness (RBE) For Photons, Neutrons, And Light Ions. *Phys. Med. Biol.* **2015**, *60* (21), 8249–8274 DOI: 10.1088/0031-9155/60/21/8249.

Stewart, R.; Streitmatter, S.; Traneus, E.; Moskvin, V.; Schuemann, J. *Benchmarks of a Proton Relative Biological Effectiveness (RBE) Model for DNA Double Strand Break (DSB) Induction in the FLUKA, MCNP, TOPAS, and RayStation™*

Treatment Planning System, 58th Annual Meeting of the American Association of Physicists in Medicine (AAPM); Washington DC, USA, July 31-August 4, 2016; American Association of Physicist in Medicine: Alexandria, VA, 2016; MO-FG-CAMPUS-TeP3-02.

Streitmatter, S.; Stewart, R.; Sandison G.; *Relative Biological Effectiveness (RBE) of Protons in Pristine Bragg Peaks*, 55th Annual Meeting of the American Association of Physicists in Medicine (AAPM); Indianapolis, IN, USA, August 4-8, 2013; American Association of Physicist in Medicine: Alexandria, VA, 2013; WE-E-108-03.

APPENDIX A

MCNP6 DOSE RESPONSE CARDS (DE/DF)

The dose response cards (DE/DF) utilized for computing dose-averaged estimates of RBE_{DSB}, $\bar{z}_F$, LET, RBE_{SSB} and RBE_{BD}, etc. contained in this dissertation are listed below. Here, the "intra-track RMF interaction term" is equal to $RBE_{DSB}^2 \times \bar{z}_F$. They are compatible with MCNP5 (electrons only), MCNPX and the most current MCNP software version, MCNP6.1.1b. Note that for heavy ions (Z>2), the additional card FT RES is needed to separate the ion of interest from all heavy ion contribution (particle identifier '#'). For example, for ^{7}Li, the card FT RES 3007 is required, where 3007 is the nuclide identification number (ZAID), with the format *ZZZAAA*. Also, listed at the header of each set of dose response cards are the corresponding DSB, SSB and BD Gy^{-1} Gbp^{-1} for ^{60}Co. To convert tally results from RBE_{DSB}, RBE_{SSB} and RBE_{BD} to absolute DSB, SSB or BD Gy^{-1} Gbp^{-1}, simply multiply the dose-averaged RBE by the ^{60}Co reference values. These lookup tables were efficiently constructed with the use of two custom Python scripts, which are contained in Appendix B. The work presented in Chapter 4 is expected to supersede this solution, but further work on the user interface and adjustable variables are needed and this will remain the best solution for use without access to the MCNP source code.

Protons

```
Proton DOSE-RESPONSE FUNCTIONS FOR USE IN MCNP6 (April 25, 2017)
Data generated using MCDS Version 3.10A  05-DEC-2011

C
C           DSB (60Co):   8.32
C           SSB (60Co): 188.63
C           BD  (60Co): 425.26
C
C    ***    ========================================================
C    ***                 Proton  DOSE, RBE AND RELATED TALLIES
C    ***    --------------------------------------------------------
C
FC1016      Proton Absorbed Dose
F1016:H     1
C
FM1016      0.1602  $MeV/g to nGy
C
C
FC1026      Proton RBE for DSB induction (100% pO2) relative to 60Co
F1026:H     1
C
FM1026      0.1602  $MeV/g to nGy
DE1026      1.000E-03 1.200E-03 1.450E-03 1.750E-03 2.100E-03 2.540E-03
            3.050E-03 3.680E-03 4.430E-03 5.340E-03 6.430E-03 7.740E-03
            9.330E-03 1.120E-02 1.350E-02 1.630E-02 1.960E-02 2.360E-02
            2.850E-02 3.430E-02 4.130E-02 4.980E-02 5.990E-02 7.220E-02
            8.700E-02 1.050E-01 1.260E-01 1.520E-01 1.830E-01 2.210E-01
            2.660E-01 3.200E-01 3.850E-01 4.640E-01 5.590E-01 6.730E-01
            8.110E-01 9.770E-01 1.180E+00 1.420E+00 1.710E+00 2.060E+00
            2.480E+00 2.980E+00 3.590E+00 4.330E+00 5.210E+00 6.280E+00
            7.560E+00 9.110E+00 1.100E+01 1.320E+01 1.590E+01 1.920E+01
            2.310E+01 2.780E+01 3.350E+01 4.040E+01 4.860E+01 5.860E+01
            7.050E+01 8.500E+01 1.020E+02 1.230E+02 1.480E+02 1.790E+02
            2.150E+02 2.600E+02 3.130E+02 3.760E+02 4.530E+02 5.460E+02
            6.580E+02 7.920E+02 9.550E+02 1.150E+03 1.380E+03 1.670E+03
            2.010E+03 2.420E+03 2.920E+03 3.510E+03 4.230E+03 5.090E+03
            6.140E+03 7.390E+03 8.900E+03 1.070E+04 1.290E+04 1.560E+04
            1.870E+04 2.260E+04 2.720E+04 3.270E+04 3.940E+04 4.750E+04
            5.720E+04 6.890E+04 8.300E+04 1.000E+05
DF1026      3.358E+00 3.356E+00 3.355E+00 3.354E+00 3.350E+00 3.349E+00
            3.350E+00 3.345E+00 3.343E+00 3.339E+00 3.336E+00 3.331E+00
            3.325E+00 3.325E+00 3.318E+00 3.309E+00 3.302E+00 3.290E+00
            3.279E+00 3.265E+00 3.248E+00 3.226E+00 3.203E+00 3.170E+00
            3.135E+00 3.094E+00 3.043E+00 2.985E+00 2.912E+00 2.829E+00
            2.741E+00 2.638E+00 2.530E+00 2.410E+00 2.288E+00 2.163E+00
            2.043E+00 1.921E+00 1.806E+00 1.704E+00 1.608E+00 1.523E+00
            1.447E+00 1.379E+00 1.322E+00 1.270E+00 1.228E+00 1.190E+00
            1.158E+00 1.131E+00 1.109E+00 1.091E+00 1.073E+00 1.060E+00
            1.047E+00 1.038E+00 1.031E+00 1.025E+00 1.020E+00 1.015E+00
            1.011E+00 1.009E+00 1.006E+00 1.001E+00 1.002E+00 9.991E-01
            9.976E-01 9.962E-01 9.979E-01 9.960E-01 9.958E-01 9.942E-01
            9.953E-01 9.950E-01 9.948E-01 9.939E-01 9.931E-01 9.941E-01
            9.940E-01 9.923E-01 9.939E-01 9.930E-01 9.942E-01 9.941E-01
            9.939E-01 9.928E-01 9.929E-01 9.921E-01 9.913E-01 9.920E-01
            9.920E-01 9.938E-01 9.938E-01 9.938E-01 9.938E-01 9.938E-01
            9.938E-01 9.938E-01 9.938E-01 9.938E-01
C
```

```
C
FC1036      Proton RBE for SSB induction (100% pO2) relative to 60Co
F1036:H     1
C
FM1036      0.1602  $MeV/g to nGy
DE1036      1.000E-03 1.200E-03 1.450E-03 1.750E-03 2.100E-03 2.540E-03
            3.050E-03 3.680E-03 4.430E-03 5.340E-03 6.430E-03 7.740E-03
            9.330E-03 1.120E-02 1.350E-02 1.630E-02 1.960E-02 2.360E-02
            2.850E-02 3.430E-02 4.130E-02 4.980E-02 5.990E-02 7.220E-02
            8.700E-02 1.050E-01 1.260E-01 1.520E-01 1.830E-01 2.210E-01
            2.660E-01 3.200E-01 3.850E-01 4.640E-01 5.590E-01 6.730E-01
            8.110E-01 9.770E-01 1.180E+00 1.420E+00 1.710E+00 2.060E+00
            2.480E+00 2.980E+00 3.590E+00 4.330E+00 5.210E+00 6.280E+00
            7.560E+00 9.110E+00 1.100E+01 1.320E+01 1.590E+01 1.920E+01
            2.310E+01 2.780E+01 3.350E+01 4.040E+01 4.860E+01 5.860E+01
            7.050E+01 8.500E+01 1.020E+02 1.230E+02 1.480E+02 1.790E+02
            2.150E+02 2.600E+02 3.130E+02 3.760E+02 4.530E+02 5.460E+02
            6.580E+02 7.920E+02 9.550E+02 1.150E+03 1.380E+03 1.670E+03
            2.010E+03 2.420E+03 2.920E+03 3.510E+03 4.230E+03 5.090E+03
            6.140E+03 7.390E+03 8.900E+03 1.070E+04 1.290E+04 1.560E+04
            1.870E+04 2.260E+04 2.720E+04 3.270E+04 3.940E+04 4.750E+04
            5.720E+04 6.890E+04 8.300E+04 1.000E+05
DF1036      3.612E-01 3.622E-01 3.634E-01 3.647E-01 3.661E-01 3.676E-01
            3.693E-01 3.713E-01 3.734E-01 3.759E-01 3.785E-01 3.817E-01
            3.853E-01 3.888E-01 3.934E-01 3.984E-01 4.040E-01 4.105E-01
            4.179E-01 4.261E-01 4.357E-01 4.465E-01 4.589E-01 4.731E-01
            4.890E-01 5.069E-01 5.267E-01 5.491E-01 5.734E-01 5.999E-01
            6.282E-01 6.575E-01 6.875E-01 7.179E-01 7.480E-01 7.772E-01
            8.048E-01 8.300E-01 8.537E-01 8.745E-01 8.930E-01 9.093E-01
            9.234E-01 9.356E-01 9.461E-01 9.550E-01 9.623E-01 9.689E-01
            9.743E-01 9.788E-01 9.827E-01 9.857E-01 9.885E-01 9.907E-01
            9.928E-01 9.943E-01 9.956E-01 9.966E-01 9.974E-01 9.981E-01
            9.988E-01 9.992E-01 9.997E-01 1.000E+00 1.000E+00 1.001E+00
            1.001E+00 1.001E+00 1.001E+00 1.001E+00 1.001E+00 1.001E+00
            1.001E+00 1.002E+00 1.001E+00 1.002E+00 1.002E+00 1.002E+00
            1.002E+00 1.002E+00 1.002E+00 1.002E+00 1.002E+00 1.002E+00
            1.002E+00 1.002E+00 1.002E+00 1.002E+00 1.002E+00 1.002E+00
            1.002E+00 1.002E+00 1.002E+00 1.002E+00 1.002E+00 1.002E+00
            1.002E+00 1.002E+00 1.002E+00 1.002E+00
C
C
FC1046      Proton RBE for BD induction (100% pO2) relative to 60Co
F1046:H     1
C
FM1046      0.1602  $MeV/g to nGy
DE1046      1.000E-03 1.200E-03 1.450E-03 1.750E-03 2.100E-03 2.540E-03
            3.050E-03 3.680E-03 4.430E-03 5.340E-03 6.430E-03 7.740E-03
            9.330E-03 1.120E-02 1.350E-02 1.630E-02 1.960E-02 2.360E-02
            2.850E-02 3.430E-02 4.130E-02 4.980E-02 5.990E-02 7.220E-02
            8.700E-02 1.050E-01 1.260E-01 1.520E-01 1.830E-01 2.210E-01
            2.660E-01 3.200E-01 3.850E-01 4.640E-01 5.590E-01 6.730E-01
            8.110E-01 9.770E-01 1.180E+00 1.420E+00 1.710E+00 2.060E+00
            2.480E+00 2.980E+00 3.590E+00 4.330E+00 5.210E+00 6.280E+00
            7.560E+00 9.110E+00 1.100E+01 1.320E+01 1.590E+01 1.920E+01
            2.310E+01 2.780E+01 3.350E+01 4.040E+01 4.860E+01 5.860E+01
            7.050E+01 8.500E+01 1.020E+02 1.230E+02 1.480E+02 1.790E+02
            2.150E+02 2.600E+02 3.130E+02 3.760E+02 4.530E+02 5.460E+02
            6.580E+02 7.920E+02 9.550E+02 1.150E+03 1.380E+03 1.670E+03
            2.010E+03 2.420E+03 2.920E+03 3.510E+03 4.230E+03 5.090E+03
            6.140E+03 7.390E+03 8.900E+03 1.070E+04 1.290E+04 1.560E+04
            1.870E+04 2.260E+04 2.720E+04 3.270E+04 3.940E+04 4.750E+04
```

```
            5.720E+04 6.890E+04 8.300E+04 1.000E+05
DF1046      1.123E-01 1.129E-01 1.135E-01 1.141E-01 1.149E-01 1.157E-01
            1.166E-01 1.176E-01 1.188E-01 1.202E-01 1.216E-01 1.233E-01
            1.253E-01 1.275E-01 1.300E-01 1.329E-01 1.362E-01 1.400E-01
            1.445E-01 1.499E-01 1.558E-01 1.631E-01 1.712E-01 1.810E-01
            1.927E-01 2.065E-01 2.221E-01 2.411E-01 2.630E-01 2.890E-01
            3.179E-01 3.507E-01 3.869E-01 4.272E-01 4.697E-01 5.142E-01
            5.596E-01 6.048E-01 6.495E-01 6.912E-01 7.303E-01 7.665E-01
            7.992E-01 8.279E-01 8.537E-01 8.765E-01 8.960E-01 9.131E-01
            9.275E-01 9.400E-01 9.505E-01 9.593E-01 9.668E-01 9.731E-01
            9.783E-01 9.827E-01 9.865E-01 9.896E-01 9.922E-01 9.942E-01
            9.960E-01 9.976E-01 9.988E-01 9.998E-01 1.001E+00 1.001E+00
            1.002E+00 1.002E+00 1.003E+00 1.003E+00 1.003E+00 1.004E+00
            1.004E+00 1.004E+00 1.004E+00 1.004E+00 1.004E+00 1.004E+00
            1.004E+00 1.004E+00 1.005E+00 1.005E+00 1.005E+00 1.004E+00
            1.005E+00 1.005E+00 1.005E+00 1.005E+00 1.005E+00 1.005E+00
            1.005E+00 1.005E+00 1.005E+00 1.005E+00 1.005E+00 1.005E+00
            1.005E+00 1.005E+00 1.005E+00 1.005E+00
C
C
FC1056      Proton LET (keV/um)
F1056:H     1
C
FM1056      0.1602  $MeV/g to nGy
DE1056      1.000E-03 1.200E-03 1.450E-03 1.750E-03 2.100E-03 2.540E-03
            3.050E-03 3.680E-03 4.430E-03 5.340E-03 6.430E-03 7.740E-03
            9.330E-03 1.120E-02 1.350E-02 1.630E-02 1.960E-02 2.360E-02
            2.850E-02 3.430E-02 4.130E-02 4.980E-02 5.990E-02 7.220E-02
            8.700E-02 1.050E-01 1.260E-01 1.520E-01 1.830E-01 2.210E-01
            2.660E-01 3.200E-01 3.850E-01 4.640E-01 5.590E-01 6.730E-01
            8.110E-01 9.770E-01 1.180E+00 1.420E+00 1.710E+00 2.060E+00
            2.480E+00 2.980E+00 3.590E+00 4.330E+00 5.210E+00 6.280E+00
            7.560E+00 9.110E+00 1.100E+01 1.320E+01 1.590E+01 1.920E+01
            2.310E+01 2.780E+01 3.350E+01 4.040E+01 4.860E+01 5.860E+01
            7.050E+01 8.500E+01 1.020E+02 1.230E+02 1.480E+02 1.790E+02
            2.150E+02 2.600E+02 3.130E+02 3.760E+02 4.530E+02 5.460E+02
            6.580E+02 7.920E+02 9.550E+02 1.150E+03 1.380E+03 1.670E+03
            2.010E+03 2.420E+03 2.920E+03 3.510E+03 4.230E+03 5.090E+03
            6.140E+03 7.390E+03 8.900E+03 1.070E+04 1.290E+04 1.560E+04
            1.870E+04 2.260E+04 2.720E+04 3.270E+04 3.940E+04 4.750E+04
            5.720E+04 6.890E+04 8.300E+04 1.000E+05
DF1056      1.737E+01 1.811E+01 1.905E+01 2.018E+01 2.148E+01 2.310E+01
            2.492E+01 2.709E+01 2.955E+01 3.237E+01 3.551E+01 3.897E+01
            4.276E+01 4.673E+01 5.098E+01 5.537E+01 5.966E+01 6.385E+01
            6.782E+01 7.130E+01 7.421E+01 7.643E+01 7.781E+01 7.831E+01
            7.788E+01 7.649E+01 7.429E+01 7.124E+01 6.755E+01 6.327E+01
            5.869E+01 5.391E+01 4.907E+01 4.424E+01 3.960E+01 3.522E+01
            3.113E+01 2.738E+01 2.394E+01 2.091E+01 1.821E+01 1.581E+01
            1.370E+01 1.188E+01 1.026E+01 8.837E+00 7.620E+00 6.556E+00
            5.641E+00 4.848E+00 4.157E+00 3.582E+00 3.077E+00 2.638E+00
            2.269E+00 1.953E+00 1.680E+00 1.446E+00 1.250E+00 1.080E+00
            9.369E-01 8.139E-01 7.120E-01 6.231E-01 5.487E-01 4.842E-01
            4.318E-01 3.861E-01 3.488E-01 3.181E-01 2.921E-01 2.707E-01
            2.533E-01 2.393E-01 2.281E-01 2.194E-01 2.129E-01 2.078E-01
            2.044E-01 2.021E-01 2.008E-01 2.003E-01 2.004E-01 2.009E-01
            2.018E-01 2.029E-01 2.041E-01 2.055E-01 2.070E-01 2.085E-01
            2.099E-01 2.114E-01 2.129E-01 2.143E-01 2.157E-01 2.170E-01
            2.183E-01 2.196E-01 2.208E-01 2.220E-01
C
C
FC1066      Proton ZF (mean specific energy)
```

```
F1066:H     1
C
FM1066      0.1602  $MeV/g to nGy
DE1066      1.000E-03 1.200E-03 1.450E-03 1.750E-03 2.100E-03 2.540E-03
            3.050E-03 3.680E-03 4.430E-03 5.340E-03 6.430E-03 7.740E-03
            9.330E-03 1.120E-02 1.350E-02 1.630E-02 1.960E-02 2.360E-02
            2.850E-02 3.430E-02 4.130E-02 4.980E-02 5.990E-02 7.220E-02
            8.700E-02 1.050E-01 1.260E-01 1.520E-01 1.830E-01 2.210E-01
            2.660E-01 3.200E-01 3.850E-01 4.640E-01 5.590E-01 6.730E-01
            8.110E-01 9.770E-01 1.180E+00 1.420E+00 1.710E+00 2.060E+00
            2.480E+00 2.980E+00 3.590E+00 4.330E+00 5.210E+00 6.280E+00
            7.560E+00 9.110E+00 1.100E+01 1.320E+01 1.590E+01 1.920E+01
            2.310E+01 2.780E+01 3.350E+01 4.040E+01 4.860E+01 5.860E+01
            7.050E+01 8.500E+01 1.020E+02 1.230E+02 1.480E+02 1.790E+02
            2.150E+02 2.600E+02 3.130E+02 3.760E+02 4.530E+02 5.460E+02
            6.580E+02 7.920E+02 9.550E+02 1.150E+03 1.380E+03 1.670E+03
            2.010E+03 2.420E+03 2.920E+03 3.510E+03 4.230E+03 5.090E+03
            6.140E+03 7.390E+03 8.900E+03 1.070E+04 1.290E+04 1.560E+04
            1.870E+04 2.260E+04 2.720E+04 3.270E+04 3.940E+04 4.750E+04
            5.720E+04 6.890E+04 8.300E+04 1.000E+05
DF1066      2.448E-03 2.937E-03 3.549E-03 4.283E-03 5.139E-03 6.216E-03
            7.463E-03 9.004E-03 1.084E-02 1.306E-02 1.573E-02 1.893E-02
            2.281E-02 2.738E-02 3.299E-02 3.981E-02 4.785E-02 5.758E-02
            6.948E-02 8.353E-02 1.004E-01 1.209E-01 1.450E-01 1.742E-01
            2.088E-01 2.500E-01 2.965E-01 3.511E-01 4.101E-01 4.704E-01
            5.175E-01 5.246E-01 4.717E-01 4.100E-01 3.557E-01 3.088E-01
            2.679E-01 2.324E-01 2.011E-01 1.743E-01 1.509E-01 1.304E-01
            1.127E-01 9.747E-02 8.404E-02 7.232E-02 6.231E-02 5.357E-02
            4.608E-02 3.958E-02 3.394E-02 2.924E-02 2.511E-02 2.152E-02
            1.852E-02 1.593E-02 1.371E-02 1.180E-02 1.020E-02 8.810E-03
            7.645E-03 6.641E-03 5.809E-03 5.084E-03 4.477E-03 3.950E-03
            3.523E-03 3.150E-03 2.846E-03 2.595E-03 2.383E-03 2.209E-03
            2.067E-03 1.952E-03 1.861E-03 1.790E-03 1.737E-03 1.696E-03
            1.668E-03 1.649E-03 1.638E-03 1.634E-03 1.635E-03 1.639E-03
            1.646E-03 1.655E-03 1.666E-03 1.677E-03 1.689E-03 1.701E-03
            1.713E-03 1.725E-03 1.737E-03 1.748E-03 1.760E-03 1.771E-03
            1.781E-03 1.792E-03 1.802E-03 1.812E-03
C
C
FC1076      Proton RMF intra-track DSB interaction term (100% pO2)
F1076:H     1
C
FM1076      0.1602  $MeV to nGy
DE1076      1.000E-03 1.200E-03 1.450E-03 1.750E-03 2.100E-03 2.540E-03
            3.050E-03 3.680E-03 4.430E-03 5.340E-03 6.430E-03 7.740E-03
            9.330E-03 1.120E-02 1.350E-02 1.630E-02 1.960E-02 2.360E-02
            2.850E-02 3.430E-02 4.130E-02 4.980E-02 5.990E-02 7.220E-02
            8.700E-02 1.050E-01 1.260E-01 1.520E-01 1.830E-01 2.210E-01
            2.660E-01 3.200E-01 3.850E-01 4.640E-01 5.590E-01 6.730E-01
            8.110E-01 9.770E-01 1.180E+00 1.420E+00 1.710E+00 2.060E+00
            2.480E+00 2.980E+00 3.590E+00 4.330E+00 5.210E+00 6.280E+00
            7.560E+00 9.110E+00 1.100E+01 1.320E+01 1.590E+01 1.920E+01
            2.310E+01 2.780E+01 3.350E+01 4.040E+01 4.860E+01 5.860E+01
            7.050E+01 8.500E+01 1.020E+02 1.230E+02 1.480E+02 1.790E+02
            2.150E+02 2.600E+02 3.130E+02 3.760E+02 4.530E+02 5.460E+02
            6.580E+02 7.920E+02 9.550E+02 1.150E+03 1.380E+03 1.670E+03
            2.010E+03 2.420E+03 2.920E+03 3.510E+03 4.230E+03 5.090E+03
            6.140E+03 7.390E+03 8.900E+03 1.070E+04 1.290E+04 1.560E+04
            1.870E+04 2.260E+04 2.720E+04 3.270E+04 3.940E+04 4.750E+04
            5.720E+04 6.890E+04 8.300E+04 1.000E+05
DF1076      2.759E-02 3.308E-02 3.993E-02 4.818E-02 5.766E-02 6.972E-02
```

```
            8.375E-02 1.007E-01 1.211E-01 1.456E-01 1.750E-01 2.100E-01
            2.522E-01 3.026E-01 3.630E-01 4.360E-01 5.217E-01 6.231E-01
            7.470E-01 8.904E-01 1.059E+00 1.258E+00 1.488E+00 1.751E+00
            2.052E+00 2.394E+00 2.745E+00 3.129E+00 3.479E+00 3.764E+00
            3.888E+00 3.651E+00 3.019E+00 2.382E+00 1.863E+00 1.445E+00
            1.118E+00 8.579E-01 6.556E-01 5.063E-01 3.901E-01 3.024E-01
            2.359E-01 1.854E-01 1.468E-01 1.166E-01 9.403E-02 7.587E-02
            6.184E-02 5.066E-02 4.173E-02 3.482E-02 2.891E-02 2.420E-02
            2.030E-02 1.716E-02 1.456E-02 1.239E-02 1.060E-02 9.082E-03
            7.819E-03 6.760E-03 5.884E-03 5.094E-03 4.491E-03 3.943E-03
            3.506E-03 3.126E-03 2.834E-03 2.574E-03 2.364E-03 2.183E-03
            2.047E-03 1.933E-03 1.841E-03 1.768E-03 1.713E-03 1.676E-03
            1.648E-03 1.624E-03 1.619E-03 1.612E-03 1.616E-03 1.620E-03
            1.626E-03 1.631E-03 1.642E-03 1.650E-03 1.660E-03 1.674E-03
            1.685E-03 1.704E-03 1.715E-03 1.727E-03 1.738E-03 1.749E-03
            1.760E-03 1.770E-03 1.780E-03 1.789E-03

Proton DOSE-RESPONSE FUNCTIONS FOR USE IN MCNP6 (April 25, 2017)
Data generated using MCDS Version 3.10A  05-DEC-2011

C
C           DSB (60Co):   2.86
C           SSB (60Co): 115.53
C           BD  (60Co): 293.98
C
C    ***    ============================================================
C    ***                 Proton  DOSE, RBE AND RELATED TALLIES
C    ***    ------------------------------------------------------------
C
FC2016      Proton Absorbed Dose
F2016:H     1
C
FM2016      0.1602  $MeV/g to nGy
C
C
FC2026      Proton RBE for DSB induction (0% pO2) relative to 60Co
F2026:H     1
C
FM2026      0.1602  $MeV/g to nGy
DE2026      1.000E-03 1.200E-03 1.450E-03 1.750E-03 2.100E-03 2.540E-03
            3.050E-03 3.680E-03 4.430E-03 5.340E-03 6.430E-03 7.740E-03
            9.330E-03 1.120E-02 1.350E-02 1.630E-02 1.960E-02 2.360E-02
            2.850E-02 3.430E-02 4.130E-02 4.980E-02 5.990E-02 7.220E-02
            8.700E-02 1.050E-01 1.260E-01 1.520E-01 1.830E-01 2.210E-01
            2.660E-01 3.200E-01 3.850E-01 4.640E-01 5.590E-01 6.730E-01
            8.110E-01 9.770E-01 1.180E+00 1.420E+00 1.710E+00 2.060E+00
            2.480E+00 2.980E+00 3.590E+00 4.330E+00 5.210E+00 6.280E+00
            7.560E+00 9.110E+00 1.100E+01 1.320E+01 1.590E+01 1.920E+01
            2.310E+01 2.780E+01 3.350E+01 4.040E+01 4.860E+01 5.860E+01
            7.050E+01 8.500E+01 1.020E+02 1.230E+02 1.480E+02 1.790E+02
            2.150E+02 2.600E+02 3.130E+02 3.760E+02 4.530E+02 5.460E+02
            6.580E+02 7.920E+02 9.550E+02 1.150E+03 1.380E+03 1.670E+03
            2.010E+03 2.420E+03 2.920E+03 3.510E+03 4.230E+03 5.090E+03
            6.140E+03 7.390E+03 8.900E+03 1.070E+04 1.290E+04 1.560E+04
            1.870E+04 2.260E+04 2.720E+04 3.270E+04 3.940E+04 4.750E+04
            5.720E+04 6.890E+04 8.300E+04 1.000E+05
DF2026      9.741E+00 9.726E+00 9.722E+00 9.720E+00 9.707E+00 9.706E+00
            9.709E+00 9.683E+00 9.679E+00 9.667E+00 9.648E+00 9.624E+00
            9.606E+00 9.595E+00 9.565E+00 9.532E+00 9.499E+00 9.443E+00
            9.391E+00 9.320E+00 9.228E+00 9.124E+00 8.992E+00 8.812E+00
            8.616E+00 8.360E+00 8.037E+00 7.654E+00 7.178E+00 6.625E+00
```

```
            6.021E+00 5.362E+00 4.710E+00 4.084E+00 3.521E+00 3.046E+00
            2.651E+00 2.343E+00 2.090E+00 1.898E+00 1.744E+00 1.613E+00
            1.512E+00 1.424E+00 1.353E+00 1.292E+00 1.242E+00 1.205E+00
            1.168E+00 1.137E+00 1.113E+00 1.094E+00 1.073E+00 1.063E+00
            1.047E+00 1.038E+00 1.030E+00 1.023E+00 1.021E+00 1.013E+00
            1.011E+00 1.007E+00 1.005E+00 9.996E-01 9.985E-01 9.958E-01
            9.959E-01 9.929E-01 9.949E-01 9.945E-01 9.952E-01 9.924E-01
            9.923E-01 9.924E-01 9.928E-01 9.907E-01 9.902E-01 9.929E-01
            9.907E-01 9.913E-01 9.925E-01 9.917E-01 9.922E-01 9.931E-01
            9.912E-01 9.916E-01 9.905E-01 9.907E-01 9.872E-01 9.918E-01
            9.918E-01 9.917E-01 9.917E-01 9.917E-01 9.917E-01 9.917E-01
            9.917E-01 9.917E-01 9.917E-01 9.917E-01
C
C
FC2036      Proton RBE for SSB induction (0% pO2) relative to 60Co
F2036:H     1
C
FM2036      0.1602  $MeV/g to nGy
DE2036      1.000E-03 1.200E-03 1.450E-03 1.750E-03 2.100E-03 2.540E-03
            3.050E-03 3.680E-03 4.430E-03 5.340E-03 6.430E-03 7.740E-03
            9.330E-03 1.120E-02 1.350E-02 1.630E-02 1.960E-02 2.360E-02
            2.850E-02 3.430E-02 4.130E-02 4.980E-02 5.990E-02 7.220E-02
            8.700E-02 1.050E-01 1.260E-01 1.520E-01 1.830E-01 2.210E-01
            2.660E-01 3.200E-01 3.850E-01 4.640E-01 5.590E-01 6.730E-01
            8.110E-01 9.770E-01 1.180E+00 1.420E+00 1.710E+00 2.060E+00
            2.480E+00 2.980E+00 3.590E+00 4.330E+00 5.210E+00 6.280E+00
            7.560E+00 9.110E+00 1.100E+01 1.320E+01 1.590E+01 1.920E+01
            2.310E+01 2.780E+01 3.350E+01 4.040E+01 4.860E+01 5.860E+01
            7.050E+01 8.500E+01 1.020E+02 1.230E+02 1.480E+02 1.790E+02
            2.150E+02 2.600E+02 3.130E+02 3.760E+02 4.530E+02 5.460E+02
            6.580E+02 7.920E+02 9.550E+02 1.150E+03 1.380E+03 1.670E+03
            2.010E+03 2.420E+03 2.920E+03 3.510E+03 4.230E+03 5.090E+03
            6.140E+03 7.390E+03 8.900E+03 1.070E+04 1.290E+04 1.560E+04
            1.870E+04 2.260E+04 2.720E+04 3.270E+04 3.940E+04 4.750E+04
            5.720E+04 6.890E+04 8.300E+04 1.000E+05
DF2036      5.910E-01 5.929E-01 5.948E-01 5.969E-01 5.993E-01 6.018E-01
            6.046E-01 6.080E-01 6.116E-01 6.157E-01 6.202E-01 6.257E-01
            6.316E-01 6.376E-01 6.453E-01 6.537E-01 6.632E-01 6.744E-01
            6.869E-01 7.008E-01 7.170E-01 7.354E-01 7.561E-01 7.798E-01
            8.058E-01 8.345E-01 8.646E-01 8.967E-01 9.280E-01 9.572E-01
            9.808E-01 9.974E-01 1.005E+00 1.005E+00 9.985E-01 9.896E-01
            9.796E-01 9.732E-01 9.683E-01 9.660E-01 9.669E-01 9.684E-01
            9.704E-01 9.737E-01 9.771E-01 9.794E-01 9.823E-01 9.855E-01
            9.872E-01 9.898E-01 9.918E-01 9.920E-01 9.936E-01 9.948E-01
            9.959E-01 9.966E-01 9.973E-01 9.979E-01 9.982E-01 9.987E-01
            9.990E-01 9.992E-01 9.995E-01 9.998E-01 1.000E+00 1.000E+00
            1.000E+00 1.000E+00 1.000E+00 1.000E+00 1.000E+00 1.000E+00
            1.000E+00 1.000E+00 1.000E+00 1.001E+00 1.001E+00 1.000E+00
            1.001E+00 1.001E+00 1.001E+00 1.001E+00 1.001E+00 1.001E+00
            1.001E+00 1.000E+00 1.001E+00 1.001E+00 1.001E+00 1.001E+00
            1.001E+00 1.000E+00 1.000E+00 1.000E+00 1.000E+00 1.000E+00
            1.000E+00 1.000E+00 1.000E+00 1.000E+00
C
C
FC2046      Proton RBE for BD induction (0% pO2) relative to 60Co
F2046:H     1
C
FM2046      0.1602  $MeV/g to nGy
DE2046      1.000E-03 1.200E-03 1.450E-03 1.750E-03 2.100E-03 2.540E-03
            3.050E-03 3.680E-03 4.430E-03 5.340E-03 6.430E-03 7.740E-03
            9.330E-03 1.120E-02 1.350E-02 1.630E-02 1.960E-02 2.360E-02
```

```
            2.850E-02 3.430E-02 4.130E-02 4.980E-02 5.990E-02 7.220E-02
            8.700E-02 1.050E-01 1.260E-01 1.520E-01 1.830E-01 2.210E-01
            2.660E-01 3.200E-01 3.850E-01 4.640E-01 5.590E-01 6.730E-01
            8.110E-01 9.770E-01 1.180E+00 1.420E+00 1.710E+00 2.060E+00
            2.480E+00 2.980E+00 3.590E+00 4.330E+00 5.210E+00 6.280E+00
            7.560E+00 9.110E+00 1.100E+01 1.320E+01 1.590E+01 1.920E+01
            2.310E+01 2.780E+01 3.350E+01 4.040E+01 4.860E+01 5.860E+01
            7.050E+01 8.500E+01 1.020E+02 1.230E+02 1.480E+02 1.790E+02
            2.150E+02 2.600E+02 3.130E+02 3.760E+02 4.530E+02 5.460E+02
            6.580E+02 7.920E+02 9.550E+02 1.150E+03 1.380E+03 1.670E+03
            2.010E+03 2.420E+03 2.920E+03 3.510E+03 4.230E+03 5.090E+03
            6.140E+03 7.390E+03 8.900E+03 1.070E+04 1.290E+04 1.560E+04
            1.870E+04 2.260E+04 2.720E+04 3.270E+04 3.940E+04 4.750E+04
            5.720E+04 6.890E+04 8.300E+04 1.000E+05
DF2046      1.633E-01 1.643E-01 1.652E-01 1.662E-01 1.673E-01 1.685E-01
            1.698E-01 1.715E-01 1.733E-01 1.753E-01 1.776E-01 1.803E-01
            1.832E-01 1.867E-01 1.906E-01 1.951E-01 2.002E-01 2.063E-01
            2.135E-01 2.221E-01 2.319E-01 2.437E-01 2.573E-01 2.740E-01
            2.937E-01 3.176E-01 3.453E-01 3.786E-01 4.171E-01 4.614E-01
            5.090E-01 5.586E-01 6.073E-01 6.535E-01 6.942E-01 7.296E-01
            7.601E-01 7.867E-01 8.117E-01 8.339E-01 8.542E-01 8.732E-01
            8.905E-01 9.058E-01 9.198E-01 9.319E-01 9.428E-01 9.522E-01
            9.599E-01 9.668E-01 9.727E-01 9.776E-01 9.819E-01 9.854E-01
            9.884E-01 9.907E-01 9.929E-01 9.943E-01 9.957E-01 9.969E-01
            9.979E-01 9.988E-01 9.994E-01 9.999E-01 1.001E+00 1.001E+00
            1.001E+00 1.001E+00 1.002E+00 1.002E+00 1.002E+00 1.002E+00
            1.002E+00 1.002E+00 1.002E+00 1.003E+00 1.002E+00 1.003E+00
            1.003E+00 1.003E+00 1.003E+00 1.003E+00 1.003E+00 1.003E+00
            1.003E+00 1.003E+00 1.003E+00 1.003E+00 1.003E+00 1.003E+00
            1.003E+00 1.003E+00 1.003E+00 1.003E+00 1.003E+00 1.003E+00
            1.003E+00 1.003E+00 1.003E+00 1.003E+00
C
C
```

Electrons

```
e- DOSE-RESPONSE FUNCTIONS FOR USE IN MCNP6 (December 28, 2016)
Data generated using MCDS Version 3.10A  05-DEC-2011

C
C           DSB (60Co):   8.32
C           SSB (60Co): 188.63
C           BD  (60Co): 425.26
C
C    ***    ============================================================
C    ***                 e-  DOSE, RBE AND RELATED TALLIES
C    ***    ------------------------------------------------------------
C
FC6016      e- Absorbed Dose
F6016:E     1
C
FM6016      0.1602  $MeV/g to nGy
C
C
FC6026      e- RBE for DSB induction (100% pO2) relative to 60Co
F6026:E     1
```

```
C
FM6026      0.1602  $MeV/g to nGy
DE6026      1.000E-05 1.200E-05 1.450E-05 1.750E-05 2.100E-05 2.540E-05
            3.050E-05 3.680E-05 4.430E-05 5.340E-05 6.430E-05 7.740E-05
            9.330E-05 1.120E-04 1.350E-04 1.630E-04 1.960E-04 2.360E-04
            2.850E-04 3.430E-04 4.130E-04 4.980E-04 5.990E-04 7.220E-04
            8.700E-04 1.050E-03 1.260E-03 1.520E-03 1.830E-03 2.210E-03
            2.660E-03 3.200E-03 3.850E-03 4.640E-03 5.590E-03 6.730E-03
            8.110E-03 9.770E-03 1.180E-02 1.420E-02 1.710E-02 2.060E-02
            2.480E-02 2.980E-02 3.590E-02 4.330E-02 5.210E-02 6.280E-02
            7.560E-02 9.110E-02 1.100E-01 1.320E-01 1.590E-01 1.920E-01
            2.310E-01 2.780E-01 3.350E-01 4.040E-01 4.860E-01 5.860E-01
            7.050E-01 8.500E-01 1.020E+00 1.230E+00 1.480E+00 1.790E+00
            2.150E+00 2.600E+00 3.130E+00 3.760E+00 4.530E+00 5.460E+00
            6.580E+00 7.920E+00 9.550E+00 1.150E+01 1.380E+01 1.670E+01
            2.010E+01 2.420E+01 2.920E+01 3.510E+01 4.230E+01 5.090E+01
            6.140E+01 7.390E+01 8.900E+01 1.070E+02 1.290E+02 1.560E+02
            1.870E+02 2.260E+02 2.720E+02 3.270E+02 3.940E+02 4.750E+02
            5.720E+02 6.890E+02 8.300E+02 1.000E+03
DF6026      3.383E+00 3.378E+00 3.371E+00 3.362E+00 3.354E+00 3.337E+00
            3.317E+00 3.293E+00 3.259E+00 3.218E+00 3.166E+00 3.104E+00
            3.031E+00 2.945E+00 2.842E+00 2.732E+00 2.611E+00 2.487E+00
            2.353E+00 2.222E+00 2.094E+00 1.966E+00 1.852E+00 1.743E+00
            1.642E+00 1.554E+00 1.473E+00 1.402E+00 1.341E+00 1.287E+00
            1.242E+00 1.203E+00 1.168E+00 1.141E+00 1.115E+00 1.095E+00
            1.077E+00 1.064E+00 1.053E+00 1.042E+00 1.034E+00 1.026E+00
            1.023E+00 1.016E+00 1.013E+00 1.008E+00 1.006E+00 1.004E+00
            1.002E+00 1.001E+00 9.991E-01 9.976E-01 9.982E-01 9.958E-01
            9.970E-01 9.960E-01 9.941E-01 9.938E-01 9.941E-01 9.938E-01
            9.945E-01 9.932E-01 9.938E-01 9.939E-01 9.924E-01 9.944E-01
            9.940E-01 9.931E-01 9.931E-01 9.928E-01 9.929E-01 9.921E-01
            9.913E-01 9.920E-01 9.920E-01 9.920E-01 9.938E-01 9.938E-01
            9.938E-01 9.938E-01 9.938E-01 9.938E-01 9.938E-01 9.938E-01
            9.938E-01 9.938E-01 9.938E-01 9.938E-01 9.938E-01 9.938E-01
            9.938E-01 9.938E-01 9.938E-01 9.938E-01 9.938E-01 9.938E-01
            9.938E-01 9.938E-01 9.938E-01 9.938E-01
C
C
FC6036      e- RBE for SSB induction (100% pO2) relative to 60Co
F6036:E     1
C
FM6036      0.1602  $MeV/g to nGy
DE6036      1.000E-05 1.200E-05 1.450E-05 1.750E-05 2.100E-05 2.540E-05
            3.050E-05 3.680E-05 4.430E-05 5.340E-05 6.430E-05 7.740E-05
            9.330E-05 1.120E-04 1.350E-04 1.630E-04 1.960E-04 2.360E-04
            2.850E-04 3.430E-04 4.130E-04 4.980E-04 5.990E-04 7.220E-04
            8.700E-04 1.050E-03 1.260E-03 1.520E-03 1.830E-03 2.210E-03
            2.660E-03 3.200E-03 3.850E-03 4.640E-03 5.590E-03 6.730E-03
            8.110E-03 9.770E-03 1.180E-02 1.420E-02 1.710E-02 2.060E-02
            2.480E-02 2.980E-02 3.590E-02 4.330E-02 5.210E-02 6.280E-02
            7.560E-02 9.110E-02 1.100E-01 1.320E-01 1.590E-01 1.920E-01
            2.310E-01 2.780E-01 3.350E-01 4.040E-01 4.860E-01 5.860E-01
            7.050E-01 8.500E-01 1.020E+00 1.230E+00 1.480E+00 1.790E+00
            2.150E+00 2.600E+00 3.130E+00 3.760E+00 4.530E+00 5.460E+00
            6.580E+00 7.920E+00 9.550E+00 1.150E+01 1.380E+01 1.670E+01
            2.010E+01 2.420E+01 2.920E+01 3.510E+01 4.230E+01 5.090E+01
            6.140E+01 7.390E+01 8.900E+01 1.070E+02 1.290E+02 1.560E+02
            1.870E+02 2.260E+02 2.720E+02 3.270E+02 3.940E+02 4.750E+02
            5.720E+02 6.890E+02 8.300E+02 1.000E+03
DF6036      3.319E-01 3.382E-01 3.460E-01 3.551E-01 3.653E-01 3.782E-01
            3.926E-01 4.095E-01 4.287E-01 4.506E-01 4.750E-01 5.020E-01
```

```
            5.317E-01 5.627E-01 5.959E-01 6.304E-01 6.648E-01 6.989E-01
            7.321E-01 7.635E-01 7.931E-01 8.201E-01 8.444E-01 8.667E-01
            8.864E-01 9.035E-01 9.184E-01 9.315E-01 9.425E-01 9.521E-01
            9.600E-01 9.668E-01 9.726E-01 9.773E-01 9.815E-01 9.848E-01
            9.877E-01 9.901E-01 9.920E-01 9.937E-01 9.950E-01 9.963E-01
            9.969E-01 9.979E-01 9.985E-01 9.993E-01 9.997E-01 9.999E-01
            1.000E+00 1.001E+00 1.001E+00 1.001E+00 1.001E+00 1.001E+00
            1.001E+00 1.001E+00 1.002E+00 1.002E+00 1.002E+00 1.002E+00
            1.002E+00 1.002E+00 1.002E+00 1.002E+00 1.002E+00 1.002E+00
            1.002E+00 1.002E+00 1.002E+00 1.002E+00 1.002E+00 1.002E+00
            1.002E+00 1.002E+00 1.002E+00 1.002E+00 1.002E+00 1.002E+00
            1.002E+00 1.002E+00 1.002E+00 1.002E+00 1.002E+00 1.002E+00
            1.002E+00 1.002E+00 1.002E+00 1.002E+00 1.002E+00 1.002E+00
            1.002E+00 1.002E+00 1.002E+00 1.002E+00
C
C
FC6046      e- RBE for BD induction (100% pO2) relative to 60Co
F6046:E     1
C
FM6046      0.1602  $MeV/g to nGy
DE6046      1.000E-05 1.200E-05 1.450E-05 1.750E-05 2.100E-05 2.540E-05
            3.050E-05 3.680E-05 4.430E-05 5.340E-05 6.430E-05 7.740E-05
            9.330E-05 1.120E-04 1.350E-04 1.630E-04 1.960E-04 2.360E-04
            2.850E-04 3.430E-04 4.130E-04 4.980E-04 5.990E-04 7.220E-04
            8.700E-04 1.050E-03 1.260E-03 1.520E-03 1.830E-03 2.210E-03
            2.660E-03 3.200E-03 3.850E-03 4.640E-03 5.590E-03 6.730E-03
            8.110E-03 9.770E-03 1.180E-02 1.420E-02 1.710E-02 2.060E-02
            2.480E-02 2.980E-02 3.590E-02 4.330E-02 5.210E-02 6.280E-02
            7.560E-02 9.110E-02 1.100E-01 1.320E-01 1.590E-01 1.920E-01
            2.310E-01 2.780E-01 3.350E-01 4.040E-01 4.860E-01 5.860E-01
            7.050E-01 8.500E-01 1.020E+00 1.230E+00 1.480E+00 1.790E+00
            2.150E+00 2.600E+00 3.130E+00 3.760E+00 4.530E+00 5.460E+00
            6.580E+00 7.920E+00 9.550E+00 1.150E+01 1.380E+01 1.670E+01
            2.010E+01 2.420E+01 2.920E+01 3.510E+01 4.230E+01 5.090E+01
            6.140E+01 7.390E+01 8.900E+01 1.070E+02 1.290E+02 1.560E+02
            1.870E+02 2.260E+02 2.720E+02 3.270E+02 3.940E+02 4.750E+02
            5.720E+02 6.890E+02 8.300E+02 1.000E+03
DF6046      9.752E-02 1.005E-01 1.044E-01 1.091E-01 1.146E-01 1.215E-01
            1.295E-01 1.394E-01 1.513E-01 1.656E-01 1.826E-01 2.026E-01
            2.264E-01 2.533E-01 2.849E-01 3.206E-01 3.591E-01 4.012E-01
            4.468E-01 4.929E-01 5.398E-01 5.868E-01 6.320E-01 6.755E-01
            7.161E-01 7.539E-01 7.872E-01 8.180E-01 8.448E-01 8.690E-01
            8.896E-01 9.073E-01 9.224E-01 9.357E-01 9.469E-01 9.563E-01
            9.643E-01 9.709E-01 9.766E-01 9.812E-01 9.853E-01 9.886E-01
            9.913E-01 9.935E-01 9.955E-01 9.971E-01 9.983E-01 9.994E-01
            1.000E+00 1.001E+00 1.002E+00 1.002E+00 1.003E+00 1.003E+00
            1.003E+00 1.004E+00 1.004E+00 1.004E+00 1.004E+00 1.004E+00
            1.004E+00 1.004E+00 1.004E+00 1.004E+00 1.005E+00 1.004E+00
            1.005E+00 1.004E+00 1.005E+00 1.005E+00 1.005E+00 1.005E+00
            1.005E+00 1.005E+00 1.005E+00 1.005E+00 1.005E+00 1.005E+00
            1.005E+00 1.005E+00 1.005E+00 1.005E+00 1.005E+00 1.005E+00
            1.005E+00 1.005E+00 1.005E+00 1.005E+00 1.005E+00 1.005E+00
            1.005E+00 1.005E+00 1.005E+00 1.005E+00
C
C
FC6056      e- LET (keV/um)
F6056:E     1
C
FM6056      0.1602  $MeV/g to nGy
```

```
DE6056      1.000E-05 1.200E-05 1.450E-05 1.750E-05 2.100E-05 2.540E-05
            3.050E-05 3.680E-05 4.430E-05 5.340E-05 6.430E-05 7.740E-05
            9.330E-05 1.120E-04 1.350E-04 1.630E-04 1.960E-04 2.360E-04
            2.850E-04 3.430E-04 4.130E-04 4.980E-04 5.990E-04 7.220E-04
            8.700E-04 1.050E-03 1.260E-03 1.520E-03 1.830E-03 2.210E-03
            2.660E-03 3.200E-03 3.850E-03 4.640E-03 5.590E-03 6.730E-03
            8.110E-03 9.770E-03 1.180E-02 1.420E-02 1.710E-02 2.060E-02
            2.480E-02 2.980E-02 3.590E-02 4.330E-02 5.210E-02 6.280E-02
            7.560E-02 9.110E-02 1.100E-01 1.320E-01 1.590E-01 1.920E-01
            2.310E-01 2.780E-01 3.350E-01 4.040E-01 4.860E-01 5.860E-01
            7.050E-01 8.500E-01 1.020E+00 1.230E+00 1.480E+00 1.790E+00
            2.150E+00 2.600E+00 3.130E+00 3.760E+00 4.530E+00 5.460E+00
            6.580E+00 7.920E+00 9.550E+00 1.150E+01 1.380E+01 1.670E+01
            2.010E+01 2.420E+01 2.920E+01 3.510E+01 4.230E+01 5.090E+01
            6.140E+01 7.390E+01 8.900E+01 1.070E+02 1.290E+02 1.560E+02
            1.870E+02 2.260E+02 2.720E+02 3.270E+02 3.940E+02 4.750E+02
            5.720E+02 6.890E+02 8.300E+02 1.000E+03
DF6056      1.632E+01 1.750E+01 1.862E+01 1.960E+01 2.041E+01 2.111E+01
            2.163E+01 2.201E+01 2.223E+01 2.230E+01 2.222E+01 2.200E+01
            2.164E+01 2.117E+01 2.057E+01 1.985E+01 1.905E+01 1.818E+01
            1.722E+01 1.622E+01 1.520E+01 1.414E+01 1.310E+01 1.205E+01
            1.102E+01 1.002E+01 9.091E+00 8.183E+00 7.339E+00 6.539E+00
            5.814E+00 5.150E+00 4.545E+00 3.993E+00 3.498E+00 3.058E+00
            2.664E+00 2.317E+00 2.009E+00 1.743E+00 1.511E+00 1.309E+00
            1.135E+00 9.862E-01 8.562E-01 7.441E-01 6.496E-01 5.682E-01
            4.995E-01 4.410E-01 3.911E-01 3.505E-01 3.157E-01 2.863E-01
            2.625E-01 2.428E-01 2.267E-01 2.137E-01 2.036E-01 1.956E-01
            1.898E-01 1.855E-01 1.827E-01 1.809E-01 1.802E-01 1.802E-01
            1.808E-01 1.820E-01 1.834E-01 1.851E-01 1.871E-01 1.891E-01
            1.913E-01 1.935E-01 1.957E-01 1.979E-01 2.000E-01 2.022E-01
            2.044E-01 2.064E-01 2.085E-01 2.105E-01 2.125E-01 2.144E-01
            2.163E-01 2.182E-01 2.200E-01 2.218E-01 2.235E-01 2.253E-01
            2.270E-01 2.287E-01 2.303E-01 2.319E-01 2.335E-01 2.350E-01
            2.366E-01 2.381E-01 2.396E-01 2.410E-01
C
C
FC6066      e- ZF (mean specific energy)
F6066:E     1
C
FM6066      0.1602  $MeV/g to nGy
DE6066      1.000E-05 1.200E-05 1.450E-05 1.750E-05 2.100E-05 2.540E-05
            3.050E-05 3.680E-05 4.430E-05 5.340E-05 6.430E-05 7.740E-05
            9.330E-05 1.120E-04 1.350E-04 1.630E-04 1.960E-04 2.360E-04
            2.850E-04 3.430E-04 4.130E-04 4.980E-04 5.990E-04 7.220E-04
            8.700E-04 1.050E-03 1.260E-03 1.520E-03 1.830E-03 2.210E-03
            2.660E-03 3.200E-03 3.850E-03 4.640E-03 5.590E-03 6.730E-03
            8.110E-03 9.770E-03 1.180E-02 1.420E-02 1.710E-02 2.060E-02
            2.480E-02 2.980E-02 3.590E-02 4.330E-02 5.210E-02 6.280E-02
            7.560E-02 9.110E-02 1.100E-01 1.320E-01 1.590E-01 1.920E-01
            2.310E-01 2.780E-01 3.350E-01 4.040E-01 4.860E-01 5.860E-01
            7.050E-01 8.500E-01 1.020E+00 1.230E+00 1.480E+00 1.790E+00
            2.150E+00 2.600E+00 3.130E+00 3.760E+00 4.530E+00 5.460E+00
            6.580E+00 7.920E+00 9.550E+00 1.150E+01 1.380E+01 1.670E+01
            2.010E+01 2.420E+01 2.920E+01 3.510E+01 4.230E+01 5.090E+01
            6.140E+01 7.390E+01 8.900E+01 1.070E+02 1.290E+02 1.560E+02
            1.870E+02 2.260E+02 2.720E+02 3.270E+02 3.940E+02 4.750E+02
            5.720E+02 6.890E+02 8.300E+02 1.000E+03
DF6066      2.448E-05 2.937E-05 3.549E-05 4.283E-05 5.140E-05 6.217E-05
            7.465E-05 9.007E-05 1.084E-04 1.307E-04 1.574E-04 1.894E-04
            2.284E-04 2.741E-04 3.304E-04 3.990E-04 4.797E-04 5.776E-04
            6.976E-04 8.395E-04 1.011E-03 1.219E-03 1.466E-03 1.767E-03
```

```
            2.129E-03 2.570E-03 3.084E-03 3.720E-03 4.477E-03 5.405E-03
            6.501E-03 7.811E-03 9.376E-03 1.125E-02 1.344E-02 1.594E-02
            1.863E-02 2.111E-02 2.238E-02 1.984E-02 1.473E-02 1.197E-02
            9.993E-03 8.478E-03 7.243E-03 6.226E-03 5.394E-03 4.693E-03
            4.111E-03 3.620E-03 3.204E-03 2.868E-03 2.581E-03 2.339E-03
            2.144E-03 1.982E-03 1.851E-03 1.744E-03 1.661E-03 1.596E-03
            1.548E-03 1.513E-03 1.490E-03 1.476E-03 1.470E-03 1.470E-03
            1.475E-03 1.484E-03 1.497E-03 1.510E-03 1.526E-03 1.543E-03
            1.561E-03 1.578E-03 1.597E-03 1.614E-03 1.632E-03 1.650E-03
            1.667E-03 1.684E-03 1.701E-03 1.718E-03 1.734E-03 1.749E-03
            1.765E-03 1.780E-03 1.795E-03 1.809E-03 1.824E-03 1.838E-03
            1.852E-03 1.866E-03 1.879E-03 1.892E-03 1.905E-03 1.918E-03
            1.930E-03 1.942E-03 1.955E-03 1.966E-03

C
C
FC6076      e- RMF intra-track DSB interaction term (100% pO2)
F6076:E     1
C
FM6076      0.1602  $MeV/g to nGy
DE6076      1.000E-05 1.200E-05 1.450E-05 1.750E-05 2.100E-05 2.540E-05
            3.050E-05 3.680E-05 4.430E-05 5.340E-05 6.430E-05 7.740E-05
            9.330E-05 1.120E-04 1.350E-04 1.630E-04 1.960E-04 2.360E-04
            2.850E-04 3.430E-04 4.130E-04 4.980E-04 5.990E-04 7.220E-04
            8.700E-04 1.050E-03 1.260E-03 1.520E-03 1.830E-03 2.210E-03
            2.660E-03 3.200E-03 3.850E-03 4.640E-03 5.590E-03 6.730E-03
            8.110E-03 9.770E-03 1.180E-02 1.420E-02 1.710E-02 2.060E-02
            2.480E-02 2.980E-02 3.590E-02 4.330E-02 5.210E-02 6.280E-02
            7.560E-02 9.110E-02 1.100E-01 1.320E-01 1.590E-01 1.920E-01
            2.310E-01 2.780E-01 3.350E-01 4.040E-01 4.860E-01 5.860E-01
            7.050E-01 8.500E-01 1.020E+00 1.230E+00 1.480E+00 1.790E+00
            2.150E+00 2.600E+00 3.130E+00 3.760E+00 4.530E+00 5.460E+00
            6.580E+00 7.920E+00 9.550E+00 1.150E+01 1.380E+01 1.670E+01
            2.010E+01 2.420E+01 2.920E+01 3.510E+01 4.230E+01 5.090E+01
            6.140E+01 7.390E+01 8.900E+01 1.070E+02 1.290E+02 1.560E+02
            1.870E+02 2.260E+02 2.720E+02 3.270E+02 3.940E+02 4.750E+02
            5.720E+02 6.890E+02 8.300E+02 1.000E+03
DF6076      2.801E-04 3.352E-04 4.034E-04 4.842E-04 5.781E-04 6.923E-04
            8.215E-04 9.766E-04 1.152E-03 1.354E-03 1.578E-03 1.826E-03
            2.097E-03 2.378E-03 2.670E-03 2.979E-03 3.271E-03 3.572E-03
            3.864E-03 4.146E-03 4.433E-03 4.712E-03 5.027E-03 5.368E-03
            5.743E-03 6.209E-03 6.694E-03 7.310E-03 8.048E-03 8.958E-03
            1.003E-02 1.130E-02 1.279E-02 1.464E-02 1.672E-02 1.911E-02
            2.162E-02 2.389E-02 2.481E-02 2.155E-02 1.575E-02 1.261E-02
            1.047E-02 8.754E-03 7.436E-03 6.329E-03 5.458E-03 4.732E-03
            4.129E-03 3.628E-03 3.199E-03 2.854E-03 2.572E-03 2.320E-03
            2.131E-03 1.967E-03 1.829E-03 1.723E-03 1.642E-03 1.577E-03
            1.531E-03 1.493E-03 1.472E-03 1.458E-03 1.448E-03 1.454E-03
            1.458E-03 1.464E-03 1.476E-03 1.489E-03 1.505E-03 1.519E-03
            1.534E-03 1.553E-03 1.571E-03 1.589E-03 1.612E-03 1.630E-03
            1.647E-03 1.664E-03 1.680E-03 1.696E-03 1.712E-03 1.728E-03
            1.743E-03 1.758E-03 1.773E-03 1.787E-03 1.802E-03 1.816E-03
            1.829E-03 1.843E-03 1.856E-03 1.869E-03 1.881E-03 1.894E-03
            1.906E-03 1.919E-03 1.931E-03 1.942E-03
```

```
e- DOSE-RESPONSE FUNCTIONS FOR USE IN MCNP6 (June 11, 2016)
Data generated using MCDS Version 3.10A  05-DEC-2011

C
C           DSB (60Co):   2.86
C           SSB (60Co): 115.53
C           BD  (60Co): 293.98
C
C    ***    ============================================================
C    ***                 e-  DOSE, RBE AND RELATED TALLIES
C    ***    ------------------------------------------------------------
C
FC6016      e- Absorbed Dose
F6016:E     1
C
FM6016      0.1602  $MeV/g to nGy
C
C
FC6026      e- RBE for DSB induction (0% pO2) relative to 60Co
F6026:E     1
C
FM6026      0.1602  $MeV/g to nGy
DE6026      1.000E-05 1.200E-05 1.450E-05 1.750E-05 2.100E-05 2.540E-05
            3.050E-05 3.680E-05 4.430E-05 5.340E-05 6.430E-05 7.740E-05
            9.330E-05 1.120E-04 1.350E-04 1.630E-04 1.960E-04 2.360E-04
            2.850E-04 3.430E-04 4.130E-04 4.980E-04 5.990E-04 7.220E-04
            8.700E-04 1.050E-03 1.260E-03 1.520E-03 1.830E-03 2.210E-03
            2.660E-03 3.200E-03 3.850E-03 4.640E-03 5.590E-03 6.730E-03
            8.110E-03 9.770E-03 1.180E-02 1.420E-02 1.710E-02 2.060E-02
            2.480E-02 2.980E-02 3.590E-02 4.330E-02 5.210E-02 6.280E-02
            7.560E-02 9.110E-02 1.100E-01 1.320E-01 1.590E-01 1.920E-01
            2.310E-01 2.780E-01 3.350E-01 4.040E-01 4.860E-01 5.860E-01
            7.050E-01 8.500E-01 1.020E+00 1.230E+00 1.480E+00 1.790E+00
            2.150E+00 2.600E+00 3.130E+00 3.760E+00 4.530E+00 5.460E+00
            6.580E+00 7.920E+00 9.550E+00 1.150E+01 1.380E+01 1.670E+01
            2.010E+01 2.420E+01 2.920E+01 3.510E+01 4.230E+01 5.090E+01
            6.140E+01 7.390E+01 8.900E+01 1.070E+02 1.290E+02 1.560E+02
            1.870E+02 2.260E+02 2.720E+02 3.270E+02 3.940E+02 4.750E+02
            5.720E+02 6.890E+02 8.300E+02 1.000E+03
DF6026      9.831E+00 9.819E+00 9.790E+00 9.753E+00 9.719E+00 9.652E+00
            9.564E+00 9.452E+00 9.291E+00 9.077E+00 8.791E+00 8.423E+00
            7.961E+00 7.392E+00 6.711E+00 5.960E+00 5.198E+00 4.466E+00
            3.811E+00 3.259E+00 2.812E+00 2.456E+00 2.186E+00 1.968E+00
            1.795E+00 1.659E+00 1.546E+00 1.452E+00 1.375E+00 1.316E+00
            1.258E+00 1.216E+00 1.178E+00 1.146E+00 1.123E+00 1.098E+00
            1.079E+00 1.066E+00 1.054E+00 1.040E+00 1.032E+00 1.027E+00
            1.022E+00 1.016E+00 1.014E+00 1.007E+00 1.007E+00 1.003E+00
            9.999E-01 9.989E-01 9.990E-01 9.963E-01 9.970E-01 9.935E-01
            9.953E-01 9.929E-01 9.934E-01 9.931E-01 9.941E-01 9.910E-01
            9.923E-01 9.904E-01 9.915E-01 9.912E-01 9.907E-01 9.932E-01
            9.922E-01 9.908E-01 9.920E-01 9.916E-01 9.905E-01 9.907E-01
            9.872E-01 9.918E-01 9.918E-01 9.918E-01 9.917E-01 9.917E-01
            9.917E-01 9.917E-01 9.917E-01 9.917E-01 9.917E-01 9.917E-01
            9.917E-01 9.917E-01 9.917E-01 9.917E-01 9.917E-01 9.917E-01
            9.917E-01 9.917E-01 9.917E-01 9.917E-01 9.917E-01 9.917E-01
            9.917E-01 9.917E-01 9.917E-01 9.917E-01
```

```
C
C
FC6036      e- RBE for SSB induction (0% pO2) relative to 60Co
F6036:E     1
C
FM6036      0.1602  $MeV/g to nGy
DE6036      1.000E-05 1.200E-05 1.450E-05 1.750E-05 2.100E-05 2.540E-05
            3.050E-05 3.680E-05 4.430E-05 5.340E-05 6.430E-05 7.740E-05
            9.330E-05 1.120E-04 1.350E-04 1.630E-04 1.960E-04 2.360E-04
            2.850E-04 3.430E-04 4.130E-04 4.980E-04 5.990E-04 7.220E-04
            8.700E-04 1.050E-03 1.260E-03 1.520E-03 1.830E-03 2.210E-03
            2.660E-03 3.200E-03 3.850E-03 4.640E-03 5.590E-03 6.730E-03
            8.110E-03 9.770E-03 1.180E-02 1.420E-02 1.710E-02 2.060E-02
            2.480E-02 2.980E-02 3.590E-02 4.330E-02 5.210E-02 6.280E-02
            7.560E-02 9.110E-02 1.100E-01 1.320E-01 1.590E-01 1.920E-01
            2.310E-01 2.780E-01 3.350E-01 4.040E-01 4.860E-01 5.860E-01
            7.050E-01 8.500E-01 1.020E+00 1.230E+00 1.480E+00 1.790E+00
            2.150E+00 2.600E+00 3.130E+00 3.760E+00 4.530E+00 5.460E+00
            6.580E+00 7.920E+00 9.550E+00 1.150E+01 1.380E+01 1.670E+01
            2.010E+01 2.420E+01 2.920E+01 3.510E+01 4.230E+01 5.090E+01
            6.140E+01 7.390E+01 8.900E+01 1.070E+02 1.290E+02 1.560E+02
            1.870E+02 2.260E+02 2.720E+02 3.270E+02 3.940E+02 4.750E+02
            5.720E+02 6.890E+02 8.300E+02 1.000E+03
DF6036      5.423E-01 5.527E-01 5.657E-01 5.809E-01 5.979E-01 6.197E-01
            6.439E-01 6.726E-01 7.053E-01 7.423E-01 7.829E-01 8.265E-01
            8.720E-01 9.145E-01 9.529E-01 9.823E-01 9.997E-01 1.005E+00
            1.002E+00 9.937E-01 9.840E-01 9.753E-01 9.694E-01 9.666E-01
            9.666E-01 9.674E-01 9.703E-01 9.727E-01 9.752E-01 9.789E-01
            9.808E-01 9.845E-01 9.863E-01 9.890E-01 9.910E-01 9.916E-01
            9.932E-01 9.943E-01 9.954E-01 9.964E-01 9.971E-01 9.976E-01
            9.980E-01 9.985E-01 9.988E-01 9.992E-01 9.994E-01 9.996E-01
            9.998E-01 1.000E+00 9.999E-01 1.000E+00 1.000E+00 1.000E+00
            1.000E+00 1.000E+00 1.000E+00 1.000E+00 1.000E+00 1.001E+00
            1.000E+00 1.001E+00 1.001E+00 1.001E+00 1.001E+00 1.000E+00
            1.001E+00 1.001E+00 1.000E+00 1.000E+00 1.001E+00 1.001E+00
            1.001E+00 1.001E+00 1.001E+00 1.001E+00 1.000E+00 1.000E+00
            1.000E+00 1.000E+00 1.000E+00 1.000E+00 1.000E+00 1.000E+00
            1.000E+00 1.000E+00 1.000E+00 1.000E+00 1.000E+00 1.000E+00
            1.000E+00 1.000E+00 1.000E+00 1.000E+00 1.000E+00 1.000E+00
            1.000E+00 1.000E+00 1.000E+00 1.000E+00
C
C
FC6046      e- RBE for BD induction (0% pO2) relative to 60Co
F6046:E     1
C
FM6046      0.1602  $MeV/g to nGy
DE6046      1.000E-05 1.200E-05 1.450E-05 1.750E-05 2.100E-05 2.540E-05
            3.050E-05 3.680E-05 4.430E-05 5.340E-05 6.430E-05 7.740E-05
            9.330E-05 1.120E-04 1.350E-04 1.630E-04 1.960E-04 2.360E-04
            2.850E-04 3.430E-04 4.130E-04 4.980E-04 5.990E-04 7.220E-04
            8.700E-04 1.050E-03 1.260E-03 1.520E-03 1.830E-03 2.210E-03
            2.660E-03 3.200E-03 3.850E-03 4.640E-03 5.590E-03 6.730E-03
            8.110E-03 9.770E-03 1.180E-02 1.420E-02 1.710E-02 2.060E-02
            2.480E-02 2.980E-02 3.590E-02 4.330E-02 5.210E-02 6.280E-02
            7.560E-02 9.110E-02 1.100E-01 1.320E-01 1.590E-01 1.920E-01
            2.310E-01 2.780E-01 3.350E-01 4.040E-01 4.860E-01 5.860E-01
            7.050E-01 8.500E-01 1.020E+00 1.230E+00 1.480E+00 1.790E+00
            2.150E+00 2.600E+00 3.130E+00 3.760E+00 4.530E+00 5.460E+00
            6.580E+00 7.920E+00 9.550E+00 1.150E+01 1.380E+01 1.670E+01
            2.010E+01 2.420E+01 2.920E+01 3.510E+01 4.230E+01 5.090E+01
            6.140E+01 7.390E+01 8.900E+01 1.070E+02 1.290E+02 1.560E+02
```

```
            1.870E+02 2.260E+02 2.720E+02 3.270E+02 3.940E+02 4.750E+02
            5.720E+02 6.890E+02 8.300E+02 1.000E+03
DF6046      1.413E-01 1.457E-01 1.515E-01 1.586E-01 1.669E-01 1.774E-01
            1.899E-01 2.054E-01 2.244E-01 2.480E-01 2.766E-01 3.111E-01
            3.526E-01 4.002E-01 4.546E-01 5.132E-01 5.707E-01 6.249E-01
            6.733E-01 7.134E-01 7.475E-01 7.766E-01 8.023E-01 8.253E-01
            8.467E-01 8.668E-01 8.841E-01 9.002E-01 9.149E-01 9.279E-01
            9.392E-01 9.488E-01 9.574E-01 9.646E-01 9.707E-01 9.758E-01
            9.804E-01 9.841E-01 9.873E-01 9.899E-01 9.924E-01 9.938E-01
            9.952E-01 9.964E-01 9.976E-01 9.985E-01 9.991E-01 9.996E-01
            1.000E+00 1.001E+00 1.001E+00 1.001E+00 1.002E+00 1.002E+00
            1.002E+00 1.002E+00 1.002E+00 1.002E+00 1.002E+00 1.002E+00
            1.002E+00 1.003E+00 1.003E+00 1.003E+00 1.003E+00 1.003E+00
            1.003E+00 1.003E+00 1.003E+00 1.003E+00 1.003E+00 1.003E+00
            1.003E+00 1.003E+00 1.003E+00 1.003E+00 1.003E+00 1.003E+00
            1.003E+00 1.003E+00 1.003E+00 1.003E+00 1.003E+00 1.003E+00
            1.003E+00 1.003E+00 1.003E+00 1.003E+00 1.003E+00 1.003E+00
            1.003E+00 1.003E+00 1.003E+00 1.003E+00
C
C
FC6076      e- RMF intra-track DSB interaction term (0% pO2)
F6076:E     1
C
FM6076      0.1602  $MeV/g to nGy
DE6076      1.000E-05 1.200E-05 1.450E-05 1.750E-05 2.100E-05 2.540E-05
            3.050E-05 3.680E-05 4.430E-05 5.340E-05 6.430E-05 7.740E-05
            9.330E-05 1.120E-04 1.350E-04 1.630E-04 1.960E-04 2.360E-04
            2.850E-04 3.430E-04 4.130E-04 4.980E-04 5.990E-04 7.220E-04
            8.700E-04 1.050E-03 1.260E-03 1.520E-03 1.830E-03 2.210E-03
            2.660E-03 3.200E-03 3.850E-03 4.640E-03 5.590E-03 6.730E-03
            8.110E-03 9.770E-03 1.180E-02 1.420E-02 1.710E-02 2.060E-02
            2.480E-02 2.980E-02 3.590E-02 4.330E-02 5.210E-02 6.280E-02
            7.560E-02 9.110E-02 1.100E-01 1.320E-01 1.590E-01 1.920E-01
            2.310E-01 2.780E-01 3.350E-01 4.040E-01 4.860E-01 5.860E-01
            7.050E-01 8.500E-01 1.020E+00 1.230E+00 1.480E+00 1.790E+00
            2.150E+00 2.600E+00 3.130E+00 3.760E+00 4.530E+00 5.460E+00
            6.580E+00 7.920E+00 9.550E+00 1.150E+01 1.380E+01 1.670E+01
            2.010E+01 2.420E+01 2.920E+01 3.510E+01 4.230E+01 5.090E+01
            6.140E+01 7.390E+01 8.900E+01 1.070E+02 1.290E+02 1.560E+02
            1.870E+02 2.260E+02 2.720E+02 3.270E+02 3.940E+02 4.750E+02
            5.720E+02 6.890E+02 8.300E+02 1.000E+03
DF6076      2.366E-03 2.832E-03 3.401E-03 4.074E-03 4.856E-03 5.792E-03
            6.829E-03 8.047E-03 9.360E-03 1.077E-02 1.216E-02 1.344E-02
            1.448E-02 1.498E-02 1.488E-02 1.417E-02 1.296E-02 1.152E-02
            1.013E-02 8.915E-03 7.994E-03 7.350E-03 7.003E-03 6.847E-03
            6.861E-03 7.070E-03 7.367E-03 7.839E-03 8.463E-03 9.366E-03
            1.029E-02 1.154E-02 1.300E-02 1.477E-02 1.697E-02 1.920E-02
            2.168E-02 2.400E-02 2.485E-02 2.147E-02 1.570E-02 1.262E-02
            1.044E-02 8.747E-03 7.442E-03 6.313E-03 5.465E-03 4.723E-03
            4.110E-03 3.612E-03 3.198E-03 2.847E-03 2.566E-03 2.309E-03
            2.124E-03 1.954E-03 1.826E-03 1.720E-03 1.642E-03 1.568E-03
            1.524E-03 1.484E-03 1.465E-03 1.450E-03 1.443E-03 1.450E-03
            1.452E-03 1.457E-03 1.473E-03 1.485E-03 1.497E-03 1.514E-03
            1.521E-03 1.553E-03 1.570E-03 1.588E-03 1.605E-03 1.623E-03
            1.640E-03 1.657E-03 1.673E-03 1.689E-03 1.705E-03 1.721E-03
            1.736E-03 1.751E-03 1.765E-03 1.780E-03 1.794E-03 1.808E-03
            1.821E-03 1.835E-03 1.848E-03 1.861E-03 1.873E-03 1.886E-03
            1.898E-03 1.910E-03 1.922E-03 1.934E-03
```

Alpha Particles

```
4He DOSE-RESPONSE FUNCTIONS FOR USE IN MCNP6 (April 25, 2016)
Data generated using MCDS Version 3.10A  05-DEC-2011

C
C           DSB (60Co):   8.32
C           SSB (60Co): 188.63
C           BD  (60Co): 425.26
C
C    ***    ========================================================
C    ***                 4He  DOSE, RBE AND RELATED TALLIES
C    ***    --------------------------------------------------------
C
FC1016      4He Absorbed Dose
F1016:A     1
FM1016      0.1602  $MeV/g to nGy
C
C
FC5026      4He RBE for DSB induction (100% pO2) relative to 60Co
F5026:A     1
FM5026      0.1602  $MeV/g to nGy
DE5026      1.000E-03 1.500E-03 2.000E-03 2.500E-03 3.000E-03 4.000E-03
            5.000E-03 6.000E-03 7.000E-03 8.000E-03 9.000E-03 1.000E-02
            1.250E-02 1.500E-02 1.750E-02 2.000E-02 2.250E-02 2.500E-02
            2.750E-02 3.000E-02 3.500E-02 4.000E-02 4.500E-02 5.000E-02
            5.500E-02 6.000E-02 6.500E-02 7.000E-02 7.500E-02 8.000E-02
            8.500E-02 9.000E-02 9.500E-02 1.000E-01 1.250E-01 1.500E-01
            1.750E-01 2.000E-01 2.250E-01 2.500E-01 2.750E-01 3.000E-01
            3.500E-01 4.000E-01 4.500E-01 5.000E-01 5.500E-01 6.000E-01
            6.500E-01 7.000E-01 7.500E-01 8.000E-01 8.500E-01 9.000E-01
            9.500E-01 1.000E+00 1.250E+00 1.500E+00 1.750E+00 2.000E+00
            2.250E+00 2.500E+00 2.750E+00 3.000E+00 3.500E+00 4.000E+00
            4.500E+00 5.000E+00 5.500E+00 6.000E+00 6.500E+00 7.000E+00
            7.500E+00 8.000E+00 8.500E+00 9.000E+00 9.500E+00 1.000E+01
            1.250E+01 1.500E+01 1.750E+01 2.000E+01 2.500E+01 2.750E+01
            3.000E+01 3.500E+01 4.000E+01 4.500E+01 5.000E+01 5.500E+01
            6.000E+01 6.500E+01 7.000E+01 7.500E+01 8.000E+01 8.500E+01
            9.000E+01 9.500E+01 1.000E+02 1.250E+02 1.500E+02 1.750E+02
            2.000E+02 2.250E+02 2.500E+02 2.750E+02 3.000E+02 3.500E+02
            3.750E+02 4.000E+02 4.500E+02 5.000E+02 5.500E+02 6.000E+02
            6.500E+02 7.000E+02 7.500E+02 8.000E+02 8.500E+02 9.000E+02
            9.500E+02 1.000E+03 2.000E+03 5.000E+03 7.500E+03 1.000E+04
DF5026      3.381E+00 3.379E+00 3.381E+00 3.380E+00 3.378E+00 3.379E+00
            3.378E+00 3.377E+00 3.378E+00 3.378E+00 3.377E+00 3.377E+00
            3.377E+00 3.376E+00 3.374E+00 3.375E+00 3.375E+00 3.373E+00
            3.371E+00 3.372E+00 3.372E+00 3.370E+00 3.371E+00 3.370E+00
            3.367E+00 3.368E+00 3.369E+00 3.365E+00 3.365E+00 3.366E+00
            3.365E+00 3.364E+00 3.362E+00 3.362E+00 3.358E+00 3.355E+00
            3.352E+00 3.349E+00 3.345E+00 3.342E+00 3.338E+00 3.334E+00
            3.329E+00 3.323E+00 3.317E+00 3.309E+00 3.303E+00 3.294E+00
            3.289E+00 3.283E+00 3.276E+00 3.270E+00 3.263E+00 3.253E+00
            3.247E+00 3.239E+00 3.204E+00 3.165E+00 3.129E+00 3.092E+00
            3.055E+00 3.018E+00 2.979E+00 2.945E+00 2.869E+00 2.804E+00
            2.739E+00 2.679E+00 2.622E+00 2.567E+00 2.513E+00 2.466E+00
            2.417E+00 2.373E+00 2.332E+00 2.291E+00 2.255E+00 2.222E+00
            2.070E+00 1.948E+00 1.852E+00 1.774E+00 1.654E+00 1.607E+00
            1.566E+00 1.500E+00 1.444E+00 1.402E+00 1.367E+00 1.338E+00
            1.311E+00 1.288E+00 1.271E+00 1.254E+00 1.240E+00 1.224E+00
```

```
            1.216E+00 1.204E+00 1.195E+00 1.158E+00 1.131E+00 1.115E+00
            1.100E+00 1.088E+00 1.079E+00 1.072E+00 1.067E+00 1.057E+00
            1.053E+00 1.051E+00 1.044E+00 1.041E+00 1.037E+00 1.031E+00
            1.032E+00 1.029E+00 1.027E+00 1.027E+00 1.024E+00 1.022E+00
            1.020E+00 1.020E+00 1.010E+00 1.004E+00 1.004E+00 1.002E+00
C
C
FC5036      4He RBE for SSB induction (100% pO2) relative to 60Co
F5036:A     1
FM5036      0.1602  $MeV/g to nGy
DE5036      1.000E-03 1.500E-03 2.000E-03 2.500E-03 3.000E-03 4.000E-03
            5.000E-03 6.000E-03 7.000E-03 8.000E-03 9.000E-03 1.000E-02
            1.250E-02 1.500E-02 1.750E-02 2.000E-02 2.250E-02 2.500E-02
            2.750E-02 3.000E-02 3.500E-02 4.000E-02 4.500E-02 5.000E-02
            5.500E-02 6.000E-02 6.500E-02 7.000E-02 7.500E-02 8.000E-02
            8.500E-02 9.000E-02 9.500E-02 1.000E-01 1.250E-01 1.500E-01
            1.750E-01 2.000E-01 2.250E-01 2.500E-01 2.750E-01 3.000E-01
            3.500E-01 4.000E-01 4.500E-01 5.000E-01 5.500E-01 6.000E-01
            6.500E-01 7.000E-01 7.500E-01 8.000E-01 8.500E-01 9.000E-01
            9.500E-01 1.000E+00 1.250E+00 1.500E+00 1.750E+00 2.000E+00
            2.250E+00 2.500E+00 2.750E+00 3.000E+00 3.500E+00 4.000E+00
            4.500E+00 5.000E+00 5.500E+00 6.000E+00 6.500E+00 7.000E+00
            7.500E+00 8.000E+00 8.500E+00 9.000E+00 9.500E+00 1.000E+01
            1.250E+01 1.500E+01 1.750E+01 2.000E+01 2.500E+01 2.750E+01
            3.000E+01 3.500E+01 4.000E+01 4.500E+01 5.000E+01 5.500E+01
            6.000E+01 6.500E+01 7.000E+01 7.500E+01 8.000E+01 8.500E+01
            9.000E+01 9.500E+01 1.000E+02 1.250E+02 1.500E+02 1.750E+02
            2.000E+02 2.250E+02 2.500E+02 2.750E+02 3.000E+02 3.500E+02
            3.750E+02 4.000E+02 4.500E+02 5.000E+02 5.500E+02 6.000E+02
            6.500E+02 7.000E+02 7.500E+02 8.000E+02 8.500E+02 9.000E+02
            9.500E+02 1.000E+03 2.000E+03 5.000E+03 7.500E+03 1.000E+04
DF5036      3.349E-01 3.353E-01 3.356E-01 3.359E-01 3.363E-01 3.368E-01
            3.372E-01 3.378E-01 3.380E-01 3.384E-01 3.388E-01 3.393E-01
            3.401E-01 3.407E-01 3.415E-01 3.422E-01 3.428E-01 3.434E-01
            3.439E-01 3.444E-01 3.454E-01 3.465E-01 3.475E-01 3.482E-01
            3.492E-01 3.501E-01 3.510E-01 3.517E-01 3.524E-01 3.532E-01
            3.540E-01 3.546E-01 3.554E-01 3.563E-01 3.594E-01 3.627E-01
            3.657E-01 3.685E-01 3.713E-01 3.741E-01 3.768E-01 3.793E-01
            3.843E-01 3.890E-01 3.936E-01 3.984E-01 4.026E-01 4.072E-01
            4.116E-01 4.156E-01 4.197E-01 4.236E-01 4.279E-01 4.319E-01
            4.356E-01 4.396E-01 4.580E-01 4.756E-01 4.921E-01 5.075E-01
            5.223E-01 5.365E-01 5.501E-01 5.629E-01 5.867E-01 6.081E-01
            6.279E-01 6.458E-01 6.623E-01 6.775E-01 6.916E-01 7.044E-01
            7.159E-01 7.270E-01 7.373E-01 7.469E-01 7.557E-01 7.639E-01
            7.986E-01 8.242E-01 8.442E-01 8.604E-01 8.841E-01 8.932E-01
            9.011E-01 9.137E-01 9.237E-01 9.314E-01 9.379E-01 9.431E-01
            9.478E-01 9.516E-01 9.549E-01 9.578E-01 9.603E-01 9.628E-01
            9.645E-01 9.664E-01 9.681E-01 9.744E-01 9.787E-01 9.818E-01
            9.841E-01 9.860E-01 9.874E-01 9.887E-01 9.896E-01 9.912E-01
            9.918E-01 9.922E-01 9.932E-01 9.939E-01 9.946E-01 9.953E-01
            9.955E-01 9.959E-01 9.962E-01 9.965E-01 9.967E-01 9.970E-01
            9.972E-01 9.974E-01 9.990E-01 9.999E-01 1.000E+00 1.000E+00
C
C
```

```
FC5046      4He RBE for BD induction (100% pO2) relative to 60Co
F5046:A     1
FM5046      0.1602  $MeV/g to nGy
DE5046      1.000E-03 1.500E-03 2.000E-03 2.500E-03 3.000E-03 4.000E-03
            5.000E-03 6.000E-03 7.000E-03 8.000E-03 9.000E-03 1.000E-02
            1.250E-02 1.500E-02 1.750E-02 2.000E-02 2.250E-02 2.500E-02
            2.750E-02 3.000E-02 3.500E-02 4.000E-02 4.500E-02 5.000E-02
            5.500E-02 6.000E-02 6.500E-02 7.000E-02 7.500E-02 8.000E-02
            8.500E-02 9.000E-02 9.500E-02 1.000E-01 1.250E-01 1.500E-01
            1.750E-01 2.000E-01 2.250E-01 2.500E-01 2.750E-01 3.000E-01
            3.500E-01 4.000E-01 4.500E-01 5.000E-01 5.500E-01 6.000E-01
            6.500E-01 7.000E-01 7.500E-01 8.000E-01 8.500E-01 9.000E-01
            9.500E-01 1.000E+00 1.250E+00 1.500E+00 1.750E+00 2.000E+00
            2.250E+00 2.500E+00 2.750E+00 3.000E+00 3.500E+00 4.000E+00
            4.500E+00 5.000E+00 5.500E+00 6.000E+00 6.500E+00 7.000E+00
            7.500E+00 8.000E+00 8.500E+00 9.000E+00 9.500E+00 1.000E+01
            1.250E+01 1.500E+01 1.750E+01 2.000E+01 2.500E+01 2.750E+01
            3.000E+01 3.500E+01 4.000E+01 4.500E+01 5.000E+01 5.500E+01
            6.000E+01 6.500E+01 7.000E+01 7.500E+01 8.000E+01 8.500E+01
            9.000E+01 9.500E+01 1.000E+02 1.250E+02 1.500E+02 1.750E+02
            2.000E+02 2.250E+02 2.500E+02 2.750E+02 3.000E+02 3.500E+02
            3.750E+02 4.000E+02 4.500E+02 5.000E+02 5.500E+02 6.000E+02
            6.500E+02 7.000E+02 7.500E+02 8.000E+02 8.500E+02 9.000E+02
            9.500E+02 1.000E+03 2.000E+03 5.000E+03 7.500E+03 1.000E+04
DF5046      9.896E-02 9.915E-02 9.933E-02 9.947E-02 9.965E-02 9.991E-02
            1.001E-01 1.004E-01 1.006E-01 1.008E-01 1.009E-01 1.011E-01
            1.015E-01 1.018E-01 1.022E-01 1.026E-01 1.028E-01 1.031E-01
            1.034E-01 1.037E-01 1.043E-01 1.047E-01 1.052E-01 1.056E-01
            1.061E-01 1.066E-01 1.069E-01 1.073E-01 1.078E-01 1.081E-01
            1.086E-01 1.089E-01 1.093E-01 1.096E-01 1.114E-01 1.130E-01
            1.147E-01 1.162E-01 1.177E-01 1.191E-01 1.206E-01 1.220E-01
            1.248E-01 1.275E-01 1.302E-01 1.328E-01 1.355E-01 1.380E-01
            1.405E-01 1.432E-01 1.457E-01 1.482E-01 1.507E-01 1.532E-01
            1.558E-01 1.582E-01 1.706E-01 1.828E-01 1.949E-01 2.070E-01
            2.188E-01 2.304E-01 2.419E-01 2.533E-01 2.757E-01 2.971E-01
            3.177E-01 3.376E-01 3.564E-01 3.745E-01 3.919E-01 4.084E-01
            4.244E-01 4.395E-01 4.540E-01 4.677E-01 4.809E-01 4.935E-01
            5.489E-01 5.940E-01 6.312E-01 6.624E-01 7.113E-01 7.309E-01
            7.481E-01 7.767E-01 7.995E-01 8.182E-01 8.336E-01 8.468E-01
            8.578E-01 8.677E-01 8.761E-01 8.835E-01 8.901E-01 8.961E-01
            9.016E-01 9.061E-01 9.108E-01 9.277E-01 9.393E-01 9.478E-01
            9.543E-01 9.594E-01 9.636E-01 9.669E-01 9.697E-01 9.742E-01
            9.760E-01 9.775E-01 9.802E-01 9.823E-01 9.839E-01 9.854E-01
            9.866E-01 9.877E-01 9.886E-01 9.895E-01 9.902E-01 9.909E-01
            9.914E-01 9.920E-01 9.967E-01 9.994E-01 9.999E-01 1.000E+00
C
C
FC5056      4He LET (keV/um)
F5056:A     1
FM5056      0.1602  $MeV/g to nGy
DE5056      1.000E-03 1.500E-03 2.000E-03 2.500E-03 3.000E-03 4.000E-03
            5.000E-03 6.000E-03 7.000E-03 8.000E-03 9.000E-03 1.000E-02
            1.250E-02 1.500E-02 1.750E-02 2.000E-02 2.250E-02 2.500E-02
            2.750E-02 3.000E-02 3.500E-02 4.000E-02 4.500E-02 5.000E-02
            5.500E-02 6.000E-02 6.500E-02 7.000E-02 7.500E-02 8.000E-02
            8.500E-02 9.000E-02 9.500E-02 1.000E-01 1.250E-01 1.500E-01
            1.750E-01 2.000E-01 2.250E-01 2.500E-01 2.750E-01 3.000E-01
            3.500E-01 4.000E-01 4.500E-01 5.000E-01 5.500E-01 6.000E-01
            6.500E-01 7.000E-01 7.500E-01 8.000E-01 8.500E-01 9.000E-01
            9.500E-01 1.000E+00 1.250E+00 1.500E+00 1.750E+00 2.000E+00
            2.250E+00 2.500E+00 2.750E+00 3.000E+00 3.500E+00 4.000E+00
```

```
            4.500E+00 5.000E+00 5.500E+00 6.000E+00 6.500E+00 7.000E+00
            7.500E+00 8.000E+00 8.500E+00 9.000E+00 9.500E+00 1.000E+01
            1.250E+01 1.500E+01 1.750E+01 2.000E+01 2.500E+01 2.750E+01
            3.000E+01 3.500E+01 4.000E+01 4.500E+01 5.000E+01 5.500E+01
            6.000E+01 6.500E+01 7.000E+01 7.500E+01 8.000E+01 8.500E+01
            9.000E+01 9.500E+01 1.000E+02 1.250E+02 1.500E+02 1.750E+02
            2.000E+02 2.250E+02 2.500E+02 2.750E+02 3.000E+02 3.500E+02
            3.750E+02 4.000E+02 4.500E+02 5.000E+02 5.500E+02 6.000E+02
            6.500E+02 7.000E+02 7.500E+02 8.000E+02 8.500E+02 9.000E+02
            9.500E+02 1.000E+03 2.000E+03 5.000E+03 7.500E+03 1.000E+04
DF5056      3.298E+01 3.310E+01 3.329E+01 3.359E+01 3.397E+01 3.494E+01
            3.609E+01 3.734E+01 3.866E+01 4.000E+01 4.135E+01 4.270E+01
            4.602E+01 4.923E+01 5.231E+01 5.526E+01 5.809E+01 6.079E+01
            6.339E+01 6.588E+01 7.060E+01 7.501E+01 7.914E+01 8.304E+01
            8.674E+01 9.027E+01 9.364E+01 9.687E+01 9.998E+01 1.030E+02
            1.059E+02 1.087E+02 1.114E+02 1.141E+02 1.265E+02 1.377E+02
            1.480E+02 1.576E+02 1.665E+02 1.747E+02 1.823E+02 1.892E+02
            2.011E+02 2.104E+02 2.174E+02 2.223E+02 2.255E+02 2.272E+02
            2.277E+02 2.273E+02 2.262E+02 2.244E+02 2.223E+02 2.199E+02
            2.172E+02 2.143E+02 1.993E+02 1.848E+02 1.718E+02 1.604E+02
            1.503E+02 1.415E+02 1.336E+02 1.266E+02 1.148E+02 1.050E+02
            9.694E+01 9.008E+01 8.419E+01 7.908E+01 7.460E+01 7.064E+01
            6.711E+01 6.395E+01 6.110E+01 5.851E+01 5.615E+01 5.399E+01
            4.545E+01 3.941E+01 3.491E+01 3.140E+01 2.629E+01 2.436E+01
            2.272E+01 2.007E+01 1.802E+01 1.639E+01 1.505E+01 1.393E+01
            1.299E+01 1.217E+01 1.146E+01 1.084E+01 1.029E+01 9.793E+00
            9.350E+00 8.950E+00 8.586E+00 7.171E+00 6.194E+00 5.477E+00
            4.927E+00 4.491E+00 4.136E+00 3.842E+00 3.593E+00 3.196E+00
            3.035E+00 2.893E+00 2.653E+00 2.459E+00 2.299E+00 2.163E+00
            2.048E+00 1.949E+00 1.862E+00 1.786E+00 1.718E+00 1.657E+00
            1.603E+00 1.554E+00 1.083E+00 8.129E-01 7.635E-01 7.436E-01
C
C
FC5066      4He ZF (mean specific energy)
F5066:A     1
FM5066      0.1602  $MeV/g to nGy
DE5066      1.000E-03 1.500E-03 2.000E-03 2.500E-03 3.000E-03 4.000E-03
            5.000E-03 6.000E-03 7.000E-03 8.000E-03 9.000E-03 1.000E-02
            1.250E-02 1.500E-02 1.750E-02 2.000E-02 2.250E-02 2.500E-02
            2.750E-02 3.000E-02 3.500E-02 4.000E-02 4.500E-02 5.000E-02
            5.500E-02 6.000E-02 6.500E-02 7.000E-02 7.500E-02 8.000E-02
            8.500E-02 9.000E-02 9.500E-02 1.000E-01 1.250E-01 1.500E-01
            1.750E-01 2.000E-01 2.250E-01 2.500E-01 2.750E-01 3.000E-01
            3.500E-01 4.000E-01 4.500E-01 5.000E-01 5.500E-01 6.000E-01
            6.500E-01 7.000E-01 7.500E-01 8.000E-01 8.500E-01 9.000E-01
            9.500E-01 1.000E+00 1.250E+00 1.500E+00 1.750E+00 2.000E+00
            2.250E+00 2.500E+00 2.750E+00 3.000E+00 3.500E+00 4.000E+00
            4.500E+00 5.000E+00 5.500E+00 6.000E+00 6.500E+00 7.000E+00
            7.500E+00 8.000E+00 8.500E+00 9.000E+00 9.500E+00 1.000E+01
            1.250E+01 1.500E+01 1.750E+01 2.000E+01 2.500E+01 2.750E+01
            3.000E+01 3.500E+01 4.000E+01 4.500E+01 5.000E+01 5.500E+01
            6.000E+01 6.500E+01 7.000E+01 7.500E+01 8.000E+01 8.500E+01
            9.000E+01 9.500E+01 1.000E+02 1.250E+02 1.500E+02 1.750E+02
            2.000E+02 2.250E+02 2.500E+02 2.750E+02 3.000E+02 3.500E+02
            3.750E+02 4.000E+02 4.500E+02 5.000E+02 5.500E+02 6.000E+02
            6.500E+02 7.000E+02 7.500E+02 8.000E+02 8.500E+02 9.000E+02
            9.500E+02 1.000E+03 2.000E+03 5.000E+03 7.500E+03 1.000E+04
DF5066      2.448E-03 3.671E-03 4.895E-03 6.119E-03 7.342E-03 9.789E-03
            1.223E-02 1.468E-02 1.713E-02 1.957E-02 2.201E-02 2.445E-02
            3.056E-02 3.665E-02 4.274E-02 4.882E-02 5.490E-02 6.097E-02
            6.704E-02 7.310E-02 8.520E-02 9.728E-02 1.093E-01 1.213E-01
```

```
            1.333E-01 1.453E-01 1.573E-01 1.692E-01 1.811E-01 1.930E-01
            2.048E-01 2.166E-01 2.284E-01 2.402E-01 2.986E-01 3.564E-01
            4.135E-01 4.699E-01 5.256E-01 5.807E-01 6.350E-01 6.886E-01
            7.935E-01 8.952E-01 9.935E-01 1.088E+00 1.177E+00 1.262E+00
            1.341E+00 1.415E+00 1.481E+00 1.540E+00 1.591E+00 1.635E+00
            1.673E+00 1.703E+00 1.754E+00 1.679E+00 1.556E+00 1.435E+00
            1.329E+00 1.238E+00 1.159E+00 1.091E+00 9.777E-01 8.878E-01
            8.145E-01 7.534E-01 7.017E-01 6.573E-01 6.186E-01 5.847E-01
            5.546E-01 5.278E-01 5.037E-01 4.819E-01 4.621E-01 4.440E-01
            3.728E-01 3.228E-01 2.857E-01 2.568E-01 2.148E-01 1.990E-01
            1.856E-01 1.639E-01 1.472E-01 1.338E-01 1.229E-01 1.137E-01
            1.060E-01 9.932E-02 9.353E-02 8.844E-02 8.394E-02 7.991E-02
            7.630E-02 7.303E-02 7.006E-02 5.851E-02 5.054E-02 4.469E-02
            4.020E-02 3.664E-02 3.375E-02 3.134E-02 2.932E-02 2.608E-02
            2.476E-02 2.360E-02 2.165E-02 2.006E-02 1.876E-02 1.765E-02
            1.671E-02 1.590E-02 1.519E-02 1.457E-02 1.402E-02 1.352E-02
            1.308E-02 1.268E-02 8.837E-03 6.632E-03 6.230E-03 6.067E-03
C
C
FC5076      4He intra-track RMF interaction term (100% pO2)
F5076:A     1
FM5076      0.1602  $MeV to nGy
DE5076      1.000E-03 1.500E-03 2.000E-03 2.500E-03 3.000E-03 4.000E-03
            5.000E-03 6.000E-03 7.000E-03 8.000E-03 9.000E-03 1.000E-02
            1.250E-02 1.500E-02 1.750E-02 2.000E-02 2.250E-02 2.500E-02
            2.750E-02 3.000E-02 3.500E-02 4.000E-02 4.500E-02 5.000E-02
            5.500E-02 6.000E-02 6.500E-02 7.000E-02 7.500E-02 8.000E-02
            8.500E-02 9.000E-02 9.500E-02 1.000E-01 1.250E-01 1.500E-01
            1.750E-01 2.000E-01 2.250E-01 2.500E-01 2.750E-01 3.000E-01
            3.500E-01 4.000E-01 4.500E-01 5.000E-01 5.500E-01 6.000E-01
            6.500E-01 7.000E-01 7.500E-01 8.000E-01 8.500E-01 9.000E-01
            9.500E-01 1.000E+00 1.250E+00 1.500E+00 1.750E+00 2.000E+00
            2.250E+00 2.500E+00 2.750E+00 3.000E+00 3.500E+00 4.000E+00
            4.500E+00 5.000E+00 5.500E+00 6.000E+00 6.500E+00 7.000E+00
            7.500E+00 8.000E+00 8.500E+00 9.000E+00 9.500E+00 1.000E+01
            1.250E+01 1.500E+01 1.750E+01 2.000E+01 2.500E+01 2.750E+01
            3.000E+01 3.500E+01 4.000E+01 4.500E+01 5.000E+01 5.500E+01
            6.000E+01 6.500E+01 7.000E+01 7.500E+01 8.000E+01 8.500E+01
            9.000E+01 9.500E+01 1.000E+02 1.250E+02 1.500E+02 1.750E+02
            2.000E+02 2.250E+02 2.500E+02 2.750E+02 3.000E+02 3.500E+02
            3.750E+02 4.000E+02 4.500E+02 5.000E+02 5.500E+02 6.000E+02
            6.500E+02 7.000E+02 7.500E+02 8.000E+02 8.500E+02 9.000E+02
            9.500E+02 1.000E+03 2.000E+03 5.000E+03 7.500E+03 1.000E+04
DF5076      2.797E-02 4.191E-02 5.597E-02 6.988E-02 8.379E-02 1.118E-01
            1.396E-01 1.674E-01 1.954E-01 2.234E-01 2.510E-01 2.789E-01
            3.485E-01 4.178E-01 4.866E-01 5.562E-01 6.253E-01 6.936E-01
            7.620E-01 8.313E-01 9.689E-01 1.105E+00 1.242E+00 1.378E+00
            1.512E+00 1.649E+00 1.785E+00 1.916E+00 2.051E+00 2.186E+00
            2.319E+00 2.451E+00 2.582E+00 2.715E+00 3.367E+00 4.012E+00
            4.645E+00 5.269E+00 5.882E+00 6.487E+00 7.074E+00 7.653E+00
            8.795E+00 9.887E+00 1.093E+01 1.191E+01 1.284E+01 1.369E+01
            1.451E+01 1.524E+01 1.589E+01 1.646E+01 1.694E+01 1.731E+01
            1.763E+01 1.786E+01 1.801E+01 1.682E+01 1.523E+01 1.373E+01
            1.241E+01 1.128E+01 1.029E+01 9.461E+00 8.045E+00 6.980E+00
            6.108E+00 5.408E+00 4.824E+00 4.331E+00 3.908E+00 3.556E+00
            3.241E+00 2.972E+00 2.739E+00 2.530E+00 2.350E+00 2.191E+00
            1.598E+00 1.225E+00 9.801E-01 8.084E-01 5.877E-01 5.140E-01
            4.553E-01 3.688E-01 3.070E-01 2.631E-01 2.295E-01 2.035E-01
            1.821E-01 1.649E-01 1.511E-01 1.390E-01 1.290E-01 1.198E-01
            1.128E-01 1.059E-01 1.001E-01 7.845E-02 6.464E-02 5.554E-02
            4.866E-02 4.339E-02 3.933E-02 3.604E-02 3.337E-02 2.913E-02
```

```
            2.744E-02 2.606E-02 2.361E-02 2.176E-02 2.019E-02 1.877E-02
            1.780E-02 1.682E-02 1.603E-02 1.536E-02 1.468E-02 1.412E-02
            1.362E-02 1.318E-02 9.013E-03 6.688E-03 6.277E-03 6.088E-03

4He DOSE-RESPONSE FUNCTIONS FOR USE IN MCNP6 (April 25, 2016)
Data generated using MCDS Version 3.10A  05-DEC-2011

C
C           DSB (60Co):   2.86
C           SSB (60Co): 115.53
C           BD  (60Co): 293.98
C
C    ***    ============================================================
C    ***                 4He  DOSE, RBE AND RELATED TALLIES
C    ***    ------------------------------------------------------------
C
FC1016      4He Absorbed Dose
F1016:A     1
FM1016      0.1602  $MeV/g to nGy
C
C
FC5026      4He RBE for DSB induction (0% pO2) relative to 60Co
F5026:A     1
FM5026      0.1602  $MeV/g to nGy
DE5026      1.000E-03 1.500E-03 2.000E-03 2.500E-03 3.000E-03 4.000E-03
            5.000E-03 6.000E-03 7.000E-03 8.000E-03 9.000E-03 1.000E-02
            1.250E-02 1.500E-02 1.750E-02 2.000E-02 2.250E-02 2.500E-02
            2.750E-02 3.000E-02 3.500E-02 4.000E-02 4.500E-02 5.000E-02
            5.500E-02 6.000E-02 6.500E-02 7.000E-02 7.500E-02 8.000E-02
            8.500E-02 9.000E-02 9.500E-02 1.000E-01 1.250E-01 1.500E-01
            1.750E-01 2.000E-01 2.250E-01 2.500E-01 2.750E-01 3.000E-01
            3.500E-01 4.000E-01 4.500E-01 5.000E-01 5.500E-01 6.000E-01
            6.500E-01 7.000E-01 7.500E-01 8.000E-01 8.500E-01 9.000E-01
            9.500E-01 1.000E+00 1.250E+00 1.500E+00 1.750E+00 2.000E+00
            2.250E+00 2.500E+00 2.750E+00 3.000E+00 3.500E+00 4.000E+00
            4.500E+00 5.000E+00 5.500E+00 6.000E+00 6.500E+00 7.000E+00
            7.500E+00 8.000E+00 8.500E+00 9.000E+00 9.500E+00 1.000E+01
            1.250E+01 1.500E+01 1.750E+01 2.000E+01 2.500E+01 2.750E+01
            3.000E+01 3.500E+01 4.000E+01 4.500E+01 5.000E+01 5.500E+01
            6.000E+01 6.500E+01 7.000E+01 7.500E+01 8.000E+01 8.500E+01
            9.000E+01 9.500E+01 1.000E+02 1.250E+02 1.500E+02 1.750E+02
            2.000E+02 2.250E+02 2.500E+02 2.750E+02 3.000E+02 3.500E+02
            3.750E+02 4.000E+02 4.500E+02 5.000E+02 5.500E+02 6.000E+02
            6.500E+02 7.000E+02 7.500E+02 8.000E+02 8.500E+02 9.000E+02
            9.500E+02 1.000E+03 2.000E+03 5.000E+03 7.500E+03 1.000E+04
DF5026      9.826E+00 9.820E+00 9.828E+00 9.823E+00 9.818E+00 9.821E+00
            9.819E+00 9.815E+00 9.818E+00 9.820E+00 9.815E+00 9.816E+00
            9.817E+00 9.814E+00 9.808E+00 9.810E+00 9.799E+00 9.794E+00
            9.789E+00 9.792E+00 9.792E+00 9.785E+00 9.788E+00 9.786E+00
            9.778E+00 9.781E+00 9.782E+00 9.772E+00 9.772E+00 9.773E+00
            9.761E+00 9.758E+00 9.752E+00 9.753E+00 9.742E+00 9.723E+00
            9.713E+00 9.705E+00 9.685E+00 9.677E+00 9.653E+00 9.642E+00
            9.619E+00 9.592E+00 9.563E+00 9.530E+00 9.501E+00 9.467E+00
            9.442E+00 9.402E+00 9.372E+00 9.344E+00 9.303E+00 9.264E+00
            9.226E+00 9.191E+00 8.996E+00 8.787E+00 8.574E+00 8.344E+00
            8.114E+00 7.871E+00 7.627E+00 7.388E+00 6.912E+00 6.457E+00
            6.015E+00 5.619E+00 5.255E+00 4.925E+00 4.619E+00 4.357E+00
            4.119E+00 3.898E+00 3.713E+00 3.543E+00 3.389E+00 3.250E+00
            2.740E+00 2.405E+00 2.190E+00 2.030E+00 1.816E+00 1.736E+00
            1.676E+00 1.582E+00 1.507E+00 1.455E+00 1.405E+00 1.372E+00
            1.339E+00 1.313E+00 1.293E+00 1.274E+00 1.258E+00 1.240E+00
```

```
            1.230E+00 1.221E+00 1.210E+00 1.167E+00 1.137E+00 1.121E+00
            1.101E+00 1.088E+00 1.079E+00 1.074E+00 1.067E+00 1.059E+00
            1.054E+00 1.049E+00 1.042E+00 1.039E+00 1.035E+00 1.031E+00
            1.033E+00 1.027E+00 1.026E+00 1.027E+00 1.023E+00 1.022E+00
            1.020E+00 1.019E+00 1.006E+00 1.002E+00 1.002E+00 1.000E+00
C
C
FC5036      4He RBE for SSB induction (0% pO2) relative to 60Co
F5036:A     1
FM5036      0.1602  $MeV/g to nGy
DE5036      1.000E-03 1.500E-03 2.000E-03 2.500E-03 3.000E-03 4.000E-03
            5.000E-03 6.000E-03 7.000E-03 8.000E-03 9.000E-03 1.000E-02
            1.250E-02 1.500E-02 1.750E-02 2.000E-02 2.250E-02 2.500E-02
            2.750E-02 3.000E-02 3.500E-02 4.000E-02 4.500E-02 5.000E-02
            5.500E-02 6.000E-02 6.500E-02 7.000E-02 7.500E-02 8.000E-02
            8.500E-02 9.000E-02 9.500E-02 1.000E-01 1.250E-01 1.500E-01
            1.750E-01 2.000E-01 2.250E-01 2.500E-01 2.750E-01 3.000E-01
            3.500E-01 4.000E-01 4.500E-01 5.000E-01 5.500E-01 6.000E-01
            6.500E-01 7.000E-01 7.500E-01 8.000E-01 8.500E-01 9.000E-01
            9.500E-01 1.000E+00 1.250E+00 1.500E+00 1.750E+00 2.000E+00
            2.250E+00 2.500E+00 2.750E+00 3.000E+00 3.500E+00 4.000E+00
            4.500E+00 5.000E+00 5.500E+00 6.000E+00 6.500E+00 7.000E+00
            7.500E+00 8.000E+00 8.500E+00 9.000E+00 9.500E+00 1.000E+01
            1.250E+01 1.500E+01 1.750E+01 2.000E+01 2.500E+01 2.750E+01
            3.000E+01 3.500E+01 4.000E+01 4.500E+01 5.000E+01 5.500E+01
            6.000E+01 6.500E+01 7.000E+01 7.500E+01 8.000E+01 8.500E+01
            9.000E+01 9.500E+01 1.000E+02 1.250E+02 1.500E+02 1.750E+02
            2.000E+02 2.250E+02 2.500E+02 2.750E+02 3.000E+02 3.500E+02
            3.750E+02 4.000E+02 4.500E+02 5.000E+02 5.500E+02 6.000E+02
            6.500E+02 7.000E+02 7.500E+02 8.000E+02 8.500E+02 9.000E+02
            9.500E+02 1.000E+03 2.000E+03 5.000E+03 7.500E+03 1.000E+04
DF5036      5.472E-01 5.479E-01 5.483E-01 5.489E-01 5.495E-01 5.503E-01
            5.510E-01 5.520E-01 5.523E-01 5.531E-01 5.538E-01 5.545E-01
            5.558E-01 5.568E-01 5.581E-01 5.593E-01 5.604E-01 5.614E-01
            5.622E-01 5.630E-01 5.647E-01 5.664E-01 5.682E-01 5.694E-01
            5.710E-01 5.724E-01 5.740E-01 5.752E-01 5.763E-01 5.776E-01
            5.790E-01 5.801E-01 5.813E-01 5.828E-01 5.881E-01 5.936E-01
            5.987E-01 6.032E-01 6.080E-01 6.128E-01 6.173E-01 6.214E-01
            6.299E-01 6.379E-01 6.458E-01 6.538E-01 6.609E-01 6.687E-01
            6.761E-01 6.830E-01 6.900E-01 6.967E-01 7.038E-01 7.108E-01
            7.168E-01 7.238E-01 7.547E-01 7.840E-01 8.109E-01 8.353E-01
            8.579E-01 8.789E-01 8.981E-01 9.149E-01 9.436E-01 9.647E-01
            9.806E-01 9.917E-01 9.988E-01 1.003E+00 1.005E+00 1.006E+00
            1.005E+00 1.003E+00 1.001E+00 9.991E-01 9.964E-01 9.933E-01
            9.825E-01 9.744E-01 9.704E-01 9.681E-01 9.662E-01 9.660E-01
            9.672E-01 9.685E-01 9.707E-01 9.725E-01 9.739E-01 9.754E-01
            9.768E-01 9.789E-01 9.794E-01 9.810E-01 9.809E-01 9.824E-01
            9.834E-01 9.842E-01 9.851E-01 9.874E-01 9.897E-01 9.912E-01
            9.913E-01 9.924E-01 9.931E-01 9.936E-01 9.942E-01 9.949E-01
            9.953E-01 9.957E-01 9.962E-01 9.965E-01 9.969E-01 9.972E-01
            9.972E-01 9.975E-01 9.977E-01 9.977E-01 9.979E-01 9.980E-01
            9.981E-01 9.983E-01 9.992E-01 9.996E-01 9.996E-01 9.998E-01
```

```
C
C
FC5046      4He RBE for BD induction (0% pO2) relative to 60Co
F5046:A     1
FM5046      0.1602  $MeV/g to nGy
DE5046      1.000E-03 1.500E-03 2.000E-03 2.500E-03 3.000E-03 4.000E-03
            5.000E-03 6.000E-03 7.000E-03 8.000E-03 9.000E-03 1.000E-02
            1.250E-02 1.500E-02 1.750E-02 2.000E-02 2.250E-02 2.500E-02
            2.750E-02 3.000E-02 3.500E-02 4.000E-02 4.500E-02 5.000E-02
            5.500E-02 6.000E-02 6.500E-02 7.000E-02 7.500E-02 8.000E-02
            8.500E-02 9.000E-02 9.500E-02 1.000E-01 1.250E-01 1.500E-01
            1.750E-01 2.000E-01 2.250E-01 2.500E-01 2.750E-01 3.000E-01
            3.500E-01 4.000E-01 4.500E-01 5.000E-01 5.500E-01 6.000E-01
            6.500E-01 7.000E-01 7.500E-01 8.000E-01 8.500E-01 9.000E-01
            9.500E-01 1.000E+00 1.250E+00 1.500E+00 1.750E+00 2.000E+00
            2.250E+00 2.500E+00 2.750E+00 3.000E+00 3.500E+00 4.000E+00
            4.500E+00 5.000E+00 5.500E+00 6.000E+00 6.500E+00 7.000E+00
            7.500E+00 8.000E+00 8.500E+00 9.000E+00 9.500E+00 1.000E+01
            1.250E+01 1.500E+01 1.750E+01 2.000E+01 2.500E+01 2.750E+01
            3.000E+01 3.500E+01 4.000E+01 4.500E+01 5.000E+01 5.500E+01
            6.000E+01 6.500E+01 7.000E+01 7.500E+01 8.000E+01 8.500E+01
            9.000E+01 9.500E+01 1.000E+02 1.250E+02 1.500E+02 1.750E+02
            2.000E+02 2.250E+02 2.500E+02 2.750E+02 3.000E+02 3.500E+02
            3.750E+02 4.000E+02 4.500E+02 5.000E+02 5.500E+02 6.000E+02
            6.500E+02 7.000E+02 7.500E+02 8.000E+02 8.500E+02 9.000E+02
            9.500E+02 1.000E+03 2.000E+03 5.000E+03 7.500E+03 1.000E+04
DF5046      1.434E-01 1.437E-01 1.439E-01 1.441E-01 1.444E-01 1.448E-01
            1.451E-01 1.454E-01 1.458E-01 1.461E-01 1.462E-01 1.466E-01
            1.472E-01 1.476E-01 1.481E-01 1.487E-01 1.492E-01 1.497E-01
            1.501E-01 1.504E-01 1.513E-01 1.520E-01 1.527E-01 1.533E-01
            1.540E-01 1.547E-01 1.552E-01 1.558E-01 1.565E-01 1.570E-01
            1.578E-01 1.583E-01 1.588E-01 1.593E-01 1.619E-01 1.645E-01
            1.670E-01 1.692E-01 1.716E-01 1.738E-01 1.760E-01 1.781E-01
            1.825E-01 1.867E-01 1.909E-01 1.950E-01 1.991E-01 2.032E-01
            2.071E-01 2.114E-01 2.155E-01 2.195E-01 2.236E-01 2.276E-01
            2.318E-01 2.357E-01 2.564E-01 2.769E-01 2.975E-01 3.186E-01
            3.393E-01 3.598E-01 3.800E-01 4.001E-01 4.387E-01 4.750E-01
            5.088E-01 5.393E-01 5.668E-01 5.913E-01 6.137E-01 6.330E-01
            6.505E-01 6.663E-01 6.801E-01 6.924E-01 7.036E-01 7.140E-01
            7.531E-01 7.808E-01 8.016E-01 8.185E-01 8.443E-01 8.547E-01
            8.637E-01 8.787E-01 8.908E-01 9.005E-01 9.088E-01 9.163E-01
            9.220E-01 9.272E-01 9.321E-01 9.357E-01 9.394E-01 9.430E-01
            9.459E-01 9.482E-01 9.509E-01 9.600E-01 9.664E-01 9.712E-01
            9.747E-01 9.776E-01 9.800E-01 9.818E-01 9.835E-01 9.860E-01
            9.870E-01 9.879E-01 9.894E-01 9.906E-01 9.915E-01 9.922E-01
            9.926E-01 9.932E-01 9.938E-01 9.942E-01 9.946E-01 9.950E-01
            9.951E-01 9.956E-01 9.984E-01 9.998E-01 1.000E+00 1.000E+00
C
C
FC5076      4He intra-track RMF interaction term (0% pO2)
F5076:A     1
FM5076      0.1602  $MeV to nGy
DE5076      1.000E-03 1.500E-03 2.000E-03 2.500E-03 3.000E-03 4.000E-03
            5.000E-03 6.000E-03 7.000E-03 8.000E-03 9.000E-03 1.000E-02
            1.250E-02 1.500E-02 1.750E-02 2.000E-02 2.250E-02 2.500E-02
            2.750E-02 3.000E-02 3.500E-02 4.000E-02 4.500E-02 5.000E-02
            5.500E-02 6.000E-02 6.500E-02 7.000E-02 7.500E-02 8.000E-02
            8.500E-02 9.000E-02 9.500E-02 1.000E-01 1.250E-01 1.500E-01
            1.750E-01 2.000E-01 2.250E-01 2.500E-01 2.750E-01 3.000E-01
            3.500E-01 4.000E-01 4.500E-01 5.000E-01 5.500E-01 6.000E-01
            6.500E-01 7.000E-01 7.500E-01 8.000E-01 8.500E-01 9.000E-01
```

```
             9.500E-01 1.000E+00 1.250E+00 1.500E+00 1.750E+00 2.000E+00
             2.250E+00 2.500E+00 2.750E+00 3.000E+00 3.500E+00 4.000E+00
             4.500E+00 5.000E+00 5.500E+00 6.000E+00 6.500E+00 7.000E+00
             7.500E+00 8.000E+00 8.500E+00 9.000E+00 9.500E+00 1.000E+01
             1.250E+01 1.500E+01 1.750E+01 2.000E+01 2.500E+01 2.750E+01
             3.000E+01 3.500E+01 4.000E+01 4.500E+01 5.000E+01 5.500E+01
             6.000E+01 6.500E+01 7.000E+01 7.500E+01 8.000E+01 8.500E+01
             9.000E+01 9.500E+01 1.000E+02 1.250E+02 1.500E+02 1.750E+02
             2.000E+02 2.250E+02 2.500E+02 2.750E+02 3.000E+02 3.500E+02
             3.750E+02 4.000E+02 4.500E+02 5.000E+02 5.500E+02 6.000E+02
             6.500E+02 7.000E+02 7.500E+02 8.000E+02 8.500E+02 9.000E+02
             9.500E+02 1.000E+03 2.000E+03 5.000E+03 7.500E+03 1.000E+04
DF5076       2.363E-01 3.540E-01 4.728E-01 5.904E-01 7.078E-01 9.441E-01
             1.180E+00 1.414E+00 1.651E+00 1.887E+00 2.120E+00 2.356E+00
             2.945E+00 3.530E+00 4.111E+00 4.699E+00 5.272E+00 5.848E+00
             6.425E+00 7.009E+00 8.169E+00 9.313E+00 1.047E+01 1.162E+01
             1.275E+01 1.390E+01 1.505E+01 1.616E+01 1.729E+01 1.843E+01
             1.952E+01 2.063E+01 2.173E+01 2.285E+01 2.834E+01 3.369E+01
             3.901E+01 4.426E+01 4.931E+01 5.437E+01 5.917E+01 6.402E+01
             7.342E+01 8.235E+01 9.086E+01 9.879E+01 1.063E+02 1.131E+02
             1.196E+02 1.250E+02 1.301E+02 1.344E+02 1.377E+02 1.404E+02
             1.424E+02 1.439E+02 1.420E+02 1.297E+02 1.144E+02 9.994E+01
             8.752E+01 7.671E+01 6.744E+01 5.954E+01 4.671E+01 3.702E+01
             2.947E+01 2.379E+01 1.938E+01 1.594E+01 1.320E+01 1.110E+01
             9.408E+00 8.020E+00 6.945E+00 6.048E+00 5.306E+00 4.689E+00
             2.799E+00 1.867E+00 1.370E+00 1.058E+00 7.086E-01 5.998E-01
             5.210E-01 4.104E-01 3.341E-01 2.833E-01 2.426E-01 2.140E-01
             1.901E-01 1.712E-01 1.563E-01 1.436E-01 1.329E-01 1.229E-01
             1.154E-01 1.088E-01 1.025E-01 7.967E-02 6.534E-02 5.613E-02
             4.876E-02 4.339E-02 3.928E-02 3.618E-02 3.338E-02 2.924E-02
             2.751E-02 2.597E-02 2.351E-02 2.167E-02 2.008E-02 1.876E-02
             1.784E-02 1.677E-02 1.599E-02 1.535E-02 1.466E-02 1.411E-02
             1.361E-02 1.316E-02 8.952E-03 6.662E-03 6.250E-03 6.072E-03
```

Lithium Ions

```
7Li DOSE-RESPONSE FUNCTIONS FOR USE IN MCNP6 (May 25, 2016)
Data generated using MCDS Version 3.10A  05-DEC-2011

C
C           DSB (60Co):   8.32
C           SSB (60Co): 188.63
C           BD  (60Co): 425.26
C
C    ***    ============================================================
C    ***                 7Li  DOSE, RBE AND RELATED TALLIES
C    ***    ------------------------------------------------------------
C
FC6016      7Li Absorbed Dose
F6016:#     1
FT6016      RES 3007
FM6016      0.1602  $MeV/g to nGy
C
C
FC6026      7Li RBE for DSB induction (100% pO2) relative to 60Co
F6026:#     1
FT6026      RES 3007
```

```
FM6026      0.1602  $MeV/g to nGy
DE6026      1.000E-03 1.200E-03 1.450E-03 1.750E-03 2.100E-03 2.540E-03
            3.050E-03 3.680E-03 4.430E-03 5.340E-03 6.430E-03 7.740E-03
            9.330E-03 1.120E-02 1.350E-02 1.630E-02 1.960E-02 2.360E-02
            2.850E-02 3.430E-02 4.130E-02 4.980E-02 5.990E-02 7.220E-02
            8.700E-02 1.050E-01 1.260E-01 1.520E-01 1.830E-01 2.210E-01
            2.660E-01 3.200E-01 3.850E-01 4.640E-01 5.590E-01 6.730E-01
            8.110E-01 9.770E-01 1.180E+00 1.420E+00 1.710E+00 2.060E+00
            2.480E+00 2.980E+00 3.590E+00 4.330E+00 5.210E+00 6.280E+00
            7.560E+00 9.110E+00 1.100E+01 1.320E+01 1.590E+01 1.920E+01
            2.310E+01 2.780E+01 3.350E+01 4.040E+01 4.860E+01 5.860E+01
            7.050E+01 8.500E+01 1.020E+02 1.230E+02 1.480E+02 1.790E+02
            2.150E+02 2.600E+02 3.130E+02 3.760E+02 4.530E+02 5.460E+02
            6.580E+02 7.920E+02 9.550E+02 1.150E+03 1.380E+03 1.670E+03
            2.010E+03 2.420E+03 2.920E+03 3.510E+03 4.230E+03 5.090E+03
            6.140E+03 7.390E+03 8.900E+03 1.070E+04 1.290E+04 1.560E+04
            1.870E+04 2.260E+04 2.720E+04 3.270E+04 3.940E+04 4.750E+04
            5.720E+04 6.890E+04 8.300E+04 1.000E+05
DF6026      3.386E+00 3.386E+00 3.385E+00 3.385E+00 3.385E+00 3.386E+00
            3.385E+00 3.386E+00 3.388E+00 3.384E+00 3.387E+00 3.386E+00
            3.385E+00 3.384E+00 3.385E+00 3.383E+00 3.385E+00 3.383E+00
            3.385E+00 3.384E+00 3.385E+00 3.384E+00 3.382E+00 3.380E+00
            3.382E+00 3.381E+00 3.380E+00 3.379E+00 3.377E+00 3.376E+00
            3.377E+00 3.374E+00 3.372E+00 3.370E+00 3.365E+00 3.363E+00
            3.361E+00 3.358E+00 3.350E+00 3.343E+00 3.332E+00 3.320E+00
            3.307E+00 3.291E+00 3.270E+00 3.245E+00 3.212E+00 3.172E+00
            3.125E+00 3.065E+00 2.992E+00 2.911E+00 2.815E+00 2.707E+00
            2.590E+00 2.469E+00 2.339E+00 2.209E+00 2.086E+00 1.962E+00
            1.847E+00 1.740E+00 1.643E+00 1.553E+00 1.477E+00 1.407E+00
            1.348E+00 1.295E+00 1.249E+00 1.214E+00 1.181E+00 1.154E+00
            1.129E+00 1.110E+00 1.092E+00 1.079E+00 1.067E+00 1.058E+00
            1.051E+00 1.043E+00 1.037E+00 1.033E+00 1.030E+00 1.026E+00
            1.024E+00 1.021E+00 1.020E+00 1.018E+00 1.020E+00 1.017E+00
            1.018E+00 1.015E+00 1.016E+00 1.015E+00 1.017E+00 1.015E+00
            1.016E+00 1.016E+00 1.016E+00 1.015E+00
C
C
FC6036      7Li RBE for SSB induction (100% pO2) relative to 60Co
F6036:#     1
FT6036      RES 3007
FM6036      0.1602  $MeV/g to nGy
DE6036      1.000E-03 1.200E-03 1.450E-03 1.750E-03 2.100E-03 2.540E-03
            3.050E-03 3.680E-03 4.430E-03 5.340E-03 6.430E-03 7.740E-03
            9.330E-03 1.120E-02 1.350E-02 1.630E-02 1.960E-02 2.360E-02
            2.850E-02 3.430E-02 4.130E-02 4.980E-02 5.990E-02 7.220E-02
            8.700E-02 1.050E-01 1.260E-01 1.520E-01 1.830E-01 2.210E-01
            2.660E-01 3.200E-01 3.850E-01 4.640E-01 5.590E-01 6.730E-01
            8.110E-01 9.770E-01 1.180E+00 1.420E+00 1.710E+00 2.060E+00
            2.480E+00 2.980E+00 3.590E+00 4.330E+00 5.210E+00 6.280E+00
            7.560E+00 9.110E+00 1.100E+01 1.320E+01 1.590E+01 1.920E+01
            2.310E+01 2.780E+01 3.350E+01 4.040E+01 4.860E+01 5.860E+01
            7.050E+01 8.500E+01 1.020E+02 1.230E+02 1.480E+02 1.790E+02
            2.150E+02 2.600E+02 3.130E+02 3.760E+02 4.530E+02 5.460E+02
            6.580E+02 7.920E+02 9.550E+02 1.150E+03 1.380E+03 1.670E+03
            2.010E+03 2.420E+03 2.920E+03 3.510E+03 4.230E+03 5.090E+03
            6.140E+03 7.390E+03 8.900E+03 1.070E+04 1.290E+04 1.560E+04
            1.870E+04 2.260E+04 2.720E+04 3.270E+04 3.940E+04 4.750E+04
            5.720E+04 6.890E+04 8.300E+04 1.000E+05
DF6036      3.259E-01 3.261E-01 3.261E-01 3.261E-01 3.263E-01 3.265E-01
            3.268E-01 3.268E-01 3.267E-01 3.271E-01 3.272E-01 3.275E-01
            3.278E-01 3.281E-01 3.283E-01 3.287E-01 3.289E-01 3.295E-01
```

```
            3.298E-01 3.304E-01 3.309E-01 3.315E-01 3.322E-01 3.331E-01
            3.340E-01 3.351E-01 3.358E-01 3.372E-01 3.386E-01 3.402E-01
            3.419E-01 3.439E-01 3.460E-01 3.486E-01 3.519E-01 3.551E-01
            3.590E-01 3.634E-01 3.686E-01 3.748E-01 3.817E-01 3.898E-01
            3.991E-01 4.098E-01 4.224E-01 4.370E-01 4.536E-01 4.726E-01
            4.943E-01 5.186E-01 5.459E-01 5.742E-01 6.050E-01 6.380E-01
            6.708E-01 7.035E-01 7.353E-01 7.666E-01 7.951E-01 8.215E-01
            8.455E-01 8.673E-01 8.862E-01 9.034E-01 9.177E-01 9.307E-01
            9.413E-01 9.506E-01 9.585E-01 9.649E-01 9.704E-01 9.752E-01
            9.792E-01 9.825E-01 9.854E-01 9.875E-01 9.895E-01 9.910E-01
            9.923E-01 9.935E-01 9.945E-01 9.951E-01 9.957E-01 9.963E-01
            9.967E-01 9.971E-01 9.973E-01 9.975E-01 9.975E-01 9.977E-01
            9.977E-01 9.980E-01 9.979E-01 9.981E-01 9.979E-01 9.980E-01
            9.980E-01 9.980E-01 9.980E-01 9.981E-01
C
C
FC6046      7Li RBE for BD induction (100% pO2) relative to 60Co
F6046:#     1
FT6046      RES 3007
FM6046      0.1602  $MeV/g to nGy
DE6046      1.000E-03 1.200E-03 1.450E-03 1.750E-03 2.100E-03 2.540E-03
            3.050E-03 3.680E-03 4.430E-03 5.340E-03 6.430E-03 7.740E-03
            9.330E-03 1.120E-02 1.350E-02 1.630E-02 1.960E-02 2.360E-02
            2.850E-02 3.430E-02 4.130E-02 4.980E-02 5.990E-02 7.220E-02
            8.700E-02 1.050E-01 1.260E-01 1.520E-01 1.830E-01 2.210E-01
            2.660E-01 3.200E-01 3.850E-01 4.640E-01 5.590E-01 6.730E-01
            8.110E-01 9.770E-01 1.180E+00 1.420E+00 1.710E+00 2.060E+00
            2.480E+00 2.980E+00 3.590E+00 4.330E+00 5.210E+00 6.280E+00
            7.560E+00 9.110E+00 1.100E+01 1.320E+01 1.590E+01 1.920E+01
            2.310E+01 2.780E+01 3.350E+01 4.040E+01 4.860E+01 5.860E+01
            7.050E+01 8.500E+01 1.020E+02 1.230E+02 1.480E+02 1.790E+02
            2.150E+02 2.600E+02 3.130E+02 3.760E+02 4.530E+02 5.460E+02
            6.580E+02 7.920E+02 9.550E+02 1.150E+03 1.380E+03 1.670E+03
            2.010E+03 2.420E+03 2.920E+03 3.510E+03 4.230E+03 5.090E+03
            6.140E+03 7.390E+03 8.900E+03 1.070E+04 1.290E+04 1.560E+04
            1.870E+04 2.260E+04 2.720E+04 3.270E+04 3.940E+04 4.750E+04
            5.720E+04 6.890E+04 8.300E+04 1.000E+05
DF6046      9.464E-02 9.468E-02 9.480E-02 9.486E-02 9.484E-02 9.489E-02
            9.497E-02 9.504E-02 9.510E-02 9.524E-02 9.531E-02 9.546E-02
            9.554E-02 9.568E-02 9.577E-02 9.599E-02 9.619E-02 9.633E-02
            9.649E-02 9.681E-02 9.712E-02 9.736E-02 9.770E-02 9.809E-02
            9.846E-02 9.897E-02 9.953E-02 1.001E-01 1.008E-01 1.016E-01
            1.024E-01 1.035E-01 1.045E-01 1.059E-01 1.074E-01 1.092E-01
            1.112E-01 1.135E-01 1.163E-01 1.196E-01 1.234E-01 1.280E-01
            1.333E-01 1.396E-01 1.473E-01 1.567E-01 1.677E-01 1.810E-01
            1.968E-01 2.157E-01 2.383E-01 2.640E-01 2.941E-01 3.286E-01
            3.662E-01 4.072E-01 4.514E-01 4.972E-01 5.432E-01 5.897E-01
            6.340E-01 6.766E-01 7.156E-01 7.525E-01 7.856E-01 8.160E-01
            8.418E-01 8.654E-01 8.852E-01 9.024E-01 9.173E-01 9.299E-01
            9.407E-01 9.497E-01 9.575E-01 9.639E-01 9.693E-01 9.738E-01
            9.777E-01 9.807E-01 9.833E-01 9.853E-01 9.871E-01 9.886E-01
            9.898E-01 9.907E-01 9.915E-01 9.921E-01 9.925E-01 9.928E-01
            9.930E-01 9.932E-01 9.934E-01 9.936E-01 9.938E-01 9.938E-01
            9.938E-01 9.940E-01 9.938E-01 9.938E-01
```

```
C
C
FC6056      7Li LET (keV/um)
F6056:#     1
FT6056      RES 3007
FM6056      0.1602  $MeV/g to nGy
DE6056      1.000E-03 1.200E-03 1.450E-03 1.750E-03 2.100E-03 2.540E-03
            3.050E-03 3.680E-03 4.430E-03 5.340E-03 6.430E-03 7.740E-03
            9.330E-03 1.120E-02 1.350E-02 1.630E-02 1.960E-02 2.360E-02
            2.850E-02 3.430E-02 4.130E-02 4.980E-02 5.990E-02 7.220E-02
            8.700E-02 1.050E-01 1.260E-01 1.520E-01 1.830E-01 2.210E-01
            2.660E-01 3.200E-01 3.850E-01 4.640E-01 5.590E-01 6.730E-01
            8.110E-01 9.770E-01 1.180E+00 1.420E+00 1.710E+00 2.060E+00
            2.480E+00 2.980E+00 3.590E+00 4.330E+00 5.210E+00 6.280E+00
            7.560E+00 9.110E+00 1.100E+01 1.320E+01 1.590E+01 1.920E+01
            2.310E+01 2.780E+01 3.350E+01 4.040E+01 4.860E+01 5.860E+01
            7.050E+01 8.500E+01 1.020E+02 1.230E+02 1.480E+02 1.790E+02
            2.150E+02 2.600E+02 3.130E+02 3.760E+02 4.530E+02 5.460E+02
            6.580E+02 7.920E+02 9.550E+02 1.150E+03 1.380E+03 1.670E+03
            2.010E+03 2.420E+03 2.920E+03 3.510E+03 4.230E+03 5.090E+03
            6.140E+03 7.390E+03 8.900E+03 1.070E+04 1.290E+04 1.560E+04
            1.870E+04 2.260E+04 2.720E+04 3.270E+04 3.940E+04 4.750E+04
            5.720E+04 6.890E+04 8.300E+04 1.000E+05
DF6056      4.348E+01 4.359E+01 4.370E+01 4.380E+01 4.391E+01 4.406E+01
            4.426E+01 4.455E+01 4.499E+01 4.562E+01 4.651E+01 4.771E+01
            4.931E+01 5.130E+01 5.384E+01 5.698E+01 6.066E+01 6.503E+01
            7.020E+01 7.606E+01 8.273E+01 9.033E+01 9.874E+01 1.082E+02
            1.187E+02 1.305E+02 1.431E+02 1.574E+02 1.732E+02 1.912E+02
            2.110E+02 2.331E+02 2.576E+02 2.846E+02 3.129E+02 3.404E+02
            3.650E+02 3.836E+02 3.942E+02 3.956E+02 3.887E+02 3.748E+02
            3.559E+02 3.339E+02 3.095E+02 2.840E+02 2.587E+02 2.337E+02
            2.097E+02 1.868E+02 1.652E+02 1.459E+02 1.280E+02 1.115E+02
            9.713E+01 8.433E+01 7.296E+01 6.298E+01 5.439E+01 4.683E+01
            4.036E+01 3.471E+01 2.995E+01 2.574E+01 2.215E+01 1.899E+01
            1.638E+01 1.406E+01 1.213E+01 1.049E+01 9.070E+00 7.856E+00
            6.824E+00 5.953E+00 5.207E+00 4.580E+00 4.059E+00 3.601E+00
            3.227E+00 2.914E+00 2.650E+00 2.436E+00 2.257E+00 2.111E+00
            1.992E+00 1.898E+00 1.824E+00 1.766E+00 1.722E+00 1.688E+00
            1.666E+00 1.650E+00 1.640E+00 1.634E+00 1.632E+00 1.633E+00
            1.635E+00 1.639E+00 1.643E+00 1.648E+00
C
C
FC6066      7Li ZF (mean specific energy)
F6066:#     1
FT6066      RES 3007
FM6066      0.1602  $MeV/g to nGy
DE6066      1.000E-03 1.200E-03 1.450E-03 1.750E-03 2.100E-03 2.540E-03
            3.050E-03 3.680E-03 4.430E-03 5.340E-03 6.430E-03 7.740E-03
            9.330E-03 1.120E-02 1.350E-02 1.630E-02 1.960E-02 2.360E-02
            2.850E-02 3.430E-02 4.130E-02 4.980E-02 5.990E-02 7.220E-02
            8.700E-02 1.050E-01 1.260E-01 1.520E-01 1.830E-01 2.210E-01
            2.660E-01 3.200E-01 3.850E-01 4.640E-01 5.590E-01 6.730E-01
            8.110E-01 9.770E-01 1.180E+00 1.420E+00 1.710E+00 2.060E+00
            2.480E+00 2.980E+00 3.590E+00 4.330E+00 5.210E+00 6.280E+00
            7.560E+00 9.110E+00 1.100E+01 1.320E+01 1.590E+01 1.920E+01
            2.310E+01 2.780E+01 3.350E+01 4.040E+01 4.860E+01 5.860E+01
            7.050E+01 8.500E+01 1.020E+02 1.230E+02 1.480E+02 1.790E+02
            2.150E+02 2.600E+02 3.130E+02 3.760E+02 4.530E+02 5.460E+02
            6.580E+02 7.920E+02 9.550E+02 1.150E+03 1.380E+03 1.670E+03
            2.010E+03 2.420E+03 2.920E+03 3.510E+03 4.230E+03 5.090E+03
            6.140E+03 7.390E+03 8.900E+03 1.070E+04 1.290E+04 1.560E+04
```

```
            1.870E+04 2.260E+04 2.720E+04 3.270E+04 3.940E+04 4.750E+04
            5.720E+04 6.890E+04 8.300E+04 1.000E+05
DF6066      2.448E-03 2.937E-03 3.549E-03 4.283E-03 5.140E-03 6.217E-03
            7.465E-03 9.007E-03 1.084E-02 1.307E-02 1.573E-02 1.894E-02
            2.283E-02 2.739E-02 3.301E-02 3.984E-02 4.788E-02 5.762E-02
            6.953E-02 8.360E-02 1.006E-01 1.211E-01 1.454E-01 1.749E-01
            2.102E-01 2.529E-01 3.024E-01 3.631E-01 4.349E-01 5.218E-01
            6.234E-01 7.432E-01 8.846E-01 1.052E+00 1.248E+00 1.474E+00
            1.734E+00 2.020E+00 2.329E+00 2.629E+00 2.895E+00 3.071E+00
            3.094E+00 2.958E+00 2.730E+00 2.475E+00 2.227E+00 1.989E+00
            1.768E+00 1.564E+00 1.375E+00 1.208E+00 1.056E+00 9.175E-01
            7.973E-01 6.911E-01 5.972E-01 5.150E-01 4.445E-01 3.826E-01
            3.296E-01 2.834E-01 2.445E-01 2.100E-01 1.808E-01 1.550E-01
            1.337E-01 1.148E-01 9.896E-02 8.560E-02 7.400E-02 6.410E-02
            5.568E-02 4.857E-02 4.248E-02 3.737E-02 3.312E-02 2.938E-02
            2.633E-02 2.378E-02 2.162E-02 1.987E-02 1.841E-02 1.723E-02
            1.625E-02 1.549E-02 1.488E-02 1.441E-02 1.405E-02 1.378E-02
            1.359E-02 1.346E-02 1.338E-02 1.333E-02 1.332E-02 1.332E-02
            1.334E-02 1.337E-02 1.341E-02 1.345E-02
C
C
FC6076      7Li RMF intra-track DSB interaction term (100% pO2)
F6076:#     1
FT6076      RES 3007
FM6076      0.1602  $MeV/g to nGy
DE6076      1.000E-03 1.200E-03 1.450E-03 1.750E-03 2.100E-03 2.540E-03
            3.050E-03 3.680E-03 4.430E-03 5.340E-03 6.430E-03 7.740E-03
            9.330E-03 1.120E-02 1.350E-02 1.630E-02 1.960E-02 2.360E-02
            2.850E-02 3.430E-02 4.130E-02 4.980E-02 5.990E-02 7.220E-02
            8.700E-02 1.050E-01 1.260E-01 1.520E-01 1.830E-01 2.210E-01
            2.660E-01 3.200E-01 3.850E-01 4.640E-01 5.590E-01 6.730E-01
            8.110E-01 9.770E-01 1.180E+00 1.420E+00 1.710E+00 2.060E+00
            2.480E+00 2.980E+00 3.590E+00 4.330E+00 5.210E+00 6.280E+00
            7.560E+00 9.110E+00 1.100E+01 1.320E+01 1.590E+01 1.920E+01
            2.310E+01 2.780E+01 3.350E+01 4.040E+01 4.860E+01 5.860E+01
            7.050E+01 8.500E+01 1.020E+02 1.230E+02 1.480E+02 1.790E+02
            2.150E+02 2.600E+02 3.130E+02 3.760E+02 4.530E+02 5.460E+02
            6.580E+02 7.920E+02 9.550E+02 1.150E+03 1.380E+03 1.670E+03
            2.010E+03 2.420E+03 2.920E+03 3.510E+03 4.230E+03 5.090E+03
            6.140E+03 7.390E+03 8.900E+03 1.070E+04 1.290E+04 1.560E+04
            1.870E+04 2.260E+04 2.720E+04 3.270E+04 3.940E+04 4.750E+04
            5.720E+04 6.890E+04 8.300E+04 1.000E+05
DF6076      2.807E-02 3.368E-02 4.066E-02 4.908E-02 5.890E-02 7.127E-02
            8.556E-02 1.033E-01 1.245E-01 1.496E-01 1.805E-01 2.171E-01
            2.615E-01 3.137E-01 3.782E-01 4.559E-01 5.488E-01 6.596E-01
            7.967E-01 9.576E-01 1.152E+00 1.387E+00 1.662E+00 1.997E+00
            2.404E+00 2.890E+00 3.455E+00 4.147E+00 4.960E+00 5.947E+00
            7.109E+00 8.459E+00 1.006E+01 1.195E+01 1.413E+01 1.667E+01
            1.958E+01 2.278E+01 2.614E+01 2.938E+01 3.214E+01 3.386E+01
            3.384E+01 3.203E+01 2.919E+01 2.607E+01 2.298E+01 2.002E+01
            1.727E+01 1.469E+01 1.231E+01 1.024E+01 8.364E+00 6.721E+00
            5.347E+00 4.211E+00 3.268E+00 2.512E+00 1.933E+00 1.472E+00
            1.125E+00 8.576E-01 6.602E-01 5.066E-01 3.945E-01 3.067E-01
            2.429E-01 1.925E-01 1.545E-01 1.261E-01 1.033E-01 8.532E-02
            7.095E-02 5.981E-02 5.063E-02 4.354E-02 3.772E-02 3.291E-02
            2.910E-02 2.586E-02 2.326E-02 2.122E-02 1.952E-02 1.815E-02
            1.705E-02 1.615E-02 1.548E-02 1.494E-02 1.461E-02 1.424E-02
            1.409E-02 1.387E-02 1.382E-02 1.375E-02 1.376E-02 1.373E-02
            1.378E-02 1.381E-02 1.384E-02 1.386E-02
```

```
7Li DOSE-RESPONSE FUNCTIONS FOR USE IN MCNP6 (May 25, 2016)
Data generated using MCDS Version 3.10A  05-DEC-2011

C
C           DSB (60Co):   2.86
C           SSB (60Co): 115.53
C           BD  (60Co): 293.98
C
C    ***    ============================================================
C    ***                 7Li  DOSE, RBE AND RELATED TALLIES
C    ***    ------------------------------------------------------------
C
FC6016      7Li Absorbed Dose
F6016:#     1
FT6016      RES 3007
FM6016      0.1602  $MeV/g to nGy
C
C
FC6026      7Li RBE for DSB induction (0% pO2) relative to 60Co
F6026:#     1
FT6026      RES 3007
FM6026      0.1602  $MeV/g to nGy
DE6026      1.000E-03 1.200E-03 1.450E-03 1.750E-03 2.100E-03 2.540E-03
            3.050E-03 3.680E-03 4.430E-03 5.340E-03 6.430E-03 7.740E-03
            9.330E-03 1.120E-02 1.350E-02 1.630E-02 1.960E-02 2.360E-02
            2.850E-02 3.430E-02 4.130E-02 4.980E-02 5.990E-02 7.220E-02
            8.700E-02 1.050E-01 1.260E-01 1.520E-01 1.830E-01 2.210E-01
            2.660E-01 3.200E-01 3.850E-01 4.640E-01 5.590E-01 6.730E-01
            8.110E-01 9.770E-01 1.180E+00 1.420E+00 1.710E+00 2.060E+00
            2.480E+00 2.980E+00 3.590E+00 4.330E+00 5.210E+00 6.280E+00
            7.560E+00 9.110E+00 1.100E+01 1.320E+01 1.590E+01 1.920E+01
            2.310E+01 2.780E+01 3.350E+01 4.040E+01 4.860E+01 5.860E+01
            7.050E+01 8.500E+01 1.020E+02 1.230E+02 1.480E+02 1.790E+02
            2.150E+02 2.600E+02 3.130E+02 3.760E+02 4.530E+02 5.460E+02
            6.580E+02 7.920E+02 9.550E+02 1.150E+03 1.380E+03 1.670E+03
            2.010E+03 2.420E+03 2.920E+03 3.510E+03 4.230E+03 5.090E+03
            6.140E+03 7.390E+03 8.900E+03 1.070E+04 1.290E+04 1.560E+04
            1.870E+04 2.260E+04 2.720E+04 3.270E+04 3.940E+04 4.750E+04
            5.720E+04 6.890E+04 8.300E+04 1.000E+05
DF6026      9.842E+00 9.843E+00 9.838E+00 9.838E+00 9.839E+00 9.841E+00
            9.840E+00 9.841E+00 9.847E+00 9.835E+00 9.843E+00 9.840E+00
            9.838E+00 9.835E+00 9.838E+00 9.832E+00 9.839E+00 9.833E+00
            9.838E+00 9.837E+00 9.837E+00 9.836E+00 9.828E+00 9.823E+00
            9.829E+00 9.826E+00 9.825E+00 9.822E+00 9.817E+00 9.812E+00
            9.816E+00 9.796E+00 9.793E+00 9.786E+00 9.772E+00 9.756E+00
            9.749E+00 9.731E+00 9.710E+00 9.679E+00 9.626E+00 9.583E+00
            9.524E+00 9.447E+00 9.345E+00 9.220E+00 9.052E+00 8.828E+00
            8.545E+00 8.171E+00 7.705E+00 7.164E+00 6.525E+00 5.795E+00
            5.071E+00 4.372E+00 3.739E+00 3.208E+00 2.781E+00 2.446E+00
            2.174E+00 1.965E+00 1.800E+00 1.657E+00 1.551E+00 1.457E+00
            1.387E+00 1.324E+00 1.269E+00 1.228E+00 1.192E+00 1.162E+00
            1.135E+00 1.115E+00 1.093E+00 1.082E+00 1.068E+00 1.059E+00
            1.052E+00 1.041E+00 1.036E+00 1.033E+00 1.029E+00 1.027E+00
            1.023E+00 1.020E+00 1.020E+00 1.017E+00 1.017E+00 1.016E+00
            1.019E+00 1.014E+00 1.016E+00 1.015E+00 1.016E+00 1.016E+00
            1.016E+00 1.016E+00 1.013E+00 1.013E+00
C
C
FC6036      7Li RBE for SSB induction (0% pO2) relative to 60Co
F6036:#     1
FT6036      RES 3007
```

```
FM6036      0.1602  $MeV/g to nGy
DE6036      1.000E-03 1.200E-03 1.450E-03 1.750E-03 2.100E-03 2.540E-03
            3.050E-03 3.680E-03 4.430E-03 5.340E-03 6.430E-03 7.740E-03
            9.330E-03 1.120E-02 1.350E-02 1.630E-02 1.960E-02 2.360E-02
            2.850E-02 3.430E-02 4.130E-02 4.980E-02 5.990E-02 7.220E-02
            8.700E-02 1.050E-01 1.260E-01 1.520E-01 1.830E-01 2.210E-01
            2.660E-01 3.200E-01 3.850E-01 4.640E-01 5.590E-01 6.730E-01
            8.110E-01 9.770E-01 1.180E+00 1.420E+00 1.710E+00 2.060E+00
            2.480E+00 2.980E+00 3.590E+00 4.330E+00 5.210E+00 6.280E+00
            7.560E+00 9.110E+00 1.100E+01 1.320E+01 1.590E+01 1.920E+01
            2.310E+01 2.780E+01 3.350E+01 4.040E+01 4.860E+01 5.860E+01
            7.050E+01 8.500E+01 1.020E+02 1.230E+02 1.480E+02 1.790E+02
            2.150E+02 2.600E+02 3.130E+02 3.760E+02 4.530E+02 5.460E+02
            6.580E+02 7.920E+02 9.550E+02 1.150E+03 1.380E+03 1.670E+03
            2.010E+03 2.420E+03 2.920E+03 3.510E+03 4.230E+03 5.090E+03
            6.140E+03 7.390E+03 8.900E+03 1.070E+04 1.290E+04 1.560E+04
            1.870E+04 2.260E+04 2.720E+04 3.270E+04 3.940E+04 4.750E+04
            5.720E+04 6.890E+04 8.300E+04 1.000E+05
DF6036      5.325E-01 5.327E-01 5.327E-01 5.327E-01 5.331E-01 5.334E-01
            5.339E-01 5.339E-01 5.338E-01 5.344E-01 5.346E-01 5.351E-01
            5.355E-01 5.360E-01 5.363E-01 5.370E-01 5.373E-01 5.383E-01
            5.388E-01 5.397E-01 5.405E-01 5.416E-01 5.427E-01 5.442E-01
            5.458E-01 5.475E-01 5.487E-01 5.510E-01 5.534E-01 5.560E-01
            5.587E-01 5.622E-01 5.657E-01 5.700E-01 5.755E-01 5.809E-01
            5.874E-01 5.947E-01 6.035E-01 6.138E-01 6.256E-01 6.391E-01
            6.551E-01 6.733E-01 6.946E-01 7.193E-01 7.474E-01 7.791E-01
            8.143E-01 8.525E-01 8.921E-01 9.290E-01 9.618E-01 9.873E-01
            1.002E+00 1.006E+00 1.001E+00 9.931E-01 9.827E-01 9.752E-01
            9.692E-01 9.670E-01 9.663E-01 9.675E-01 9.697E-01 9.722E-01
            9.756E-01 9.781E-01 9.813E-01 9.835E-01 9.852E-01 9.878E-01
            9.899E-01 9.916E-01 9.920E-01 9.931E-01 9.941E-01 9.948E-01
            9.955E-01 9.963E-01 9.968E-01 9.971E-01 9.974E-01 9.976E-01
            9.979E-01 9.982E-01 9.982E-01 9.983E-01 9.985E-01 9.984E-01
            9.983E-01 9.986E-01 9.984E-01 9.986E-01 9.985E-01 9.985E-01
            9.985E-01 9.985E-01 9.987E-01 9.987E-01
C
C
FC6046      7Li RBE for BD induction (0% pO2) relative to 60Co
F6046:#     1
FT6046      RES 3007
FM6046      0.1602  $MeV/g to nGy
DE6046      1.000E-03 1.200E-03 1.450E-03 1.750E-03 2.100E-03 2.540E-03
            3.050E-03 3.680E-03 4.430E-03 5.340E-03 6.430E-03 7.740E-03
            9.330E-03 1.120E-02 1.350E-02 1.630E-02 1.960E-02 2.360E-02
            2.850E-02 3.430E-02 4.130E-02 4.980E-02 5.990E-02 7.220E-02
            8.700E-02 1.050E-01 1.260E-01 1.520E-01 1.830E-01 2.210E-01
            2.660E-01 3.200E-01 3.850E-01 4.640E-01 5.590E-01 6.730E-01
            8.110E-01 9.770E-01 1.180E+00 1.420E+00 1.710E+00 2.060E+00
            2.480E+00 2.980E+00 3.590E+00 4.330E+00 5.210E+00 6.280E+00
            7.560E+00 9.110E+00 1.100E+01 1.320E+01 1.590E+01 1.920E+01
            2.310E+01 2.780E+01 3.350E+01 4.040E+01 4.860E+01 5.860E+01
            7.050E+01 8.500E+01 1.020E+02 1.230E+02 1.480E+02 1.790E+02
            2.150E+02 2.600E+02 3.130E+02 3.760E+02 4.530E+02 5.460E+02
            6.580E+02 7.920E+02 9.550E+02 1.150E+03 1.380E+03 1.670E+03
            2.010E+03 2.420E+03 2.920E+03 3.510E+03 4.230E+03 5.090E+03
            6.140E+03 7.390E+03 8.900E+03 1.070E+04 1.290E+04 1.560E+04
            1.870E+04 2.260E+04 2.720E+04 3.270E+04 3.940E+04 4.750E+04
            5.720E+04 6.890E+04 8.300E+04 1.000E+05
DF6046      1.371E-01 1.372E-01 1.373E-01 1.374E-01 1.374E-01 1.375E-01
            1.376E-01 1.377E-01 1.378E-01 1.380E-01 1.381E-01 1.383E-01
            1.384E-01 1.386E-01 1.387E-01 1.391E-01 1.394E-01 1.396E-01
```

```
            1.398E-01 1.403E-01 1.407E-01 1.410E-01 1.415E-01 1.422E-01
            1.427E-01 1.434E-01 1.442E-01 1.451E-01 1.461E-01 1.472E-01
            1.485E-01 1.501E-01 1.517E-01 1.538E-01 1.559E-01 1.587E-01
            1.617E-01 1.652E-01 1.694E-01 1.744E-01 1.804E-01 1.873E-01
            1.957E-01 2.057E-01 2.181E-01 2.332E-01 2.513E-01 2.738E-01
            3.009E-01 3.339E-01 3.738E-01 4.187E-01 4.700E-01 5.257E-01
            5.803E-01 6.318E-01 6.777E-01 7.167E-01 7.497E-01 7.783E-01
            8.033E-01 8.259E-01 8.467E-01 8.660E-01 8.832E-01 8.994E-01
            9.133E-01 9.261E-01 9.368E-01 9.462E-01 9.543E-01 9.614E-01
            9.672E-01 9.724E-01 9.766E-01 9.802E-01 9.832E-01 9.858E-01
            9.879E-01 9.897E-01 9.912E-01 9.922E-01 9.928E-01 9.938E-01
            9.943E-01 9.950E-01 9.953E-01 9.956E-01 9.959E-01 9.961E-01
            9.962E-01 9.963E-01 9.965E-01 9.966E-01 9.966E-01 9.966E-01
            9.966E-01 9.967E-01 9.967E-01 9.967E-01
C
C
FC6076      7Li RMF intra-track DSB interaction term (0% pO2)
F6076:#     1
FT6076      RES 3007
FM6076      0.1602  $MeV/g to nGy
DE6076      1.000E-03 1.200E-03 1.450E-03 1.750E-03 2.100E-03 2.540E-03
            3.050E-03 3.680E-03 4.430E-03 5.340E-03 6.430E-03 7.740E-03
            9.330E-03 1.120E-02 1.350E-02 1.630E-02 1.960E-02 2.360E-02
            2.850E-02 3.430E-02 4.130E-02 4.980E-02 5.990E-02 7.220E-02
            8.700E-02 1.050E-01 1.260E-01 1.520E-01 1.830E-01 2.210E-01
            2.660E-01 3.200E-01 3.850E-01 4.640E-01 5.590E-01 6.730E-01
            8.110E-01 9.770E-01 1.180E+00 1.420E+00 1.710E+00 2.060E+00
            2.480E+00 2.980E+00 3.590E+00 4.330E+00 5.210E+00 6.280E+00
            7.560E+00 9.110E+00 1.100E+01 1.320E+01 1.590E+01 1.920E+01
            2.310E+01 2.780E+01 3.350E+01 4.040E+01 4.860E+01 5.860E+01
            7.050E+01 8.500E+01 1.020E+02 1.230E+02 1.480E+02 1.790E+02
            2.150E+02 2.600E+02 3.130E+02 3.760E+02 4.530E+02 5.460E+02
            6.580E+02 7.920E+02 9.550E+02 1.150E+03 1.380E+03 1.670E+03
            2.010E+03 2.420E+03 2.920E+03 3.510E+03 4.230E+03 5.090E+03
            6.140E+03 7.390E+03 8.900E+03 1.070E+04 1.290E+04 1.560E+04
            1.870E+04 2.260E+04 2.720E+04 3.270E+04 3.940E+04 4.750E+04
            5.720E+04 6.890E+04 8.300E+04 1.000E+05
DF6076      2.371E-01 2.845E-01 3.435E-01 4.145E-01 4.976E-01 6.021E-01
            7.227E-01 8.722E-01 1.051E+00 1.264E+00 1.524E+00 1.834E+00
            2.209E+00 2.650E+00 3.195E+00 3.852E+00 4.636E+00 5.572E+00
            6.730E+00 8.089E+00 9.730E+00 1.171E+01 1.404E+01 1.687E+01
            2.030E+01 2.441E+01 2.919E+01 3.503E+01 4.191E+01 5.024E+01
            6.006E+01 7.132E+01 8.483E+01 1.008E+02 1.192E+02 1.403E+02
            1.648E+02 1.913E+02 2.196E+02 2.463E+02 2.682E+02 2.821E+02
            2.807E+02 2.640E+02 2.384E+02 2.104E+02 1.825E+02 1.550E+02
            1.291E+02 1.044E+02 8.161E+01 6.203E+01 4.495E+01 3.082E+01
            2.050E+01 1.321E+01 8.348E+00 5.299E+00 3.439E+00 2.288E+00
            1.557E+00 1.094E+00 7.923E-01 5.769E-01 4.352E-01 3.292E-01
            2.571E-01 2.012E-01 1.594E-01 1.291E-01 1.051E-01 8.653E-02
            7.173E-02 6.042E-02 5.075E-02 4.374E-02 3.777E-02 3.295E-02
            2.912E-02 2.578E-02 2.320E-02 2.122E-02 1.948E-02 1.816E-02
            1.702E-02 1.612E-02 1.549E-02 1.490E-02 1.452E-02 1.422E-02
            1.410E-02 1.384E-02 1.382E-02 1.373E-02 1.376E-02 1.375E-02
            1.376E-02 1.379E-02 1.376E-02 1.379E-02
```

APPENDIX B

PYTHON SCRIPTS

MCDS Input Generator Script

This script was developed to quickly generate the MCDS input files for a span of ion kinetic energies and the .bat or .sh file for sequentially running them on a Windows or Linux system, respectively. User defined variables include minimum and maximum kinetic energy, number of energy bins, oxygenation percentage, particle type and the cell-specific geometry variables (generally unchanged). Currently it is setup for log spacing of bins, but linear spacing can be selected by commenting out lines 32-33 and uncommenting lines 29-30. The .out files generated after the MCDS batch simulations are used in a subsequent script to create the lookup tables for integration into MCNP. The numpy external library is needed for the script to function.

```
################################################################################
#########################  MCDS Input Generator v1.1  (05/10/16, SS)  ###############
################################################################################

#import necessary libraries and functions

import numpy as np
import matplotlib.pyplot as plt

#############################################################
#####################  adjustable parameters  ###############
#############################################################

E_min = float(1E-5)    #minimum kinetic energy (MeV)
E_max = float(1E+3)    #maximum kinetic energy (MeV)
N_steps = int(100)    #number of energy bins
O1 = int(0)    #Oxygenation (%)
P1 = 'e'    #MCDS particle type
Gbp = int(1)    #Gbp of DNA
ndia = int(5)    #nucleus diameter in microns
cdia = int(5)    #cell diameter in microns
wem = int(0)    #water equivalent material between source and cell
nocs = int(25000)    #number of cell simulations

#############################################################

File_num = np.arange(0,N_steps,1)

E_bins = np.logspace(np.log10(E_min),np.log10(E_max), num=N_steps)  #log bin spacing
E_bins2 = ["{0:.2E}".format(float(x)) for x in E_bins]

'''E_bins = np.linspace(E_min,E_max, num=N_steps)  #lin bin spacing, uncomment to use linear bin spacing
E_bins2 = ["{0:.2E}".format(float(x)) for x in E_bins]'''

table = open('mcds_run.sh', 'w')  #create .sh file for batch Linux runs
table.write('#!/bin/bash'+'\n')
table.write('# Script for running MCDS simulations on Neva (Linux server)'+'\n')
table.write('\n')
a=0
while a<N_steps:
    table.write('../mcds mcds'+str(File_num[a])+'.inp'+'\n')
    a=a+1
table.close

for i in File_num:
    table = open('mcds'+str(File_num[i])+'.inp', 'w')  #create MCDS input files
    table.write('\n')
    table.write('CELL: DNA='+str(Gbp)+'  NDIA='+str(ndia)+' CDIA='+str(cdia)+' WEM='+str(wem)+'\n')
    table.write('RADX: PAR='+str(P1)+' KE='+str(E_bins2[i])+'\n')
    table.write('EVO2: pO2='+str(O1)+'\n')
    table.write('\n')
    table.write('SIMCON: nocs='+str(nocs)+' seed=987654321')
    table.close()
```

MCDS to MCNP Parse Script

This script was developed to quickly construct dose-response cards (DE/DF), which modify a standard heating tally (F6) in MCNP6 (or MCNPX), with an array of MCDS output files (sequentially numbered .out files of monotonically increasing kinetic energy). This script is meant to be run in the directory containing the output files and it produces a table of values, plot and dose-response cards ready to copy into MCNP input files. Dose-response cards include: RBE_{DSB}, RBE_{SSB}, RBE_{BD}, LET (keV/μm), $\bar{z}_F$ (Gy) and the RMF intra-track DSB interaction term ($RBE_{DSB}^2 \times \bar{z}_F$), where the output is dose-averaged.

```
################################################################################
#########################  MCDS Parsing Script v4.7  (4/29/16, SS)  ############################
################################################################################

#import necessary libraries and functions

import sys
import glob
import fileinput
import numpy as np
import matplotlib.pyplot as plt
from decimal import *
import datetime
import textwrap
import re

#################################################################
####################  adjustable parameters  ####################
#################################################################

DSB_60Co_aer = float(8.32)  #DSB, Co-60, 100% O2
SSB_60Co_aer = float(188.63)  #SSB, Co-60, 100% O2
BD_60Co_aer = float(425.26)  #BD, Co-60, 100% O2

DSB_60Co_an = float(2.86)  #DSB, Co-60, 0% O2
SSB_60Co_an = float(115.53)  #SSB, Co-60, 0% O2
BD_60Co_an = float(293.98)  #BD, Co-60, 0% O2

DE_DF_width = int(72)  #column termination for text wrap, shouldn't need to change
Tally_num = str(6)  #changes first number for all dose response card tallies, use only integers 1-9

#################################################################

def natural_key(string_):
    return [int(s) if s.isdigit() else s for s in re.split(r'(\d+)', string_)]   #function to sort MCDS output
files in ascending order

File = sorted(glob.glob("*.out"), key=natural_key)  #searches current directory for ".out" files, sorts

T = np.count_nonzero(File)  #number of MCDS output files in directory
print (str(T)+'   MCDS files')

#find particle type in all files

P1 = []
b=0
while b<T:
         a=0
         for line in open(str(File[b])):
```

```
                if "INCIDENT PARTICLE:" in line:
                        data = line.strip().split()
                        P1.append(data[a+2])
        b=b+1

#find oxygenation

O1 = []
b=0
while b<T:
        a=0
        for line in open(str(File[b])):
                if "% O2" in line:
                        data = line.strip().split()
                        O1.append(data[a])
        b=b+1
        O2 = ["{0:.3E}".format(float(x)) for x in O1]

#find particle energy

E1 = []
b=0
while b<T:
        a=0
        for line in open(str(File[b])):
                if "MeV >=" in line:
                        data = line.strip().split()
                        E1.append(data[a])
        b=b+1
        E2 = ["{0:.3E}".format(float(x)) for x in E1]  #convert string to float to scientific notation with 4
sig figs

#find CSDA range (cm)

CSDA1 = []
b=0
while b<T:
        a=0
        for line in open(str(File[b])):
                if "CSDA" in line:
                        data = line.strip().split()
                        CSDA1.append(data[a])
        b=b+1
        CSDA2 = ["{0:.3E}".format(float(x)) for x in CSDA1]

#find LET

LET = []
b=0
while b<T:
        a=0
        for line in open(str(File[b])):
                if "LET (keV/um)" in line:
                        data = line.strip().split()
                        LET.append(data[a+5])  #nucleus entry, use a+2 for incident, a+3 for cell entry
        b=b+1
        LET2 = ["{0:.3E}".format(float(x)) for x in LET]

#find (Zeff/beta)^2

Zeff_b2 = []
b=0
while b<T:
        a=0
        for line in open(str(File[b])):
                if "(Zeff/beta)^2" in line:
                        data = line.strip().split()
                        Zeff_b2.append(data[a+4])  #nucleus entry, use a+1 for incident, a+2 for cell entry
        b=b+1
        Zeff_b3 = ["{0:.3E}".format(float(x)) for x in Zeff_b2]

#find ZF

ZF = []
b=0
while b<T:
        a=0
        for line in open(str(File[b])):
                if "ZF (Gy)" in line:
                        data = line.strip().split()
                        ZF.append(data[a+5])  #nucleus entry, use a+2 for incident, a+3 for cell entry
        b=b+1
        ZF2 = ["{0:.3E}".format(float(x)) for x in ZF]

#find DSB, SSB, BD and ALL, append to list
```

```
DSB = []
SSB = []
BD = []
ALL = []
b=0
while b<T:
         a=0
         for i,line in enumerate(open(str(File[b]))):
                  if i ==151:                                #line-1 that contains Table 2 output (number of
clusters per cell)
                           data = line.strip().split()
                           DSB.append(data[a+1])
                           SSB.append(data[a+3])
                           BD.append(data[a+5])
                           ALL.append(data[a+7])
         b=b+1
         DSB2 = ["{0:.3E}".format(float(x)) for x in DSB]
         SSB2 = ["{0:.3E}".format(float(x)) for x in SSB]
         BD2 = ["{0:.3E}".format(float(x)) for x in BD]
         ALL2 = ["{0:.3E}".format(float(x)) for x in ALL]

#################################################################

if O1[0] == '1.0000E+02':
    DSB_60Co = DSB_60Co_aer
    SSB_60Co = SSB_60Co_aer
    BD_60Co = BD_60Co_aer
else:
    DSB_60Co = DSB_60Co_an
    SSB_60Co = SSB_60Co_an
    BD_60Co = BD_60Co_an

print(str(DSB_60Co)+'  DSB/Gy/Gbp (60Co)')

RBE_DSB = [float(x)/DSB_60Co for x in DSB]
RBE_SSB = [float(x)/SSB_60Co for x in SSB]
RBE_BD = [float(x)/BD_60Co for x in BD]

a=0
RMF2=[]
while a <T:
    RMF2.append(float(RBE_DSB[a])*float(RBE_DSB[a])*float(ZF[a]))
    a=a+1

RBE_DSB2 = ["{0:.3E}".format(float(x)) for x in RBE_DSB]
RBE_SSB2 = ["{0:.3E}".format(float(x)) for x in RBE_SSB]
RBE_BD2 = ["{0:.3E}".format(float(x)) for x in RBE_BD]
RMF3 = ["{0:.3E}".format(float(x)) for x in RMF2]

#################################################################
######################  Write data to a table  ##################
#################################################################

table = open(str(P1[0])+'_'+str(int(float(O1[0])))+'_O2_MCDS_output.txt', 'w')

table.write('Data generated using MCDS Version 3.10A  05-DEC-2011'+'
('+datetime.date.today().strftime("%B %d, %Y")+')'+'\n')
table.write('=============================================================================================================
=================================== \n')
table.write('PARTICLE   OXYGEN        E(MeV)      (Zeff/Beta)^2   LET(keV/um)     CSDA(cm)       ZF(Gy)
DSB/Gy/Gbp    SSB/Gy/Gbp     BD/Gy/Gbp\n')
table.write('=============================================================================================================
================================== \n')

a=0
while a<T:
        table.write('   ' +P1[a]+'    '+ str(O2[a]).ljust(11) +'   '+ str(E2[a]).ljust(11) + '   ' +
str(Zeff_b3[a]).ljust(11) + '    ' + str(LET2[a]).ljust(11) + '   ' +  str(CSDA2[a]).ljust(11) +  '   ' +
str(ZF2[a]).ljust(11) + '   ' +  str(DSB2[a]).ljust(11) +'   ' +  str(SSB2[a]).ljust(11) +'   ' +
str(BD2[a]).ljust(11) +'\n')
        a=a+1
print(str(P1[0])+'_'+str(int(float(O1[0])))+'_O2_MCDS_output.txt  created')
table.close()

#################################################################
###############  Select MCNP particle type for DE/DF  #################
#################################################################

if P1[0] == '4He':    #MCDS particle identifier
    P2 = 'A   '       #MCNP particle identifier
    P16=P26=P36=P46=P56=P66=P76='C'
else:
    if P1[0]== '3He':
        P2 = 'S   '
```

```
    P16=P26=P36=P46=P56=P66=P76='C'
else:
    if P1[0] == '3H':
        P2 = 'T   '
        P16=P26=P36=P46=P56=P66=P76='C'
    else:
        if P1[0] == '2H':
            P2 = 'D   '
            P16=P26=P36=P46=P56=P66=P76='C'
        else:
            if P1[0] == 'proton':
                P2 = 'H   '
                P16=P26=P36=P46=P56=P66=P76='C'
            else:
                if P1[0] == 'e-':
                    P2 = 'E   '
                    P16=P26=P36=P46=P56=P66=P76='C'
                else:
                    if P1[0] == '12C':
                        P2 = '#   '
                        P16 = 'FT'+str(Tally_num)+'016      RES 6012'
                        P26 = 'FT'+str(Tally_num)+'026      RES 6012'
                        P36 = 'FT'+str(Tally_num)+'036      RES 6012'
                        P46 = 'FT'+str(Tally_num)+'046      RES 6012'
                        P56 = 'FT'+str(Tally_num)+'056      RES 6012'
                        P66 = 'FT'+str(Tally_num)+'066      RES 6012'
                        P76 = 'FT'+str(Tally_num)+'076      RES 6012'
                    else:
                        if P1[0] == '7Li':
                            P2 = '#   '
                            P16 = 'FT'+str(Tally_num)+'016      RES 3007'
                            P26 = 'FT'+str(Tally_num)+'026      RES 3007'
                            P36 = 'FT'+str(Tally_num)+'036      RES 3007'
                            P46 = 'FT'+str(Tally_num)+'046      RES 3007'
                            P56 = 'FT'+str(Tally_num)+'056      RES 3007'
                            P66 = 'FT'+str(Tally_num)+'066      RES 3007'
                            P76 = 'FT'+str(Tally_num)+'076      RES 3007'
                        else:
                            if P1[0] == '6Li':
                                P2 = '#   '
                                P16 = 'FT'+str(Tally_num)+'016      RES 3006'
                                P26 = 'FT'+str(Tally_num)+'026      RES 3006'
                                P36 = 'FT'+str(Tally_num)+'036      RES 3006'
                                P46 = 'FT'+str(Tally_num)+'046      RES 3006'
                                P56 = 'FT'+str(Tally_num)+'056      RES 3006'
                                P66 = 'FT'+str(Tally_num)+'066      RES 3006'
                                P76 = 'FT'+str(Tally_num)+'076      RES 3006'
                            else:
                                if P1[0] == '14N':
                                    P2 = '#   '
                                    P16 = 'FT'+str(Tally_num)+'016      RES 7014'
                                    P26 = 'FT'+str(Tally_num)+'026      RES 7014'
                                    P36 = 'FT'+str(Tally_num)+'036      RES 7014'
                                    P46 = 'FT'+str(Tally_num)+'046      RES 7014'
                                    P56 = 'FT'+str(Tally_num)+'056      RES 7014'
                                    P66 = 'FT'+str(Tally_num)+'066      RES 7014'
                                    P76 = 'FT'+str(Tally_num)+'076      RES 7014'
                                else:
                                    if P1[0] == '16O':
                                        P2 = '#   '
                                        P16 = 'FT'+str(Tally_num)+'016      RES 8016'
                                        P26 = 'FT'+str(Tally_num)+'026      RES 8016'
                                        P36 = 'FT'+str(Tally_num)+'036      RES 8016'
                                        P46 = 'FT'+str(Tally_num)+'046      RES 8016'
                                        P56 = 'FT'+str(Tally_num)+'056      RES 8016'
                                        P66 = 'FT'+str(Tally_num)+'066      RES 8016'
                                        P76 = 'FT'+str(Tally_num)+'076      RES 8016'
                                    else:
                                        if P1[0] == '20Ne':
                                            P2 = '#   '
                                            P16 = 'FT'+str(Tally_num)+'016      RES 10020'
                                            P26 = 'FT'+str(Tally_num)+'026      RES 10020'
                                            P36 = 'FT'+str(Tally_num)+'036      RES 10020'
                                            P46 = 'FT'+str(Tally_num)+'046      RES 10020'
                                            P56 = 'FT'+str(Tally_num)+'056      RES 10020'
                                            P66 = 'FT'+str(Tally_num)+'066      RES 10020'
                                            P76 = 'FT'+str(Tally_num)+'076      RES 10020'
                                        else:
                                            if P1[0] == '16N':
                                                P2 = '#   '
                                                P16 = 'FT'+str(Tally_num)+'016      RES 7016'
                                                P26 = 'FT'+str(Tally_num)+'026      RES 7016'
                                                P36 = 'FT'+str(Tally_num)+'036      RES 7016'
                                                P46 = 'FT'+str(Tally_num)+'046      RES 7016'
                                                P56 = 'FT'+str(Tally_num)+'056      RES 7016'
```

```
                                        P66 = 'FT'+str(Tally_num)+'066      RES 7016'
                                        P76 = 'FT'+str(Tally_num)+'076      RES 7016'
                                    else:
                                        if P1[0] == '13C':
                                            P2 = '#    '
                                            P16 = 'FT'+str(Tally_num)+'016      RES 6013'
                                            P26 = 'FT'+str(Tally_num)+'026      RES 6013'
                                            P36 = 'FT'+str(Tally_num)+'036      RES 6013'
                                            P46 = 'FT'+str(Tally_num)+'046      RES 6013'
                                            P56 = 'FT'+str(Tally_num)+'056      RES 6013'
                                            P66 = 'FT'+str(Tally_num)+'066      RES 6013'
                                            P76 = 'FT'+str(Tally_num)+'076      RES 6013'
                                        else:
                                            if P1[0] == '56Fe':
                                                P2 = '#    '
                                                P16 = 'FT'+str(Tally_num)+'016      RES 26056'
                                                P26 = 'FT'+str(Tally_num)+'026      RES 26056'
                                                P36 = 'FT'+str(Tally_num)+'036      RES 26056'
                                                P46 = 'FT'+str(Tally_num)+'046      RES 26056'
                                                P56 = 'FT'+str(Tally_num)+'056      RES 26056'
                                                P66 = 'FT'+str(Tally_num)+'066      RES 26056'
                                                P76 = 'FT'+str(Tally_num)+'076      RES 26056'

############################################################
######################  Write data to DE/DF  ######################
############################################################

table = open(str(P1[0])+'_'+str(int(float(O1[0])))+'_O2_MCNP_dose_response.dedf', 'w')

table.write(str(P1[0])+' DOSE-RESPONSE FUNCTIONS FOR USE IN MCNP6
'+'('+datetime.date.today().strftime("%B %d, %Y")+')'+'\n')
table.write('Data generated using MCDS Version 3.10A  05-DEC-2011'+'\n')
table.write('\n')
table.write('C'+'\n')
table.write('C           DSB (60Co):   '+str(DSB_60Co)+'\n')
table.write('C           SSB (60Co): '+str(SSB_60Co)+'\n')
table.write('C           BD  (60Co): '+str(BD_60Co)+'\n')
table.write('C'+'\n')
table.write('C    ***    ============================================================'+'\n')
table.write('C    ***'+'                 '+str(P1[0])+ '  DOSE, RBE AND RELATED TALLIES'+'\n')
table.write('C    ***    ------------------------------------------------------------'+'\n')

table.write('C'+'\n')
table.write('FC'+str(Tally_num)+'016'+'      '+str(P1[0])+' '+'Absorbed Dose ' +'\n')
table.write('F'+str(Tally_num)+'016:'+str(P2)+'  '+'1'+'\n')
table.write(str(P16)+'\n')
table.write('FM'+str(Tally_num)+'016'+'      '+'0.1602  $MeV/g to nGy'+ '\n')

###### RBE[DSB] card

table.write('C'+'\n')
table.write('C'+'\n')
table.write('FC'+str(Tally_num)+'026'+'      '+str(P1[0])+' '+'RBE for DSB induction '
+'('+str(int(float(O1[0])))+'% pO2)'+' relative to 60Co' + '\n')
table.write('F'+str(Tally_num)+'026:'+str(P2)+'  '+'1'+'\n')
table.write(str(P26)+'\n')
table.write('FM'+str(Tally_num)+'026'+'      '+'0.1602  $MeV/g to nGy'+ '\n')

wrapper = textwrap.TextWrapper(initial_indent='DE'+str(Tally_num)+'026'+'      ',width=DE_DF_width,
                               subsequent_indent='            ')
E2 = map(str, E2)
E3 = ' '.join(E2)
table.write(wrapper.fill(str(E3)))
table.write('\n')

wrapper = textwrap.TextWrapper(initial_indent='DF'+str(Tally_num)+'026'+'      ',width=DE_DF_width,
                               subsequent_indent='            ')
RBE_DSB2 = map(str, RBE_DSB2)
RBE_DSB3 = ' '.join(RBE_DSB2)
table.write(wrapper.fill(str(RBE_DSB3)))
table.write('\n')

###### RBE[SSB] card

table.write('C'+'\n')
table.write('C'+'\n')
table.write('FC'+str(Tally_num)+'036'+'      '+str(P1[0])+' '+'RBE for SSB induction '
+'('+str(int(float(O1[0])))+'% pO2)'+' relative to 60Co' + '\n')
table.write('F'+str(Tally_num)+'036:'+str(P2)+'  '+'1'+'\n')
table.write(str(P36)+'\n')
table.write('FM'+str(Tally_num)+'036'+'      '+'0.1602  $MeV/g to nGy'+ '\n')

wrapper = textwrap.TextWrapper(initial_indent='DE'+str(Tally_num)+'036'+'      ',width=DE_DF_width,
                               subsequent_indent='            ')
E2 = map(str, E2)
```

```
E3 = ' '.join(E2)
table.write(wrapper.fill(str(E3)))
table.write('\n')

wrapper = textwrap.TextWrapper(initial_indent='DF'+str(Tally_num)+'036'+'      ',width=DE_DF_width,
                               subsequent_indent='            ')
RBE_SSB2 = map(str, RBE_SSB2)
RBE_SSB3 = ' '.join(RBE_SSB2)
table.write(wrapper.fill(str(RBE_SSB3)))
table.write('\n')

###### RBE[BD] card

table.write('C'+'\n')
table.write('C'+'\n')
table.write('FC'+str(Tally_num)+'046'+'      '+str(P1[0])+' '+'RBE for BD induction '
+'('+str(int(float(O1[0])))+'% pO2)'+' relative to 60Co'+ '\n')
table.write('F'+str(Tally_num)+'046:'+str(P2)+'  '+'1'+'\n')
table.write(str(P46)+'\n')
table.write('FM'+str(Tally_num)+'046'+'      '+'0.1602  $MeV/g to nGy'+ '\n')

wrapper = textwrap.TextWrapper(initial_indent='DE'+str(Tally_num)+'046'+'      ',width=DE_DF_width,
                               subsequent_indent='            ')
E2 = map(str, E2)
E3 = ' '.join(E2)
table.write(wrapper.fill(str(E3)))
table.write('\n')

wrapper = textwrap.TextWrapper(initial_indent='DF'+str(Tally_num)+'046'+'      ',width=DE_DF_width,
                               subsequent_indent='            ')
RBE_BD2 = map(str, RBE_BD2)
RBE_BD3 = ' '.join(RBE_BD2)
table.write(wrapper.fill(str(RBE_BD3)))
table.write('\n')

###### LET card

table.write('C'+'\n')
table.write('C'+'\n')
table.write('FC'+str(Tally_num)+'056'+'      '+str(P1[0])+' '+'LET (keV/um) '+'\n')
table.write('F'+str(Tally_num)+'056:'+str(P2)+'  '+'1'+'\n')
table.write(str(P56)+'\n')
table.write('FM'+str(Tally_num)+'056'+'      '+'0.1602  $MeV/g to nGy'+ '\n')

wrapper = textwrap.TextWrapper(initial_indent='DE'+str(Tally_num)+'056'+'      ',width=DE_DF_width,
                               subsequent_indent='            ')
E2 = map(str, E2)
E3 = ' '.join(E2)
table.write(wrapper.fill(str(E3)))
table.write('\n')

wrapper = textwrap.TextWrapper(initial_indent='DF'+str(Tally_num)+'056'+'      ',width=DE_DF_width,
                               subsequent_indent='            ')
LET2 = map(str, LET2)
LET3 = ' '.join(LET2)
table.write(wrapper.fill(str(LET3)))
table.write('\n')

###### ZF card

table.write('C'+'\n')
table.write('C'+'\n')
table.write('FC'+str(Tally_num)+'066'+'      '+str(P1[0])+' '+'ZF (mean specific energy) ' +'\n')
table.write('F'+str(Tally_num)+'066:'+str(P2)+'  '+'1'+'\n')
table.write(str(P66)+'\n')
table.write('FM'+str(Tally_num)+'066'+'      '+'0.1602  $MeV/g to nGy'+ '\n')

wrapper = textwrap.TextWrapper(initial_indent='DE'+str(Tally_num)+'066'+'      ',width=DE_DF_width,
                               subsequent_indent='            ')
E2 = map(str, E2)
E3 = ' '.join(E2)
table.write(wrapper.fill(str(E3)))
table.write('\n')

wrapper = textwrap.TextWrapper(initial_indent='DF'+str(Tally_num)+'066'+'      ',width=DE_DF_width,
                               subsequent_indent='            ')
ZF2 = map(str, ZF2)
ZF3 = ' '.join(ZF2)
table.write(wrapper.fill(str(ZF3)))
table.write('\n')

###### RMF card

table.write('C'+'\n')
table.write('C'+'\n')
```

```
table.write('FC'+str(Tally_num)+'076'+'      '+str(P1[0])+' '+'RMF intra-track DSB interaction term '
+'('+str(int(float(O1[0])))+'% pO2)'+'\n')
table.write('F'+str(Tally_num)+'076:'+str(P2)+'  '+'1'+'\n')
table.write(str(P76)+'\n')
table.write('FM'+str(Tally_num)+'076'+'      '+'0.1602  $MeV to nGy'+ '\n')

wrapper = textwrap.TextWrapper(initial_indent='DE'+str(Tally_num)+'076'+'      ',width=DE_DF_width,
                               subsequent_indent='             ')
E2 = map(str, E2)
E3 = ' '.join(E2)
table.write(wrapper.fill(str(E3)))
table.write('\n')

wrapper = textwrap.TextWrapper(initial_indent='DF'+str(Tally_num)+'076'+'      ',width=DE_DF_width,
                               subsequent_indent='             ')
RMF3 = map(str, RMF3)
RMF4 = ' '.join(RMF3)
table.write(wrapper.fill(str(RMF4)))
table.write('\n')

print(str(P1[0])+'_'+str(int(float(O1[0])))+'_O2_MCNP_dose_response.dedf  created')
table.close()

############################################################
##########################  Plot Data  #####################
############################################################

plt.figure(1)
plt.semilogx()
plt.plot(E1,DSB,'.', label='DSB')
plt.plot(E1,SSB,'.', label='SSB')
plt.plot(E1,BD,'.',label='BD')
plt.plot(E1,ALL,'.', label='ALL')
plt.title(str(P1[0])+' ions,  '+str(int(float(O1[0])))+'% O2')
plt.xlabel('Energy (MeV)', fontsize = 12)
plt.ylabel('number of clusters per cell', fontsize = 12)
plt.minorticks_on()
plt.legend(loc=9,ncol=5 ,fontsize=10)
plt.savefig(str(P1[0])+'_'+str(int(float(O1[0])))+'_O2_MCDS_plot.png')
print(str(P1[0])+'_'+str(int(float(O1[0])))+'_O2_MCDS_plot.png  created')

plt.show()
```

APPENDIX C

TALLYX.F90 SUBROUTINE

```
!+ $Id: tallyx.F90,v 1.4 2009/09/15 16:58:25 hgh Exp $
! Copyright LANS/LANL/DOE - see file COPYRIGHT_INFO

subroutine tallyx(t,ib)
  ! dummy for user-supplied tallyx subroutine.
  ! t is the input and output tally score value.
  ! ib controls scoring.  see the user's manual.

  ! .. Use Statements ..
  use fixcom,          only: jtlx
  use errprn_mod,      only: errprn
  use mcnp_global,     only: iptal, tds, tally_for_par
  use mcnp_params,     only: dknd, one, zero
  use mcnp_particles,  only: charge, gpt           !charge of particle, string
  use fluence_to_dose, only: dfact
  use pblcom,          only: pbl
  use tskcom,          only: ital
  use ephcom,          only: stppwr
  use varcom,          only: ion_a, ion_z, ion_src_a, ion_src_z, ion_chg
  use mcnp_debug

  implicit real(dknd) (a-h,o-z)

  ! .. Scalar Arguments ..
  real(dknd) :: t
  integer :: ib

  func=RDUM(1)
  dtar=RDUM(2)

  if (pbl%i%ipt==3) then
    ion_a2=0.00054857           ! electron (e) rest mass (amu)
    v=pbl%r%erg
    c=charge(pbl%i%ipt)
  else if (pbl%i%ipt==9) then
    ion_a2=1.00727647           ! proton (h) rest mass (amu)
    v=pbl%r%erg
    c=charge(pbl%i%ipt)
  else if (pbl%i%ipt==31) then
    ion_a2=2.01355556           ! deuteron (d) rest mass (amu)
    v=pbl%r%erg
    c=charge(pbl%i%ipt)
  else if (pbl%i%ipt==32) then
    ion_a2=3.01551369           ! triton (t) rest mass (amu)
    v=pbl%r%erg
    c=charge(pbl%i%ipt)
  else if (pbl%i%ipt==33) then
    ion_a2=3.01494471           ! helion (s) rest mass (amu)
    v=pbl%r%erg
    c=charge(pbl%i%ipt)
  else if (pbl%i%ipt==34) then
    ion_a2=4.00150618           ! alpha (a) rest mass (amu)
    v=pbl%r%erg
    c=charge(pbl%i%ipt)
  else
    ion_a2=ion_a
    v=pbl%r%vel
    c=ion_chg
  end if

 !-----------------------------------------------------------------------
 ! Calculate beta, zeff, x
 !-----------------------------------------------------------------------
```

```
 b=sqrt(1.-(1./((1.+(v/(ion_a2*931.5)))**2))) ! beta
 zeff=c*(1-exp(-125*b*c**(-2./3.)))           ! Zeff
 x=(zeff/b)**2                                ! (Zeff/beta)^2

!-----------------------------------------------------------------------
! Calculate RBE(DSB), RBE(SSB), RBE(BD)
!
! pO2 = 100%
! DSB (60Co):   8.32
! SSB (60Co): 188.63
! BD  (60Co): 425.26
!
! po2 = 0%
! DSB (60Co):   2.86
! SSB (60Co): 115.53
! BD  (60Co): 293.98
!-----------------------------------------------------------------------

 RBE_DSB_100=0.9902+2.411-(2.411**(1.-1.539)+0.000732*x*(1.539-1))** &
 &(1./(1-1.539))

 RBE_DSB_0=(1.502+sqrt(x)*(1.037+sqrt(x)*(0.135+sqrt(x)*(-0.00823+0.0003077* &
 &sqrt(x)))))/(1.+sqrt(x)*(1.611+sqrt(x)*(-0.0115+sqrt(x)*(-0.0006096+ &
 &0.00003047*sqrt(x)))))

 RBE_SSB_100=((1.001-0.003468*sqrt(x)+0.0002142*x)/(1-0.003754*sqrt(x)+ &
 &0.0006658*x+0.0000001028*x**1.5))

 RBE_SSB_0=((0.99954102-0.44385537*alog(x)+0.075736504*alog(x)**2-0.00592203 &
 &*alog(x)**3+0.000181752*alog(x)**4)/(1-0.44572796*alog(x)+0.076670658* &
 &alog(x)**2-0.00597358*log(x)**3+0.000160081*alog(x)**4+0.00000217649* &
 &alog(x)**5))

 RBE_BD_100=((0.99999501-0.0073091938*sqrt(x)+0.00016008872*x)/ &
 &(1-0.0080920565*sqrt(x)+0.0014413807*x+8.643173e-7*x**1.5))

 RBE_BD_0=((1.0003012-0.41085633*alog(x)+0.065436498*alog(x)**2- &
 &0.00482080*alog(x)**3+0.000140979*alog(x)**4)/(1-0.40744935*alog(x)+ &
 &0.061453313*alog(x)**2-0.00302474*alog(x)**3-0.00016191*alog(x)**4+ &
 &1.73989e-5*alog(x)**5))

!-----------------------------------------------------------------------
! Calculate ZF (ICRU Report 36 definition)
!-----------------------------------------------------------------------

 ZF=(0.204*stppwr*0.1)/(dtar**2)  ! frequency-mean specific energy in Gy
 LET=stppwr*0.1

 RMF_100=((RBE_100**2)*ZF)
 RMF_0= ((RBE_0**2)*ZF)

 !print *, "velocity=  ", pbl%r%vel
 !print *, "energy=  ", pbl%r%erg
 ! print *, "ion Z=  ", ion_z
 ! print *, "ion A=  ", ion_a
 ! print *, "ion chg=  ", ion_chg
 ! print *, "ion ipt=  ", pbl%i%ipt
 !print *, "beta=  ", b
 !print *, "zeff=  ", zeff
 !print *, "x=  ", x
 !print *, "RBE 100=  ", RBE_DSB_100
 !print *, "RBE 0=  ", RBE_DSB_0
 !print *, "ZF=  ", ZF
 ! print *, "RMF_100=  ", RMF_100
 ! print *,  charge(pbl%i%ipt)
 !print *, ion_a2
 !print *, v
 !print *, stppwr
 ! print *, gpt
 ! print *, charge
 ! print *, iptal

 if (func==100) then
   t=t*RBE_DSB_100
 else if (func==0) then
   t=t*RBE_DSB_0
 else if (func == 1) then
   t=t*ZF
 else if (func == 2) then
   t=t*RMF100
 else if (func == 3) then
   t=t*RBE_SSB_100
 else if (func == 4) then
```

```
    t=t*RBE_SSB_0
  else if (func == 5) then
    t=t*RBE_BD_100
  else if (func == 6) then
    t=t*RBE_BD_0
  else if (func == 7) then
    t=t*LET
  else
    ib=-1
  end if

  return
end subroutine tallyx
```